2000

Feasibility study of road substitution technique for accelerated laboratory road test simulation.

Mirella T. Rennert
University of Windsor

INFORMATION TO USERS

This manuscript has been reproduced from the microfilm master. UMI films the text directly from the original or copy submitted. Thus, some thesis and dissertation copies are in typewriter face, while others may be from any type of computer printer.

The quality of this reproduction is dependent upon the quality of the copy submitted. Broken or indistinct print, colored or poor quality illustrations and photographs, print bleedthrough, substandard margins, and improper alignment can adversely affect reproduction.

in the unlikely event that the author did not send UMI a complete manuscript and there are missing pages, these will be noted. Also, if unauthorized copyright material had to be removed, a note will indicate the deletion.

Oversize materials (e.g., maps, drawings, charts) are reproduced by sectioning the original, beginning at the upper left-hand corner and continuing from left to right in equal sections with small overlaps.

Photographs included in the original manuscript have been reproduced xerographically in this copy. Higher quality 6" x 9" black and white photographic prints are available for any photographs or illustrations appearing in this copy for an additional charge. Contact UMI directly to order.

ProQuest Information and Learning
300 North Zeeb Road, Ann Arbor, MI 48106-1346 USA
800-521-0600

FEASIBILITY STUDY OF ROAD SUBSTITUTION TECHNIQUE FOR ACCELERATED LABORATORY ROAD TEST SIMULATION

by

Mirella T. Rennert
Research Assistant
University of Windsor / DaimlerChrysler Canada Automotive Research and Development Center
Road Test Simulation Department

A Thesis
Submitted to the College of Graduate Studies and Research
through Mechanical, Automotive and Materials Engineering
in Partial Fulfillment of the Requirements for
The Degree of Master of Applied Science at the
University of Windsor

Windsor, Ontario, Canada

September, 2000

ABSTRACT

A study of the feasibility of road substitution to accelerate the simulation of vehicle use has been conducted using an off-road test (OR test) at the Proving Grounds (PG) as a test case. The purpose of the study was to examine the possibility of accelerating and optimizing the testing conducted at the vehicle proving grounds. This was performed by investigating the similarities in vehicle responses collected from various roads included in the test. The goal was to ultimately reduce the data acquisition period, data analysis as well as the durability cycle replicated in the laboratory environment.

The initial study was performed on the data collected for a vehicle durability project. Sixteen channels of transducer data were utilized (out of 39 available) in the analysis. The selected sixteen channels were used in the project to develop computer control or drive files for a vehicle on an MTS Model 329 spindle coupled simulator. Out of the sixteen channels, four channels measuring spindle to body displacement of the vehicle were selected to perform fatigue analysis. The results of the study were later verified with the data collected for two other durability projects.

There are ten roads included in the OR test. The vehicle responses collected from these roads were analyzed and compared using the following methods:

- Time histories and statistical analysis
- Cyclic content based on "rainflow counted" histograms
- Probability density functions relating the amplitude distribution
- Power spectral density
- Fatigue analysis

In addition, road profile analyses from a report on the OR test course roughness comparison were used to further verify the results.

The results of the above analyses showed that five groups of roads could be formed to simplify the OR test at the PG. A representative road can then be selected from each group, to represent the remaining roads in that group. The representative road can be selected based on two factors:

1. road stability, as determined by road profiling analyses conducted over several years, and
2. process optimization.

The second factor, being process optimization, should then take into account:

- the duration of the time history, and
- the damage induced in the vehicle by the representative road.

Ultimately the shortest, most damaging road would be selected as a group representative. Since experience shows that repeated field tests over same road tracks show variance in the measurement data due to changes in speed, drivers and weather, as well as different data editing procedures being implemented by companies, the selection of the representative road may change with each test. Thus optimization will have to be performed with each project. This study purely focuses on grouping roads with similar vehicle characteristic to simplify the data analysis period.

ACKNOWLEDGEMENTS

I would like to acknowledge my thanks to my supervisor Dr. Peter Frise, Professor and DaimlerChrysler Canada/NSERC Industrial Research Chair in Mechanical Design at the University of Windsor, Department of Mechanical Engineering. Dr. Frise provided me with a great opportunity of pursuing my educational career in a true engineering environment. I appreciate his efforts in bringing valuable technical experience and skills into his methods of teaching. His presence at the University of Windsor will surely benefit many to come.

I would also like to thank the following who helped:

Stuart Shaw from Product & Development Engineering at the DaimlerChrysler Automotive Research & Development Center (ARDC) in Windsor, Canada for his guidance and supervision during my stay at ARDC;

Martin Vander Baaren who worked at ARDC as a product engineer within the Road Test Simulation Department. His knowledge, experience and constant support played a significant part in the completion of this work;

Steven Schleuter, a duty cycle specialist from DaimlerChrysler Arizona Proving Grounds for an amazing tour of his facilities and for his assistance in my work;

DaimlerChrysler ARDC employees, especially the Road Test Simulation Engineers, for their gracious welcome and support;

The Natural Sciences and Engineering Research Council and University of Windsor for providing me with financial assistance in forms of scholarships;

Lastly I would like to acknowledge my peers and wish them best of luck in completion of their degree.

TABLE OF CONTENTS

LIST OF FIGURES

LIST OF TABLES

LIST OF ABBREVIATIONS

ADAMS – Automated Dynamic Analysis of Mechanical Systems
ADR – Automated Durability Road
APG – Arizona Proving Grounds
ARDC – Automotive Research and Development Center
ASD – Auto Spectral Density
ASTM – American Society for Testing and Materials
Avg. - Average
CAE – Computer Aided Engineering
CCW – Counter Clockwise
Ch - Channel
Cm – Centimeter
CSD – Cross Spectral Density
CW – Clockwise
DFMV – Dynamic Force Measurement Vehicle
ERPC – Effective Road Profile Control
FEA – Finite Element Analysis
FIR – Finite Impulse Response
FRF – Frequency Response Function
Ft – Feet/foot
G – Gravity acceleration
HCF – High Cycle Fatigue
Hz. – Hertz
In – Inches
Kg – Kilograms
Km – Kilometers
Km/h – Kilometer per hour
L – Liter
Lbs – Pounds
LCF – Low Cycle Fatigue
LFCS or LFCoil– Left front coil spring
LFKnZa01 – Left front knuckle vertical acceleration
LFLBJX05 – Left front lower ball joint longitudinal load
LFLBJY09 – Left front lower ball joint lateral load
LFLgBo – Left front longitudinal outer bending
LFLnAxBd – Left front longitudinal axle bending
LFLtBo – Left front lateral outer bending
LFSprD36 – Left front coil spring axial displacement
LFVA or LFvertAc – Left front vertical acceleration
LRAxZa02 – Left rear outboard axle tube vertical acceleration
LRCS – Left rear coil spring
LRLnAxBd – Left rear longitudinal axle bending
LRLtB – Left rear lateral bending
LRSltX06 – Left rear axle tube outboard longitudinal bending (slotted location)
LRSltY10 – Left rear axle tube outboard lateral bending (slotted location)

LRSprD37 – Left rear coil spring axial displacement
LRStrPot – Left rear string pot
LRTAS – Left rear trailing arm support
LRVA or LRvertAc – Left rear vertical acceleration
Max – Maximum
MIMO – Multiple Input – Multiple Output
Min – Minimum
MPa – MegaPascals
M.P.H. – Miles per hour
NATC – Nevada Automotive Test Center
NSERC – National Science and Engineering Research Council
OR – Off –road
PDF – Probability Density Function
PID – Proportional Integral Controller
PG – Proving Grounds
PSD – Power Spectral Density
QT – Quenched and tempered
Rd - Road
RFCS or RFCoil– Right front coil spring
RFKnZa03 – Right front knuckle vertical acceleration
RFLBJX07 – Right front lower ball joint longitudinal load
RFLBJY011 – Right front lower ball joint lateral load
RFLgBo – Right front longitudinal outer bending
RFLnAxBd – Right front longitudinal axle bending
RFLtBo – Right front lateral outer bending
RFSprD37 – Right front coil spring axial displacement
RFVA or RFvertAc – Right front vertical acceleration
RRAxZa04 – Right rear outboard axle tube vertical acceleration
RRCS – Right rear coil spring
RRLatAcc – Right rear lateral acceleration
RRLnAxBd – Right rear longitudinal axle bending
RRLtB – Right rear lateral bending
RRSltX08 – Right rear axle tube outboard longitudinal bending (slotted location)
RRSltY12 – Right rear axle tube outboard lateral bending (slotted location)
RRSprD39 – Right rear coil spring axial displacement
RRStrPot – Right rear string pot
RRTS – Right rear trailing arm support
RRVA or RRvertAc– Right rear vertical acceleration
RMS – Root Mean Square
RPC – Remote Parameter Control
RTS – Road Test Simulation (Simulator)
R2 – Fit coefficient
SAE – Society of Automotive Engineers
SUV – Sport Utility Vehicle
S-W-T – Smith-Watson-Topper
TRN – Transfer Function

Ue or $\mu\varepsilon$ – Microstrain
USD – U.S. dollars
VDF – Vehicles Dynamics Facility

NOMENCLATURE

$A_1, B_1, C_1, \ldots Z_1$	– Multipliers of sample data for channel 1
$A_m, B_m, C_m, \ldots Z_m$	– Multipliers of sample data for channel m
$[X1_1], [X2_1], \ldots [Xn_1]$	– Matrix of sample measurements for channel 1
$[X1_m], [X2_m], \ldots [Xn_m]$	– Matrix of sample measurements for channel m
$[Y_1]$	– Matrix of target measurement for channel 1
$[Y_m]$	– Matrix of target measurement for channel m
$Cov(x,y)$	– Covariance of two data sets
$\rho(x,y)$	– Correlation coefficient
σ_x	– Standard deviation of data set x
σ_y	– Standard deviation of data set y
μ_x	– Mean value of data set x
μ_y	– Mean value of data set y
N	– Total number of samples
n	– sample size at a particular magnitude
T	– Total time period
t	– Time period
p(y)	– Probability density function
t(y)	– Time-at-Level function
Di	– Damage/cycle at the ith constant amplitude stress (strain)
n_i	– Number of occurrences of the ith constant amplitude stress (strain)
N_i	– Number of cycles to failures at the ith stress (strain) amplitude
$\Delta\varepsilon$	– Total strain range
$\sigma_f^{'}$	– Fatigue strength coefficient
$\varepsilon_f^{'}$	– Fatigue ductility coefficient
E	– Modulus of elasticity
c	– Fatigue ductility exponent
b	– Fatigue strength exponent (Basquin's exponent)
$2N_f$	– Reversals to failure
$2N_t$	– Transition fatigue life
K_σ and K_ε	– Stress and strain concentration factors
σ and S	– Local and nominal stress range
ε and e	– Local and nominal strain range
ρ	– Material constant (related to grain size of the material and its strength)
r	– Radius at the root of the notch.
q	– Number of standard errors from the mean life
e	– Standard error of 2Nf for elastic life line

p	– Standard error of 2Nf for plastic life line
Pk_{err}	– Percent error on peaks/100
f_d	– Data frequency
f_s	– Sampling frequency
π	– Pi value, approx. 3.14

1 PURPOSE OF THE STUDY

A study was requested by the Road Test Simulation (RTS) group to examine the feasibility of simplifying laboratory road testing of vehicles. Durability schedules replicated in the laboratory environment consist of a variety of proving ground roads from which vehicle responses are collected. This research involves characterizing the conditions of these roads based on the behavior they induce in the vehicles to determine similarities/differences between them. This research will serve as a thesis for the author's Master's degree in Mechanical Engineering, under the supervision of Dr. Peter Frise (Professor and DaimlerChrysler Canada/NSERC Industrial Research Chair in Mechanical Design), and under the guidance of the Product and Development Engineering Department at the DaimlerChrysler Automotive Research and Development Center (ARDC) in Windsor, Ontario. The example set of ten roads used in the study is from a representative proving ground's (PG) off-road (OR) test.

Currently, the studied OR test involves collecting data from ten roads in two directions, with multiple ballast load conditions. Data for each ballast weight configuration is acquired with the vehicle being run at least twice in each direction for repeatability and statistical analysis. Test vehicle instrumentation includes numerous transducers suitable for gathering data to assist with road simulation, varying in amount based on the test. In total, this accounts for a substantial number of data files, which must be analyzed upon return to the laboratory.

Past experience of the road data acquisition group suggested that there are similarities in vehicle responses collected from different roads included in the investigated OR test. The similarities were detected through personal experiences while driving over the roads, visual inspections of load time histories and frequency responses collected from the vehicles. If this was actually true, then roads exhibiting similar response characteristics could be grouped together, and the data from only one representative road from that group would have to be included in the OR durability cycle. Other roads from the group

could then be related to the representative road through various methods, as discussed within the body of this report.

Based on that suggestion, an extensive study of the characteristics of various road responses collected from the OR test on the Proving Grounds was conducted and five sets of data were analyzed. They were project #P1 under full rated load, project #P2 under half payload and two-passenger payload, and project #P3 under full and two-passenger rated loads. All five data sets contained sixteen channels of information obtained from transducers located on the instrumented vehicle.

The main objective of this study was to assess whether it is feasible to substitute road responses from various roads, if they have similar characteristics. If proved to be successful, the method would decrease the time it takes to collect and analyze the data from the PG's OR test, as well as possibly reduce the duration of the current 600 hour durability test developed for the MTS model 329 spindle coupled road simulator in the laboratory environment.

2 BRIEF HISTORY OF GROUND VEHICLE TESTING

2.1 Need for Test Acceleration

The automotive industry is one of the fastest growing economic sectors in the world. The global fascination with owning a car, not only for transportation but also for luxury, forces vehicle manufacturers to compete for customers and this gave rise to the concepts of "first to market" and "lowest cost", which paved the way for new research and technology in vehicle testing.

The idea of "first to market" combined with captivating advertisements allows car manufacturers to acquire a faithful group of customers early in the lifetime of the product. The key is building a reputation and trust among the customers, and to convince them of product quality and reliability. This makes it much harder for the competitors to win over the customers, as they join the market later. A great example of this strategy was introduction of the Chrysler minivan in the 1980's, which to this date dominates the market in the family vehicle category.

The concept of reducing cost relates back to the time incurred in the product development stage. Any product rework, resulting from new design, adds significant cost to the development process. The cost-development curve (dashed line), shown in Figure 1, demonstrates that the later any changes are made, the higher the overall cost of production. The second curve (solid line) represents the ideal accelerated testing method, demonstrating shorter development time and lower overall cost [1].

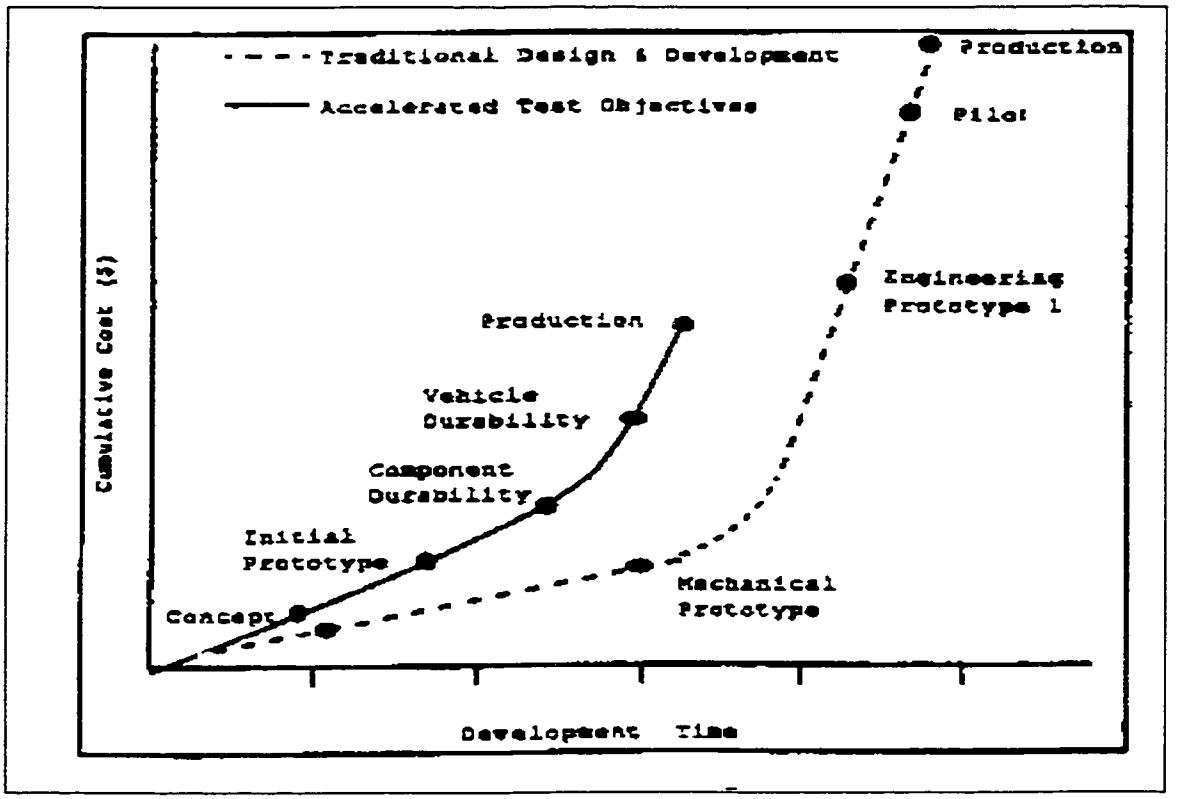

Figure 1. Shows the goal of accelerated testing. Cost reduction is related to development time of a product. Early product redesigns constitute lower overall product development costs. [1]

The overall startup costs for major new platforms are on the order of one to two billion US Dollars (USD) over a 50-60 month time period. The complete new vehicle production cost sustained by Saturn for example, from the initial concept, including manufacturing and distribution costs, totaled about three billion USD. The average engineering effort for major platform development is estimated at 2.5 million person-hours [2]. This presents a major potential for both time and cost savings in vehicle testing. As a result, new and improved methods were introduced to help in optimizing the product development process.

2.2 Methods of Vehicle Testing

The concept of smarter testing is leading the current engineering trend toward producing better quality vehicles with increased customer satisfaction and reduced time-to-market. Performing early durability assessments allows the design team to take corrective measures early in vehicle design process. Within the ground vehicle industry there are three paths (Figure 2) available to make these evaluations:

1. Computer modeling (e.g. Finite Element Analysis (FEA) or Automated Dynamic Analysis of Mechanical Systems (ADAMS)),

2. Laboratory testing (e.g. vehicle and component tests),

3. Proving ground and test track testing.

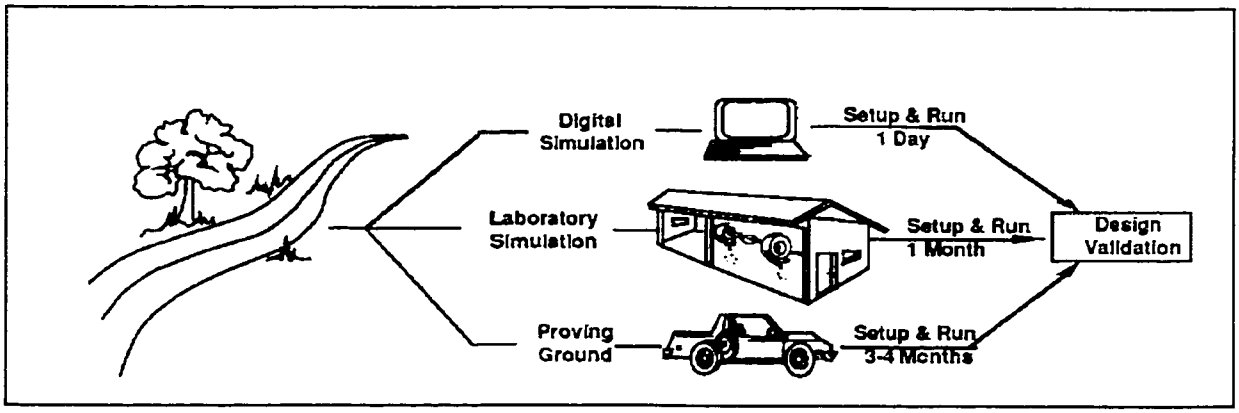

Figure 2. Paths available for durability assessment. The need for both test acceleration and better consumer satisfaction brought the evolution of vehicle evaluation based not only on proving ground/track testing, but also on laboratory and computer simulations. [3]

The methods listed above are cited in order of increasing cost and time.

2.2.1 Proving Grounds and Test Track Testing

The most customer-representative data used in the durability assessments is that of actual customers themselves. As the automotive industry developed, manufacturers tested their products in the customer's environment. Vehicles were tested on public roads and the results were then used in new product generation. Public safety, availability of roads, confidentiality of new products and the high cost incurred, were just few of the factors that prompted the automotive industry to develop new methods of vehicle testing.

Recently, attempts have been made by various companies to once again start collecting the data from customer vehicles, even to extent of basing loads and other test work on the results. The amount of data collected from these tests is enormous, but the current technology of on-board data loggers, modern instrumentation advances, faster and larger computer storage as well as sophisticated software simplifies the process of data analysis. Even with the new and advanced technology however, storage media capacity and data transfer times are often limiting factors in durability studies.

Although the data collected from customer vehicles seems ideal for any assessment, variability in drivers, road's conditions, climate, vehicle use and maintenance, makes it quite difficult to find the behavior that is most representative of customer conduct. For durability purposes, it would also require data collection throughout the whole lifetime of the vehicle (~10 years), which is not only limited by the storage capabilities but also by the ability of the engineer to analyze the data. These obstacles have to a certain extent been resolved through mathematical methods of data extrapolation.

Based on statistical information, it is quite possible to predict the trends and behavior of data on a larger scale. Extrapolation techniques can be performed based on either road length or severity of driver's maneuvers as main factors. Extrapolation in terms of length allows the data acquisition of a shorter road segment, for example 1600 km (1000 miles) of customer use, to forecast the spread of data through out the lifetime of a vehicle, or approximately 161,000 km (100,000 miles). If driver variability is of importance, an

extrapolation technique can be used to predict the data expected from the most severe driver out of a number of representative measurements collected from a variety of drivers [4].

Another disadvantage of the data collected from actual customer used vehicles is the fact that it contains high percentage of non-damaging loads. The most damaging events controlling the low cycle fatigue life of a mechanical component are typically characterized by relatively few, large amplitude, low frequency loads (below 60 Hz). The customer-acquired data contains a large number of small amplitude, high frequency loads, which may contribute little or no damage to the vehicle structure or components. This not only increases the duration of test necessary to acquire the data, but also poses problems due to data logger storage limitations.

Since testing in a customer environment is very expensive, time consuming, and often takes place in areas remote from the manufacturers' facilities, proving ground testing is utilized to accelerate the processes of data acquisition and analysis. Generally speaking, two types of tests are performed at proving ground testing facilities: Performance Testing and Endurance Testing. Performance testing attempts to address the issue of how well the product fulfills its intended function, whereas endurance testing deals with the issue of how long the product will continue to function as intended. In performance testing the goal is to replicate the operating conditions and performance criteria representative of a large mass of customers, while eliminating extraneous variables such as driver or weather variability. The priority of endurance testing on the other hand is to simulate customer usage in an accelerated time (less than normal life span of a vehicle). The aim then is to replicate the same failures as seen in customer vehicles. The failures observed in vehicles driven by actual customers should only be correlated to failures seen in production vehicles that have been subjected to accelerated testing [5]. Endurance tests designed for proving ground application can be accelerated in three different ways [5]:

- The routes could be made arbitrarily more severe than any customer would experience, for example rougher surfaces or sharper turns. This subjects the vehicle to higher stresses and loads,

- The routes could be made with approximately same severity as seen in customer usage, but omitting the mild operations, thus increasing a frequency of higher load and stress cycles,

- The vehicle can be operated for longer period of time than the average customer is able to do.

In addition, mixes of tracks, road events, distances, soils, driving and weight conditions are used to best describe a customer usage of a vehicle in a shorter period of time. The resulting time-savings can produce [6]:

- shorter time scale from concept to production,
- opportunity for repeated testing for confidence in the same time scale,
- statistical verification of results across the customer base.

There are, however some shortcomings of proving ground testing, these being:

- high cost per mile,
- slow mileage accumulation,
- limited environmental extremes,
- small sample sizes,
- inflexible,
- acceleration can introduce atypical interactions. [7]

In addition, a proving ground test may cost as much as $150,000 to $200,000, may require six to nine months (which includes vehicle instrumentation period), and will provide durability results on one specific set of specimens [8]. Proving ground testing is necessary in vehicle durability and performance assessment, since it provides the closest to real customer usage information. This opens the door for continuous improvement and the exploration of new testing and data analysis techniques.

Optimization of test configurations is one area where significant progress has been accomplished in proving ground testing. The test schedules currently implemented by the automotive industry have been designed mostly from "intelligent guesswork" of experienced engineers. The distances and number of repeats of certain tracks available on the proving ground facilities, have been estimated based on establishing the worst case conditions. These conditions include events such as potholes, Belgian blocks, and off-road tracks. [6]. Although the tests schedules have quickly been standardized, they present a need for a more efficient and "customer representative" test schedules.

Companies such as nCode International Ltd., or LMS provide automotive testing industries with software tools, which allow them to design optimized test schedules. This optimization incorporates customer-collected data so that the design of the proving ground test will be more "realistic" in nature. The whole process involves regression techniques, which handle mathematically manipulated data collected from real customers and from proving ground testing, to predict the number and types of events available on the test tracks that best describe the customer usage. The optimization can be performed with the goal of minimizing the duration, the distance, or the cost of the test itself, and with the ultimate goal being the reproduction of the same failures in accelerated testing as seen in customer-driven vehicles [4,6].

A breakthrough innovation in proving ground testing has been the design of the first and only "driverless" test track located at DaimlerChrysler Chelsea Proving Grounds. This oval track is termed Automated Durability Road (ADR) and has been in operation for the past three years. Its operation is run through control tower computer which sends

commands to the robot-driven, automatic transmission vehicles, through special relay towers (wireless network) placed around the course. The steering, shifting, braking, and acceleration maneuvers are performed by the front seat mounted robot as directed by the onboard computer, which also has a programmed path of travel [9].

Signals sent from the tower computer, instructs the vehicle to proceed or stop, while guide wires in the road direct the vehicle's path. This is performed through a signal sent by the guide wires to sensors mounted on the front of the vehicle. An antenna is also mounted on the rear of the vehicle, through which power bursts allow a signal from the track to be sent to the vehicle control computer. This in turn allows close monitoring of vehicle location and behavior throughout the test [9].

Whereas normal accelerated test at the Chelsea Proving Grounds takes on average six weeks to complete, representing 161,000 km (100,000 miles) of customer use, the ADR takes only 4,000 km (2,500 miles) or two weeks to finish (note that the acceleration factor is based on DaimlerChrysler fatigue standards for designing test tracks). The use of ADR track not only minimizes the duration and cost of the test, it also eliminates driver variability and human discomfort due to its extreme conditions [9].

Due to their limitations, proving ground tests are typically run late in the design cycle on a complete prototype vehicle, while early prototype vehicles are tested in laboratory environments.

2.2.2 Laboratory Testing

Laboratory simulation, for fatigue and durability assessment, was introduced to the automotive industry in the early 1960's. Early testing was limited in application due to poor correlation with the actual road data. It was mainly used for basic durability research applications rather than production durability assessment [10]. Limitations of the testing equipment and the number of channels available permitted only durability

testing of components rather than full vehicles. Early tests involved single axis, constant amplitude mechanical stroking tests. Technological advances in servo-hydraulics, analog and computer controls, data acquisition technology, fatigue life assessment, and experience with data editing and test system design allowed for more sophisticated system testing of full vehicles [10]. MTS has developed Remote Parameter Control (RPC) software and mechanical tests systems, which provide engineers with the tools to accurately reproduce service loads in the laboratory.

A full vehicle simulation in the testing laboratory uses two primary classes of test systems as shown in Figure 3. They are:

- tire coupled simulators,
- spindle coupled simulators.

Both systems consist of number of servo-hydraulic actuators; each controlled through a proportional-integral-derivative (PID) controller.

Figure 3. Tire coupled and Half-car spindle coupled simulators. Tire coupled or "Four Poster" simulators work by applying vertical inputs under each tire patch. The spindle coupled simulator replicates vehicle performance by applying multi-axial inputs at each corner [3].

The primary difference between the two types of test rigs is the method by which a vehicle is mounted on them and the number of degrees of freedom available at each wheel. In the case of tire coupled simulators a vehicle is placed on top of hydraulically

operated actuators. The excitation is then produced at the tires of the vehicle. The tire-coupled simulators are typically controlled through displacements at each tire. This means that the wheel displacements are proportional to the applied voltage, as regulated by the PID controller. In the spindle-coupled simulator, a vehicle is excited directly at the spindles (tires are removed). The spindle-coupled simulator can be either force or displacement controlled. There are up to sixteen actuators on a typical spindle-coupled simulator, allowing simulation in all three directions of freedom – vertical, lateral and longitudinal – and a braking torque [11].

Full vehicle simulators operate on the principle of "response simulation", rather than vehicle inputs. Response simulation is operated by a multiple input – multiple output (MIMO) control model. The method of reproducing in-service loads in a laboratory environment involves a technique of Remote Parameter Control (RPC). Coupled with servo-hydraulic systems, and sometimes with electro-dynamic systems, RPC uses field-recorded data and information about the test fixture to calculate excitation signals for the actuators. Advantage of RPC is its capability to recreate measured parameters (forces, strains, or displacements) that are remote from the points of excitation [12]. For example, RPC can be used to reproduce accelerations of a vehicle spindle by controlling the displacement of a tire, or reproduce the load in a ball joint by controlling the force across one side of a car.

2.2.3 Six Steps of Remote Parameter Control (RPC)

The six steps that comprise an RPC simulation test are shown in Figure 4.

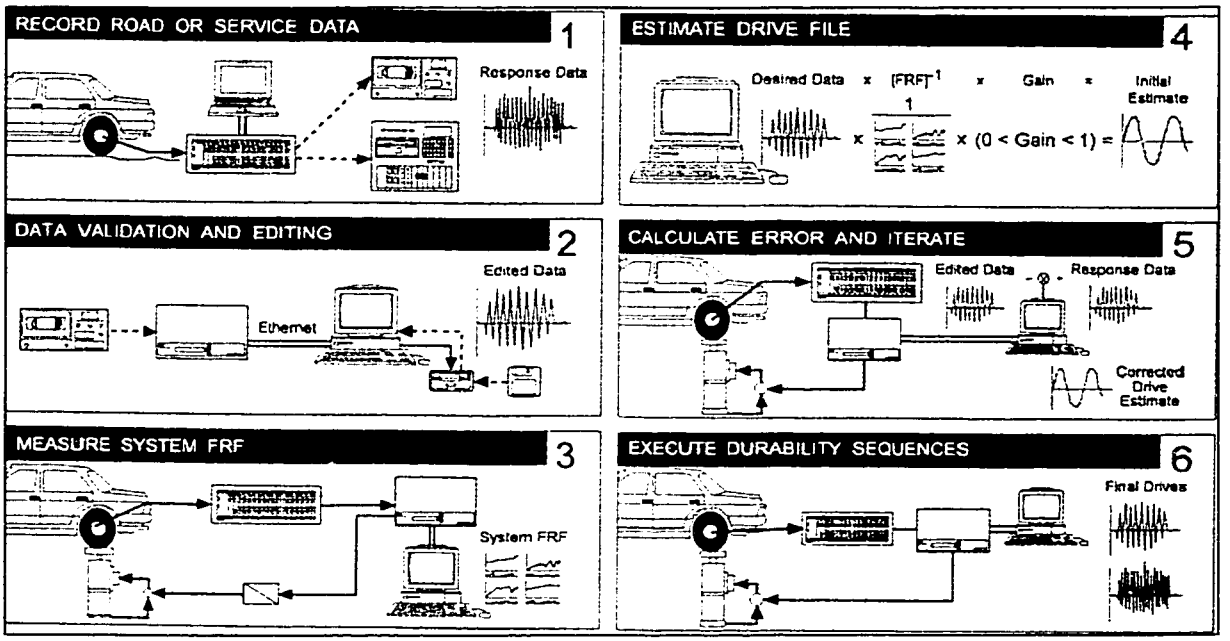

Figure 4. Six steps of Remote Parameter Control (RPC). Technique of RPC is used to accurately reproduce the load environment of a specimen in laboratory conditions. The most significant feature of RPC is its ability to recreate measured parameters that are remote from points of excitation [12].

The first step in an RPC test involves recording road or service data. Knowledge of the loading and intended purpose of the test is important in selection of transducers and their location on the specimen or vehicle. During the acquisition process, data is filtered to remove the effects of "aliasing". It is important to use a sampling rate that will cover all frequencies of interest in the field data [12]. If insufficient sampling rate is used, sampled data of a higher frequency may appear as lower frequency data, a phenomenon referred to as "aliasing". This is demonstrated in Figure 5. As a rule of thumb, the sampling frequency should be at least double the highest frequency of interest, or Nyquist Frequency.

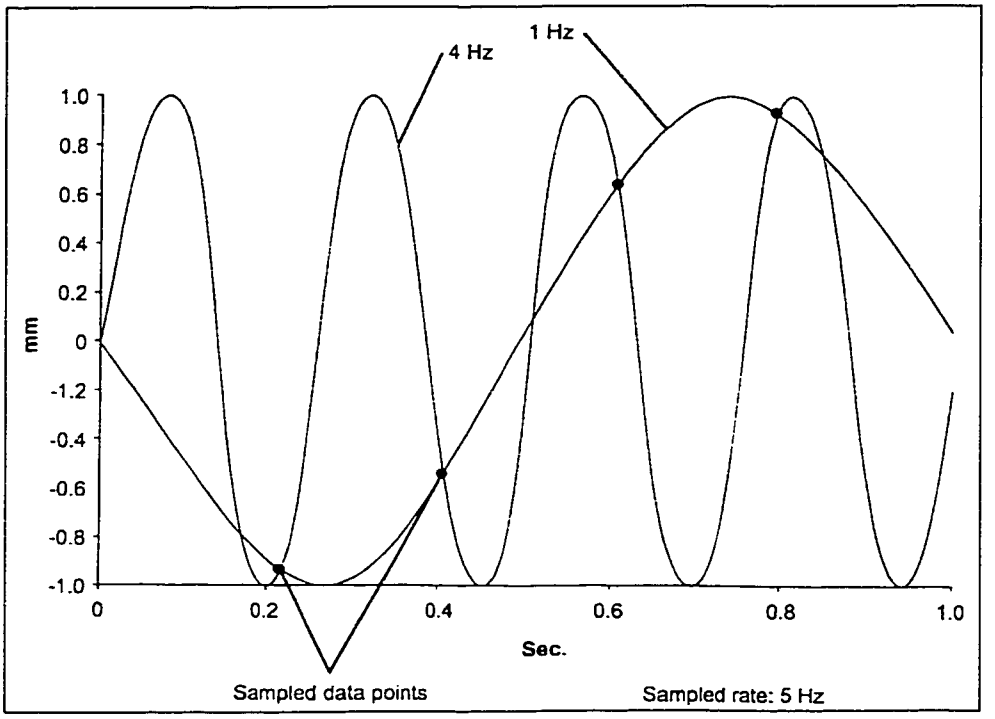

Figure 5. "Aliasing" occurs when sampled data of a higher frequency appears at lower frequency as a result of insufficient sampling rate. As a rule of thumb, the sampling frequency should be at least double the highest frequency of interest, or Nyquist frequency [13].

Proving ground data collection has been simplified further by the development of digital recording and wheel force transducers. Overall, data acquisition is one of most important steps in laboratory simulation for the simple fact that the vehicle simulation will only be as good as the data collected.

The second step of RPC simulation involves the transfer, analysis and editing of data. The data can either be stored as an analog or a digital signal. If stored in analog form, the data must be converted to a digital form and stored on a disk. The data is then grouped according to road conditions and stored for further analysis. After examining the data for any abnormalities such as drift, offsets, or unusual spikes, the data channels most appropriate for simulation are selected. Further techniques of data editing based on removing the non-damaging loads allow engineers to further accelerate vehicle simulation [12].

After preparing the data, the vehicle is mounted on the test fixture and the transducers used to measure the field data are connected through their signal conditioning electronics to the RPC computer. To successfully simulate in-service data, the RPC requires information about the test system and its influence on the remote transducers. This step is accomplished by measuring the Frequency Response Function (FRF) of the test system, which relates the input of the system to its outputs. The test system is defined as a group of: PID controller, the valve-driver, the servo-valve, the actuator, the closed-loop control transducer, the control transducer conditioner, the test fixture (kinematics and dynamics), the specimen/vehicle, the transducers used for the original data acquisition and the transducer conditioning [12]. The complete test system, for a tire-coupled simulator, is shown in Figure 6.

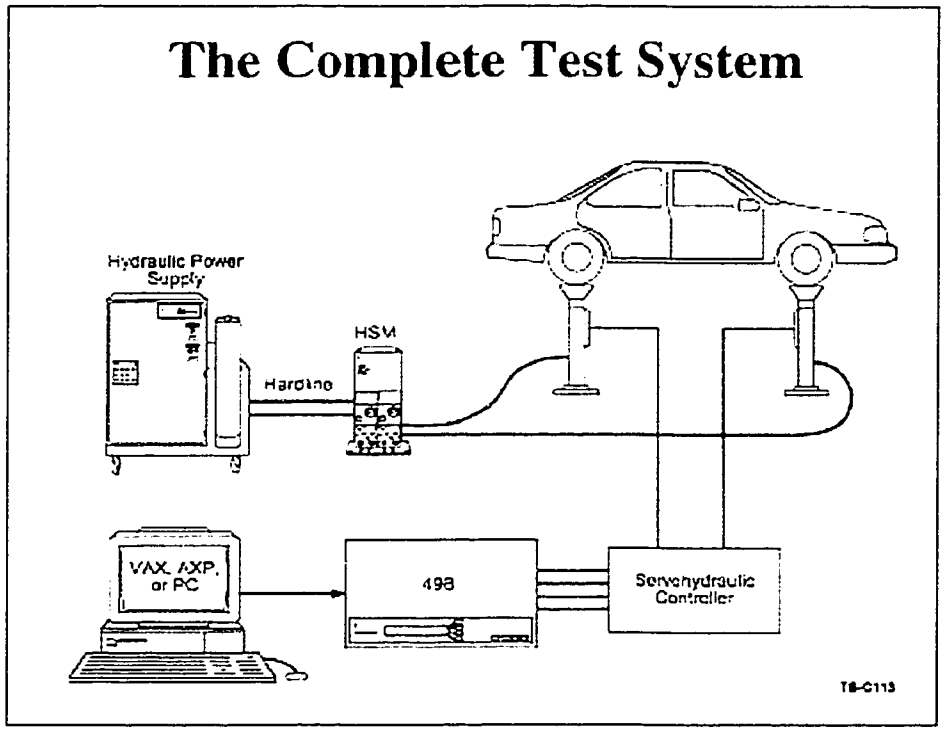

Figure 6. The complete test system includes test specimen, controllers, computer and RPC, mechanical fixtures, actuators and transducers [13].

The FRF is obtained experimentally by sending a random shaped "white noise" signal through the RPC computer system into the servo-hydraulic controllers of the test system,

while recording the outputs of the remote transducers. The FRF is then inverted and prepared for the next step of initial drive estimation, which will be explained below.

The goal of the fourth step is to estimate an initial input drive signal to reproduce the vehicle's in-service data. This data file is known as a drive file, and it is a time history file created in RPC. The drive file is used as a command signal to the rig's servo-hydraulic controllers. On a road simulator such as a 4-poster, the command signal is the displacement needed in the actuator, and the servo-hydraulic controller ensures that the piston moves to the correct position. The MTS Model 329 spindle coupled simulator uses mechanical fixtures to apply loads realistically and to act as an interface between the actuator and the specimen [12].

The whole process of creating the drive file involves a process of "convolution", which is a technique that takes a time varying signal (the desired response from Step 2), and "plays it through" the FRF mathematically. The result of this procedure is a drive (input) signal. Since the FRF is only a linear approximation of the system, a set of iterations is required [12].

Step five is an iteration process, where the error between the achieved response drives (resulting from the input signal) and the original desired response is calculated. The resulting error signal is convolved with the inverted FRF to create a drive correction, which is added to the last drive signal. The step is repeated until desired criteria, set by the testing company, are achieved. Among different tools used for analyzing convergence of iterations most common is the RMS of error signal. It is used to predict the difference between desired and achieved responses. If the iterations are converging, the RMS signal becomes smaller and smaller. Other methods of convergence testing include overlaying plots of desired and achieved responses, fatigue life calculations and among others calculating the auto-spectral density of the error to show the problem frequencies [12].

The last step in the RPC technique is performing durability testing and lab data acquisition. The final drive files are combined into durability test sequences based on the type of test required. Different road surfaces may be repeated a desired number of times and the overall sequence is referred to as a "pass". The durability cycle may then contain multiple passes, as set by the test standard [12].

2.2.4 Advantages and Disadvantages of Laboratory Simulation

Current advances in testing technology allow for full vehicle simulation to be used in multiple applications ranging from motorcycles to large agricultural and industrial equipment. Certain advantages have resulted in this technique becoming a growing trend in the automotive industry. These include:

- simulation tests can be conducted in about one fourth of the time required for road testing,
- more controlled and repeatable testing environment,
- ability to conveniently measure dynamic operating data for specific vehicle systems,
- decrease in cost-per-test basis compared to proving ground testing.

Laboratory simulation does however exhibit some shortcomings, which are continuously being addressed. These will be discussed below.

Due to limited number of control channels available with the use of a simulator, vehicle's operational dynamics are difficult to reproduce. Variability in drivers, climate, road and conditions, makes it difficult to create a true customer representative test. This poses the question of whether the automation of vehicle testing truly represents customer cycling. Component orientation can also influence the results of the durability cycle. The

boundary conditions set in the laboratory environment, such as component and/or vehicle mounting points, may introduce new types of loads not seen in a vehicle in service.

Another disadvantage of laboratory simulation is the fact that the test scripts do not account for vehicle deterioration. This happens because the system does not use an iterative open loop process. That is, the FRF will not be updated if any dynamic changes to the system occur as the result of cracking or loose parts. This inability to control changes to inputs due to vehicle degradation may significantly change the simulator's servo-hydraulic closed-loop performance.

A significant cost encountered in laboratory testing results from vehicle re-design or modifications. Simulation control parameters are specimen dependent, thus vehicle design modifications may affect the test system dynamics. This means that new data may be required and a new test performed if the vehicle dynamics have been significantly altered.

Physical limitations of the testing equipment itself affect the integrity of the simulation. System response is a function of the stiffness, damping and inertia of the system. Limitations of the testing machine such as lack of steer-control, replacement of tire and wheel with attachment fixtures, or lack of tire to road contact will influence the above-mentioned factors. If possible, overcoming these limitations would add to the complexity of the testing machines, as well as increase the research and purchase cost.

Continuous improvements and further acceleration methods are constantly being developed in the laboratory simulations. Fatigue sensitive editing techniques are now implemented that allow the non-damaging portions of the test schedule to be removed from the test cycle [8]. This cuts on both duration and expense of the testing. Other methods such as Extreme Value Analysis Techniques developed by Gumbel [14] provide ways of estimating long term high service loads from the loads measured in a shorter time interval. In addition, it allows engineers to estimate the minimum length of time for which a load history should be measured in a particular type of service environment.

Among many other breakthrough research studies in area of accelerating laboratory simulation is a development of Road Profile Control Method, a patented simulator control process developed for spindle coupled test rigs. [15]. Even though laboratory testing provides a quicker method of vehicle testing, its biggest obstacle is the fact that the process is specimen-dependent. New data must be acquired for each new vehicle to ensure the accuracy of the results. Since the simulator control is also a "closed loop" iterative process (see Section 2.2.3), in addition to being time consuming it also does not account for changes in test vehicle's parameters such as degradation. By incorporating a model of 'missing dynamics', such as tire models, an "effective" road profile can be predicted from collected vehicle spindle forces and accelerations. This profile is independent of a vehicle type, thus enabling data from one vehicle to be used to generate tests for other test vehicles [15]. The difference between the traditional and "effective road profile" simulator control methods is demonstrated in Figures 7 and 8.

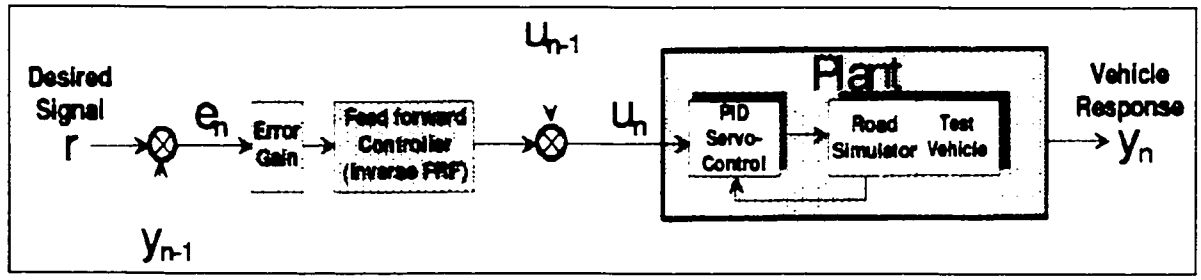

Figure 7. Feedfoward system model used in vehicle simulators. The notation is as follows: r - desired signal (vehicle response) collected during data acquisition, u - estimated drive file, y - vehicle response from a road test simulator, e-error signal. This system model is vehicle-dependent; thus new vehicle responses have to be recollected with each design change or modification [15].

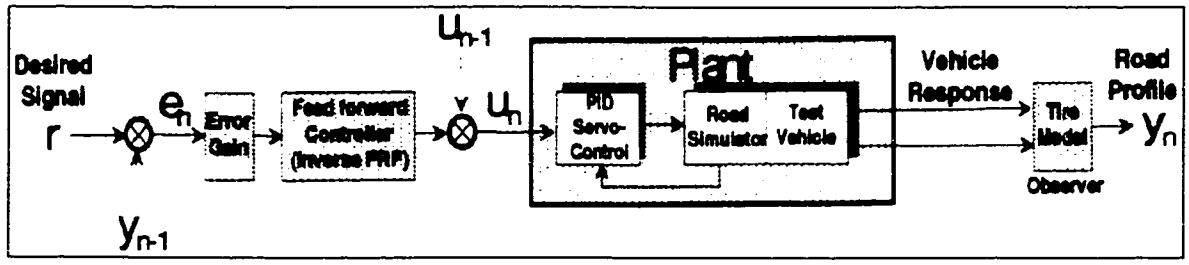

Figure 8. "Effective Road Profile Control" Feedfoward system model used in vehicle simulators. The notation is as follows: r - desired signal (vehicle response) collected during data acquisition, u - estimated drive file, y - estimated road profile, e - error signal. Vehicle responses used to estimate drive files in traditional simulator control, vary dramatically with vehicle configuration for a given road input. Used simultaneously with an accurate inverse tire model, the vehicle responses from different vehicles can be used to predict *same* road profile. This profile can then be used for subsequent vehicle tests [15].

As with any method of unconventional testing, constant improvements are a necessity. Even with the limitations posed by laboratory simulation however, test engineers are capable of reproducing actual service data typically, within 2% of load amplitudes, in only 25% of the time needed for track testing [3]. These results appeal to the automotive industry for the simple fact that the time and cost savings do not compromise the integrity of the durability test itself.

2.2.5 Mathematical Modeling

Recent advances in computer aided engineering (CAE) technology have led to utilization of computer modeling in durability testing. Finite element methods have been extensively applied to predict fatigue lives for various components. The capabilities of today's computers allow designers to create more realistic models, resulting in more accurate life predictions. There is still much research to be done to fully utilize the capabilities of computer technology. The limitation designers face while using mathematical modeling include:

- difficulty approximating the operational dynamics,

- dependency on accurate inputs such as constants, boundary conditions, and displacements,

- limitation of computer power to analyze the problem.

Even though the problems stated pose limitations on the accuracy of the results, the method of mathematical modeling proves to be very successful in early prototype designs and in determining the location of critical or "hot spots" on the vehicle's components. The benefit of quick analysis makes this method very attractive in the testing industry.

Overall, each of the three methods of vehicle testing: proving grounds, laboratory simulation and mathematical modeling serve an important purpose in the testing and evaluation of vehicles. An increased demand to shorten the time from "concept to manufacturing" puts pressure on vehicle manufacturers to accelerate their test time. Alternative methods of testing serve a vital purpose in reducing the time and cost of vehicle evaluation, although they may cause some critical failing conditions to be missed. These are vehicle aging, corrosion, weathering and soaking influences. The accelerated methods of vehicle testing are, by no means, a substitute for real vehicle testing, and should only be used in parallel to validate their results/failures.

3 PROVING GROUND UNDER INVESTIGATION

3.1 General Description

The investigated PG is used mainly for durability and development testing. The test facilities consist of a High-speed Oval, Straightaway, a Vehicles Dynamics Facility (VDF), Test Grades, Soak Sheds, Scales, Ride Road, Off-road Trails, Brake and Splash Wetting Trough, Federal and European Noise Pass-by Pad and a Material Exposure Farm. The climate is desert-like with high ambient temperatures and a great deal of dust. The following weather statistics/parameters are measured continuously: ambient temperature, test track temperature, barometric pressure and precipitation, percentage of relative humidity, rainfall, wind speed and directions at ground level (approximately 1.83 meters or 6 feet), and at tower level (9.14 meters or 30 feet).

The types of tests performed on the investigated PG include endurance tests, off-road sport utility vehicle (SUV) and truck tests, power train tests, trailer tow tests, European tests, electric vehicle tests, drag cycles, transfer case tests and axle tests.

3.2 Off-road SUV/Truck Tests

Off-road type tests are intended for all sport utility vehicles and trucks. The family of vehicles tested there covers a broad grouping of vehicles consisting of both 2-wheel drive and 4-wheel drive SUVs, pickup trucks, full size vans and cab/chassis trucks. The purpose of this type of tests is to obtain vehicle durability data on body, chassis and structural components.

The off-road type tests can be further classified based on their purpose. The investigated proving ground facility grouped their off-road tests into the following categories:

1. Full OR Durability test course for four-wheel drive light truck and utility vehicles.
2. OR Durability test course for an early off road structure evaluation of four-wheel drive light truck and utility vehicles.

3. Full OR Durability test course for two-wheel drive light truck and utility vehicles.

4. OR Durability test for early off-road structure evaluation of two-wheel drive light truck and van/utility vehicles.

3.2.1 OR Durability Test

All SUVs and light truck vehicles must be able to pass the entire OR durability test prior to going into production. However, during the early stages of a program, the interest is to primarily evaluate the development of vehicle structure. When this is the case, an abbreviated OR test is selected to run.

The studied OR test is a 24,000 km (15,000 mile) durability test conducted for sport utility and Truck platform vehicles. The course consists of ten roads - R1, R2, R3, R4, R5, R6, R7, R8, R9 and R10 – of varying characteristics. Table 1 outlines the road sections involved in off-road test cycles, in the order they are tested. It also lists the directions and corresponding road lengths. Two directions are listed, direction D1 and direction D2. No significant differences are observed in course severity relating to direction of the course. This is due to the random nature of the course, and the constant alternating of the traffic directions throughout the course

Direction D1			
Road Section	Direction	km	Miles
R9	South	0.65	0.4
R8	East	0.48	0.3
R7	North	3.39	2.1
R5	East	1.77	1.1
R3	West	3.06	1.9
R4	East	3.06	1.9
R10	East	0.16	0.1
R2	CW	1.77	1.1
R6	South	(0.96+1.77)	(0.6+1.1)
R1	CW	1.29	0.8
R6 South	South	1.13	0.7
R8	West	0.81	0.5
R9	North	0.65	0.4
Direction D2			
Road Section	Direction	km	Miles
R9	South	0.65	0.4
R8	East	0.81	0.5
R6 South	North	1.13	0.7
R1	CCW	1.29	0.8
R6	North	(0.96+1.77)	(1.1+0.6)
R2	CCW	1.77	1.1
R10	West	0.16	0.1
R4	West	3.06	1.9
R3	East	3.06	1.9
R5	West	1.77	1.1
R7	South	3.39	2.1
R8	West	0.48	0.3
R9	North	0.65	0.4

Table 1. Road Sections included in the Off-road Test Cycles. List of the OR test routes appears in order they are tested, together with corresponding directions and road lengths, given for both D1 and D2 directions of the course.

Road Data is acquired by running the vehicle in two directions D1 and D2, as shown in Table 1. Multiple ballast load schedules are collected (number depends on the vehicle tested and on the purpose of the test). Each ballast condition is acquired at least twice in each direction.

An off-road durability cycle takes at least 150-eight-hour shifts (1200 h) to complete. Depending on the number of authorized shifts per week this implies anywhere from 16 to 22 weeks. Considerations affecting test time include driver availability, vehicle

breakage, normal servicing (every 1600 km or 1000 miles), vehicle prep time (4-5 shifts), and final inspection time. According to the OR test schedule, the 24,000 km (15,000 miles) off road test is, on average, equivalent to 1094 laps in laboratory simulation. This is shown below:

$$\frac{24{,}140km[15{,}000miles]}{155km/shift[96miles/shift]} * 7[laps/shift] = 1094[laps]$$

It should be noted that one lap is considered to be a collection of all road segments in one of the directions. Therefore, the laboratory test would include 547 laps in direction D1 and 547 laps in direction D2. This could be further divided by number of ballast conditions and number of road segments to determine the amount of time each road has to be repeated during laboratory durability cycle. For example, if 3 ballast conditions are used and 13 road segments are included in each direction (as shown in Table 1), then each road section must be repeated about 14 times for each ballast condition. These numbers may once again vary depending on a test.

3.2.2 OR Durability Test Road Descriptions

Topologically, the investigated Proving Ground is located on alluvial material (unconsolidated gravel, sand, silt and clay deposited by streams). The terrain is flat, with limited natural long grades. The unpaved off-highway ("off-road") route of the studied OR test covers three types of road surfaces. These are:

- Graded gravel – a graded gravel road surface with varying degrees of washboard, typical on a non-paved "county" road surface, totaling about 1450 km (900 miles) (6% of the off-highway mileage), with average speed of 60 km/h (38 m.p.h.),

- Dry washes – dry "arroyos" (washes or dry desert gully) consisting of wash gravel and sand, with longitudinal "ruts" worn into the surface by wheel traffic. Typical depth of the gravel/sand mixture is 0.2-0.25 meters (8-10 inches). Totaling 10,645

km (6600 miles), (44% of the unpaved off-highway mileage), with average speed of 30 km/h (19 m.p.h.).

- Off-road trails – consisting of packed clay surfaces, with varying sizes of randomly spaced embedded rocks, and longitudinal wheel ruts which traverse the natural desert terrain, and are randomly crossed by naturally occurring dry washes, of widths varying between 1.5-15.2 meters (5-50 feet), and depths ranging from 0.3-3.0 meters (1-10 feet). Mileage totaling 12,000 km (7500 miles) (50% of the off-highway mileage), with average speed of approximately 24 km/h (15 m.p.h.).

Historically, the visited PG consists of two types of washboard inputs. Washboarding is a series of high and low spots formed in a wavelike pattern. The two types of washboards present at PG are:

- 0.8 to 0.9 meter (2.5 to 3.0 feet) wavelength washboards (8-10 Hz) – mostly on roads that cross the washes (R4, R3, and R5),

- 0.5 meter (1.5 foot) wavelength (16-20 Hz) – mostly on roads that run with the washes (R1, R6, R7)

The courses run either with or across these washes, thus creating two different types of roughness inputs. Generally speaking, the roads that cross the washes cause high amplitude wheel displacements and thus can be considered "stress-risers" for components. In comparison, the shorter amplitude and wavelength roads (the roads that run with the washes, which are typically heavily washboarded roads), cause stress and cracks initiated by high loads (from roads crossing the washes), to grow or propagate rapidly [18].

The test courses are dynamic by nature and are known to change characteristics based on usage, due to their deformable soil conditions. The conditions of the roads are also

affected by weather, traffic type and density, tire hardness, vehicle accelerations, decelerations, turning and speed, as well as frequency of maintenance.

Each road segment, included in the OR test, is comprised of several different road surfaces. Essentially, all of the PG's off-road trails were selected because of their random input nature. However, each was also selected for inclusion into the final test cycle, because of its specific and somewhat unique characteristics. An overview of the dominant features of each road is given with the following paragraphs [18]:

Road R1 is comprised of an eroded "arroyo", through a bed of caliche (reddish-brown to white layer found in many desert soils) clay, which has dried, hardening into deep ruts and voids. This creates large amplitude wheel displacements and torsional load inputs. The north section of the road consists primarily of low frequency high amplitude events, whereas the southern section comprises of lower amplitudes at higher frequencies. This sand-washed based course is run in direction "with the washes", at about 24 km/h (15 m.p.h.).

R2 Pit Trail is a blending of washboarding (0.5 meter/1.5-ft wavelength at 16-20 Hz at an average OR speed of 30 km/h or 18.3 m.p.h.), superimposed over longer wavelength surfaces. This is coupled with areas of severe rutting (which produces lateral wheel loading), and some "off-camber" side slopes (which also produce lateral forces). The R2 Pit trail was constructed by simply blading a path through a gravel "R2 pit", which was used to supply the gravel necessary to construct the paved test surfaces of the PG. R2 Pit was primarily to serve as a high frequency, low amplitude course coupled with high amplitude crossings.

R3, R4, and R5 trails are areas of natural desert terrain (primarily caliche clay road base, with sporadic embedded rocks similar to those found on R9 Road, and "pot-holes" in areas where the base material is not bound together by clay). These trails are laid out to cross the wash streambeds, providing large amplitude excursions through the dips/depressions, caused by driving across a "ditch-like" surface. Only the bottoms of

those depressions have any sand in them, and the width of these washes crossed is rarely more than a few feet. The courses are mainly used to create high wheel movements due to the high amplitude inputs, however over the years short stretches of these roads developed low amplitude, high frequency events.

R9 Road is a specially constructed test surface comprised of "river-run" rock (which has been smoothed by water erosion in a stream base). Rock sizing varies between 30 cm and 61 cm (12-24 inches) diameter, buried into a compacted road bed with approximately 5-15 cm (2-6 inches) of exposed surfaces, with nearly no void spacing between protruding rocks. This is intended to provide low speed, and high amplitude in vertical, lateral and longitudinal loads.

R7 Wash and R6 Wash are primarily sand based road surfaces (R7 more than R6). This allows a quick development and maintenance of consistent level of washboarding, which produces the higher frequency, low amplitude inputs. R7 and R6 road share similar characteristics, but differ in sand material size and depth.

R7 Wash sand is a finer grain size, and is much deeper, which allows for a larger amount of μ-slip displacement of the material (When a rolling pneumatic tire is subjected to lateral force, the tire will drift to the side. This tire slip will cause the displacement of the grainy surface.) causing much larger amplitude washboards, and higher rolling resistance. Typical washboard amplitudes of 13-15 cm (5-6 inches) or more are common in R7 Wash. In addition to the high frequency, low amplitude inputs, some large wheel excursions, torsional load inputs as well as breaking/accelerating events are also present.

R6 Wash sand material is sparser, with much of the wash bed tending towards small gravel in grain size. It is then overlaid on a hard-packed caliche clay surface. Thus the washboard in R6 Wash is rarely more than 8-10 cm (3-4 inches) in amplitude. R6 Wash consists mainly of high frequency low amplitude road inputs.

R10 Road is a discrete event constructed to provide torsional inputs, and high amplitude wheel movement.

R8 Road is a paved surface that must be transversed to access other test surfaces. If in good condition, it adds no input of any value to structural durability test.

As mentioned at the beginning of this section, the characteristics depicted in descriptions of each road are dominant for that road. They are, however, not homogenous throughout the whole road section.

The information on road conditions was obtained through correspondence with Steven E. Schlueter, who is a Duty Cycle Specialist at the DaimlerChrysler Arizona Proving Grounds [18].

3.3 PG Off-Road Test Course Roughness Comparison

Road roughness studies for off-road courses on PG are conducted on a yearly basis. The main objectives of those studies are to compare the profiles of the off-road courses over years for any changes, to calculate their road roughness severity, and to make recommendations on how to sustain stability of the courses.

The intention of this study is to group roads of similar characteristics based on vehicle responses, which are vehicle dependent measurements. Before this is done, it is beneficial to perform a comparison of the vehicle-independent measurements, to see whether the different courses included in the OR test share some similar road inputs. For that purpose a copy of report titled "Arizona Proving Ground Off-Road Test Course Roughness Comparison – Comparative Road Profile Analysis" was obtained [17].

The road profiling of the OR course was conducted by Nevada Automotive Test Center with the use of Dynamic Force Measurement Vehicle (DFMV). DFMV was especially designed for the use in off-road conditions, which exhibit a very dynamic behavior. The

comparison of profiles from the off-road courses was based on both vehicle and speed independent measurements of road roughness. The road roughness elevation profiles were presented in form a plot of spectral density versus wave number. The study concentrated on wave numbers between 0.033 to 3.3 cycles per meter (0.01 to 1 cycle per foot), which at average OR speeds of 29.5 km/h (18.3 m.p.h.) represent input frequencies between 0.3 to 27 Hz.

Road profiling data for all OR roads for December of 1995 is shown in Figure 9 [17]. Additional road profiling data can be obtained from the report [17].

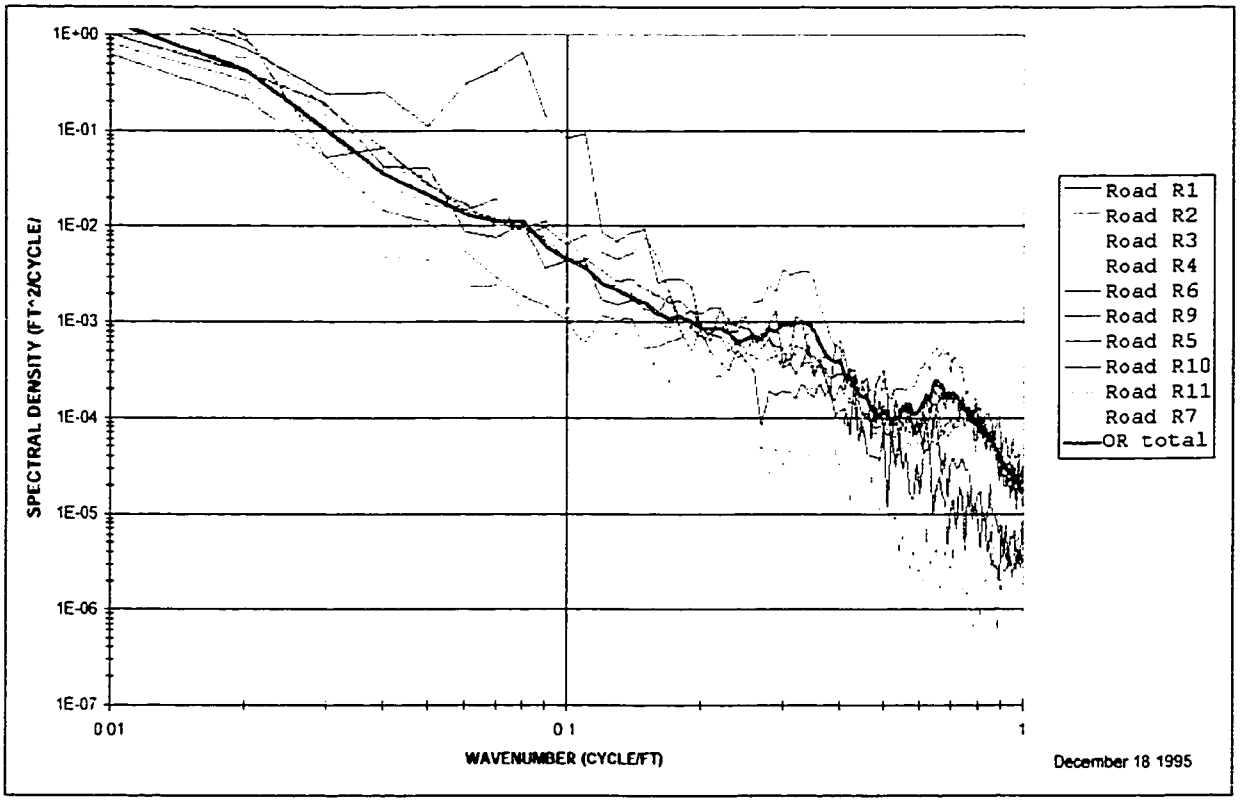

Figure 9. OR Test - Offroad road profiles for December 1995. The vehicle and speed independent measurements of road profiles are presented in form of wavenumber (cycle/foot) vs. spectral density (ft^2/cycle) [17].

It can be observed from Figure 9, that the most distinctive road sections in the OR test are R10 Road (navy) and R11 Road (blue). Their spectral density plots (relate distribution of energy with respect to frequency) differ from the other road sections for all

wavenumbers. The R11 Road however is a fairly new road, and it has not been included in any of the OR tests conducted by the RTS department. The other distinguishing road is R9 Road (brown) especially in the wavenumber range of 1.64 to 3.28 cycles/meter (0.5 to 1 cycles/foot). In addition, R6 Wash (dark magenta) and R7 Wash (light blue) show similarities amongst one another, as well as their uniqueness from the remaining road sections.

Therefore based on the provided road profiling data and in agreement with the road descriptions of Section 3.2.2, there is a possibility of combining roads into the following groups:

- R10 Road
- R9 Road
- R8 Road – not shown on the road profile graph, due to its minimal to no input in durability cycle
- R6 and R7 Roads
- R1, R2, R3, R4, and R5, especially the last three as mentioned in Section 3.2.2.

A detailed analysis of a collection of vehicle responses from different OR tests conducted over last few years will be performed, to further justify these road groupings.

4 TEST DESCRIPTIONS

An extensive study classifying the characteristics of various vehicle responses collected from OR test on the Proving Grounds was conducted, and five sets of data were analyzed. They were project #P1 under full rated load, project #P2 under half payload and two-passenger payload, and project #P3 under full and two-passenger rated loads. All five data sets contained sixteen channels of information obtained from transducers located on the instrumented vehicle. The three projects will be discussed in more detail below.

4.1 Project #P1

The feasibility study of road substitution for OR off-road test on the Proving Grounds (PG) was carried out initially on the results of September 1997 project #P1, conducted by a road test simulation group.

The purpose of the P1 test was to develop drive files for the 1999 model vehicle V1. The drive files were to simulate the 24,000 km (15,000-mile) off-road Proving Ground OR test cycle, on an MTS model 329 spindle coupled road simulator. These drive files were used to perform durability tests and collect body strain information for stress analysis. For the purpose of better understanding the analysis of the study, a brief summary of the project #P1 is included below [19].

4.1.1 Project #P1 Test Procedure

The test configuration was as follows:

Test request no.: Project #P1

Test vehicle description: 1999 110-week mule (vehicle V1)

Engine/power train: 4.0L I-6 / Auto

Accelerometers, strain gauges and string potentiometers were installed on the test vehicle at locations suitable for road simulation and fatigue damage analysis (see Appendix I). The vehicle was driven on off-road test tracks at the Proving Ground to acquire road data.

The test vehicle was shipped back to the Road Test Simulator Laboratory and mounted on the multi-axis test rig. Road data was edited in the lab to reduce the actual test time. Drive files were developed to replicate transducer responses acquired from the proving grounds using an RPC iterative process. Fatigue analysis (using RPC software) was performed to correlate the simulation in the lab and the actual test at PG. A test schedule, which would provide equivalent fatigue damage, was generated.

4.1.2 Instrumentation

Test vehicle instrumentation included 39 transducer channels suitable for road simulation. Sixteen of these 39 channels were eventually selected for drive file development according to the iteration convergence criteria set by the RTS department. These sixteen channels are listed in Table 2.

Channel No.	Tag	Unit	Tag Description
13	LFVA	g	Left front vertical acceleration
14	RFVA	g	Right front vertical acceleration
15	LRVA	g	Left rear vertical acceleration
16	RRVA	g	Right rear vertical acceleration
23	LFCS	ue	Left front coil spring
24	RFCS	ue	Right front coil spring
25	LRCS	ue	Left rear coil spring
26	RRCS	ue	Right rear coil spring
34	LRTAS	ue	Left rear trailing arm support
35	RRTAS	ue	Right rear trailing arm support
36	LRLtB	ue	Left rear lateral bending
38	RRLtB	ue	Right rear lateral bending
44	LFLtBo	ue	Left front lateral outer bending
45	RFLtBo	ue	Right front lateral outer bending
46	LFLgBo	ue	Left front longitudinal outer bending
47	RFLgBo	ue	Right front longitudinal outer bending

Table 2. Description of analyzed channels from project #P1. These sixteen channels were selected, from the 39 channels available, to perform a detailed analysis of vehicle responses from different road conditions included in the OR test. Note, g = acceleration and ue = microstrain.

The criteria, set by the RTS group, and used in selection of channels suitable for iterations are as follow:

- in the time domain:

  The RMS of the error between desired and achieved responses should be less than 2% of the absolute maximum value of the desired response, for each channel within the control band.

$$\frac{rms_{error}}{\max\left|\left(\max_{desired}, \min_{desired}\right)\right|} < 2\%$$

  The absolute maximum error between desired and achieved responses should be less than 10% of the absolute maximum of the desired response, for each channel within the control band.

$$\frac{\max_{error}}{\max\left|\left(\max_{desired}, \min_{desired}\right)\right|} < 10\%$$

- and for the frequency domain:

  The frequency-domain criterion is based on the transfer function between the achieved and desired responses. The transfer function, *TRN*, is computed from the ratio of the cross-spectral density function between the achieved and desired responses, $CSD_{achieved,desired}$, and the auto-spectral density function of the desired response, $ASD_{desired,desired}$. Information on how to obtain TRN, CSD and ASD is available in Appendix II.

  For each channel, the transfer function (TRN) must lie between 0.95 and 1.05 for all values within the control band. Mathematically, the latter can be written as:

$$\left| 1 - TRN\left(\frac{CSD_{achieved,desired}}{ASD_{desired,desired}}\right)\right| < 10\%$$

An additional 55 channels of accelerometers for the cooling module and rosette strain gauges were installed on various parts of the vehicle body for stress analysis correlation. One additional channel was used to register the voltage of a battery-powered switch for the driver to signal the beginning and end of each road section. The location and description of each transducer/channel is summarized in Appendix I.

4.1.3 Data Acquisition

Data acquisition occurred at the PG from December 3 to December 11, 1996. The sampling rate for the 6510DC Megadac data acquisition unit was 409.6 Hz, with an anti-aliasing filter of 163.84 Hz.

Three ballast load schedules shown in Table 3 were used with corner weights as determined by the assigned engineering group.

Ballast Weight Configuration	Front Axle Wt. kg (lbs.)	Rear Axle Wt. kg (lbs.)	Total Wt. Kg (lbs.)
Base vehicle + 2 passengers	1112 (2452)	928 (2046)	2040 (4498)
Base vehicle + 3 passengers + ½ cargo	1112 (2451)	1087 (2397)	2199 (4848)
Base vehicle + 5 passengers + full cargo	1123 (2475)	1303 (2873)	2426 (5348)

Table 3. Ballast Weight Configurations for project P1 used in the OR durability schedule. Only the full rated condition was utilized for the analysis in the present project.

Road Data was acquired in both directions (D1 and D2). Direction D1 runs were collected during the first week, while direction D2 runs were obtained the following week after cross-member and fuel tank changes. Due to significant ground clearance problems experienced during acquisition in direction D1, data from direction D2 was used for simulation. For each ballast weight configuration data was acquired at least twice in each direction.

In the present study only the full rated load condition data was used.

4.2 Project #P2

The feasibility study of road substitution for the OR off-road test on the Proving Grounds (PG) was verified with the results of July 1996 project #P2, conducted by the Product & Development Engineering Department.

The purpose of the P2 test was to evaluate the body structural improvements of a 1997 model vehicle, referred to as V2, by running a 12-channel simulation of the 24,000 km (15,000-mile) PG OR durability test cycle. A brief summary of the P2 test is included below [20].

4.2.1 Project #P2 Test Procedure

The test configuration was as follow:

Test request no.: Project #P2

Test vehicle description: 1994 model vehicle with 1997 hardware (vehicle V2)

Engine/power train: 4.0L I-6 / Auto

Accelerometers, strain gauges and string potentiometers were installed on the test vehicle at locations suitable for road simulation and fatigue damage analysis. The vehicle was driven on off-road test tracks at the Proving Ground to acquire road data. Upon arrival at the Road Test Simulator Laboratory in Windsor, drive files were developed and durability testing was performed.

4.2.2 Instrumentation

Test vehicle instrumentation included 35 transducer channels suitable for road simulation. Sixteen of these 35 channels were eventually selected for drive file development according to the iteration convergence criteria set by the RTS department as documented in Section 4.3. The description of the sixteen channels is listed in Table 4.

Channel No.	Tag	Unit	Tag Description
1	LFvertAc	g	Left front vertical acceleration
2	LRvertAc	g	Left rear vertical acceleration
3	RFvertAc	g	Right front vertical acceleration
4	RRvertAc	g	Right rear vertical acceleration
5	LFLnAxBd	ue	Left front longitudinal axle bending
6	LRLnAxBd	ue	Left rear longitudinal axle bending
7	RFLnAxBd	ue	Right front longitudinal axle bending
8	RRLnAxBd	ue	Right rear longitudinal axle bending
9	LFLtAxBd	ue	Left front lateral axle bending
10	LRLtAxBd	ue	Left rear lateral axle bending
11	RFLtAxBd	ue	Right front lateral axle bending
14	LRStrPot	cm	Left rear vertical string pot
16	RRStrPot	cm	Right rear vertical string pot
28	RRLatAcc	g	Right rear lateral acceleration
29	LFCoil	ue	Left front coil spring torsional
32	RFCoil	ue	Right front coil spring torsional

Table 4. Description of analyzed channels in P2 test. These sixteen channels were selected from the 35 channels available, to perform a detailed analysis of vehicle responses from different road conditions included in the OR test. Note, g = acceleration and ue = microstrain.

4.2.3 Data Acquisition

Data acquisition occurred at PG over a seven-day period from July 8th to 14th in 1996. The sampling rate for the 6510DC Megadac data acquisition unit was 409.6 Hz, with an anti-aliasing filter of 163.84 Hz.

Three ballast load schedules shown in Table 5 were used and they were replicated in the RTS lab.

Ballast Weight Configuration	Front Axle Wt. kg (lbs.)	Rear Axle Wt. kg (lbs.)	Total Wt. Kg (lbs.)
Base vehicle + 2 passengers	972 (2143)	793 (1749)	1765 (3892)
Base vehicle + half payload configuration	995 (2193)	947 (2087)	1941 (4280)
Base vehicle + full payload configuration	977 (2155)	1152 (2540)	2130 (4695)

Table 5. Ballast Weight Configurations for P2 Test used in the OR durability schedule. Both 2-passenger and half-rated load conditions were utilized for the analysis in this project.

Road Data was acquired in both directions (D1 and D2). A run of the entire OR test loop took about 50 minutes for one direction.

In the present study both 2-passenger and half payload conditions were used.

4.3 Project #P3

The feasibility study of road substitution for the off-road (OR) test on the Proving Grounds (PG) was further verified with the results of October 1999 project #P3.

The purpose of the P3 project was to develop drive files for a 2002 model vehicle referred to as vehicle V3, in a 115-week mule stage, to simulate an OR PG durability test on an MTS 329 road test simulator. A brief summary of project #P3 is included below [21].

4.3.1 Project #P3 Test Procedure

The test configuration was as follow:

Test request no.: Project #P3

Test vehicle description: 2002 model vehicle V3

Accelerometers, strain gauges and string potentiometers were installed on the test vehicle at locations suitable for road simulation and fatigue damage analysis. The vehicle was driven on the off-road test tracks at the Proving Ground to acquire road data.

4.3.2 Instrumentation

Test vehicle instrumentation included 47 transducer channels suitable for road simulation. Sixteen of these 47 channels were eventually selected for drive file development according to the iteration convergence criteria. The description of the sixteen channels is listed in Table 6.

Channel No.	Tag	Unit	Tag Description
1	LFKnZa01	g	Left Front Knuckle Vertical Acceleration
2	LRAxZa02	g	Left Rear Outboard Axle Tube Vertical Acceleration
3	RFKnZa03	g	Right Front Knuckle Vertical Acceleration
4	RRAxZa04	g	Right Rear Outboard Axle Tube Vertical Acceleration
5	LFLBJX05	lb	Left Front Lower Ball Joint Longitudinal Load
6	LRSltX06	ue	Left Rear Axle Tube Outboard Longitudinal Bending (Slotted location)
7	RFLBJX07	lb	Right Front Lower Ball Joint Longitudinal Load
8	RRSltX08	ue	Right Rear Axle Tube Outboard Longitudinal Bending (Slotted Location)
9	LFLBJY09	lb	Left Front Lower Ball Joint Lateral Load
10	LRSltY10	ue	Left Rear Axle Tube Outboard Lateral Bending (Slotted Location)
11	RFLBJY11	lb	Right Front Lower Ball Joint Lateral Load
12	RRSltY12	ue	Right Rear Axle Tube Outboard Lateral Bending (Slotted Location)
36	LFSprD36	in	Left Front Coil Spring Axial Displacement
37	LRSprD37	in	Left Rear Coil Spring Axial Displacement
38	RFSprD38	in	Right Front Coil Spring Axial Displacement
39	RRSprD39	in	Right Rear Coil Spring Axial Displacement

Table 6. Description of analyzed channels in #P3 test. These sixteen channels were selected, from the 47 channels available, to perform a detailed analysis of vehicle responses from different road conditions included in the OR test. Note, g = acceleration and ue = microstrain.

4.3.3 Data Acquisition

Data acquisition occurred at the PG over a seven-day period from October 7th to 13th in 1999. The sampling rate for the 6510DC Megadac data acquisition unit was 409.6 Hz, with an anti-aliasing filter of 163.84 Hz.

Three ballast load schedules shown in Table 7 were used for replication in the lab setting.

Ballast Weight Configuration	Front Axle Wt. kg (lbs.)	Rear Axle Wt. kg (lbs.)	Total Wt. Kg (lbs.)
Base vehicle + 2 passengers	1073 (2366)	929 (2049)	2003 (4415)
Base vehicle + half payload configuration	1097 (2419)	1101 (2427)	2198 (4846)
Base vehicle + full payload configuration	1108 (2442)	1297 (2859)	2404 (5300)

Table 7. Ballast Weight Configurations for vehicle V3 in #P3 Test used in the OR durability schedule. Both 2-passenger and full-rated load conditions were utilized for the analysis in this project.

Road Data was acquired in both directions (D1 and D2). In the present study both 2 passenger and full payload configurations were used.

5 COMPARISON OF VEHICLE RESPONSES FROM TWO/DIFFERENT ROADS – METHOD OF ANALYSIS

The objective of this study was to establish a simple method of characterizing road surfaces based on the vehicle responses collected from these roads. The method would allow the grouping of these roads that induce similar behavior in the vehicle, thus simplifying the data analysis and drive file preparation for the durability cycle. As a result, a process of comparing vehicle responses from different road surfaces included in the PG OR test has been established based on the following criteria:

- time histories and statistical analysis,
- cyclic content based on "rainflow counted" histograms,
- probability density functions relating amplitude distributions,
- power spectral density,
- fatigue analysis.

A closer look at this approach will be demonstrated below, based on a comparison of two roads (R1 and R3 Roads) using data from test #P1 under full rated load. This will lead to the next section (Section 6), which will report on the result of the full analysis of all the roads included in the OR test.

5.1 Strategy

Two roads were selected to demonstrate the procedure of classifying road surfaces of similar nature based on vehicle response characteristics. They are R1 Road and R3 Road. The methodology will be presented on the P1 project test data, collected under full rated load. Sixteen channels of data used in this analysis are listed in Table 2. The channels

selected were channels used for drive file development in the project #P1 for the MTS Model 329 spindle coupled simulator. Their location is also indicated on the diagram provided in Appendix I.

5.2 Tools Used

The full study was conducted with the use of nSoft software produced by nCode International Ltd., a company specializing in the fields of fatigue analysis, data manipulation and analysis. A variety of tools such as the correlation package, fatigue analyzer, and other analysis tools were used successfully in comparing vehicle responses from the studied roads. The results are presented in Sections 5.3 to 5.10.

5.3 Data Analysis

All of the results presented below were conducted on data collected from the R1 and R3 Roads for project #P1, under full ballast condition. The data used in this analysis is unfiltered (raw). The decision to use raw data was made after inspecting the time histories for any offsets, drifts and other abnormalities. If any of the data had exhibited the mentioned characteristics, high pass filtering techniques would have been applied, (as was necessary in project #P2 with 2-passenger payload or project #P3 under full passenger load). The decision to use raw data was also investigated with the project #P1 data, to study the effect of filtering on the fatigue damage calculations. The results of this investigation will be reported in section 5.6.5.

5.3.1 Time Histories and Statistical Comparison

Initial data analysis was conducted through a visual inspection of raw data time histories collected from two roads: R1 and R3 at full rated load. It appears that although the range (max to min) of responses experienced by a vehicle due to each road is very similar, the vehicle experiences more severe responses throughout the time when driven over R3

Road. This is demonstrated in Figure 10 which plots time histories of R1 Road and R3 Road respectively, for one of the channels (Channel 25 – Left rear coil spring strain channel).

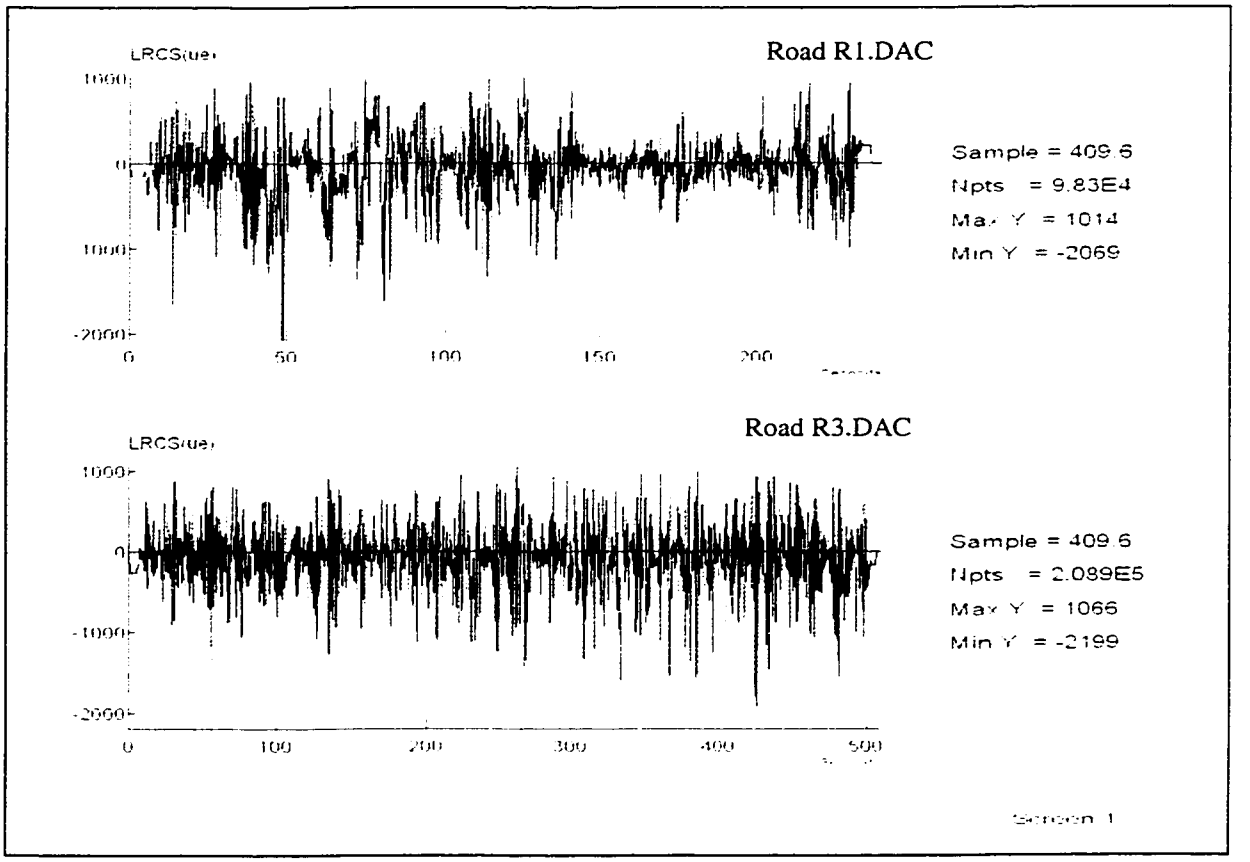

Figure 10. Time histories of left rear coil spring strain channel collected at the PG's R1 and R3 Roads during project #P1 at full rated load. The time histories exhibit the same range of amplitudes, but differ in time duration.

The fact that R3 Road shows a larger amount of damaging (high amplitude) cycles than R1 Road could be attributed simply to the fact that the duration of R3 Road is much longer than that of R1 Road.

Next, a comparison was made through statistical analyses of both roads for all sixteen channels of data, to assess whether there are similarities in vehicle responses for the two roads. A summary of the results is shown in Table 8, illustrating percent differences in

maximum (max), minimum (min), root-mean-square (RMS), and standard deviation values between the analyzed roads.

% Difference between R1 and R3 Roads				
Channel #	%Δ Max	%Δ Min	%Δ RMS	%Δ S. D.
13	5.23	24.22	2.00	2.00
14	6.19	1.47	9.73	9.75
15	18.64	9.68	8.38	8.38
16	27.06	28.83	14.28	14.31
23	3.75	3.69	7.62	0.32
24	16.32	9.24	1.58	1.02
25	5.15	6.32	2.53	0.49
26	8.79	11.65	11.90	12.94
34	11.23	27.47	32.46	25.65
35	16.66	3.96	31.87	24.31
36	9.76	4.01	2.01	2.06
38	6.70	54.26	4.60	5.96
44	63.72	4.50	18.98	20.47
45	11.18	14.07	16.35	18.19
46	25.00	17.40	15.84	12.60
47	2.50	34.82	2.98	5.01
Avg	14.87	15.98	11.45	10.22
Note: R1 Road was used as a reference Note: Analysis was performed on raw data				

% Difference between R3 and R1 Roads				
Channel #	%Δ Max	%Δ Min	%Δ RMS	%Δ S. D.
13	5.52	31.96	2.04	2.04
14	5.82	1.45	10.78	10.80
15	22.90	10.71	9.15	9.15
16	37.11	40.51	16.66	16.70
23	3.61	3.56	8.25	0.32
24	14.03	8.46	1.56	1.01
25	4.90	5.94	2.47	0.48
26	8.08	10.44	13.51	14.86
34	10.10	21.55	24.50	20.41
35	19.99	4.12	24.17	19.56
36	8.89	4.18	2.05	2.11
38	6.28	35.17	4.83	6.33
44	38.92	4.71	23.42	25.74
45	10.05	12.34	19.55	22.24
46	20.00	14.82	13.67	11.19
47	2.44	25.82	2.90	4.77
Avg	13.67	14.74	11.22	10.48
Note: R3 Road was used as a reference Note: Analysis was performed on raw data				

Table 8. Summary of statistical analysis of R1 and R3 Road. The results are presented in form of percent differences between the maximum, minimum, RMS and standard deviation values, with both R1 and R3 used as a reference.

A sample calculation of percent difference in maximum value, between R1 and R3 roads, for channel 25 is shown in Figure 11.

Channel 25 - Maximum Values

Max. Value R1 Road = 1013.7 $\mu\varepsilon$

Max. Value R3 Road = 1065.9 $\mu\varepsilon$

$$\% \Delta = \frac{1065.9 - 1013.7}{1013.7} * 100\% = 5.15\%$$

Note: R1 Road was used arbitrarily as reference

Figure 11. Sample calculation of maximum value percent difference between R1 and R3 Road calculated for channel 25 (Left Front Coil Spring strain channel)

Average values in percent differences between statistical analyses of R1 Road and R3 Road, show variations of about 16% or less (See Table 8). Although some channels show much higher differences, for example Channel 44, a closer look at the time histories indicates that the error is based on isolated incidents (global minima and maxima). Overall, the time histories show a possibility of correlating the responses from the two roads. The errors do not seem to be *too significant* considering the randomness of the data and the repeatability in data acquisition on the same road. This randomness could be attributed to variability in drivers and driving maneuvers, changes in weather conditions and static inputs (road surface conditions), as well as to vehicle degradation.

5.3.2 Cyclic Content of the Time Histories

For years the fatigue behavior of materials was estimated through constant amplitude loading tests produced in laboratory environments. In-service data, however, rarely showed constant amplitude behavior [3]. The variable load histories presented a need to reduce complex histories to a number of constant amplitude events, and the method became known in engineering practice as a cycle counting. Many attempts have been made throughout the years to develop an efficient way of cycle counting. Some of these methods are level-crossing counting, peak counting, or simple-range counting.

The early methods of cycle counting presented, however, a few shortcomings, which resulted in inaccurate fatigue life predictions. The above-mentioned techniques made no considerations of the order of applied load cycles. Since the stress-strain relationship in a material is nonlinear due to the plasticity of a material, the order in which cycles are applied has an effect on the material's response to the loading. A material's fatigue life is highly affected by mean stresses. Inducing compressive mean stresses due to tensile overload could produce crack retardation, thus increasing the life of a component. On the other hand, tensile mean stresses could result in significant reduction of component's life. A need for more efficient way of cycle counting was needed [22].

The "rainflow counting" method was developed by Matsuishi and Endo in 1968 [23]. The objective of the method was to identify closed hysteresis loops in stress-strain response of a material subjected to cyclic loading. The term "rainflow" derived from analogy of "falling rain" on a pagoda roof, where cycles are defined in the manner by which rain drips from a roof [23]. Although modern practices of "rainflow counting" no longer apply that technique, the name still remains. There are many "rainflow" counting methods:

- range pair counting,
- "race track" counting,
- ordered overall range counting,
- range-pair-range counting.

The American Society for Testing and Materials (ASTM) developed a standard algorithm, which can be implemented in computer software (as done by nCode in their nSoft package). The algorithm can be found in reference [24]. A brief description of the rainflow concept will be discussed below for clarification.

A reversal of a signal is simply defined as a change in sign of the loading direction. In general, a random time history consists of a pair of reversals: from maximum to minimum, and minimum to maximum. These maximum reversals are in turn interrupted by other smaller range reversals found in the signal. In a stress-strain diagram, each complete reversal is called a hysteresis loop. The maximum reversals form the "fattest" hysteresis loop. The smaller range reversals form smaller hysteresis loops within the biggest hysteresis loop, while remembering the prior state of deformation. This phenomenon is referred to as "material memory" [25], and is demonstrated in Figure 12.

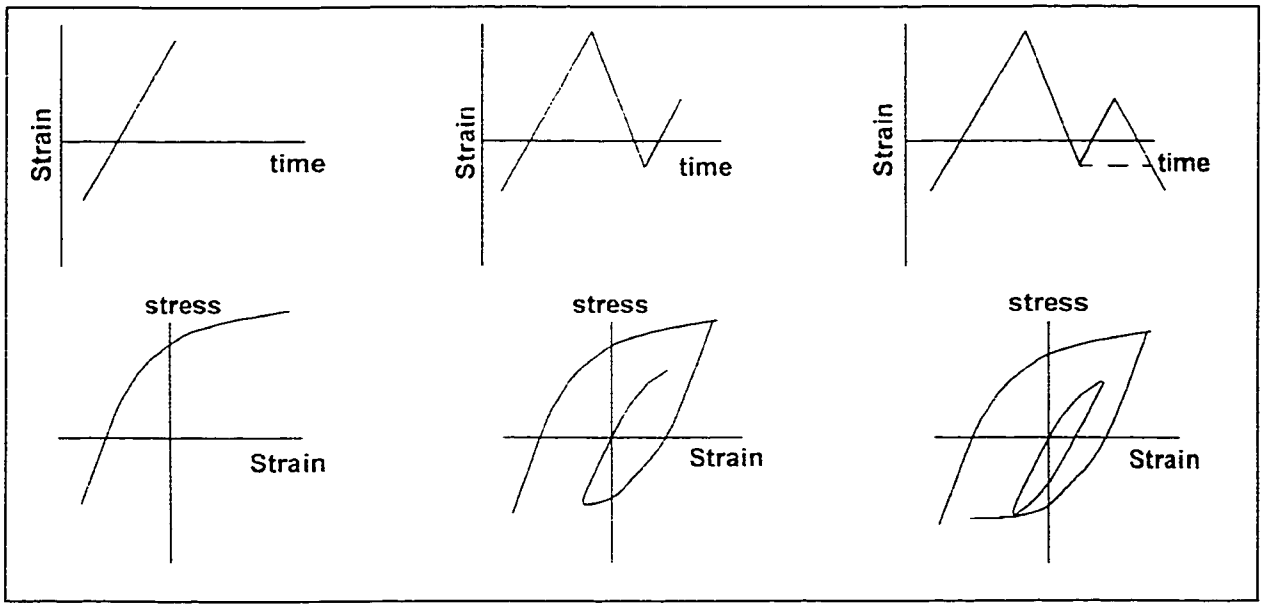

Figure 12. Material stress-strain response to a given strain history. In a random time series, a series of load reversals occur. The largest pair of reversals forms the "fattest" hysteresis loop on a strain-stress diagram. This hysteresis loop is in turn interrupted by smaller loops (smaller range reversals), in such fashion that the prior state of deformation is always remembered. This phenomenon is referred to as "material memory" [25]

Each closed hysteresis loop may be characterized in terms of strain range and mean strain. If the stress axis is ignored, the rainflow counting algorithm will extract cycles in terms of their range and mean value and store them in a range-mean matrix. The ASTM algorithm determines load cycles for closed hysteresis loops in a loading history in the steps listed below [23].

i. Arrange the history to start with either the maximum peak or the minimum valley. Let X denote range under consideration; and Y, previous range adjacent to X.

ii. Read the next peak or valley. If out of data, stop.

iii. If there are less than three points, go to step i. Form ranges X and Y using the three most recent peaks and valley that have not been discarded.

iv. Compare the absolute values of ranges X and Y.

   a) If $X<Y$, go to step i.
   b) If $X \geq Y$, go to step v.

v. Count range Y as one cycle; discard the peak and valley of Y; and go to step ii [23].

This algorithm will now be used in determining closed hysteresis loops for strain history given in Figure 13, to demonstrate the process.

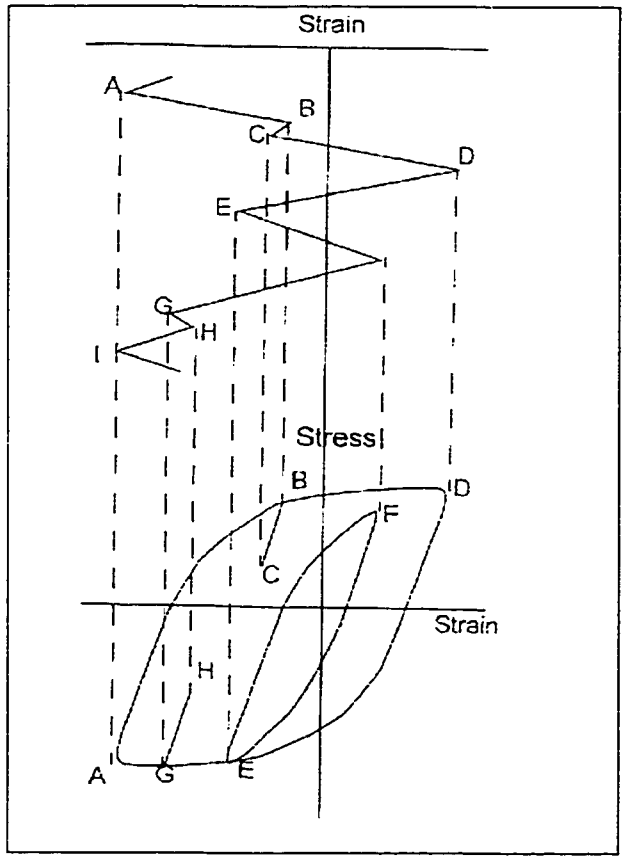

Figure 13. Rainflow counting (ASTM standard). The rainflow counting technique simplifies complicated time histories by counting load cycles for closed hysteresis loops in a loading history [25].

According to ASTM standard the rainflow technique for Figure 13 would be applied in a fashion listed below.

- Y = A-B; X = B-C; X<Y.
- Y = B-C; X = C-D; X>Y. Count B-C as one cycle and discard points B and C. Thus a cycle B-C-B is formed.

- Y = A-D; X = D-E; X<Y.
- Y = D-E; X = E-F; X<Y.
- Y = E-F; X = F-G; X>Y. Count E-F as one cycle and discard points E and F. Thus a cycle E-F-E is formed.
- Y = A-D; X = D-G; X<Y.
- Y = D-G; X = G-H ; X<Y.
- Y = G-H; X = H-I; X>Y. Count G-H as one cycle and discard points G and H. Thus a cycle G-H-G is formed.
- Y = A-D; X = D-I; X=Y. Count A-D as one cycle and discard points A and D. Thus a cycle A-D-A is formed.
- End of counting.

In summary, four hysteresis loops were identified for Figure 13. These were cycles B-C-B, E-F-E, G-H-G, and the outside loop A-D-A. Next, each of these loops can be identified in terms of their range and mean values, and counted in a matrix form. Let us arbitrarily assume the following range and mean values:

- cycle A-D-A; range = 5; mean = -1,
- cycle E-F-E; range = 4; mean = -1,
- cycle B-C-B; range = 1; mean = 2,
- cycle G-H-G; range = 1; mean = -2.

Then, the rainflow counted matrix would look as shown in Figure 14.

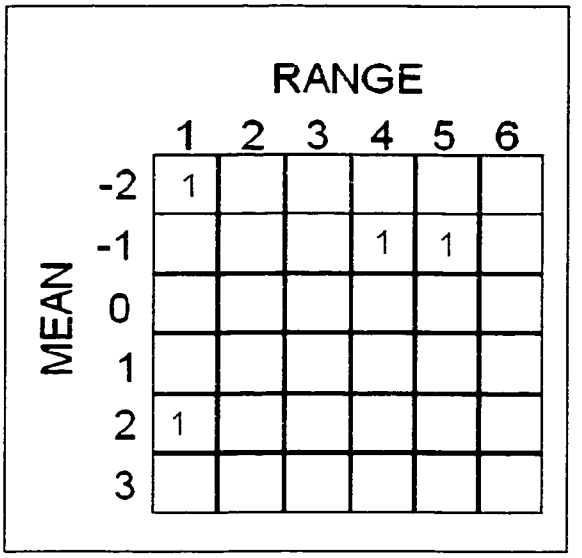

Figure 14. "Rainflow" counted matrix for time history shown in Figure 13, used as an example demonstrating the ASTM "rainflow" standard. After all the hysteresis loops are identified according to ASTM procedure, each loop is classified in terms of its range and mean value and counted in a matrix form.

Having a methodology of generating the cyclic responses of the vehicle, a comparison of "rainflow" counted time histories was performed between the sixteen channels of R1 and R3 Roads. All of the histograms were created to be the same size consisting of 64 bins (64X64 matrix). Two of the histograms for channel 25 (Left rear coil spring strain channel) are presented in Figures 15 and 16 for R1 Road and R3 Road respectively.

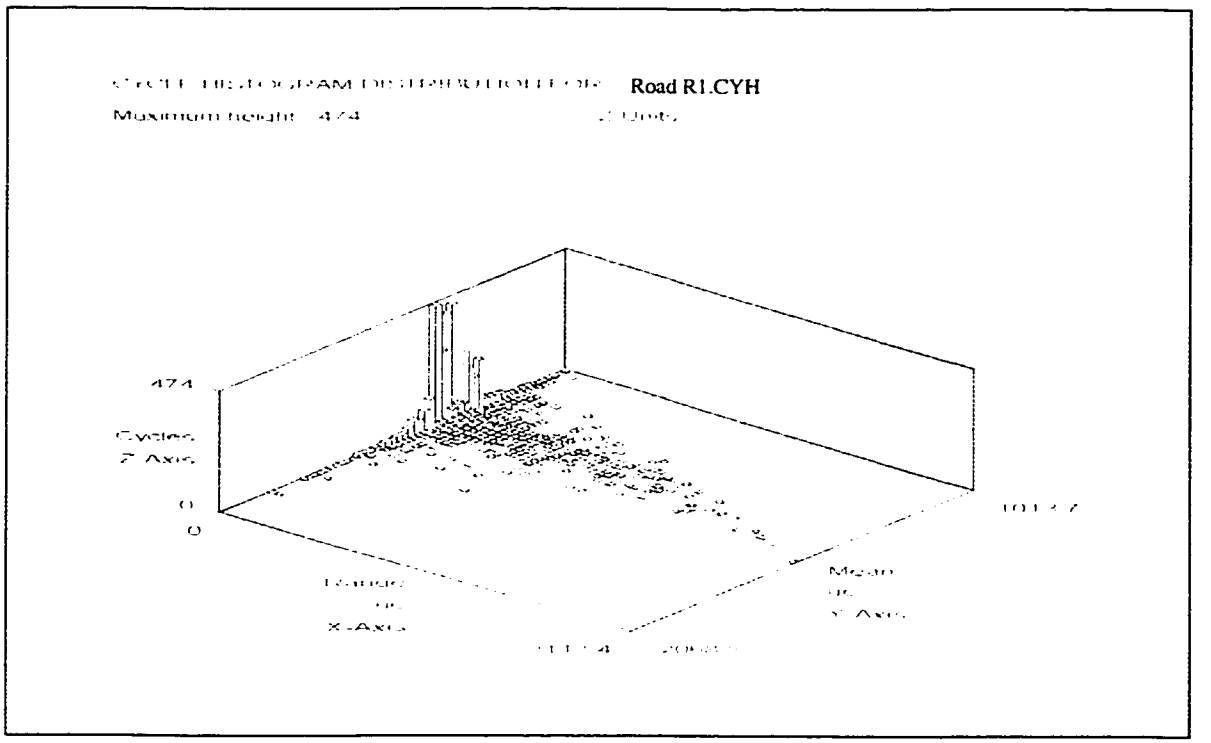

Figure 15. "Rainflow counted" histogram of time history collected for Channel 25 (Left rear coil spring strain channel) during travel over R1 road.

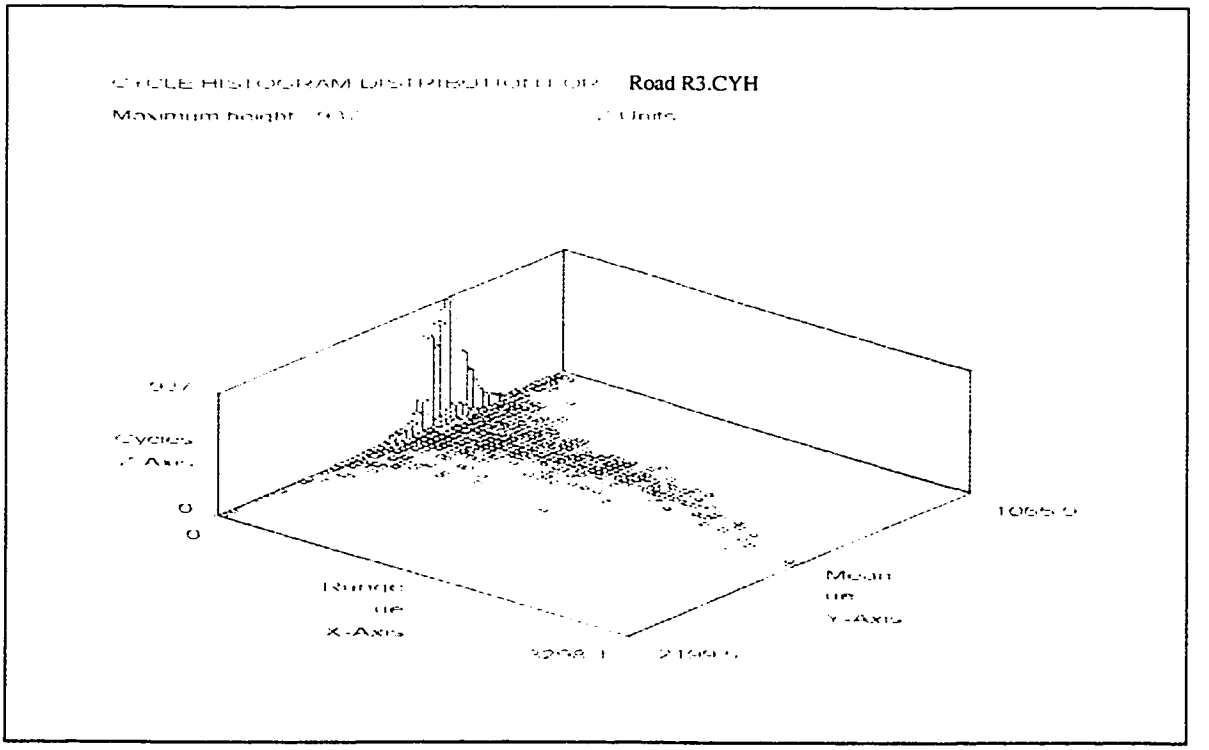

Figure 16. "Rainflow counted" histogram of time history collected for Channel 25 (Left rear coil spring strain channel) during travel over R3 road.

Visual inspection of "rainflow counted" histograms indicates similarities between the distributions of the cycles in both roads. Overall, the number of cycles introduced to a vehicle through inputs of R3 Road seems much higher than that of R1 Road (see Figures 15 and 16), especially in low amplitude regions. This is simply due to the fact that R3 Road is longer in distance (1.9 miles vs. 0.8 miles of R1 Road). Further investigation is necessary to correlate the distributions of the two loading histograms.

5.3.3 Correlation Between "Rainflow Counted" Histograms

A "Customer Correlation" tool provided by nCode in the nSoft software was utilized to correlate the "rainflow counted" cycle histograms from R1 and R3 Roads. The "Customer Correlation" attempts to match the number of cycles in the 16 amplitude bins of the target signal by summing differing proportions of sample signal(s). The mean or average (as selected by the user) contained in the last bin (16^{th} bin) is also matched. The Average option is for histograms holding other than cycle data, and shows the average value for the lost axis. The Mean option is for cycle histograms, and is the most positive mean in the largest amplitude bin, i.e. the mean of the most damaging cycle [6].

It should be noted that there is a problem inherent in attempting to sum cycle histograms, relating to the potential loss of the largest cycle, particularly when the means of the larger cycles are very different. Including the mean of the largest cycle in the correlation is the most satisfactory method of handling this, but even this cannot completely solve the problem [6].

"Customer Correlation" is achieved using Simplex Linear Programming iterated to achieve the narrowest error bounding possible, as shown below.

$$
\begin{aligned}
A_1 [X1_1] + B_1 [X2_1] + C_1 [X3_1] + \ ... + Z_1 [Xn_1] &= [Y_1] \\
A_2 [X1_2] + B_2 [X2_2] + C_2 [X3_2] + \ ... + Z_2 [Xn_1] &= [Y_2] \\
A_3 [X1_3] + B_3 [X2_3] + C_3 [X3_3] + \ ... + Z_3 [Xn_3] &= [Y_3] \\
&\vdots
\end{aligned}
$$

$$A_m [X1_m] + B_m [X2_m] + C_m [X3_m] + \ldots + Z_m [Xn_m] = [Y_m] \quad \ldots\ldots (1)$$

Where:

$A_1, B_1, C_1, \ldots Z_1$	= Multipliers of sample data for channel 1
$A_m, B_m, C_m, \ldots Z_m$	= Multipliers of sample data for channel m
$[X1_1], [X2_1], \ldots [Xn_1]$	= Matrix of sample measurements for channel 1
$[X1_m], [X2_m], \ldots [Xn_m]$	= Matrix of sample measurements for channel m
$[Y_1]$	= Matrix of target measurement for channel 1
$[Y_m]$	= Matrix of target measurement for channel m

This can be interpreted as: A times Track X1 followed by B time Track X2, and so on, that gives the same effect as Track Y of the Target for each channel from 1 to m. Each Track X1, X2, etc. could represent different individual events such as potholes, or cobblestones, respectively or a pass of a particular road. The Target Track Y could be the customer acquired data which contains a variety of events. The purpose then of the "correlation" is to design a test track from sample data that best represents the Target.

In this study only one sample measurement was considered at a time (in this case R3 Road) with all sixteen channels, to match the target (in this case R1 Road). The purpose of the correlation is then to determine if a multiple of one sample road could reproduce the same cyclic responses in a vehicle as the target road for all channels of data. More technically speaking if R3 Road is termed as track X and R1 Road is termed track Y then this can be represented as:

$$A_1 [X_1] = [Y_1]$$
$$A_2 [X_2] = [Y_2]$$
$$\vdots$$
$$A_{16} [X_{16}] = [Y_{16}] \quad \ldots\ldots (2)$$

The optimum multiplier will cause the "smallest" errors between all the target and sample histograms for all channels. The criteria used by nSoft "correlation package" for defining the optimum solution consist of correlation coefficients, average absolute cyclic errors

and RMS cyclic errors. The equations for these calculations are provided in Appendix III.

It should be noted that although the original rainflow counted histograms were constructed using 64 bins (64x64 range-mean matrix), the correlation package reduces them to sixteen bin matrices (16x16 range-mean matrix). The reason for this bin reduction is based on a fact that an optimization process cannot be performed by simply matching bins of source data to those of target data. This is because small changes during measurement process results in cycles that randomly move from one bin to neighboring bins. Thus, a look from a more global perspective is needed. The optimization process then is performed not on matching each individual bin, but rather areas of the rainflow matrix.

The "customer correlation" tool relies on the principle that exact knowledge of the damage for components is not necessary at the beginning of the analysis. A correct damage would be assumed to be done to a vehicle by virtue of reproducing the same cyclic input patterns of the target signal on the source signal(s).

When correlating the cyclic histograms, the following logic is followed in the program:

1. Vehicle life is proportional to fatigue,
2. fatigue is proportional to the cyclic strain levels,
2. cyclic strain levels are proportional to the cyclic stresses,
4. cyclic stresses are proportional to the cyclic loading, and finally
5. cyclic loading is proportional to the cyclic input history.

So, vehicle life is proportional to the cyclic input history [6].

The results of the correlation of R1 and R3 Roads indicate that in order to reproduce the cyclic inputs of the R3 road, R1 Road would have to be repeated approximately 2.3

times. Best correlation for all channels was achieved through correlating to Channel 25, as a main channel. This conclusion is based on the results presented in form of fit coefficients (r2), absolute cyclic errors, and RMS errors defined in Appendix III. When correlated to Channel 25, the fit coefficients for all channels were close to one, and the errors were the smallest.

Next, an assessment was performed to determine how well the "rainflow counted" histograms were correlated in the software. The need for this assessment was based on the fact that the "Customer correlation" tool clusters the original 64 bin-sized "rainflow counted" histograms to 16 bins (including one mean bin) using automatic scaling, to maximize bin accuracy and use.

To perform this assessment, a list containing the number of cycles at their corresponding load ranges (from original 64 bin-sized "rainflow counted" histograms), for both roads and for all the channels, was imported to a spreadsheet. The relationship between the number of cycles at particular load ranges for both roads was established through linear regression. This was done for two cases: first one relating one pass of R1 Road to one pass of R3 Road for all channels in the 64 bin-sized matrix, and the second one relating 2.3 passes of R1 Road and one pass of R3 Road. Two pieces of information were obtained as a result: slope of the line and correlation coefficients. Their significance will be discussed below.

The correlation analysis through linear regression presents two variables, which associate the cyclic inputs introduced to a vehicle by the two roads. These variables are slope and correlation coefficient. The slope shows the dependence of the two roads on one another while the correlation coefficient measures the relationship between two data sets.

The slope is simply defined as the rise over run in a line. The correlation coefficient calculation returns the covariance of two data sets divided by the product of their standard deviations (see Equation 3 and 4). This correlation tool is used to determine whether two ranges of data move together. That is, whether large values of one set are

associated with large values of the other (positive correlation), whether small values of one set are associated with large values of the other (negative correlation), or whether values in both sets are unrelated (correlation near zero).

$$\rho(x,y) = \frac{Cov(x,y)}{(\sigma_x * \sigma_y)} \quad \text{.....(3)}$$

$$Cov(x,y) = \frac{\sum_{i}^{n} (x_i - \mu_x) * (y_i - \mu_y)}{n} \quad \text{.....(4)}$$

where:

Cov (x,y) - covariance of two data sets

ρ(x,y) - correlation coefficient

σ_x – standard deviation of data set x

σ_y – standard deviation of data set y

μ_x – mean value of data set x

μ_y – mean value of data set y

As explained above, the correlation coefficient can be thought of as the "quality" of the inter-relationship between the cycles of the two studied roads, whereas the slope of the line shows the dependence that represents the "quantity" of the inter-relationship. As shown in Table 9, both the dependence and correlation must be considered in evaluating the effect of cyclic inputs from one road to the other.

High Dependence	No conclusion can be drawn	Strong Inter-relationship
Low Dependence	Weak Inter-relationship with low confidence	Weak Inter-relationship
	Low Correlation	High Correlation

Table 9. Significance of correlation and dependence on evaluating cyclic inputs for any two roads, in this case the R1 and R3 road. In order to obtain a good correlation through linear regression, the data must be able to be represented as a straight line of particular slope, and the correlation coefficient must be close to 1.0.

In order to verify the results of the "correlation package", as mentioned above, the list of ranges and corresponding number of cycles in each range (obtained through rainflow counting), was imported to a spreadsheet for all original 64 bins. Two cases of correlation were investigated:

- cycles of the R1 Road treated as the independent variable,
- cycles of the R3 Road treated as the independent variable.

Both methods of correlation show that in order to reproduce the number of cycles in one pass of R3 Road, approximately 2.3 passes of R1 Road data must be used (slope of the line $\approx$ 2.3). A chart presented in Figure 17 plots the slopes of lines relating number of cycles at particular ranges for all sixteen channels of data collected in project #P1 at full rated load, for both R1 and R3 Roads.

At this time it should be pointed out that the correlation coefficient (value of 2.3) relating R1 and R3 roads is dependent on many factors, these being road and weather conditions, driver and his/her driving maneuvers, vehicle type, payload condition and tire pressure. The value of the correlation coefficient may change as a result of these variables; however, the fact that the input cycles to a vehicle introduced by one road could be replaced by the other road inputs should still hold.

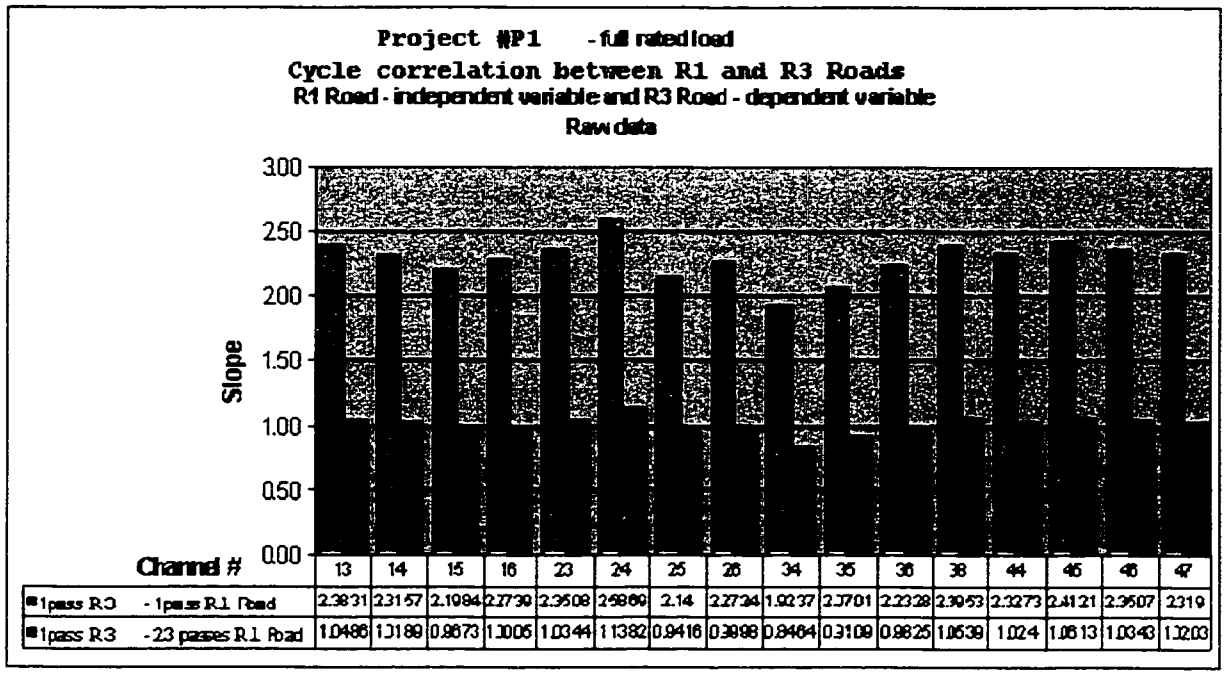

Figure 17. Results of correlation between R3 and R1 Roads presented in form of slope of a line relating number of cycles in R1 Road to number of cycles in R3 Road at particular load range. The graph shows that the number of cycles in R3 Road is equivalent to number of cycles in 2.3 passes of R1 road for all channels. This chart confirms that there are similarities in the vehicle responses collected from both R3 and R1 Roads for all considered transducer channels. Therefore, running multiple passes of one road ensures equivalent cyclic inputs of the other road considered in the correlation.

Figure 17 clearly indicates that the correlation of R1 and R3 Roads proved to be successful. That is, the number of cycles introduced to a vehicle through R3 Road is the same as number of cycles introduced through 2.3 passes of R1 Road. This relationship holds its validity for all channels of data considered in the analysis. In addition, the values of correlation coefficients for all calculation show a strong and positive correlation (correlation coefficient = 1) between the cycles of R1 and R3 Roads. Thus, based on this correlation technique it can be concluded that R1 and R3 Roads do indeed produce similar vehicle responses in the vehicle.

A correlation of range values corresponding to each of 64 bins, for both histograms was also assessed showing that corresponding bins have exact load range values for both

roads (slope = 1). This is true since the "rainflow counted" histograms for both roads were created to be of the same size (64 bins) with the same bin resolutions.

All of the correlation analyses performed in this study were done by placing equivalent importance to both high and low amplitude cycles. This was done to determine if the roads are similar for all ranges of inputs. To further accelerate the durability cycle, it is known that often cycles of low range values are edited from time histories, since they cause little or no damage. When the smaller cycles are removed, the "rainflow" counted histograms should be recalculated and the optimization process should be repeated.

Further analysis of the data collected from both roads needs to be conducted to determine the feasibility of replacing R3 Road with R1 Road or vice versa. If successful, a time saving would be realized in data analysis and drive file development duration since one set of data could be eliminated from the analysis.

5.3.4 Probability Functions

Time series signals represent variations in amplitudes, such as measured strains or accelerations, with time. Once the signal is digitized, discrete points are considered as a population of measured signals, and could be characterized by statistical methods (see Section 5.3.1). Other methods of characterizing data are:

- probability density functions,
- time-at-level functions.

5.3.4.1 Probability Density Function

Probability density function (PDF or p(y)) defines a probability of finding a value with a particular magnitude within the population. PDF can be either discrete or continuous.

Component strain and/or accelerations are considered to be continuously variable quantities.

The characteristics of PDF are as follow:

1. $p(y) \geq 0$
2. $\Sigma\, p(y) = 1$

The nSoft module calculates PDF by counting the number of individual data samples, dn, that lie in various levels or bins (y to y+dy), as a portion of the total number of samples, N, in the signal [26]. The probability density function for a particular bin is given by:

$$p(y)dy = \frac{dn}{N} \quad \text{.....(5)}$$

Probability density distribution is quite useful in signal classification, since it indicates the probability that signal value will lie between specified limits at an instant in time. It also helps to determine how close to a classical Gaussian/Normal distribution the signal behaves.

The comparison of the probability functions for one of the channels (Channel 25) is presented in Figure 18 to demonstrate the relationship between the responses of two roads.

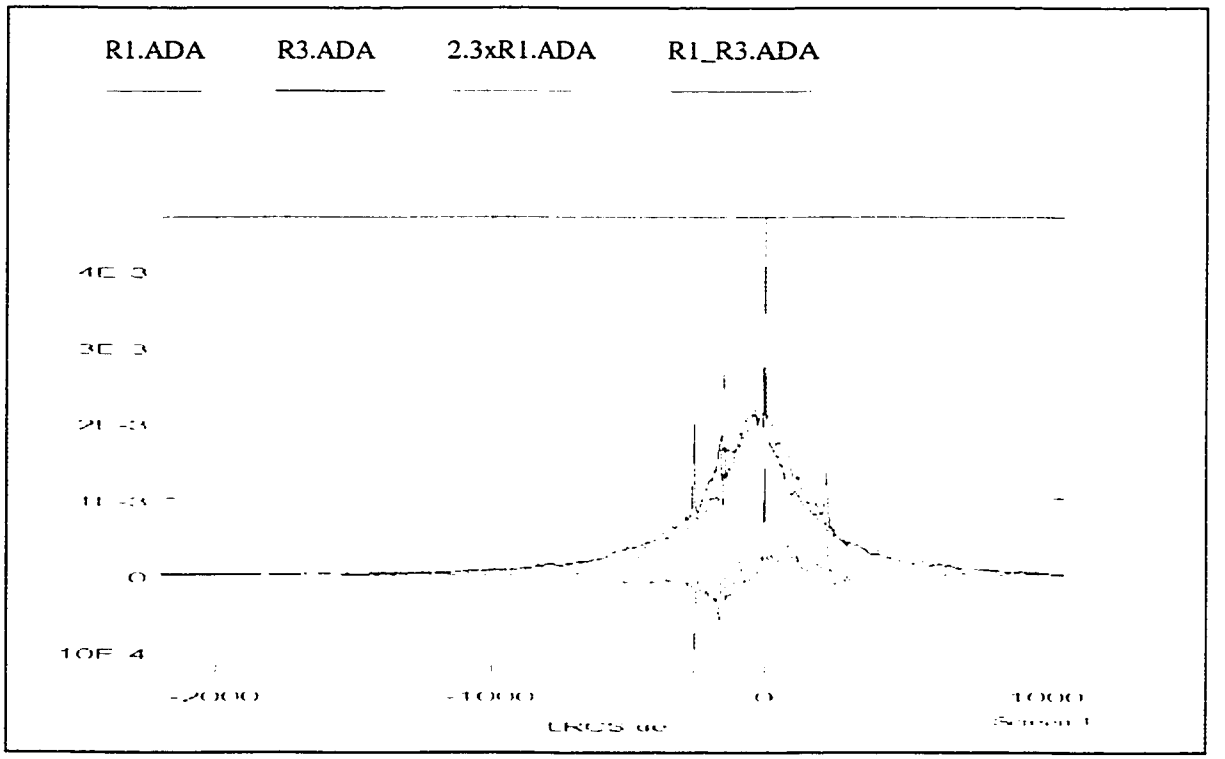

Figure 18. Relationship between probability density functions of one pass of R1 (magenta), one pass of R3 (blue) and 2.3 passes of R1 (green) roads collected from Channel 25. According to the algorithm, the PDF function is independent of number of passes (the PDF of one pass R1 road is equivalent to the PDF of 2.3 passes of R1 Road). The red line shows the error function between the PDF functions of R1 and R3 roads.

PDF functions for both roads, together with the error signal were plotted for each channel. Visual inspection indicates that the PDFs for both roads track each other fairly well. The biggest errors in PDFs are experienced at low amplitudes (spikes in the functions). However, the damage at those levels is not very significant and thus should not greatly effect the overall correlation. The spikes present in the PDF functions can simply be attributed to the algorithm used by nSoft software, and how it calculates the PDF function. The nSoft software simply divides the 'y' variable, in this case the amplitude of vehicle responses, into classes of bins. Depending on how many classes of bins the user selects, the smoothness of the function is affected. Separate modules in nSoft are available that provide averaging operations on different functions.

The PDF functions of both the R1 and R3 roads also resemble normal distributions, centered about approximately zero mean for all channels. This statement could be investigated further by calculating the skewness (representing asymmetry) and kurtosis (flattening of a curve) of the curves. Gaussian distribution gives a skewness equal to zero, and kurtosis equal to 3. Due to limitations of the software those values could not be obtained.

The probability density functions for one pass and 2.3 passes of the R1 road were identical, considering the fact that nSoft calculates the p(y) function as:

$$p(y)dy = \frac{dn}{N} \quad \text{.....(6)}$$

5.3.4.2 Time-at-Level

Time-at-level, is a method of signal classification, which defines how long the signal spends at a given magnitude. The time-at-level distribution retains physical units of time, unlike the probability density, which is normalized to one [27]. The function is defined as:

$$\frac{\Sigma t(y, y+dy)}{T} = 1 \quad \text{.....(7)}$$

where t(y, y+dy) is the time spent at level (y to y+dy) and T is the total time.

One of the plots, representing time at level curves for one pass of R1 Road, 2.3 passes of R1 Road and one pass of R3 road is shown in Figure 19 for Channel 25 data.

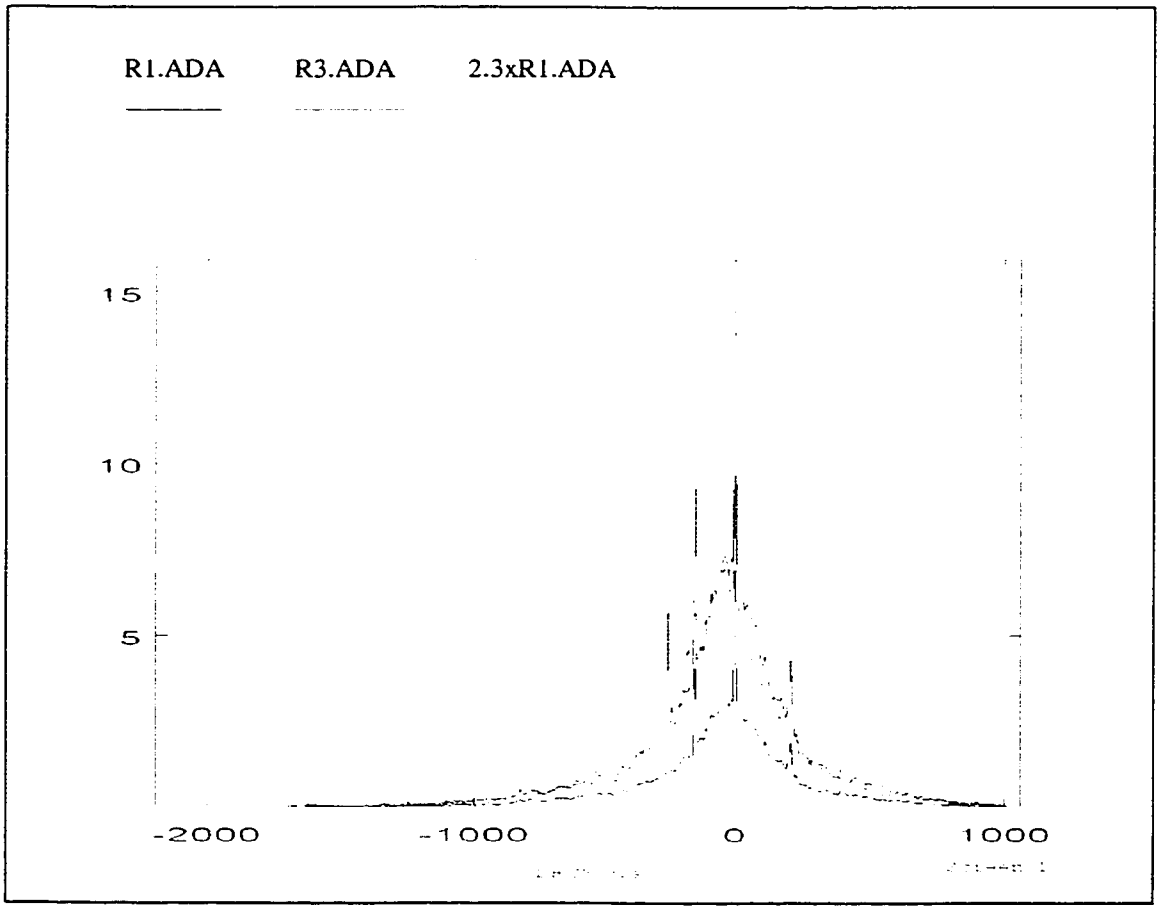

Figure 19. Plot of time at level function for one pass R1 (brown), 2.3 passes R1 (green) and one pass R3 (magenta) road for Channel 25 data. The time spent at each level of load is similar for one pass R3 and 2.3 passes of R1 road.

The time-at-level plots show clearly that the distribution of amplitudes for 2.3 passes of R1 Road tracks the R3 Road distribution better than just one pass. This is evident both at high and low amplitudes, for all channels.

5.3.5 Power Spectral Density

In addition to time history approach, there are several alternative ways of specifying the same random process. Fourier analysis allows any random time history of finite length to be represented as a series of sine waves. As an extension of Fourier analysis, Fourier transforms allow any process to be represented as a Power Spectral Density Function (PSD). This allows a representation of time history as a function of frequency thus called

"frequency domain". The amplitude, frequency and phase of sine wave is retained in both time and frequency domains [28].

PSD's are effectively obtained by taking a modulus squared of the Fourier transform. Some normalization has to take place, but it differs throughout different algorithms. In a PSD, the interest is concentrated on amplitudes, rather than on phase relationships between waves [28].

So far the only distribution of energy with relation to amplitude was analyzed through different probability density functions. The representation of a random process by a power spectral density (PSD) will show the distribution of energy with respect to frequency. The distribution of energy with respect to frequency is more evident when plotted on semi-log scale. A plot of PSD for Channel 25, comparing data from R1 and R3 roads is shown in Figure 20.

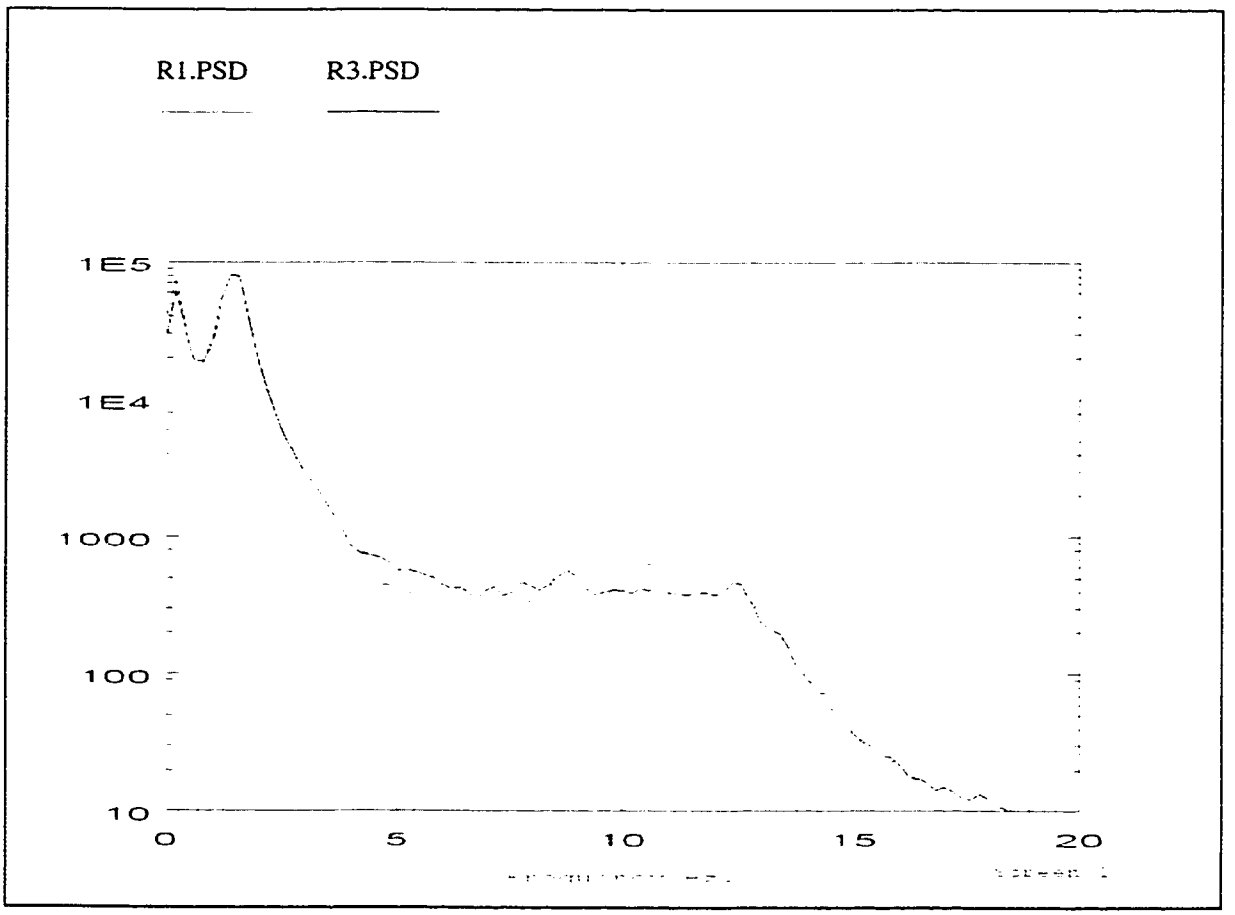

Figure 20. PSD graphs for R1 (magenta) and R3 (blue) roads for channel 25. Note the both roads induce similar frequency response in the vehicle. This is evident in both the frequency content and the profile of the PSD functions. The differences in energy content under certain frequency ranges could vary as a result of vehicle speeds, or driving maneuvers.

The PSD graphs for both roads followed each other fairly well through all frequencies. According to studies on accelerated testing, if different roads are similar in profile power spectra, the responses of the vehicle components are of the same nature. Factors such as vehicle speed or road irregularities may intensify or decrease the amplitudes of the vehicle response PSD functions; however, if similar in nature the PSD profiles should be similar [29].

The following maximum "visible" frequency spectra were observed in the project #P1 channels at full rated load, for both roads when plotted on linear axes:

Channel No.	Tag	Maximum Frequency Content Hz
13	LFVA	~30
14	RFVA	~30
15	LRVA	~30
16	RRVA	~30
23	LFCS	~5
24	RFCS	~5
25	LRCS	~5
26	RRCS	~5
34	LRTAS	~15
35	RRTAS	~15
36	LRLtB	~15
38	RRLtB	~15
44	LFLtBo	~10
45	RFLtBo	~10
46	LFLgBo	~20
47	RFLgBo	~20

Table 10. Maximum frequency contents observed in R1 and R3 Roads plotted on linear axes. Both roads showed the same frequency contents in all channels investigated.

The values of the maximum frequency ranges may vary from test to test, depending on road conditions, driving maneuvers, vehicle type or speeds. The important aspect of this analysis is to show that regardless of these variables, both roads will produce approximately the same frequency responses in the tested vehicle.

The analysis of amplitude distribution and frequency content allows us then to conclude that one pass over the R3 road will induce similar responses in a vehicle, as would 2.3 passes over the R1 Road.

The last step is to perform fatigue analysis on the vehicle responses conducted from both roads, to determine if the same damage content is induced by both road inputs.

5.4 Relative Fatigue Analysis

Relative fatigue damage analysis was performed using coil spring channels to compare the vehicle damage for both R1 and R3 Roads in P1 project, conducted at full rated load. The analysis was performed on raw data collected from the PG's OR test. The fatigue analysis was reproduced using nSoft software based on the assumptions made during original analysis of the P1 project. The intent of the original fatigue analysis was to ensure that simulator vehicle damage would be the same as proving ground road damage for development of drive files.

The fatigue analyses were performed using nSoft "critical location fatigue analysis" module. To perform damage calculations, multiple input parameters are required, these being a good description of the service loading environment, appropriate cyclic material data, and among others, component geometry. The parameters selected for the fatigue life estimations in this particular test were as follows:

Fatigue Analysis Type:	Strain-Life
Scale Factor:	30
% Certainty of Survival:	50
Mean Stress Correction:	None
Miner's Constant:	1
Material Name:	SAE5160_434_QT
Surface Finish:	Forged
Surface Treatment:	None
K_f (fatigue stress concentration factor):	1

The significance and reason for selecting the above parameters will be discussed below. It is important to point out however, that the fatigue analyses performed in this study were simply used for comparison purposes between responses of two different roads. They were not by any means absolute life estimates of any components in a tested vehicle. The most important aspect of performing relative fatigue damage comparisons is to base analysis, comparisons and decisions on *equivalent damage*. Thus when comparing two loading time histories based on their damage contributions, the selection of parameters is not important as long as they are the *same* for both analyses.

The total fatigue life of a component is made up of two stages: crack initiation and crack propagation. The initiation phase encompasses the development and initiation of cracks while crack propagation deals with crack growth to failure. The transition phase from initiation and propagation is not well defined. For most part, an initiation stage is defined as a time spent developing an engineering size crack. The software module provided by nCode predicts the presence of engineering cracks of about 2 mm length [30]. (For smaller components, an engineering crack is assumed to be on the order of 2.5 mm or 0.1 inch. [23]).

There are three primary methods of fatigue analysis: stress-life approach, strain-life approach, and fracture mechanics. Stress-life method, the first to be developed, does not account for crack initiation or propagation individually, but rather deals with total life of a component. The strain-life approach is mainly considered to be a crack initiation approach while fracture mechanics deals only with crack propagation.

Fatigue analysis was conducted in the study using a "Strain-Life" approach and using measured service time histories. Strain-Life approach is considered to be the most appropriate method of fatigue analysis in the automotive industry [22]. It is based on the observation that in many components, the behavior of material at critical locations is dependent on the strain/deformation. Automotive testing is mainly concerned with high load levels or low cycle fatigue (LCF) regime. In this regime material behavior and cyclic stress-strain response is best represented under strain-controlled conditions. In comparison, at low load levels, stresses and strains exhibit a linear relationship. As a result, in the high cycle fatigue (HCF) regime, a material's behavior can be modeled through both load controlled and/or strain controlled testing. For that reason, fatigue analysis in LCF regime should be analyzed using Strain-Life approach, whereas HCF regime could be analyzed using either Stress-Life or Strain-Life approach [23].

Strain-life analysis is very significant in fatigue analysis of automotive components as it accounts for local plasticity. The importance of considering plastic strains in fatigue is as follows:

- crack initiation is caused by local plasticity,
- by modeling residual stress, degradation on fatigue performance is accounted for,
- life estimation is made in LCF region,
- accumulation of damage caused by variable amplitude loading is accounted for [22].

The results and assumptions of fatigue analysis, using the strain responses of coil springs as a representative environment loading histories, are considered next.

As mentioned above, a strain-life approach was used for fatigue damage calculations. A scale factor was determined through an iterative process (scale factor = 30), to give meaningful damage numbers. The idea was to induce enough damage in a component in a single pass, to move its life to LCF where plastic strains form. An effect of scale factor on damage analysis will be discussed in section 5.6.1 of this report.

The large amount of scatter in data used to determine fatigue parameters introduces a measure of uncertainty to fatigue life predictions. Thus a percentage certainty-of-survival parameter can be used to specify the probability that a component will achieve a desired life [31]. Each value representing a certainty of achieving a design life is associated with the standard deviations from the mean/design life. For example 50% certainty of survival constitutes 0 standard deviations from the mean life, or 99.9% of survival represents 3 standard deviations away from the mean.

As a default, 50 percent (50%) probability of survival was used in the analysis. Knowledge of standard errors associated with regression analyses, performed to determine the material fatigue parameters, is required in order to study how the elastic and plastic life components deviate from the mean value (50% probability of survival). If the statistical information is not known, it is safe to assume a 50% uncertainty. An effect of percent probability of survival on the damage comparison between the two roads will be presented later in section 5.6.4 of this report.

The fatigue stress concentration factor, K_f, with a value equal to one was used. Once again the effect of the K_f factor on fatigue life comparison will be considered in section 5.6.2. No mean stress correction was used in the initial fatigue life calculation since mean stress relaxation occurs at high plastic strains in cyclically stable materials. A sensitivity analysis based on applying different mean stress correction factors will however be analyzed in section 5.6.3.

A description of material most appropriate for coil-spring application, is as follows:

Material Name:	SAE5160_434_QT (Quenched and tempered chromium steel)
Yield strength:	1487 MPa
Ultimate Tensile Strength:	1584 MPa
Elastic Modulus:	2.07×10^5 MPa
Work Hardening Exponent:	0.5
Work Hardening Coefficient:	1940 MPa
Fatigue Strength Coefficient:	2063 MPa
Fatigue Strength Exponent:	-0.08
Fatigue Ductility Exponent:	-1.05
Fatigue Ductility Coefficient:	9.56
Cyclic Strain-Hardening Exponent:	0.13
Cyclic Strength Coefficient:	2432 MPa
Cut-off:	2×10^8 reversals

The strain-life plot of the material is presented in Figure 21.

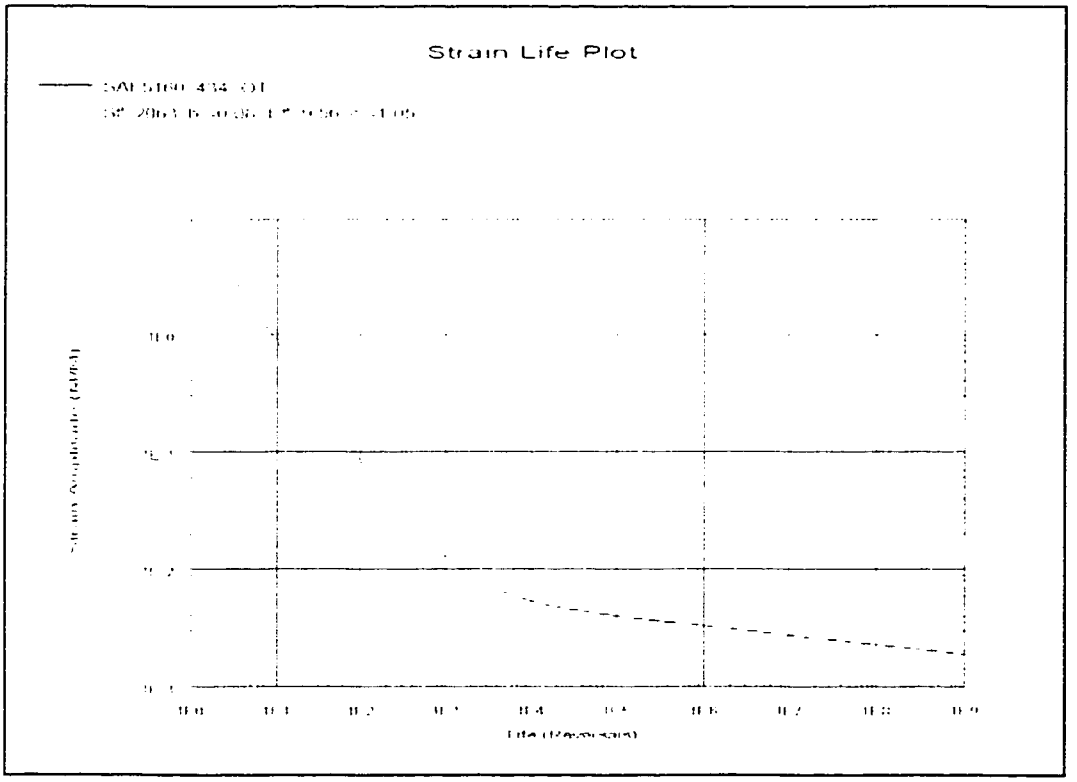

Figure 21. Strain-Life behavior of SAE5160_434_QT [nSoft Material Data Base]

The results of the fatigue analysis will be discussed next.

5.4.1 Cycle Histogram Distribution

The time histories for all channels of data were reduced through a "rainflow counting" method to range mean histograms, as described in Section 5.3.2. The correlation between the cycle histogram distributions was investigated at the beginning of the study. The results are presented in Section 5.3.2 and 5.3.3. The results of this analysis demonstrated a correlation in cyclic distributions of road responses between the R1 and R3 Roads. It was shown that the responses in a vehicle induced through driving over R3 Road, for the particular test investigated, could be simulated with 2.3 passes of R1 Road.

Once the complex time histories are simplified, a cumulative damage analysis has been conducted using a "linear damage rule" as proposed by Palmgren and Miner [23].

5.4.2 Damage Histogram Distribution

In the Palmgren-Miner approach [23], a cycle ratio is defined as:

$$Di = \frac{n_i}{N_i} \quad \text{.....(8)}$$

where:

Di - damage/cycle at the ith constant amplitude stress (strain)

n_i - the number of occurrences of the ith constant amplitude stress (strain)

N_i - the number of cycles to failures at the ith stress (strain) amplitude

A damage fraction D, is simply defined as a fraction of life consumed by an event or a series of events. A failure is considered when the summation of the damage fraction (D) is unity. That is:

$$\Sigma Di = \Sigma\left(\frac{n_i}{N_i}\right) = 1 \quad \text{.....(9)}$$

The number of occurrences (n_i) at each strain amplitude is simply obtained from the rainflow-counted matrix. In this study all matrices contain 64 bins, each bin representing a value of a particular range (amplitude is half the range value), and the corresponding number of cycles in that range. To determine the cycles to failure (N_i), at the various constant strain amplitudes, the material fatigue data presented in Section 5.4 is used. By applying the strain-life relationship (see equation 10), a Strain–Life curve is obtained [23].

$$\frac{\Delta\varepsilon}{2} = \frac{\sigma_f'}{E}(2N_f)^b + \varepsilon_f'(2N_f)^c \quad \text{.....(10)}$$

where:

$\Delta\varepsilon$ - total strain range

$2N_f$ - reversals to failure

σ_f' - fatigue strength coefficient

ε_f' - fatigue ductility coefficient

E - modulus of elasticity

c - fatigue ductility exponent

b - fatigue strength exponent (Basquin's exponent)

The last step is to calculate the cycle ratios (n_i/N_i) at each stain amplitude, and finally determine the cumulative damage [32].

Visual inspection of damage distributions resulting from fatigue analyses of coil spring responses showed similarities between the R1 and R3 Roads. An example of damage histograms for Channel 25 data is presented in Figures 22 and 23, which plot damages in one pass of R1 Road and one pass of R3 Road respectively.

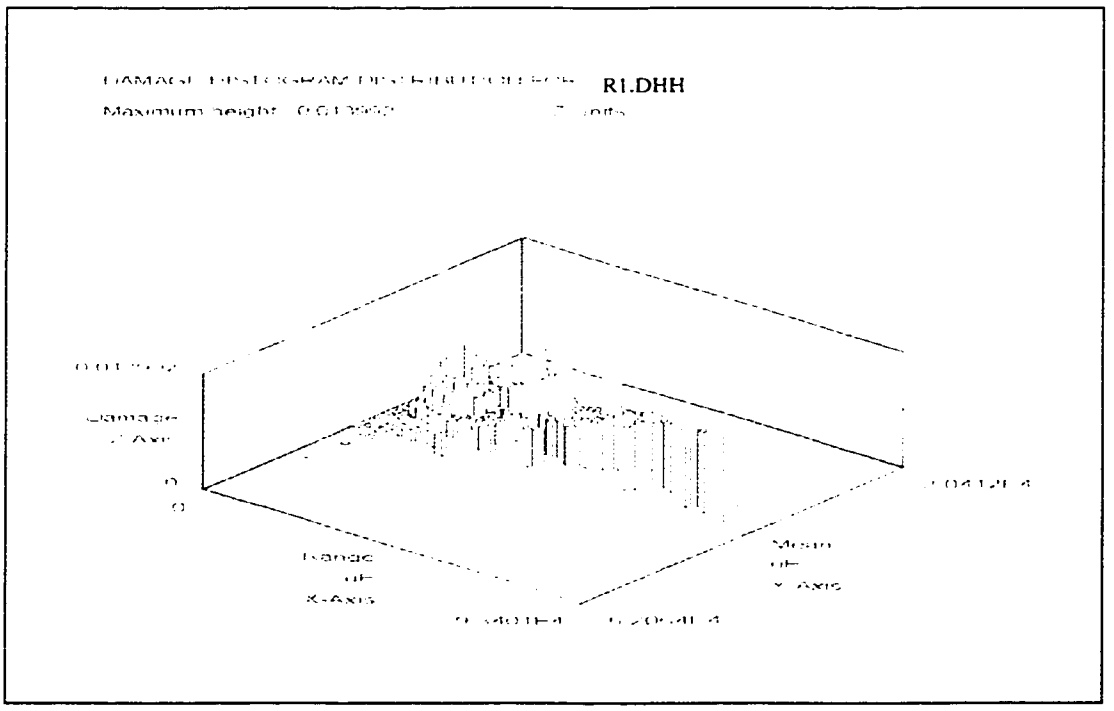

Figure 22. Damage histogram distribution in one pass of R1 road using a scale factor = 30, K_f = 1 and no mean stress correction factor.

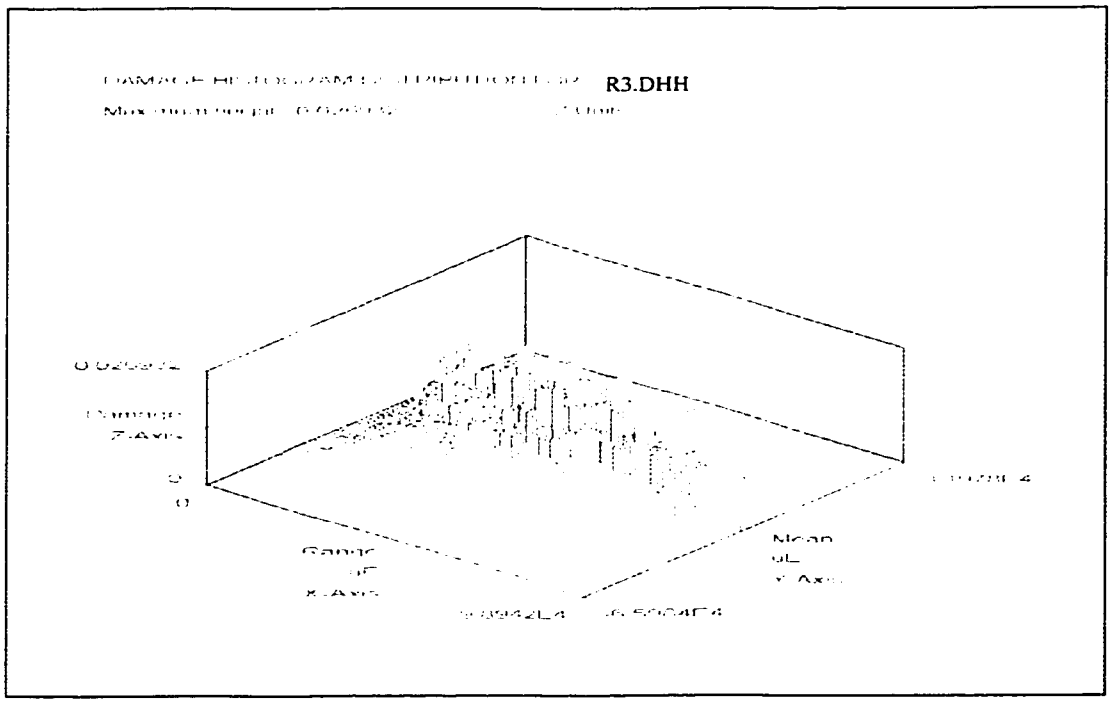

Figure 23. Damage histogram in one pass of R3 road using a scale factor = 30, $K_f = 1$ and no mean stress correction factor.

Further investigation needs to be conducted in order to assess the correlation between damage induced in a vehicle through inputs of the two roads.

Table 11, shows tabulated values of life (repeats), damage index numbers, percent low cycle damage, percent transition damage and percent high cycle damage for one pass R3 Road, one pass R1 Road, and 2.3 passes of R1 Road.

The transition life is where the elastic and plastic lines cross on the damage curve. Damage occurring within + or - 1 decade of this life is the transition damage. More than 1 decade higher in life is high cycle. More than 1 decade lower in life is low cycle. This is shown in Figure 24.

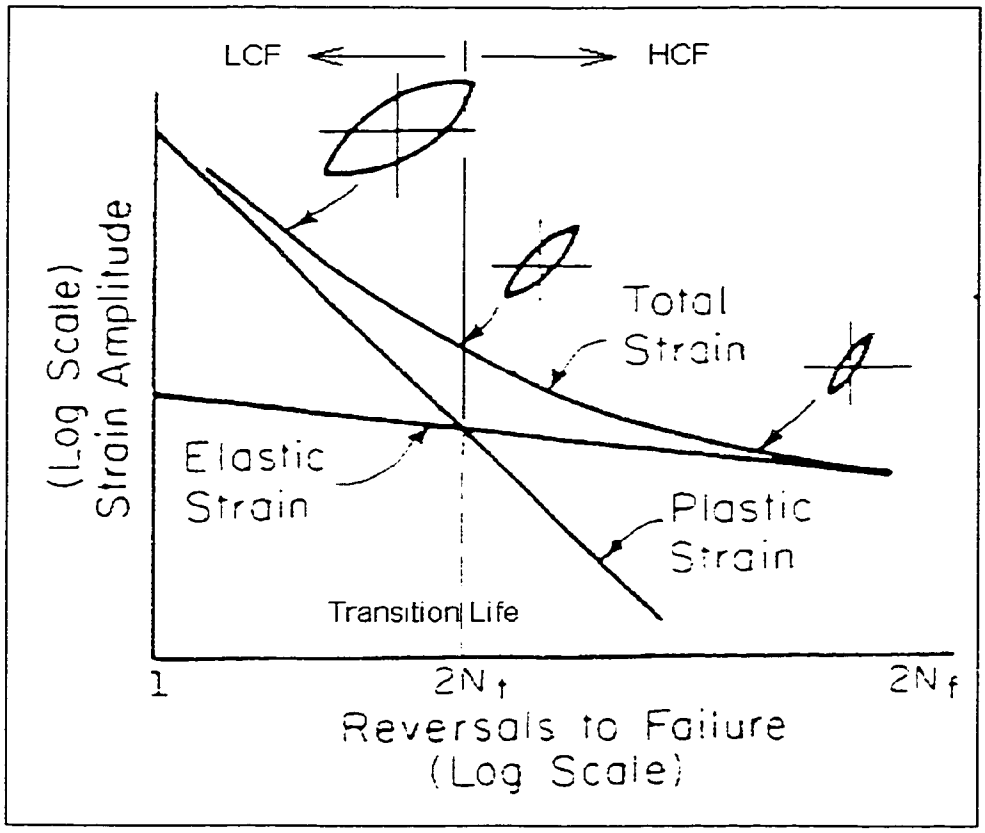

Figure 24. Strain-Life curve. At large strain amplitudes (Low Cycle Fatigue Life) the strain-life curve approaches the plastic line, and at low amplitudes (High Cycle Fatigue Life) the curve approaches the elastic line. The intersection of plastic and elastic curves represents transition life [23].

The transition life itself can be defined as [23]:

$$2N_t = \left(\frac{\varepsilon_f' E}{\sigma_f'} \right)^{1/(b-c)} \qquad \text{.....(11)}$$

where:

$2N_t$ - transition fatigue life

σ_f' - fatigue strength coefficient

E - modulus of elasticity

b - fatigue strength exponent (Basquin's exponent)

ε_f' - fatigue ductility coefficient

c - fatigue ductility exponent

The life estimates presented in Table 11 do not by any means represent the absolute/true life of the analyzed components. The fatigue analyses were strictly performed for comparison purposes of two different time histories. A failure listed in Table 11 is defined when the total damage accumulated is greater than unity, according to Miner's rule; however, it does not represent a malfunction of a component in real life. An absolute/true life estimate would require a complete knowledge of component's geometry, critical locations and material type, and would take into account a safety margin as recommended by its designer.

Ratios between the total damage numbers, and distribution of damages among high, low and transition life, were obtained in order to show the correlation between the two roads. The results are presented in Table 12.

Channel	R1 Road				
	Life (Repeats)	Damage	% Low Cycle Damage	% Transition Damage	% High Cycle Damage
23 (LFCS)	1.60	0.6250	62.10	28.20	9.61
24 (RFCS)	1.30	0.7692	63.90	27.80	8.31
25 (LRCS)	1.10	0.9091	71.30	22.00	6.72
26 (RRCS)	Failed	1.1614	73.90	20.20	5.83
Channel	2.3XR1 Road				
	Life (Repeats)	Damage	% Low Cycle Damage	% Transition Damage	% High Cycle Damage
23 (LFCS)	Failed	1.4375	62.10	28.20	9.61
24 (RFCS)	Failed	1.7692	63.90	27.80	8.31
25 (LRCS)	Failed	2.0909	71.30	22.00	6.72
26 (RRCS)	Failed	2.6712	73.90	20.20	5.83
Channel	R3 Road				
	Life (Repeats)	Damage	% Low Cycle Damage	% Transition Damage	% High Cycle Damage
23 (LFCS)	Failed	1.3936	64.10	26.30	9.60
24 (RFCS)	Failed	1.5451	67.20	23.40	9.40
25 (LRCS)	Failed	2.0018	73.20	20.70	6.11
26 (RRCS)	Failed	2.2840	75.30	19.40	5.29

Table 11. Fatigue damage analysis result summary for R3 and R1 Roads. The fatigue damage calculations were performed on four coil spring channels. The purpose of the analyses was to perform relative damage comparison between the two roads. Therefore the predicted life estimates are not by any means a representative of true components behavior. A failure was declared when the total damage ratio exceeded unity according to Miner's rule.

Channel	Damage Ratios		% Low Cycle Damage Ratio R1/R3 Road	% Transition Damage Ratio R1/R3 Road	% High Cycle Damage Ratio R1/R3 Road
	R1/R3 Road	2.3xR1/R3 Road			
25 (LRCS)	0.454	1.044	0.974	1.063	1.100
26 (RRCS)	0.508	1.170	0.981	1.041	1.102
23 (LFCS)	0.448	1.032	0.969	1.072	1.001
24 (RFCS)	0.498	1.145	0.951	1.188	0.884

Table 12. Fatigue damage correlation result summary for R3 and R1 Roads. The damage correlation shows that it is possible to achieve not only the same damage, but also the same damage distribution by substituting R1 and R3 Roads with one another during development of durability schedule in a laboratory environment.

Table 12 clearly shows that the total damage index, calculated through Miner's rule, is almost the same in one pass of R3 Road as it is in 2.3 passes of R1 Road (damage ratio

equals ≈1). The results presented in the table also indicate that the damage induced at low, transition and high cycle life regime is very similar between the two roads (ratios ≈1). The results of Table 12 clearly show that the total damage is retained through road substitution; however, a correlation of damage distribution throughout all ranges needs also to be investigated. The results of this correlation for all channels (23-26) of data are presented in Figures 25 through 28.

Figures 25 to 28 plot damage distribution throughout all range values for channels 23 to 26 respectively, together with their corresponding cumulative damage plots. The plots are obtained for one pass of R1 Road, 2.3 passes of R1 Road and one pass of R3 Road.

Although a large amount of scatter in the data was obtained in the above mentioned plots, results indicate that the scatter of damage numbers among individual bins (range values) is similar between one pass of R3 and 2.3 passes of R1 Road. The scatter is a result of data acquisition variability such as driver conduct and random events. In conclusion, road substitution of the R3 road with the R1 road or vice versa is a feasible method of test acceleration.

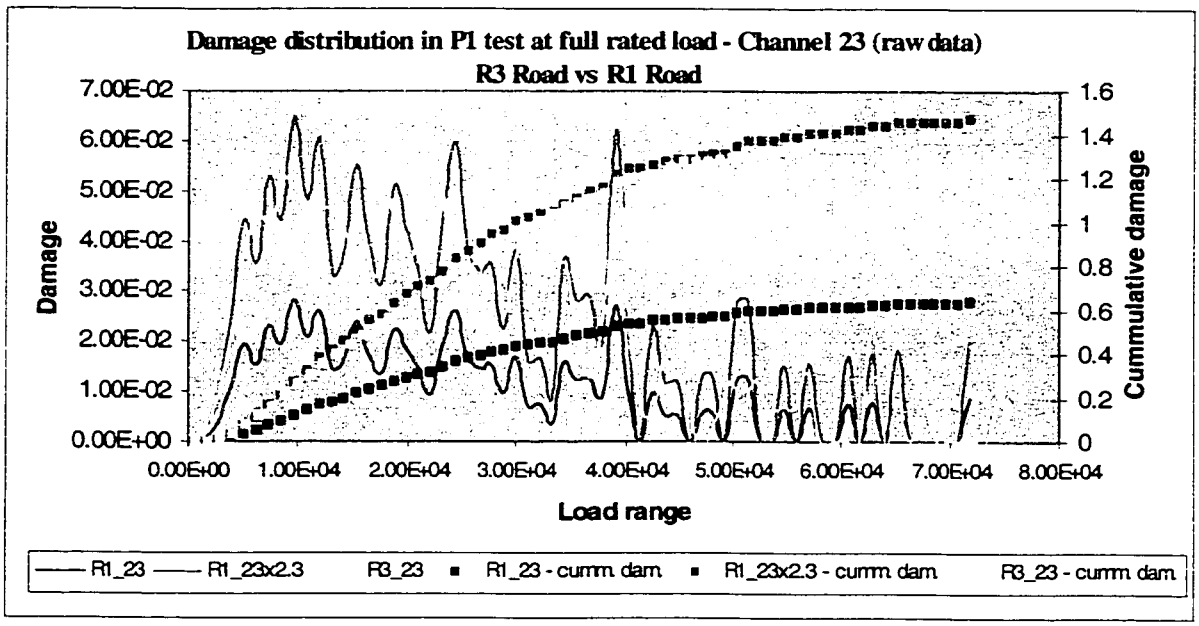

Figure 25. Damage induced at specific ranges (bins) obtained through rainflow counting methods for channel 23 data of R1 and R3 Roads, in P1 test at full rated load. Despite of the scatter in the data, one pass of R3 (yellow) produces similar damage distribution as 2.3 passes of R1 road (magenta).

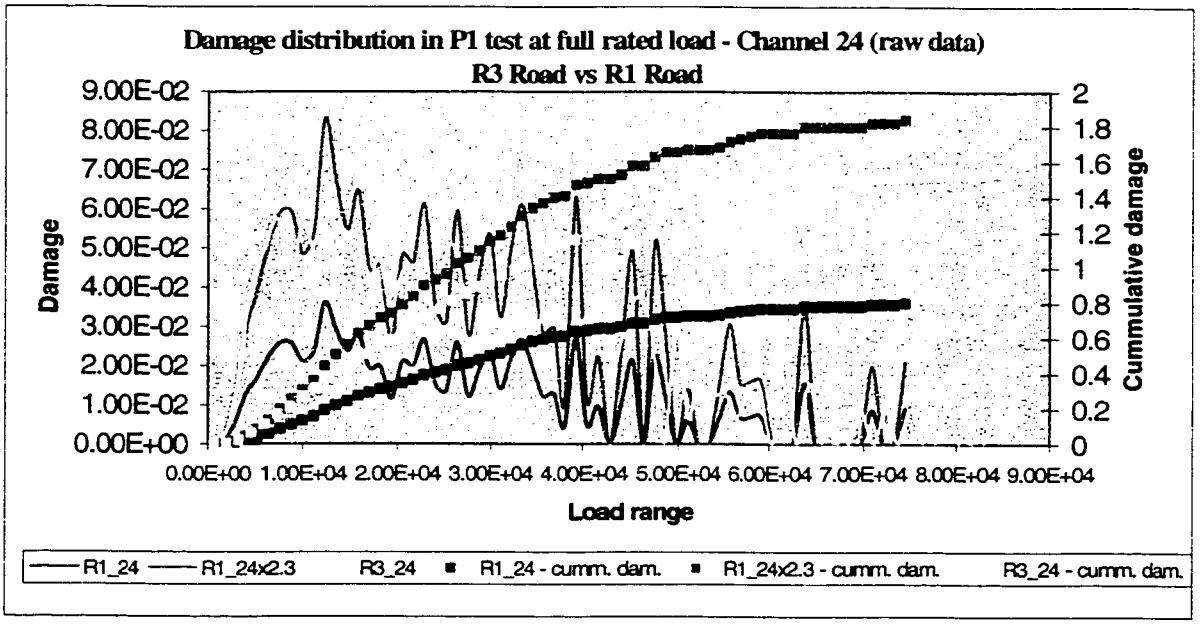

Figure 26. Damage induced at specific ranges (bins) obtained through rainflow counting methods for channel 24 data of R1 and R3 Roads, in P1 test at full rated load. Despite of the scatter in the data, one pass of R3 (yellow) produces similar damage distribution as 2.3 passes of R1 road (magenta).

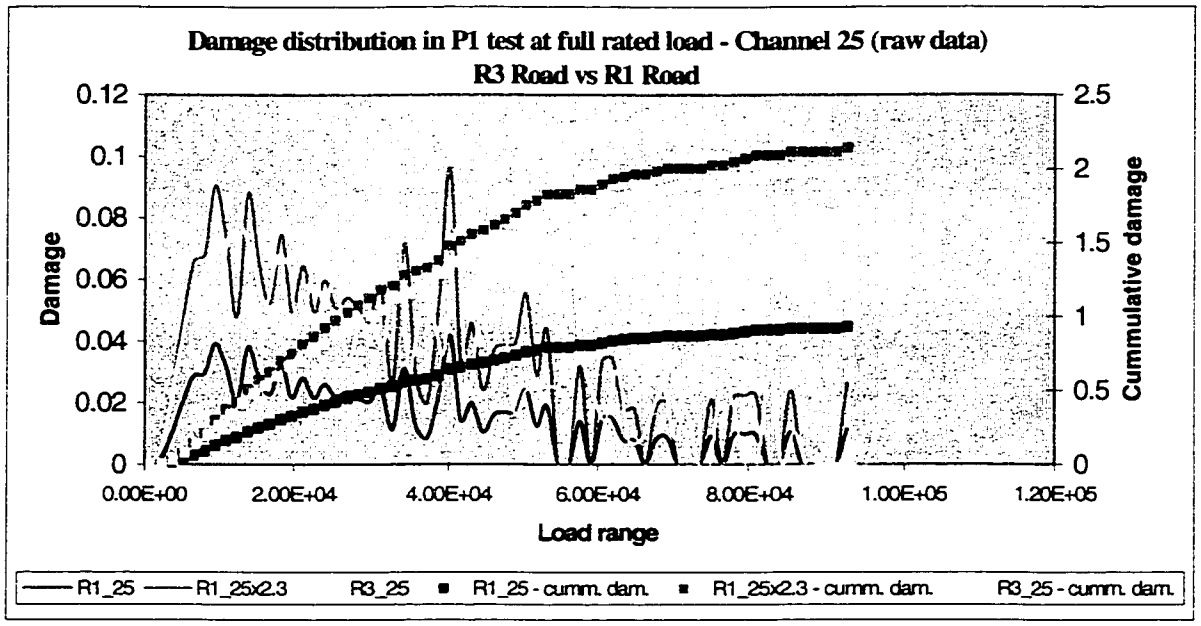

Figure 27. Damage induced at specific ranges (bins) obtained through rainflow counting methods for channel 25 data of R1 and R3 Roads, in P1 test at full rated load. Despite of the scatter in the data, one pass of R3 (yellow) produces similar damage distribution as 2.3 passes of R1 road (magenta).

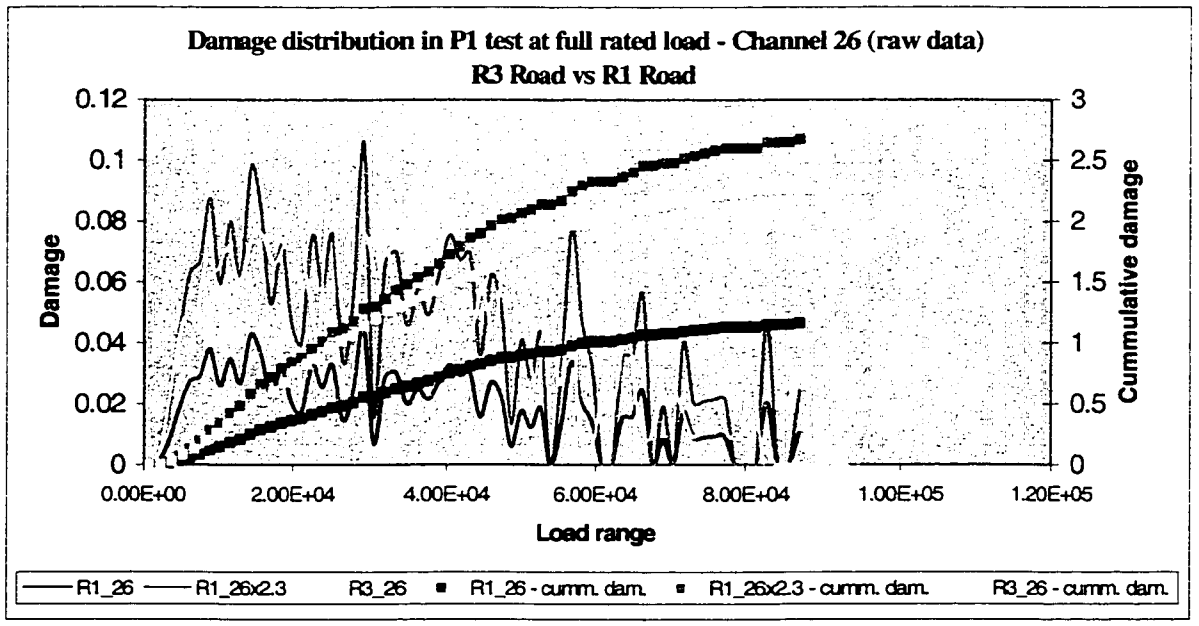

Figure 28. Damage induced at specific ranges (bins) obtained through rainflow counting methods for channel 26 data of R1 and R3 Roads, in P1 test at full rated load. Despite of the scatter in the data, one pass of R3 (yellow) produces similar damage distribution as 2.3 passes of R1 road (magenta).

It can be clearly observed that the distribution of damage in one pass of R3 Road through all ranges is closely approximated by that of 2.3 passes of R1 Road. Thus based on damage analysis, the substitution of one road with the other seems to be a feasible solution.

5.5 Hysteresis Plots of Stress vs. Strain Material Behavior

The study of cyclic stress-strain behavior plays an importance in assessing the durability of components subjected to repeated loading. The material performance due to cyclic inelastic loading can be shown in form of hysteresis loops. The total width of the loop gives the total strain range, while the total height of the loop represents the total stress range. The area within the loop is the energy per unit volume dissipated during a cycle. It also represents a measure of the plastic deformation work done on the material [23]. The bigger/fatter the loop is, the more damage is created by the cyclic input.

Comparison of hysteresis plots between the R1 and R3 Road shows that both the total stress and strain ranges are similar in all channels studied. The hysteresis loops for R1 and R3 Road in Channel 25 response are presented in Figures 29 and 30.

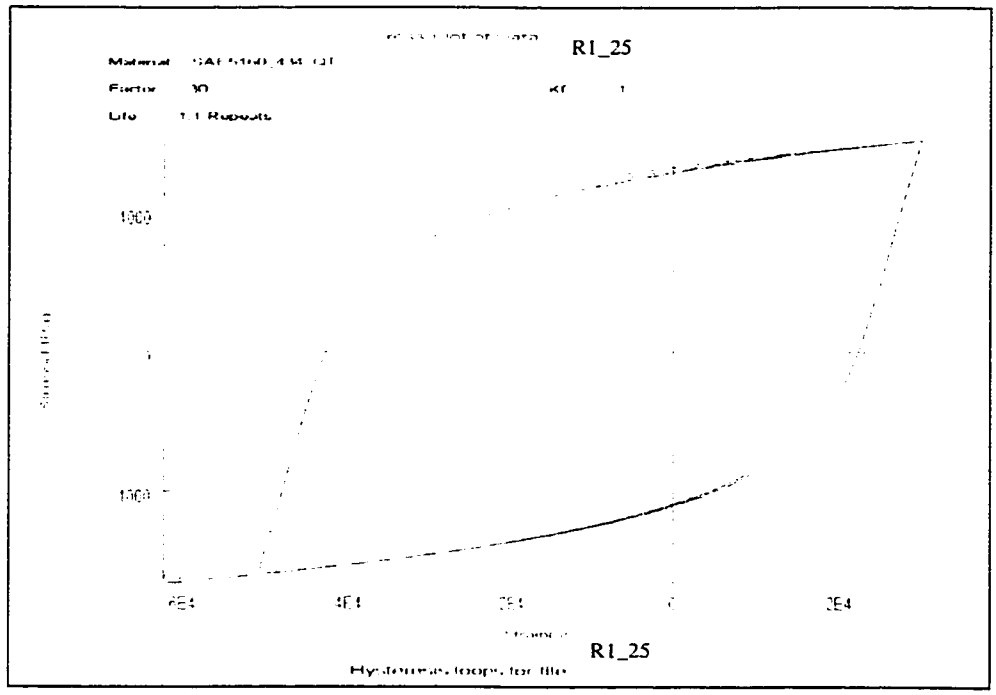

Figure 29. Hysteresis loops for R1 road Channel 25 data in P1 test at full rated load. The area within each loop represents a measure of the plastic deformation of the material.

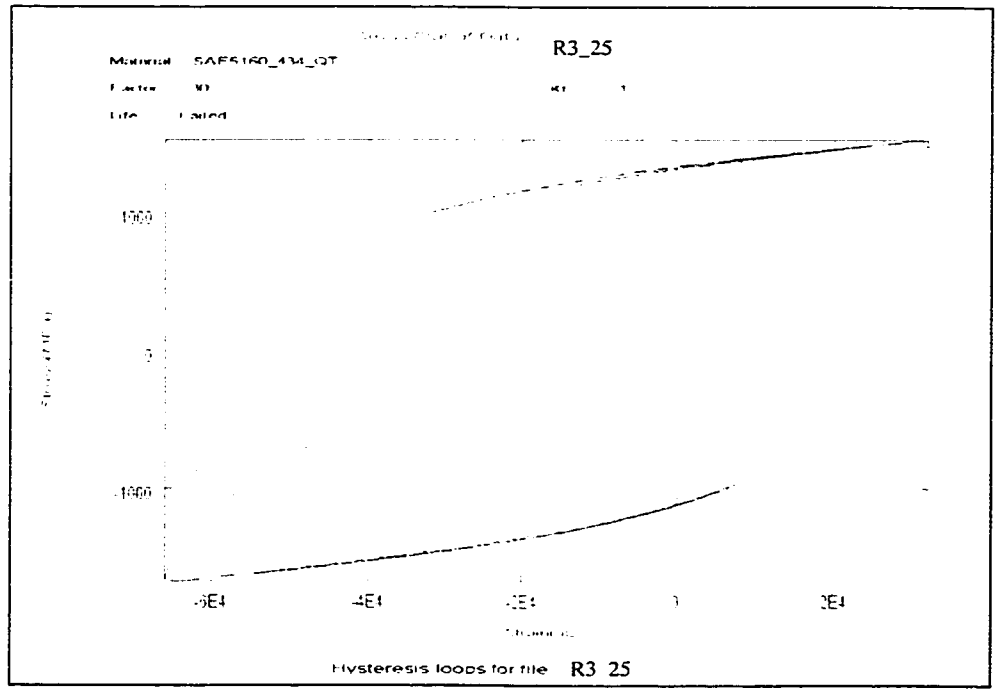

Figure 30. Hysteresis loops for R3 road Channel 25 data in P1 test at full rated load. The area within each loop represents a measure of the plastic deformation of the material.

The biggest loop is formed by the highest amplitude cyclic input located in the time history, which then creates most damage. Based on the visual inspection, a similarity in volumes of the "fattest" loop, between responses from the two roads was observed. This shows that approximately the same plastic deformation will be induced on the material/component when travelling through both R1 and R3 Roads.

5.6 Relative Fatigue Analysis – Sensitivity Analyses

The purpose of relative fatigue analysis in this study is to compare the damage induced in a vehicle being driven over different road sections in the OR test at the investigated PG. In correlating two different vehicle responses, it is essential to perform this type of analysis on the service data to assure not only that the total damage is similar but also that similar events are contributing to this damage. As discussed in Section 5.4.2 of the report, it was shown that the static inputs of both R3 and R1 Road trigger not only similar vehicle responses but also creates similar total damage.

The basis of fatigue analysis performed in Section 5.4.2 of this document is based on several assumed factors. These are:

- amplitude scale factors,
- fatigue stress concentration factor (K_f),
- mean stress correction,
- percent uncertainty of survival,
- filtering the data.

The validity of the fatigue analysis correlation is uncertain depending on how these input variables are defined. It is clear that changing one or a few factors used in the analysis will change the total damage obtained. What is questionable is whether or not the correlation between the damage induced by the two roads will be independent of these changes.

5.6.1 Amplitude Scale Factor Effect

The input load data may be scaled linearly for many reasons. These are:

- conversion of data to appropriate units,
- investigation in variation of load magnitude on the life of a component/system,
- obtaining a predetermined damage in the system/component.

The fatigue analysis of the P1 project data used a scale factor of 30. This factor was determined through iterations to predict a total damage index, i.e. Miner's sum, close to a value of one in all the channels, thus inducing plastic strains in the material behavior. Based on this assumption, a good correlation was established between the damage numbers in the responses from R1 and R3 Roads (see Table 12).

Next, retaining all other variables (see Section 5.4), a fatigue life analysis was performed using multiple scale factors. The scale factors ranged in value from 1 to 45. The result of this inquiry is presented in Figure 31.

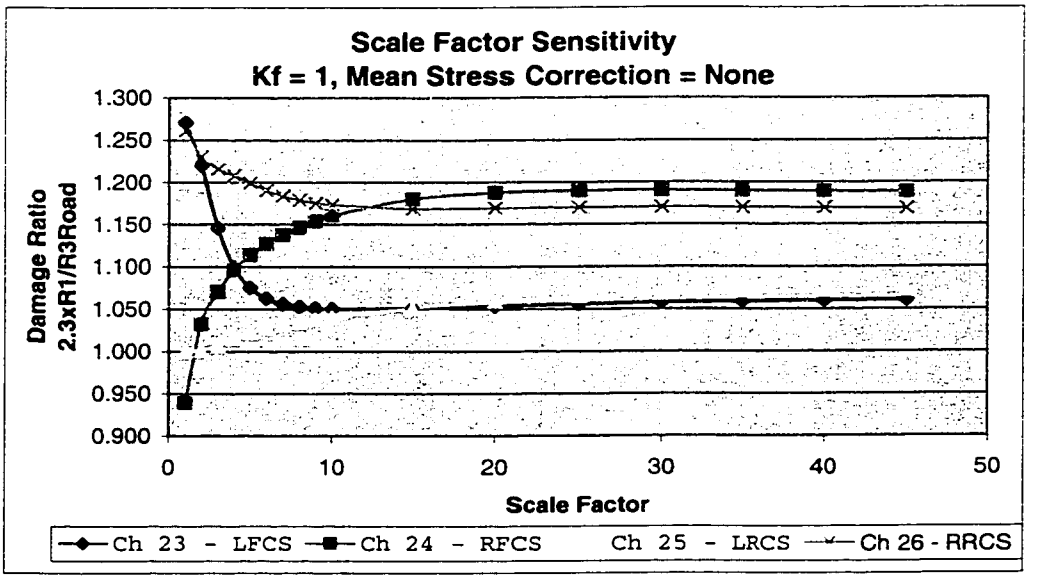

Figure 31. Scale factor sensitivity assessment on correlating the damages in coil springs channels, introduced to a vehicle by 2.3 passes of R1 Road and one pass of R3 Road in P1 test at full rated load.

It is evident that regardless of the scale factor used, the damage number ratio remained in a range from 0.9 to 1.3. This indicates that the damage induced in a vehicle by the two roads: R1 and R3 is similar regardless of the amplitudes of the vehicle responses. Another observation made by looking at Figure 31 is the fact that the damage ratio was more sensitive to changes at smaller loads (scale factor from 1 to 10), especially in the front coil springs. Nevertheless, all scale factors presented a reasonable correlation between the damage resulting from the inputs of the two studied roads. The above outcomes could serve as guidelines in the selection of scale factors for future fatigue analysis correlation studies, and are explored further below.

The durability of automotive components is concerned with low cycle fatigue or LCF (short fatigue lives and large plastic strains). Fatigue analysis of individual road responses (single passes) often does not produce enough damage to move the lives of components into the LCF regime. The signals obtained from the strain gauges are low level unless the parts have been modified to intentionally produce high stress concentration, or if a gauge was intentionally placed exactly at an existing stress concentration if it exists. This poses a problem in the analysis because very low damage numbers (high lives) are calculated and very small changes in strain seem to cause very large variations in damage (life) estimates.

The application of low scale factors may exhibit an elastic behavior in a material. This is particularly evident in Figure 32, which plots hysteresis loops obtained in fatigue analysis of R3 Road, Channel 25 (LRCS) data, using scale factor equal to one. The nature of the stress-strain curve is very linear indicating that minimal plastic strain was imposed on the material.

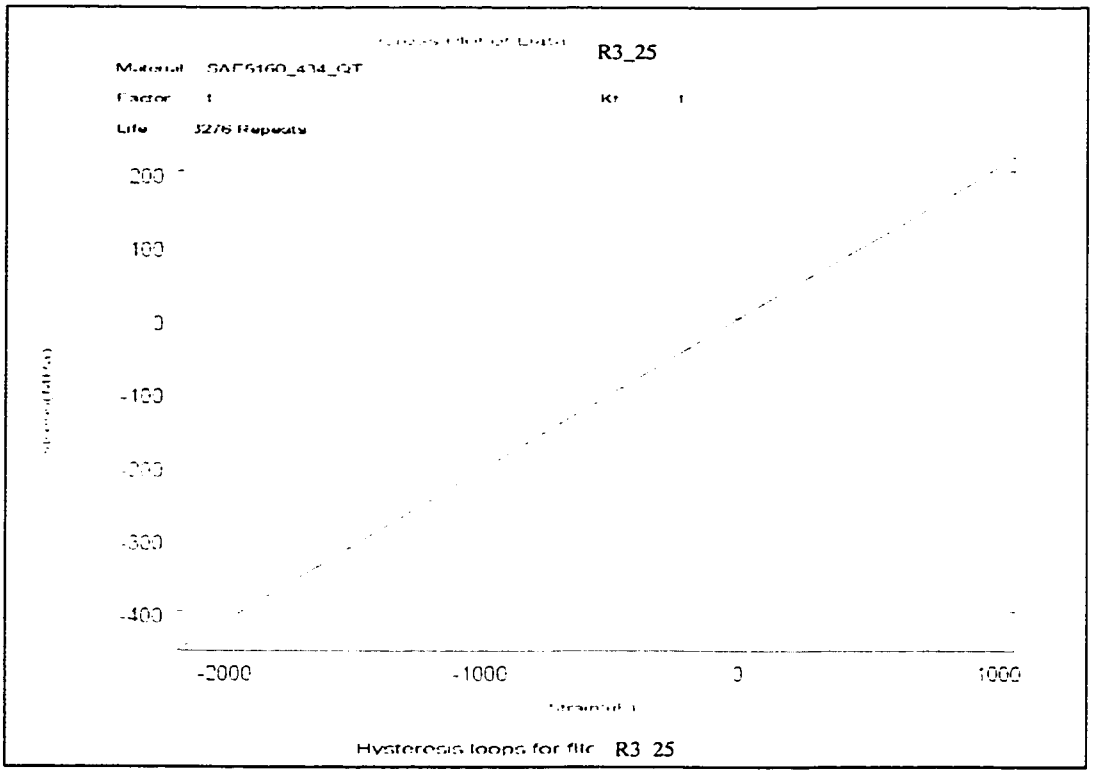

Figure 32. Hysteresis loops for channel 25 of R3 road obtained in fatigue analysis of raw data using strain-life approach, $K_f = 1$, scale factor = 1, and no mean stress correction. Note that the application of low scale factors moves the damage of the component into HCF regime (long lives) and the behavior of the material is almost elastic in nature. This graph illustrates the need to scale the time histories in order to replicate plastic deformations seen throughout the life of a vehicle. Note, this is a hysteresis loop however it is very thin due to a scale factor of 1.0.

There are two ways of assuring that the fatigue damage analysis of single pass responses is in the LCF regime where plastic strains are significant. One way is to increase the amplitude of the strain load (Figure 33), and the other is to increase the fatigue stress concentration factor (K_f) (Figure 34). The effect of K_f will be discussed further in the next section.

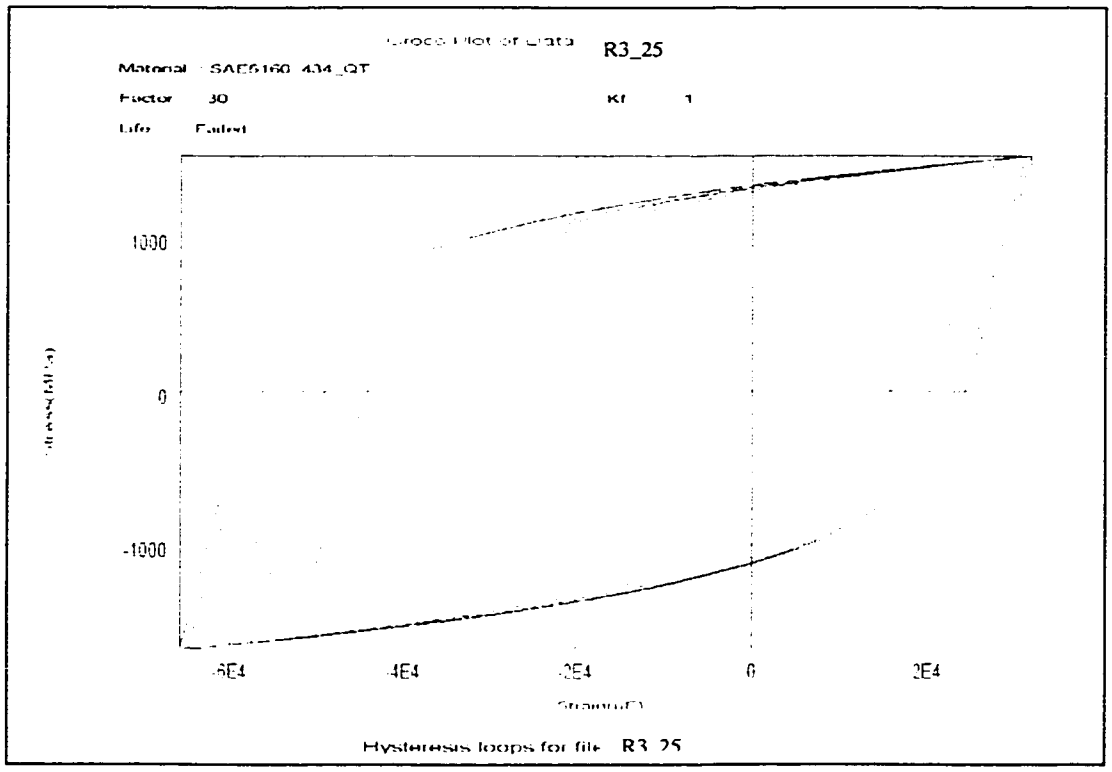

Figure 33. Hysteresis loops for channel 25 of R3 road obtained in fatigue analysis of raw data using strain-life approach, K_f = 1, scale factor = 30 and no mean stress correction. Note that the application of high scale factors moves the damage of the component into LCF regime (short lives) and induces plastic strains in the material.

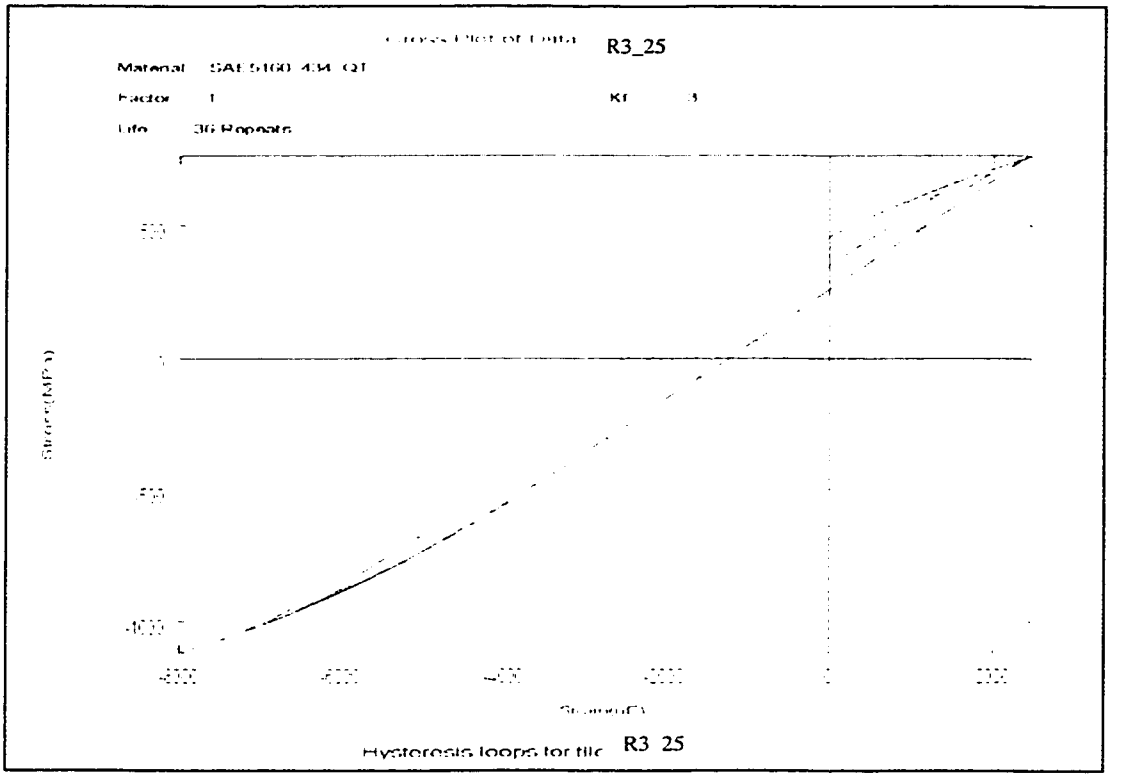

Figure 34. Hysteresis loops for channel 25 of R3 road obtained in fatigue analysis of raw data using strain-life approach, K_f = 3, scale factor = 1, and no mean stress correction. Note that increasing K_f increases the plastic strains in the material and moves the life of the component into LCF regime.

As mentioned in Section 5.5, the area inside of the hysteresis loop represents the energy per unit volume dissipated during a cycle. It also represents the plastic deformation work done on the material. Figures 33 and 34 clearly show that increasing amplitude scale factor and/or K_f will increase the amount of plastic deformation in the material. During durability tests, in the laboratory conditions, running multiple passes of different road responses on road test simulator assures that low cycle fatigue regime will dominate the fatigue of the components.

5.6.2 Fatigue Stress Concentration Factor

All engineering components contain some geometric or material stress risers. These discontinuities are sources of maximum local stresses, which are far greater than the

nominal stresses in the component. In perfectly elastic members, a stress concentration factor (Kt) can be defined as ratio of local maximum stress to nominal stress. As long as the material remains in the elastic ranges, the Kt value will remain constant. As soon as the material begins to yield however, this relationship no longer holds. Instead, the nominal and local values are related in terms of stress and strain concentration factors [22, 23]. This is demonstrated in equations 12 and 13.

$$K_\sigma = \frac{\sigma}{S} \text{ and } K_\varepsilon = \frac{\varepsilon}{e} \text{ for } \sigma > \sigma_y \quad \text{.....(12)}$$

$$K_t = \sqrt{K_\sigma K_\varepsilon} \text{ or } K_t^2 Se = \sigma\varepsilon \quad \text{.....(13)}$$

where:

K_σ and K_ε - stress and strain concentration factors

σ and S - local and nominal stress range

ε and e - local and nominal strain range

This relationship between the theoretical stress concentration factor (K_t) expressed as a geometric mean of the stress and strain concentration is referred to as Neuber's rule.

Kt factor is solely dependent on the geometry. Other factors such as absolute size and material properties must be defined separately through fatigue stress concentration factor K_f [23]. One of the methods proposed by Neuber defines Kf as follow:

$$K_f = 1 + \frac{K_t - 1}{1 + \sqrt{\frac{\rho}{r}}} \quad \text{.....(14)}$$

where:

ρ - material constant (related to grain size of the material and its strength)

r - radius at the root of the notch

Since in fatigue small notches have less effect than that indicated by K_t, it has been proposed to replace K_t in Neuber's rule by K_f (K_f values are less than K_t) [33].

The K_f value is dependent on two factors: material properties and notch size. The dependence of K_f on material properties deals with the fact that soft (ductile) materials will begin to yield at the notch, thus never reaching the stress levels predicted by K_t. Hard brittle materials on the other hand will experience the full effect of the K_t factor. The K_f value is also dependent on the size of the notch. As the size of the notch increases, the volume of the stressed material around it increases thus causing a decrease in predicted life.

Initial fatigue analysis in the present study assumed a K_f factor to have a value of one. Figures 35 to 38 show the effects of increasing the K_f factor on the predicted damage ratio. This analysis was conducted on the unfiltered (raw) data using strain-life approach, multiple scale factors (Section 5.6.1) and assuming no mean stress correction factors.

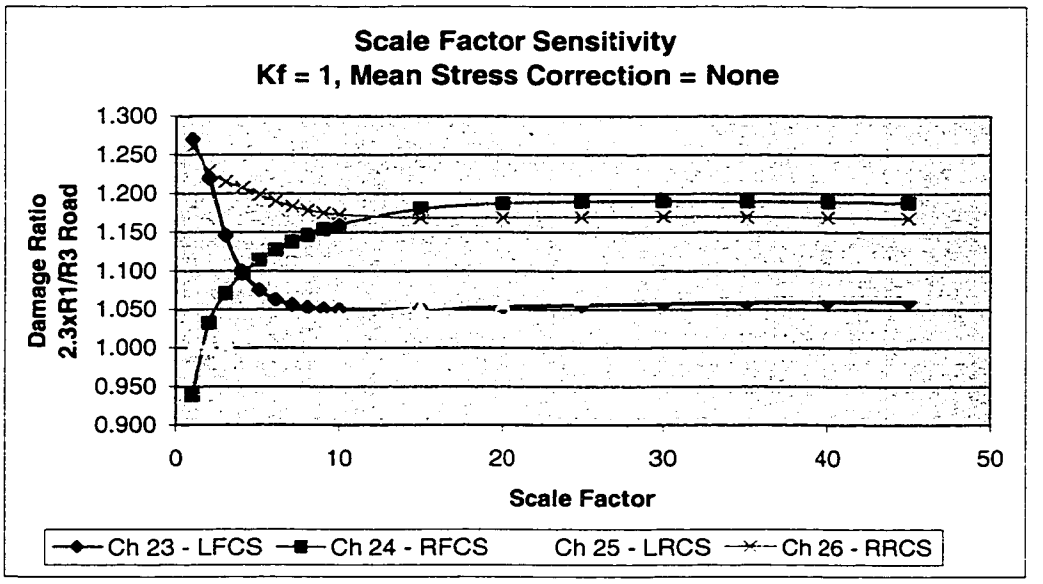

Figure 35. Scale factor sensitivity assessment on correlating the damages in coil springs channels, introduced to a vehicle by 2.3 passes of R1 Road and one pass of R3 Road in P1 test at full rated load. Among the parameters listed in Section 5.4, the following were used: $K_f = 1$, unfiltered data, and no mean stress correction factor.

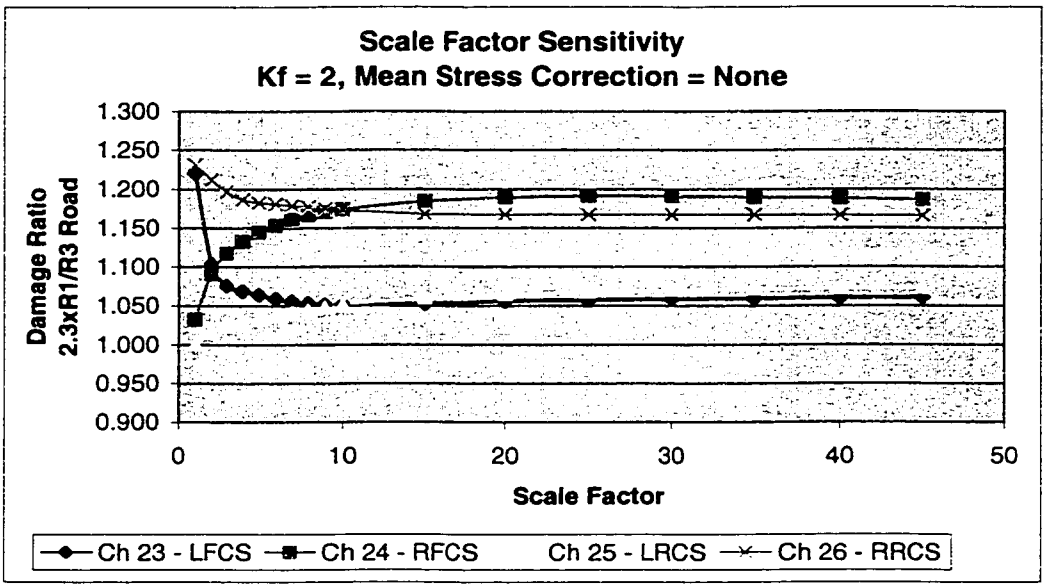

Figure 36. Scale factor sensitivity assessment on correlating the damages in coil springs channels, introduced to a vehicle by 2.3 passes of R1 Road and one pass of R3 Road in P1 test at full rated load. Among the parameters listed in Section 5.4, the following were used: $K_f = 2$, unfiltered data, and no mean stress correction factor.

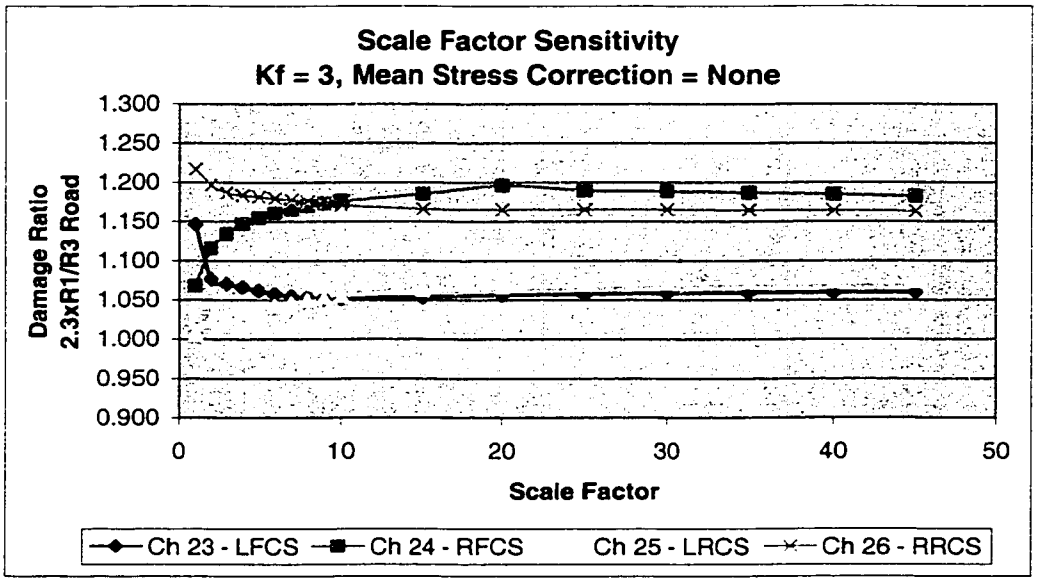

Figure 37. Scale factor sensitivity assessment on correlating the damages in coil springs channels, introduced to a vehicle by 2.3 passes of R1 Road and one pass of R3 Road in P1 test at full rated load. Among the parameters listed in Section 5.4, the following were used: $K_f = 3$, unfiltered data, and no mean stress correction factor.

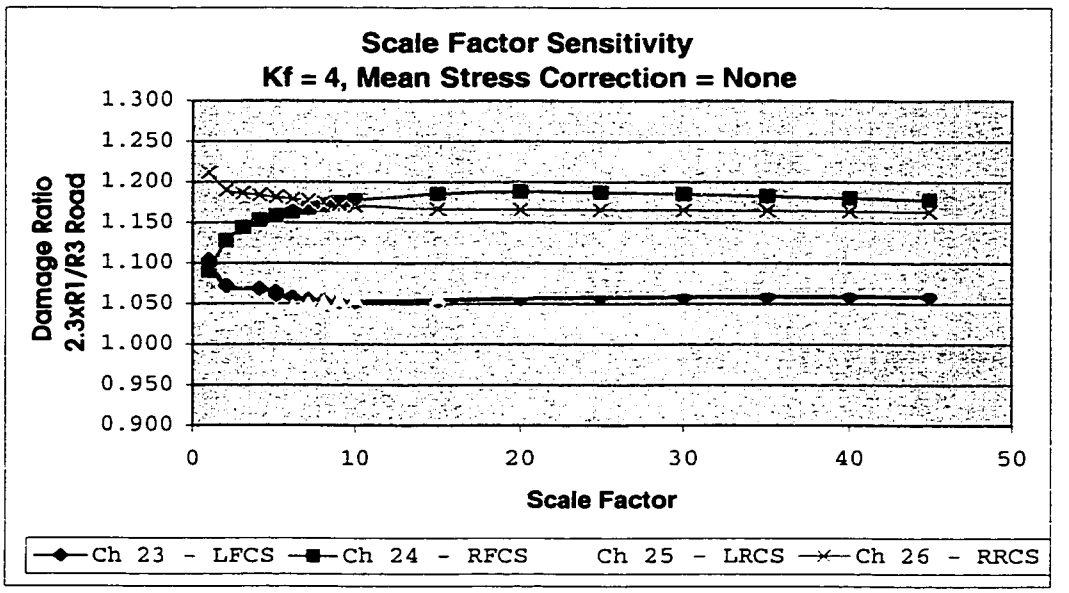

Figure 38. Scale factor sensitivity assessment on correlating the damages in coil springs channels, introduced to a vehicle by 2.3 passes of R1 Road and one pass of R3 Road in P1 test at full rated load. Among the parameters listed in Section 5.4, the following were used: $K_f = 4$, unfiltered data, and no mean stress correction factor.

It is evident in Figures 35 to 38 that all scale factors produced reasonable correlation between the calculated damages. The damage ratios were most sensitive to changes at low amplitudes (scale factors from 1 to 10). This sensitivity was most evident in front coil springs. As the K_f factor increased, the sensitivity at low amplitudes decreased (especially for the front coil spring channels). Increasing the K_f value at high loads (high scale factors) presented no evident changes in damage ratios. Thus inducing very large plastic strains produces enough damage in the material that the notch size no longer has a significant effect on fatigue results.

The sensitivity analysis based on scale factor and fatigue stress concentration effect showed that most representative results were obtained at:

- larger scale factors (in this case on the order of 10 and above, but will vary depending on units of scale, or full scale of measurement), and
- larger K_f factors ($K_f = 3$ and $K_f = 4$).

There is a limit, however, on the value of K_f. The empirical predictions of K_f show that it is only slightly smaller than the K_t value, for all values of K_t. Experimental studies however prove that the limiting value on the order of 5 to 6 (depending on material) is exhibited by K_f factors [23]. For example, hardened steel, wrought aluminum and magnesium exhibit a maximum value of K_f equal to 4, while annealed steel, and cast aluminum have a maximum K_f value equal to 3 [22]. Researchers have explained this behavior through two possibilities. The first one presumes that the limit posed by K_f is a result of blunting around the notch due to yielding. Yielding at a notch root reduces the peak stress from the value predicted by Kt. The "blunting effect" is not observed in very high strength steels. The other possibility suggests that this behavior is the result of initiation-propagation effects. For less severe notches (small Kt) the total life is dominated by crack initiation (HCF), while for more severe notches the life is spent at propagation (LCF) [9]. Therefore:

- if K_t value is small (approximately $K_t \leq 5$) then $K_t \approx K_f$, and for this notch most of the life is spent at crack initiation. Use of K_f has small influence on life.[22];
- if K_t value is large then K_f no longer equals the K_t, but reaches its maximum value ($K_f < K_t$). For this notch most of life is spent at crack propagation, and use of K_f greatly increases the predicted life [22].

The strain life method only accounts for initiation life, and cannot be used to predict propagation. Since however the automotive application is only interested in the crack initiation stage where plastic strains are significant, this approach of performing fatigue analysis is most meaningful.

In conclusion, assuming a fatigue stress concentration factor (K_f) to have a value between 3 to 5 (depending on material) seems most reasonable since it is a limiting value of K_f that moves the life of a component from HCF to LCF.

5.6.3 Mean Stress Correction

The cyclic properties of materials are obtained in laboratory conditions with fully reversed, constant amplitude strain-controlled tests. In actual use, components will rarely encounter this type of loading. Vehicle responses collected on proving grounds will exhibit some mean stresses and mean strains.

According to "Fundamentals of Metal Fatigue" by Bannantine et al. [23], mean strains affect fatigue lives of components minimally. The mean stresses will however have a significant effect on the fatigue life. The effect of mean stresses is observed predominately at longer lives.

At long lives, compressive mean stresses increase fatigue life, while tensile mean stresses will decrease the fatigue life. At short lives (high strain amplitudes), very little effect is induced on the life of a component as a result of mean stress relaxation. This is because in cyclically stable materials, the mean stress will tend toward zero upon continued cycling. It should be noted that tensile mean strains could also cause reduction in fatigue life, however the effects of mean strains is weak when the mean stress relaxes quickly. The rate of relaxation depends on the material and strain amplitude. The higher the strain amplitude the higher the relaxation rate, thus smaller effects of both mean strains and stresses. Since automotive testing involves imposing large plastic strains on components (short lives), the effect of mean stresses and strains should not be significant on the results of fatigue analysis.

The advantage of using the strain-life method in fatigue analysis also demonstrates benefits that could prove to be efficient in dealing with sequence effects. They are:

- ability to handle over-strain effects, and
- ability to deal with local mean stress effects.

In addition to mean stresses resulting from applied loads, over-strain effects may also play an influential effect on fatigue life prediction. Periodic tensile overloads cause compressive residual stresses in the material at the notch roots. The compressive residual stress has the same effect on the life of the material as an externally applied compressive mean stress of the same magnitude. Thus both externally applied mean stresses and residual stresses are accounted for in using the strain life method.

It has been established that materials undergoing variable amplitude load spectra lose their endurance limit property. This is mostly due to periodic overloads in the time history. Thus the use of endurance limits for variable amplitude history (with stress events greater than the endurance limit) is questionable. The strain-life method not only will account for the residual stresses but it also assumes that the endurance limit does not exist. This makes the strain-life method conservative enough to deal with periodic overloads, and mean stresses.

A sensitivity study was conducted on the raw data to establish the effect of using mean stress correction factor in damage ratio comparison of the two responses. Two methods of mean stress correction were utilized. These were the Morrow method and Smith-Watson-Topper method. A brief explanation of the two procedures follows.

The total strain is the sum of plastic and elastic components as shown in equation 10, and repeated below:

$$\frac{\Delta\varepsilon}{2} = \frac{\sigma_f'}{E}(2N_f)^b + \varepsilon_f'(2N_f)^c \quad \text{.....(10)}$$

The first term in the strain-life relation constitutes an elastic component while the second term refers to the plastic term. At large strain amplitudes the total strain-life curve approaches the plastic line, and at low amplitudes the elastic line.

In the first method of mean stress correction, Morrow suggested to correct the strain-life relation by modifying the elastic term with mean stress (σ_o) [23]. Thus the Morrow mean stress correction could be written as:

$$\frac{\Delta\varepsilon}{2} = \frac{\sigma_f' - \sigma_o}{E}(2N_f)^b + \varepsilon_f'(2N_f)^c \quad \text{.....(15)}$$

Although this method correctly predicts that the mean stress effect is only significant at low plastic strains, it incorrectly predicts that the ratio of elastic to plastic strain is independent of the mean stress.

The Smith-Watson-Topper (S-W-T) mean stress corrected strain-life curve [23] is defined as:

$$\sigma_{max}\frac{\Delta\varepsilon}{2} = \frac{(\sigma_f')^2}{E}(2N_f)^{2b} + \sigma_f'\varepsilon_f'(2N_f)^{b+c} \quad \text{.....(16)}$$

where:

$$\sigma_{max} = \frac{\Delta\sigma}{2} + \sigma_o \quad \text{.....(17)}$$

The S-W-T method predicts that the square root of the product of maximum stress and the total strain range is proportional to cycles to failure. It however becomes undefined when the maximum stress is zero or negative. S-W-T correction method assumes that no damage is done at zero or negative stresses which is not necessarily true.

In comparison, S-W-T is more conservative in nature when the loading is tensile in nature, while Morrow's method predicts more realistic results when the loading is mostly in compression. Application of mean stress corrections on results of fatigue correlation of R1 and R3 roads will be discussed below.

The original fatigue analysis was conducted on unfiltered data using strain-life approach, a K_f factor equal to one, the amplitude scale factor of 30 and applying no mean stress correction. While retaining the K_f factor and the scale factor, both Morrow and SWT

correction methods were applied to study the effects on fatigue damage ratios. The results of this analysis are presented in Figure 39.

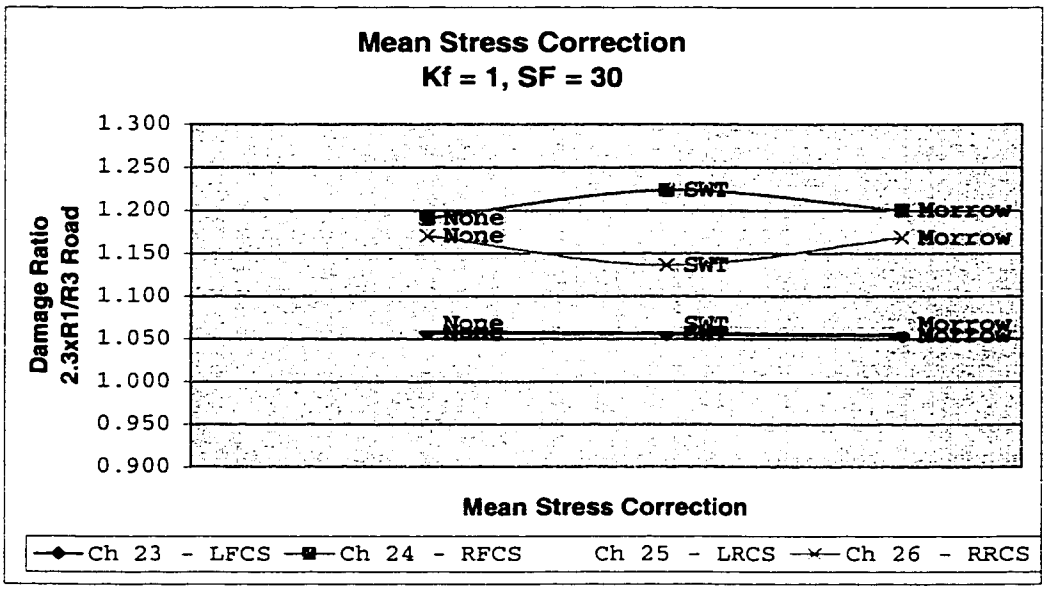

Figure 39. Effect of applying mean stress correction factor on the fatigue damage ratios (2.3 passes of R1 road to one pass of R3 road). Fatigue analysis was obtained using unfiltered data, strain-life approach, $K_f = 1$ and scale factor = 30. This figure illustrates that at high strain amplitudes, mean stress correction does not play a significant role.

It is evident that applying a mean stress correction (both SWT and Morrow) has little effect on the results of damage ratios at high plastic strains (scale factor = 30). Figures 40 and 41 investigate the sensitivity of correlating damage values at lower scale factors (10 and 1 respectively) while applying mean stress corrections.

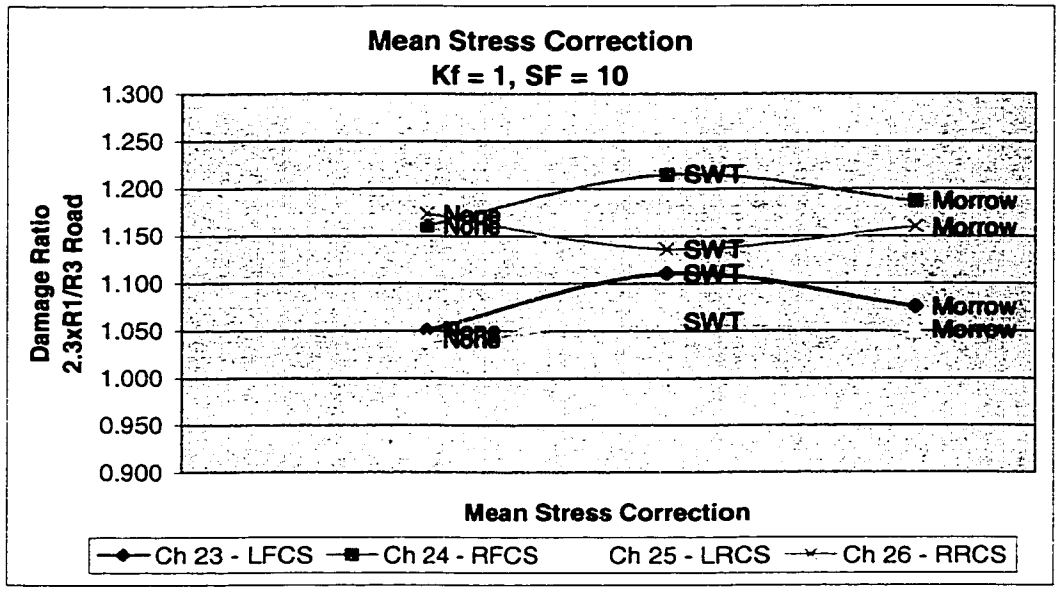

Figure 40. Effects of applying mean stress correction factor on the fatigue damage ratios (2.3 passes of R1 road to one pass of R3 road). Fatigue analysis was obtained using unfiltered data, strain-life approach, $K_f = 1$, and scale factor = 10. The effect of mean stress correction is more significant at lower strain amplitudes.

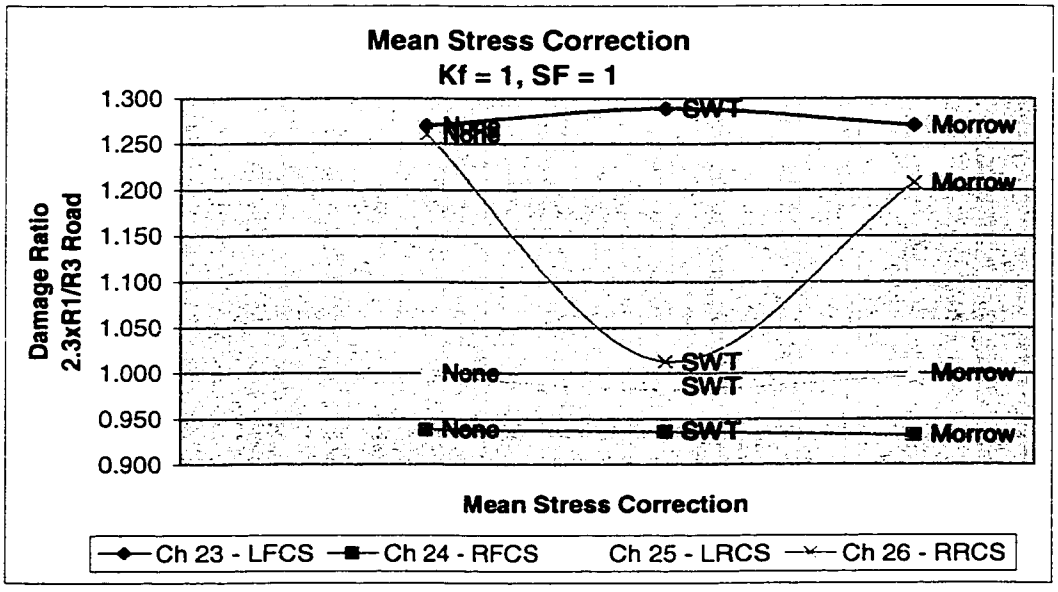

Figure 41. Effects of applying mean stress correction factor on fatigue damage ratios (2.3 passes of R1 road to one pass of R3 road). Fatigue analysis was obtained using unfiltered data, strain-life approach, $K_f = 1$ and scale factor = 1. The effect of mean stress correction is most significant at low strain amplitudes.

Figures 39 to 41 indicate that as long as there are significant plastic strains introduced to the material, the consequence of mean stress correction will not be substantial. This relates to both methods of correction. When the behavior is mostly elastic (low scale factors), the effect of mean stresses is expected to be more significant. In addition, Figures 39 to 41 show that the Morrow method of correction is less sensitive to scale factors than the SWT method.

Figure 41 illustrates the concept of applying mean stress correction at low plastic strains. It was shown in Figure 32 that when fatigue analysis was conducted using a scale factor equal to one, the stress-strain relationship was very linear in nature. This indicates minimal plastic strain induced in the material; thus it is expected that the effect of the mean stresses will be considerable on the fatigue damage analysis.

Another observation was made while analyzing Figure 41, where applied loads did not produce sufficient damage to induce plastic strains. It was noted that although damage ratios relating R1 and R3 road remained between 0.9 to 1.3, signifying a satisfactory correlation, the effects of SWT mean stress correction affected the right rear coil spring channel (Ch. 26) more drastically than other channels of data. This requires further investigation.

There are two factors that affect how sensitive the fatigue damage analysis will be to the SWT mean stress correction. The first factor deals with the amount of plastic deformation in the material. The smaller the loads, the less plastic strain will be induced in the material, and the more effect mean stresses will have on the life prediction. The second factor deals with the nature of the data itself. The SWT correction is recommended for use when the data is tensile in nature, while the Morrow mean stress correction gives better results when the mean of data is compressive [23].

The data obtained for channel 26 (right rear coil spring) exhibited both characteristics which would make it sensitive to SWT correction. These were both low amplitudes (at

scale factor of unity) and compressive mean stress. This is demonstrated in Figures 42 through 51.

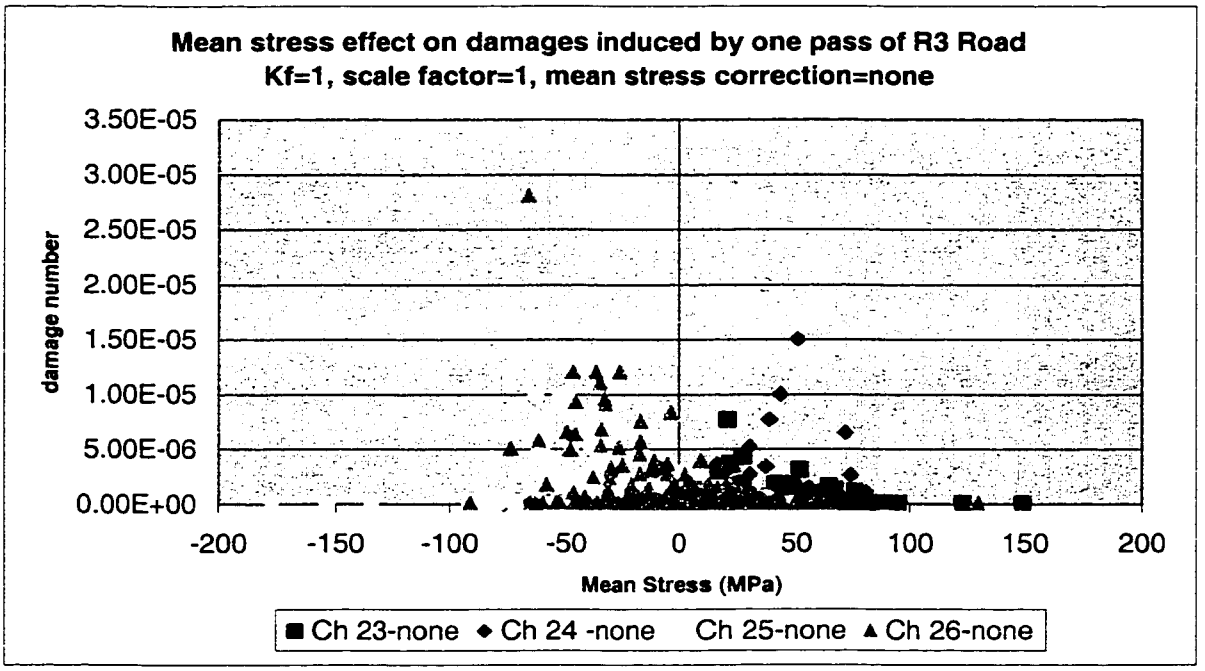

Figure 42. Mean stress effect on damage induced by one pass of R3 Road. Fatigue analysis method used $K_f = 1$, scale factor = 1, and no mean stress correction. Only channels 25 and 26 exhibit compressive mean stresses, thus are more prone to be influenced by the S-W-T mean stress correction.

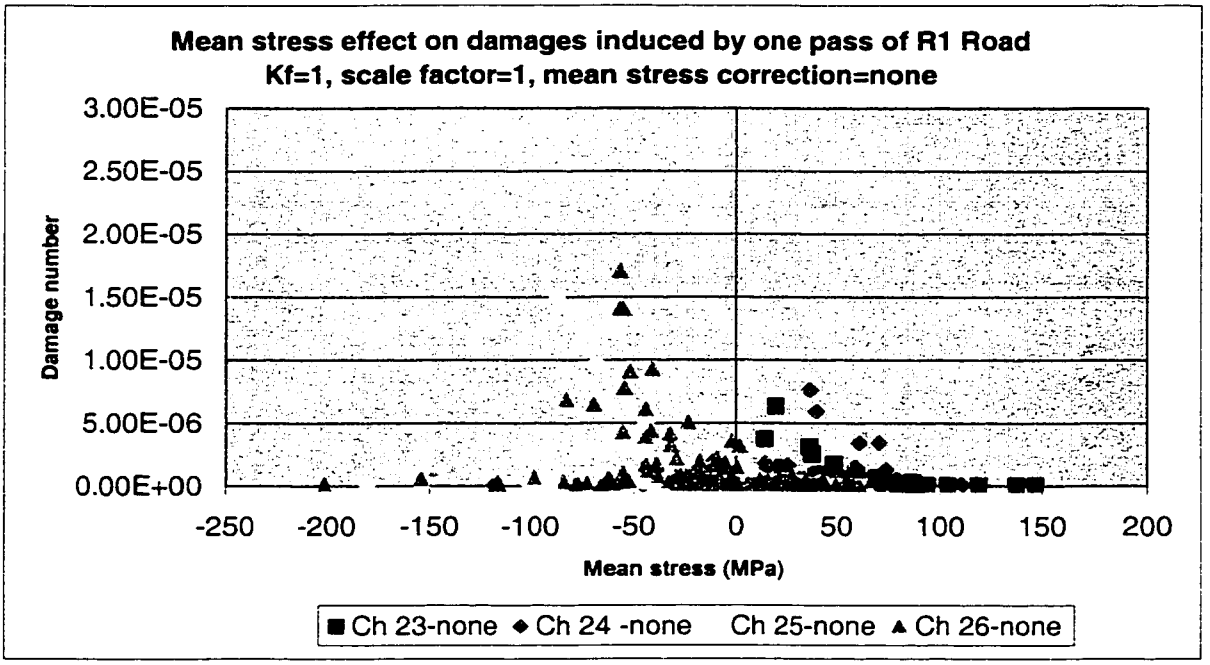

Figure 43. Mean stress effect on damage induced by one pass of R1 Road. Fatigue analysis method used K_f = 1, scale factor = 1, and no mean stress correction. Only channels 25 and 26 exhibit compressive mean stresses, thus are more prone to be influenced by the S-W-T mean stress correction.

Investigation of Figures 42 (one pass of R3 road) and Figure 43 (one pass of R1 road) shows that for both channels 25 and 26 the majority of the damage is contained in a compressive zone. Since the value of cycle ranges for channel 26, for both roads however were slightly lower (see Figures 44 and 45), the data was more sensitive to the SWT mean stress correction.

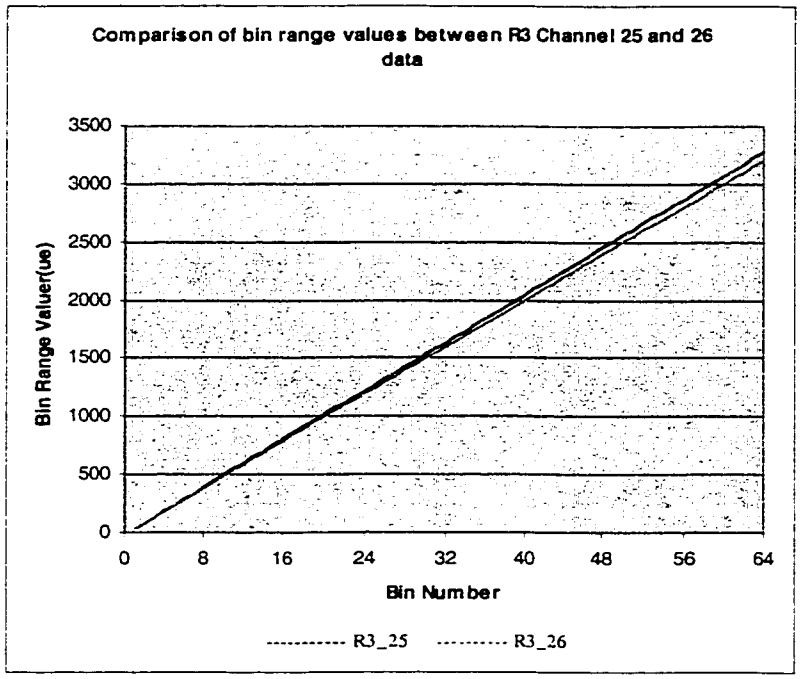

Figure 44. Range bin values for R3 Road channel 25 and 26 data. The bin values (strain ranges) for Channel 26 data (magenta) appear lower than those of Channel 25 data (navy). The lower range values of channel 26 data make it more sensitive to the SWT mean stress correction.

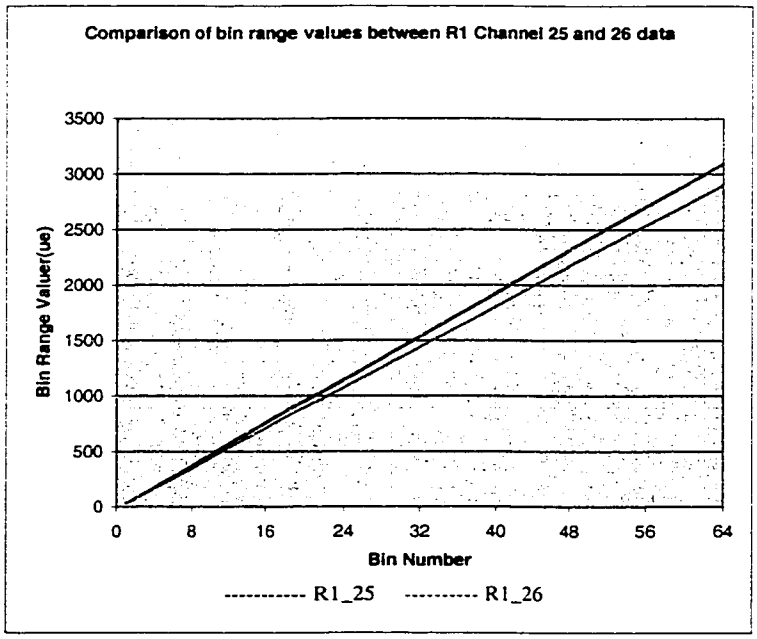

Figure 45. Range bin values for R1 Road channel 25 and 26 data. The bin values (strain ranges) for Channel 26 data (magenta) appear lower than those of Channel 25 data (navy). The lower range values of channel 26 data make it more sensitive to the SWT mean stress correction.

It is often recommended to use mean stress correction while performing fatigue analysis especially if any uncertain in whether the load amplitudes create enough damage to cause plastic strain. It should be kept in mind however that:

- mean stress correction is mostly significant at low plastic strains (HCF),
- SWT correction is more conservative for tensile mean stresses, while Morrow correction for compressive stresses, and most importantly that
- in performing a correlation of fatigue damage, **it is most important to remain consistent** in making the assumptions, thus if the mean stress correction method is used it should be applied to all of the data, at all times.

5.6.4 Percent Uncertainty of Survival

Percent uncertainty of survival is defined as the probability that a component will achieve a desired life. Knowledge of standard errors, associated with regression analyses performed to determine the fatigue parameters, is required in order to study how the elastic and plastic life components deviate from the mean value. The mean value guarantees that the tested component will have a probability of at least 50%, of survival.

The strain-life curve presented in equation 10, can be represented statistically as [23]:

$$\frac{\Delta\varepsilon}{2} = \frac{\sigma_f'}{E}(2N_f)^b \cdot 10^{qe} + \varepsilon_f'(2N_f)^c \cdot 10^{qp} \quad \text{.....(18)}$$

where:

$\Delta\varepsilon$ - total strain range

$2N_f$ - reversals to failure

σ_f' - fatigue strength coefficient

ε_f' - fatigue ductility coefficient

E - modulus of elasticity

c - fatigue ductility exponent

b - fatigue strength exponent (Basquin's exponent)

q - number of standard errors from the mean life

e - standard error of 2Nf for elastic life line

p - standard error of 2Nf for plastic life line

A default value of 50% chance of survival was assumed for all of the fatigue analyses performed. The effect of selecting other values for percent of survival on fatigue damage correlation of R1 and R3 road is investigated in this section.

Multiple factors of survival certainty ranging from 0 to 100 percent were selected for the analysis. Material parameters were altered for the analysis by assuming standard error deviations of log(e) for plastic and elastic life line, as well as for cyclic stress strain curve to be 0.5. The results for channel 25 data (strain-life approach, $K_f = 1$, SF = 30, no mean stress correction) are presented in Figure 46.

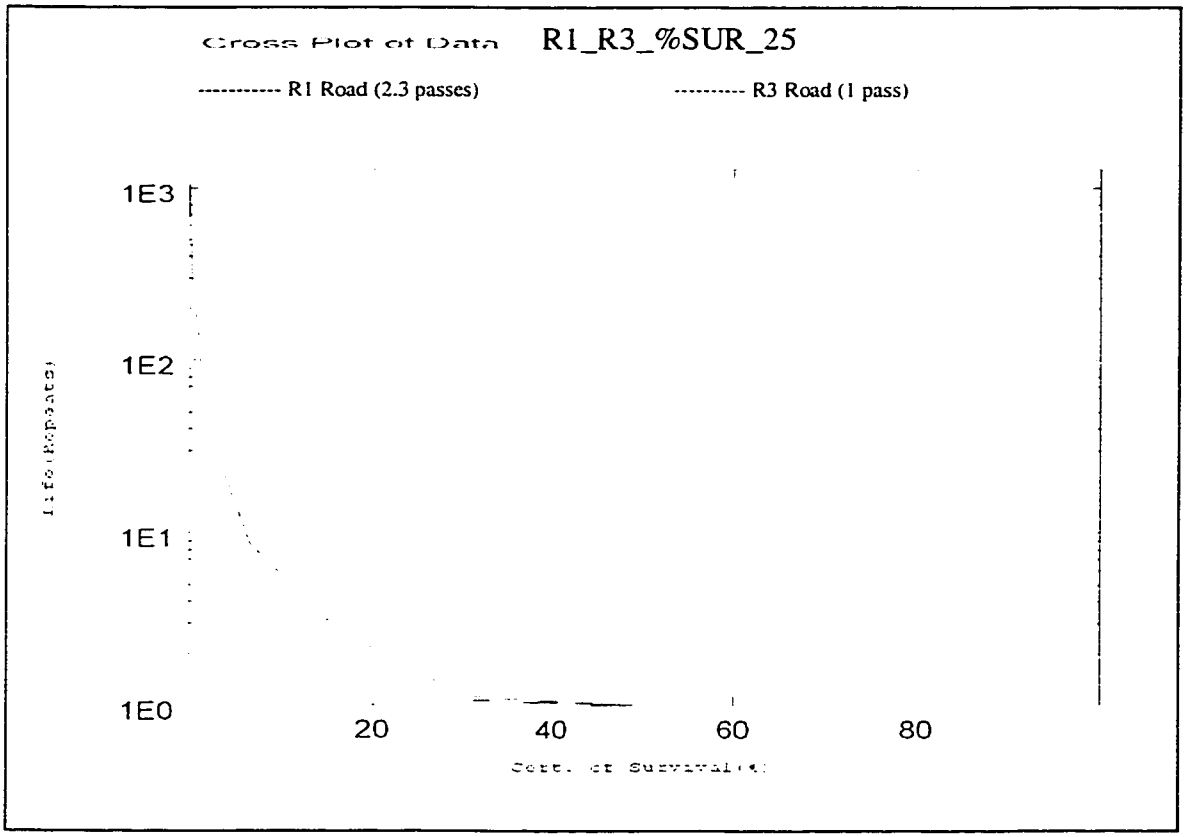

Figure 46. Effect of changing the % uncertainty of survival on life prediction of 2.3 passes of R1 road (brown) and one pass of R3 Road (magenta) (assuming standard errors to be 0.5) for channel 25 data.

It is clear that increasing the certainty of survival dramatically reduced the life of a component. Figure 46, as well as the results of other channels, shows that the life curves

of 2.3 passes of R1 road and one pass of R3 road change in the same fashion. Thus, the percent uncertainty of survival parameter does not play a big effect in correlating the data of the R1 and R3 roads.

5.6.5 Filtering the Data

One important tool of data reduction is filtering. Through its application, it is possible to isolate the signals of significance from noise or other masking frequencies. Four types of filters exist. They are low pass, high pass, band pass and band reject filters.

The use of filtering plays a great importance when collecting and analyzing data for vehicle durability assessment. Sampling criteria has been established that prevents aliasing in data acquisition. Aliasing is defined as a phenomenon that causes high frequency information to appear as low frequency due to insufficient sampling rate, and is demonstrated in Figure 5 in chapter 2.2.3. As a result anti-aliasing filters (low pass filters) are applied before the signal is sampled to attenuate or eliminate the frequencies of the original spectrum, which extend beyond the frequency of interest.

Two sampling criteria have been defined. In frequency analysis it is often appropriate to use the Nyquist or Shannon sampling theorems which state that the sample rate should be about twice the highest frequency (Nyquist frequency). This method used by frequency analysts uses averaging techniques, which only report the RMS value of amplitudes and discards the sequence of amplitudes. Although this sampling procedure provides high statistical confidence levels, it is not sufficient for fatigue analyses where both accurate amplitudes of peaks and valleys and/or sequence effects are important [34].

As a result, Donaldson [34] established a new method of sampling based on error in peak levels. Donaldson defines the error in peak resolution of a sinusoid as a function of the ratio of data frequency to sample frequency. That is:

$$Pk_{err} = 2\sin^2(\frac{\pi f_d}{2f_s}) \quad \text{.....(19)}$$

where:

Pk_{err} - percent error on peaks/100

f_d - data frequency

f_s - sampling frequency

According to the above theorem, allowing five percent error in amplitudes requires for the data to be sampled at least 10 times the highest frequency of interest. In the ground vehicle simulation the road data is usually collected at 409.6 Hz (which may vary from company to company). Before the road data is digitized, it passes through a programmable low pass analog filter at 40% the sampling rate (80% of the Nyquist frequency), internal to MEGADAC 6510DC acquisition system. When running simulations, the data of interest is below 50 Hz. Thus the road data (input/desired data) may further be filtered to capture only the frequencies of interest (0.2 Hz to 50 Hz).

The analog signal from the MTS rig (output/response data) is collected at a high frequency of 4096 Hz. Before digitization, the signal is first passed through a 400 Hz, 3 pole Bessel low pass analog filter (internal to the MTS Model 498 rig). The standard sampling rate for RPC is 409.6 Hz. Before the digitized signal is down-sampled to that rate, RPC digitally filters the data at 40% the sampling rate, or 163.8 Hz. This ensures that both the desired (road data) and response (output the MTS rig) signals are sampled at the same rate.

When developing drive files for the RTS rigs, the data is filtered through a band pass filter to capture only frequencies between 0.2 to 50 Hz on average. This poses a question whether fatigue analyses should be performed on raw (unfiltered data), low pass filtered data (0.2 Hz and above) or band pass filtered data (0.2 Hz – 50 Hz).

Fatigue damage calculations have been performed on unfiltered data (0 – 204.8 Hz), low-pass filtered data (0.2–204.8 Hz and 0.4-204.8 Hz) and high-pass filtered data (0-50 Hz) to establish the damage content in those frequency ranges. All fatigue analyses were

performed using initial assumptions (strain-life approach, scale factor = 30, K_f = 1, no mean stress correction). Data filtering was performed using the nSoft "Fast Fourier-Filtering" module which creates a finite impulse response (FIR) filter.

Fatigue analyses showed that removing frequency contents below 0.4 Hz eliminates only 2% or less of the total damage. The same can be said about frequencies above 50 Hz. The overall effects of filtering the data on damage ratios of R1 and R3 roads were minimal. This is clearly shown in Figure 47.

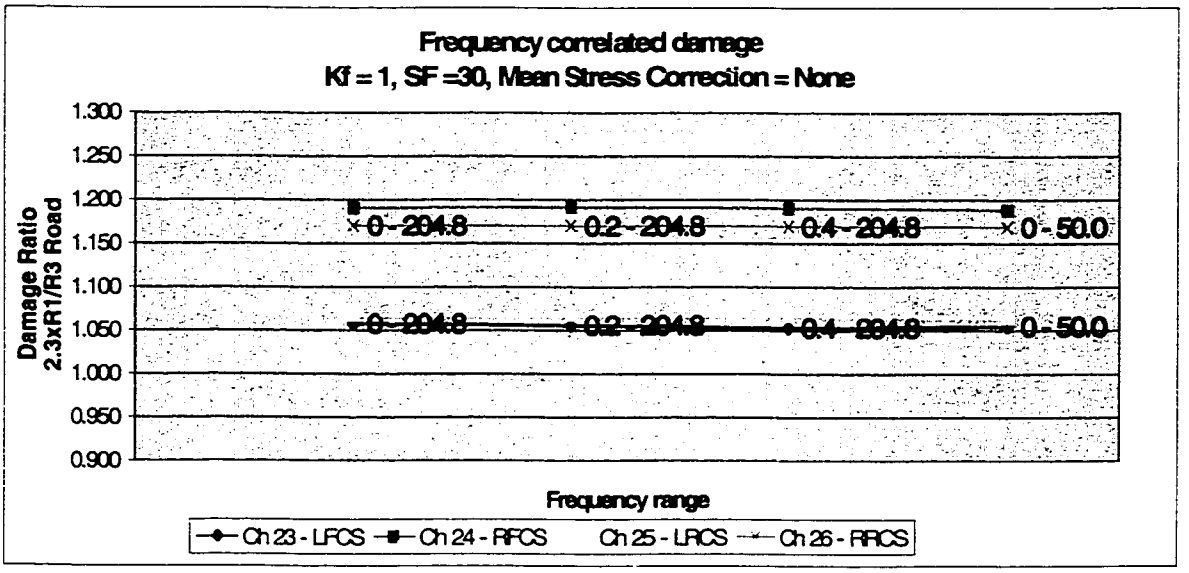

Figure 47. Effects of filtering data on damage ratio analysis of R1 road (2.3 passes) and R3 Road (1 pass). Four cases of filtering data were investigated: 0-204.8 Hz (raw data), 0.2-204.8 Hz, 0.4-204.8 Hz and 0-50 Hz. Less than 2% of total damage content was removed by filtering data in each case. Very little effect was imposed on the correlation of damage ratios between the two roads.

The above life prediction calculations show that filtering the data, although removing some damage content (less than 2%), has very little effect on correlating the road-to-road responses. This further verifies that both the frequency and damage distributions of the R1 and R3 roads are similar in nature.

6 SUMMARY OF RESULTS

6.1 Project #P1 at Full Rated Load

The method of data analysis, described in detail in Chapter 5, was developed to analyze vehicle responses from two different roads. Based on that method, the intent then was to determine whether or not the two different roads produce similar vehicle responses in the vehicle. Chapter 5 of this study only demonstrates the procedure on the unfiltered (raw) data collected from project #P1 at full rated load, for two roads, R1 and R3. The same procedure was carried out on the remaining road sections included in the OR test, as demonstrated in Table 13.

Road	R1	R2	R3	R4	R5	R6	R7	R8	R9	R10
R1										
R2	X									
R3	X	X								
R4	X	X	X							
R5	X	X	X	X						
R6	X	X	X	X	X					
R7	X	X	X	X	X	X				
R8	X	X	X	X	X	X	X			
R9	X	X	X	X	X	X	X	X		
R10	X	X	X	X	X	X	X	X	X	

Table 13. Possible road combinations necessary in the study of "Feasibility of road substitution for off-road test on the Proving Grounds (PG)".

Once the unfiltered data from project #P1 collected at full rated load has been analyzed for all road combinations, roads inducing similar vehicle responses have been grouped together. The results of the analysis show that the PG OR test could be simplified by grouping the roads in the following manner:

Group 1: R1, R2, R3, R4 and R5
Group 2: R6 and R7
Group 3: R10
Group 4: R8
Group 5: R9

More detail verification of the road groupings will be discussed next.

As presented in Chapter 5, the first form of analysis was based on visual inspection of the time histories for any trends, offsets or drifts. If the data did not appear to significantly exhibit any of the above mentioned forms of interference, the analysis was carried out on raw data (as in project P1 full rated load data). Otherwise, the time histories would have to be passed through a high pass filter at 0.2 Hz.

The next step was to perform a statistical analysis on all combination of roads. This analysis proved to be not a very efficient method of characterizing the similarities/differences in vehicle responses, due to the variability of factors associated with the data acquisition itself. Although the roads that were later verified to be similar in nature usually exhibited smaller averaged values of percent differences (less than 20%), the errors varied from channel to channel, and from test to test. Factors such as type of driver and his/her driving conduct, weather, vehicle degradation, tire pressure, or vehicle speed, surely affect the statistical values of the data. Most importantly, the randomness and dynamic nature of the roads themselves allow for significant errors to be obtained with each run over the same test track. Large global maxima or minima could be obtained if a driver drives over a significant road input that could be totally missed on the second test run. The speed at which the vehicle was operated while travelling through that input could also significantly raise/decrease the amplitudes of the measured signals.

An example of statistical analysis is shown in Figure 48 for Group 1 project #P1 data collected at full rated load. In this figure R2, R3, R4 and R5 roads are compared to R1 road (selected arbitrarily). It can be observed that on average the percent differences in maximum, minimum, RMS and standard deviation values were less than 20%. Some data channels however, presented some differences that are much higher than the average values, which is expected from such random road inputs. In comparison Figure 49 shows a statistical analysis between two roads, R1 and R10, which were found to be very distinct in nature. Once again, the percent differences, obtained from individual channels, deviated greatly from the averaged values. The differences however were exceptionally high, thus it could be assumed that these two roads will not produce similar vehicle responses. Although the statistical analysis was performed, it was not a critical

factor in road classification. Methods of including the statistical evaluations in road classification will be discussed in chapter 7 addressing recommendations for future work.

% Difference between R1 and Coyote Road				
Channel #	% Δ Max	% Δ Min	% Δ RMS	% Δ S. D.
13	5.23	24.22	2.00	2.00
14	6.19	1.47	9.73	9.75
15	18.64	9.68	8.38	8.38
16	27.06	28.83	14.28	14.31
23	3.75	3.69	7.62	0.32
24	16.32	9.24	1.58	1.02
25	5.15	6.32	2.53	0.49
26	8.79	11.65	11.90	12.94
34	11.23	27.47	32.46	25.65
35	16.66	3.96	31.87	24.31
36	9.76	4.01	2.01	2.06
38	6.70	54.26	4.60	5.96
44	63.72	4.50	18.98	20.47
45	11.18	14.07	16.35	18.19
46	25.00	17.40	15.84	12.60
47	2.50	34.82	2.98	5.01
Avg	**14.87**	**15.98**	**11.45**	**10.22**
Note: R1 Road was used arbitrarily as a reference Note: Analysis was performed on raw				

% Difference between R1 and R2 Road				
Channel #	% Δ Max	% Δ Min	% Δ RMS	% Δ S. D.
13	0.06	14.87	15.65	15.65
14	36.62	23.41	15.47	15.47
15	11.28	17.57	13.59	13.59
16	16.06	6.26	15.96	15.96
23	15.30	30.09	9.43	9.02
24	0.62	1.00	13.47	13.75
25	3.66	17.18	3.96	4.16
26	1.24	23.62	15.28	17.05
34	1.39	85.61	19.48	8.55
35	6.48	24.19	18.51	9.98
36	11.47	0.62	6.24	5.94
38	19.21	24.96	9.65	12.47
44	26.66	30.90	17.04	18.71
45	9.09	21.61	21.65	25.45
46	21.39	1.39	0.27	3.86
47	9.45	10.28	12.79	10.98
Avg	**11.87**	**20.85**	**13.03**	**12.54**
Note: R1 Road was used arbitrarily as a reference Note: Analysis was performed on raw				

% Difference between R1 and R4 Road				
Channel #	% Δ Max	% Δ Min	% Δ RMS	% Δ S. D.
13	15.48	2.90	9.57	9.57
14	33.03	3.41	9.08	9.09
15	10.26	8.71	17.06	17.06
16	7.09	2.49	13.54	13.58
23	4.03	2.15	2.36	4.21
24	10.52	7.50	0.78	0.14
25	8.80	4.06	0.43	0.27
26	8.68	17.56	9.48	9.77
34	5.37	1.36	27.23	19.63
35	6.55	13.62	26.94	19.52
36	24.43	4.22	1.03	0.72
38	20.72	35.82	3.85	4.49
44	3.04	3.99	15.20	16.77
45	13.57	9.30	14.00	15.24
46	32.24	10.57	4.08	2.16
47	22.59	21.92	3.40	2.39
Avg	**14.15**	**9.35**	**9.88**	**9.04**
Note: R1 Road was used arbitrarily as a reference Note: Analysis was performed on raw				

% Difference between R1 and R5 Road				
Channel #	% Δ Max	% Δ Min	% Δ RMS	% Δ S. D.
13	10.60	16.95	22.80	22.79
14	41.61	12.30	24.53	24.51
15	16.02	9.04	19.55	19.55
16	0.06	8.03	23.07	23.05
23	17.98	22.59	13.07	22.32
24	6.59	17.95	11.79	11.75
25	7.58	12.57	20.11	17.39
26	2.89	22.38	6.31	5.95
34	22.25	21.39	58.29	53.13
35	1.99	8.69	67.24	59.91
36	7.22	34.23	17.57	17.73
38	14.91	26.19	9.26	9.28
44	17.82	65.77	12.47	0.63
45	28.56	24.44	0.09	2.69
46	75.56	12.13	36.70	29.21
47	42.66	1.56	24.51	23.67
Avg	**19.64**	**19.76**	**22.96**	**21.47**
Note: R1 Road was used arbitrarily as a reference Note: Analysis was performed on raw				

Figure 48. Statistical analysis performed between Group 1 roads (R1, R2, R3, R4 and R5) on raw project #P1 data at full rated load. R1 road was used arbitrarily as a reference to calculate the differences as described in Figure 11. Although individual data channels showed great deviations from the averaged percent differences, the errors were significantly low to conclude that these roads have a potential for being grouped together.

% Difference between R1 and R10 Road				
Channel #	% Δ Max	% Δ Min	% Δ RMS	% Δ S. D.
13	87.18	85.58	80.67	80.67
14	90.14	88.71	81.40	81.45
15	89.28	88.76	81.43	81.43
16	90.47	90.44	82.95	82.97
23	35.05	45.77	15.74	6.53
24	52.72	24.82	6.11	17.18
25	29.22	30.49	22.75	18.04
26	35.85	26.47	8.27	8.39
34	40.85	72.36	29.31	21.49
35	46.72	76.16	25.78	13.66
36	57.10	52.82	9.67	9.37
38	50.67	48.20	15.76	16.88
44	15.98	53.82	31.27	18.75
45	33.76	75.41	36.60	0.61
46	29.32	39.72	29.43	3.15
47	28.52	38.52	14.95	0.67
Avg	**50.80**	**58.63**	**35.76**	**28.83**
Note: R1 Road was used arbitrarily as a reference Note: Analysis was performed on raw				

Figure 49. Statistical analysis performed between R1 and R10 Roads on raw project #P1 data at full rated load. R1 road was used arbitrarily as a reference to calculate the differences as described in Figure 11. Although individual channels of data showed great deviations from the averaged percent differences, the errors were great enough to conclude these two roads are somewhat distinct in nature.

A very effective way to determine the similarities in vehicle responses proved to be through "cycle correlation" as described in Sections 5.3.2 and 5.3.3. The time histories were reduced to three dimensional, 64-bin sized range-mean matrices of the same size and resolution. The transformation was performed through a rainflow counting method described in above Section 5.3.2. Each of the 64 bins represented number of cycles counted at a specific range and mean value.

A correlation based on linear regression was then used to match the number of cycles in selected areas of the "rainflow matrix", between 16 channels of vehicle response for each two-road combination. If good correlation was obtained, the following factors were satisfied:

- correlation coefficient , averaged for all channels, was close to 1.0,
- absolute cyclic error, averaged for all channels, was less than 100 units,

- RMS cyclic error, averaged for all channels, was less than 300 units.

These errors are defined in Appendix III.

In addition, the correlation was further verified by calculating the slope between the number of cycles of the two correlated roads in all 64 bins. That is the number of cycles in each bin was exported to a spreadsheet, each bin representing the same range value, for both roads. Using linear regression method, a straight line was fitted to the data and its slope was calculated. If correlation was indeed satisfactory the slope across all channels of data was uniform and close to 1. This is demonstrated in Figure 50 and 51, which plot the verification for cycle correlation for Group 1 and Group 2 results.

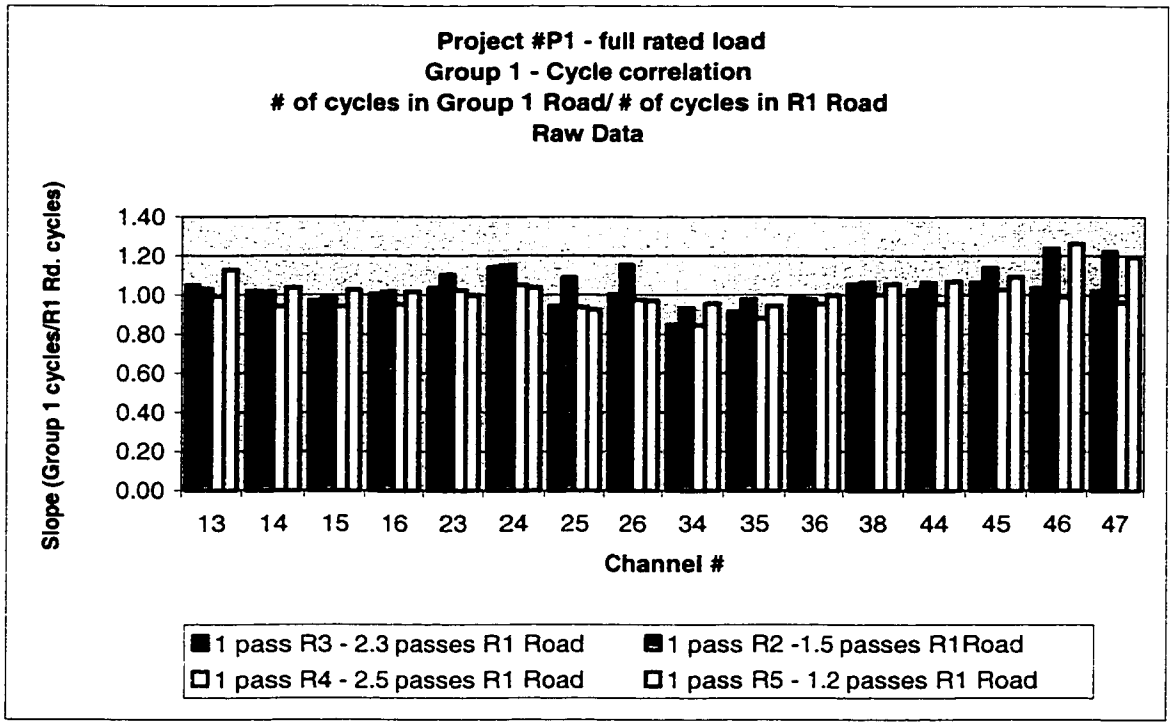

Figure 50. Verification of cycle correlation for Group 1 Roads: R1, R2, R3, R4 and R5 for P1 test at full rated load. The y-axis value represents a slope (rise/run) of a line obtained through linear regression, while trying to match number of cycles in each of 64 bins of data from R1 Road (run) to other Group 1 roads (rise). This figure clearly illustrates that the Group 1 roads do indeed produce similar responses in a vehicle in all studied channels of collected data.

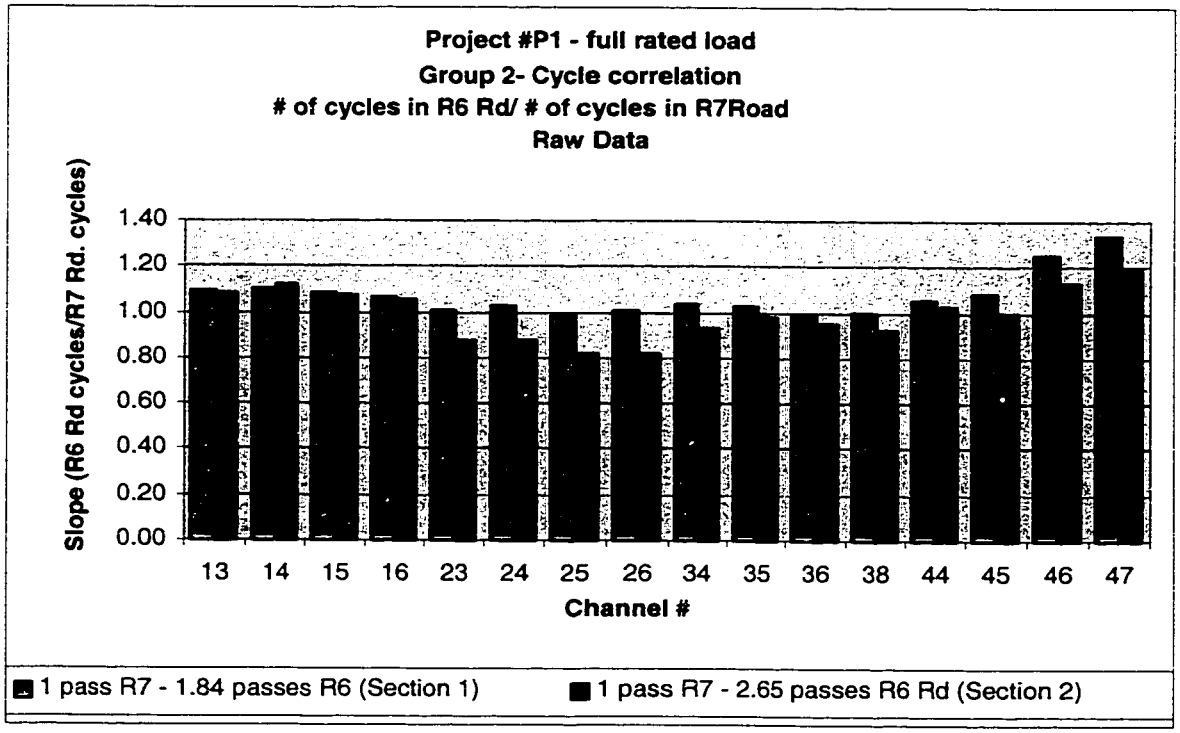

Figure 51. Verification of cycle correlation for Group 2 Roads: R7 and R6 (collected in 2 sections) for P1 test at full rated load. The y-axis value represents a slope (rise/run) of a line obtained by linear regression, while trying to match number of cycles in each of 64 bins of data from R6 Road (rise) to R7 Road (run). This figure clearly illustrates that the Group 2 roads do indeed produce similar responses in a vehicle in all studied channels of collected data.

In comparison, the roads that were determined to be distinct produced very low correlation coefficients, and high errors in absolute and RMS cycle values. The verification of this correlation showed erratic behavior in slopes obtained by matching the number of cycles in all 64 bins, for all channels of the two roads. This is demonstrated in Figure 52, which plots the results of correlation between R1 and R7 roads.

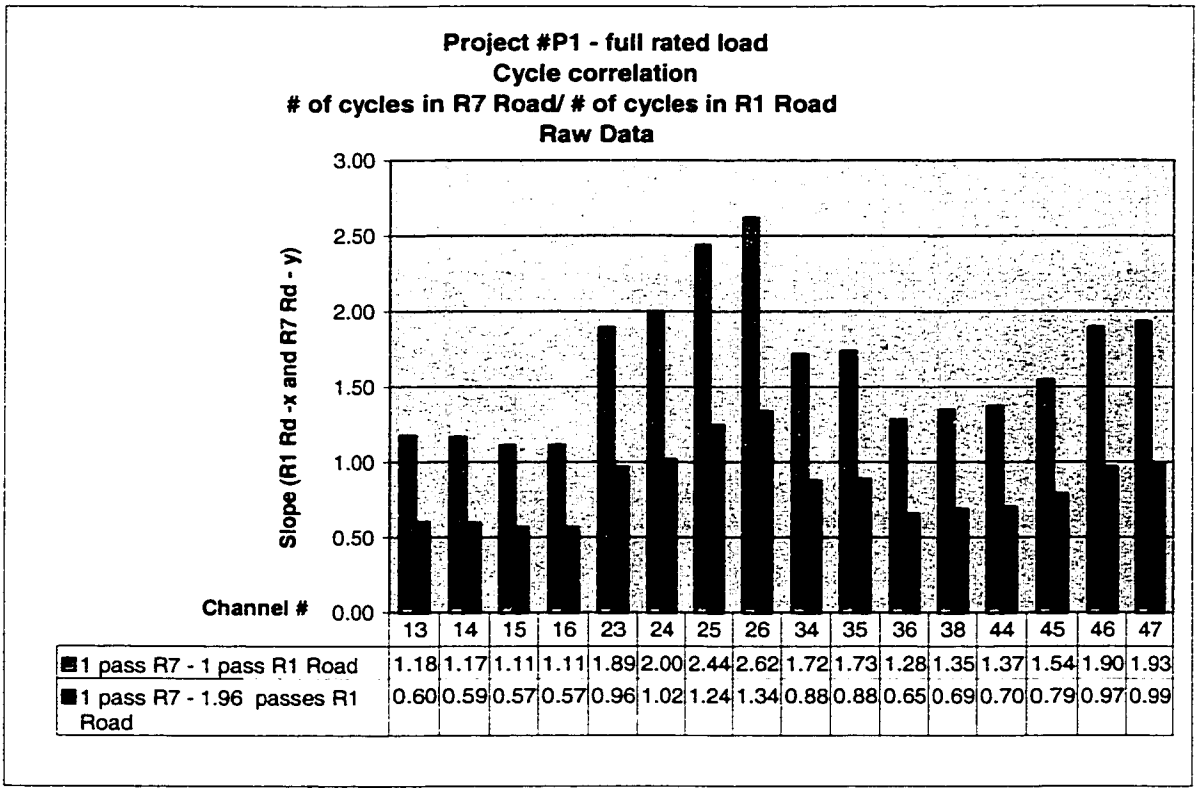

Figure 52. Verification of cycle correlation between R7 and R1 Roads for P1 test at full rated load. The y-axis value represents a slope (rise/run) of a line obtained by linear regression, while trying to match number of cycles in each of 64 bins of data from R7 Road (rise) to R1 Road (run). This figure clearly illustrates that R1 and R7 roads produce distinct responses in the tested vehicle.

Another more visual way of identifying whether the correlation results were satisfactory was by inspecting "Target versus Solution" plots for all channels, produced by the correlation tool in the nSoft package. These graphs plotted on the x-axis the bin numbers of reduced rainflow matrix (16 bins) and on y-logarithmic axis, the number of cycles in each of these bins. An example of these plots is shown in Figures 53 and 54, which produce the results of correlation between R1 and R3 roads, as well as R1 and R7 roads respectively.

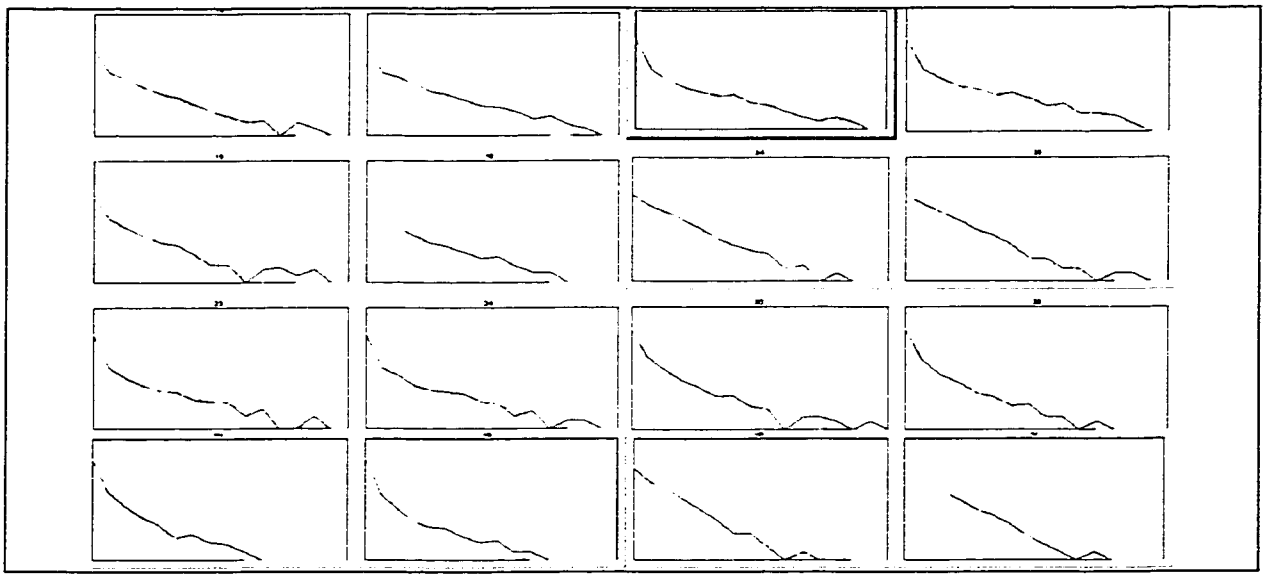

Figure 53. "Target vs. Solution" plot produced by a correlation tool in the nSoft software for R1 and R3 Roads in P1 test at full rated load. The x-axis represents the sixteen bins of reduced rainflow matrix and the y axis plots number of cycles in each of these bins. The black lines show the targets and the red lines represent the solution. These plots demonstrate that the correlation of R1 and R3 road was satisfactory for all channels studied.

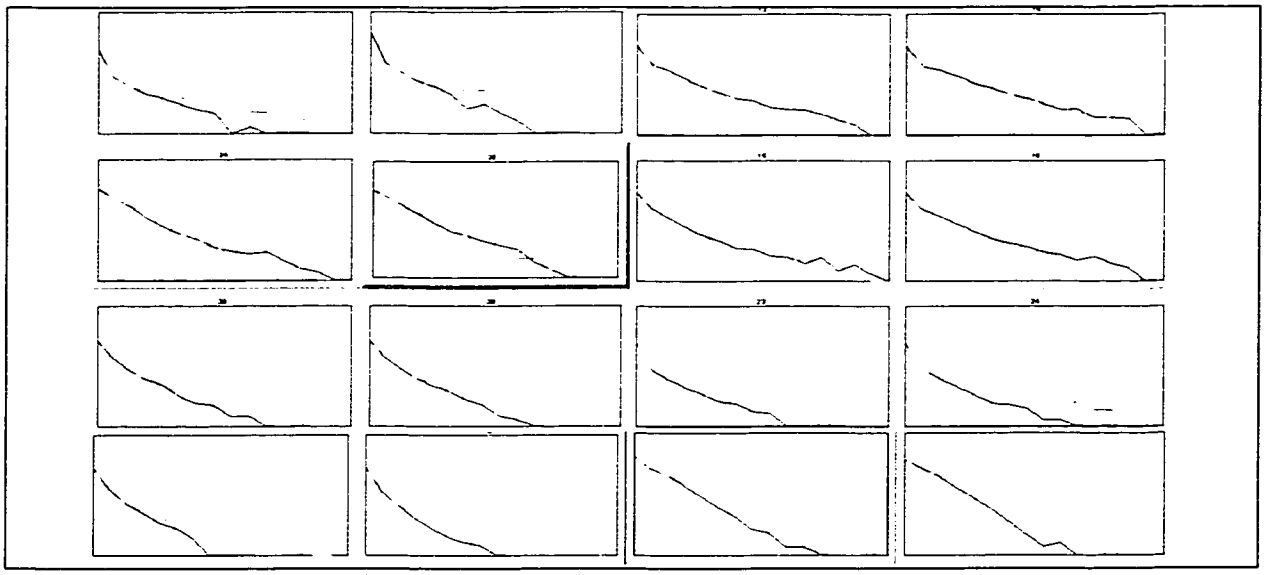

Figure 54. "Target vs. Solution" plot produced by a correlation tool in the nSoft software for R1 and R7 Roads in P1 test at full rated load. The x-axis represents the sixteen bins of reduced rainflow matrix and the y axis plots number of cycles in each of these bins. Each box represents a channel of data. The black lines show the targets and the red lines represent the solution. These plots demonstrate that the correlation of R1 and R7 roads was not satisfactory for the investigated channels.

There were instances where cycle correlation proved to be somewhat satisfactory; however, the roads were classified as dissimilar. This is because other criteria, discussed next, had to be satisfied as well.

The main goal behind correlating the cyclic histograms is to reproduce the same damage distribution. As assumed in Section 5.3.3, the fatigue is proportional to the cyclic input history. Thus upon performing fatigue analysis (as explained in Section 5.4) it is expected to obtain a good correlation between the damages in the correlated roads.

Relative fatigue analysis was performed on the signals from four coil spring channels (channels 23 to 26), measuring spindle to body displacements. The results of the analysis were total damage index, percent low cycle fatigue, percent transition fatigue, percent high cycle damage fatigue. To correlate the roads based on these results, ratios of these values were obtained. The averaged ratios for the four channels are presented in Figure 55 for Group 1 Roads and in Figure 56 for Group 2 Roads.

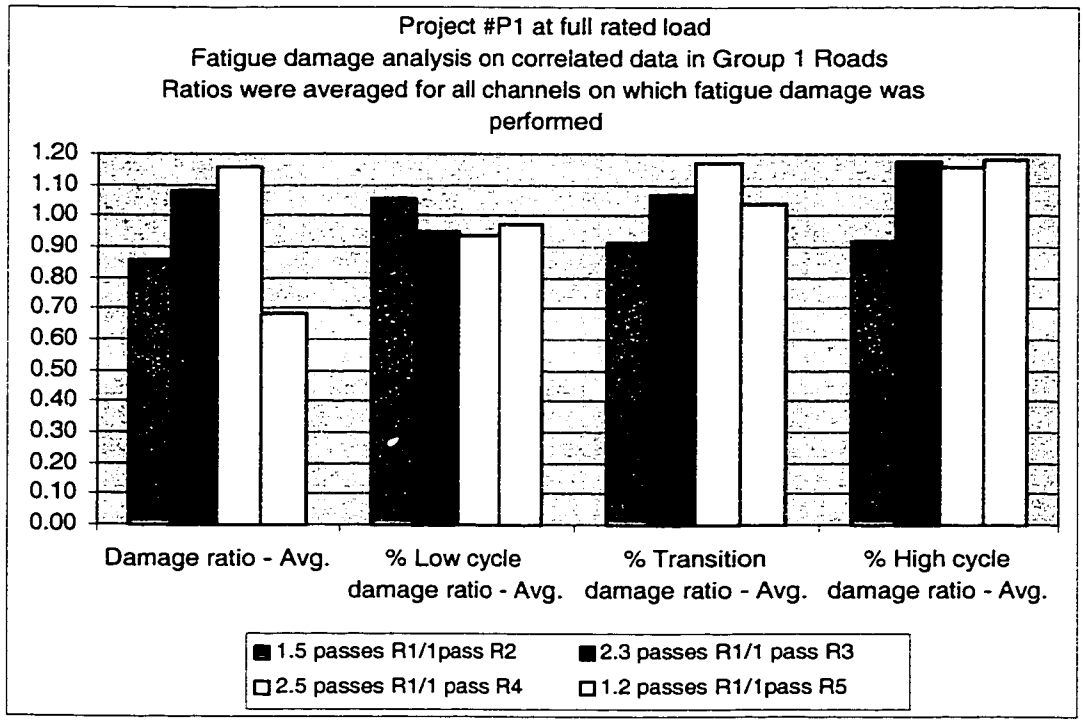

Figure 55. Fatigue damage correlation between R1 Road and the remaining roads of Group 1 (R2, R3, R4 and R5). This figure illustrates that by correlating the roads of Group 1 based on their cyclic inputs, it is possible to obtain similar damages and their distribution. The relative damage correlation could be improved by removing small amplitude cycles from the cycle correlation, since they dominate the rainflow matrix in number but contribute very little to the damage.

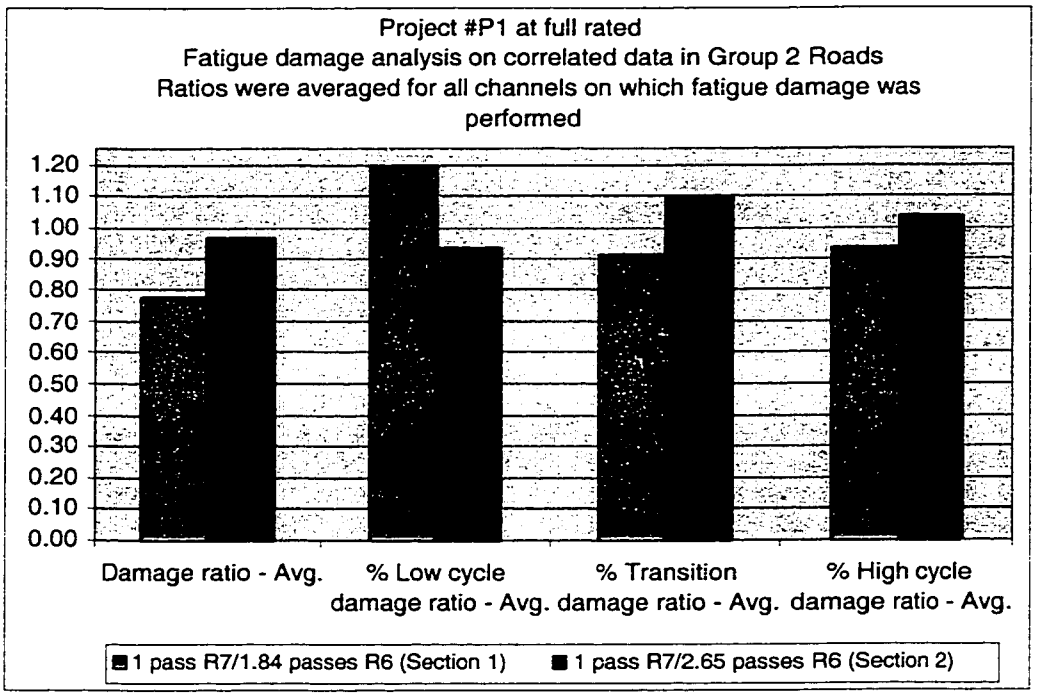

Figure 56. Fatigue damage correlation between R1 Road and the correlated R6 Road Sections. This figure illustrates that by correlating the roads of Group 2 based on their cyclic inputs, it is possible to obtain similar damages and their distribution. Once again, the relative damage correlation could be improved by removing small amplitude cycles from the cycle correlation, since they dominate the rainflow matrix in number but contribute very little to the damage.

Overall, it is shown in Figures 55 and 56 that both Groups 1 and 2 show a good correlation among the percent damage distribution for low, transition and high cycle life (percent damage ratios vary between 0.9 to 1.2). This verifies that a good correlation between the number of cycles at all range values will guarantee a satisfactory damage distribution.

The total damage ratios on the other hand ranged between 0.7 to 1.2. This correlation could be improved by editing the non-damaging (low amplitude) cycles from the time histories, and repeating the process of cycle correlation on the edited roads. Since the time histories are dominated by the number of low amplitude cycles, the correlation coefficients are expected to be different; however, the integrity of correlation should not be compromised. The purpose of the present study was just to determine if the certain

roads in OR test exhibit the same characteristics over entire road sections; thus both low and high amplitude inputs were considered in the correlation.

Based purely on cycle correlation and damage analysis, it was easily observed which vehicle responses were similar in nature, and which ones were distinct. The most important aspect of both cycle and damage correlation was to ensure that all the vehicle response signals collected from the grouped roads could be simultaneously reproduced through road substitution. Only if this criterion was satisfied, the integrity of the accelerated test could be secured.

The frequency content of excitation also plays an important role in endurance tests of subassembly or full vehicles [35]. Thus analysis of frequency content was necessary in grouping the roads. It was observed that the frequency content and the profiles of power spectral density (PSD) functions for all channels in the grouped roads were the same. The differences were mainly observed in the energy content at certain frequencies. It was impossible however to determine which road in a particular group had the highest energy content, since that varied from test to test, from channel to channel, and for values at different frequencies themselves. Thus as long as the frequency content and PSD profile was preserved, it was satisfactory to consider vehicle responses from different roads to have a potential for classifying as similar or distinct.

This method of thinking was confirmed by a study published by Yu et al [29] on the "Effects of Test Conditions on Vehicle Structural Accelerated Testing". In their study it was concluded that if different roads are similar in profile power spectra, the responses of the vehicle components will be of the same nature. The energy contained at each frequency can easily be intensified with increase in speed of a vehicle or with increase in irregularities of the roads. The irregularity of a road is referenced in the study to be determined by irregularity coefficient and index calculated from road surface profile signal measured by road profile meter [29]. Both speed and road irregularities are subject to variability due to factors such as type of driver and his/her conduct, traffic congestion, road maintenance, traffic type, as well as weather conditions.

Although the proving ground engineers regulate speed limits, which are set based on a road type condition, it is expected that the driver will not be able to maintain constant speed throughout the data acquisition period. Upon approaching high input road events, the driver is likely to slow down, brake or decelerate. In turn the higher the speed the larger the amplitudes of the response PSD functions will be obtained.

Changes in surface irregularities may also intensify or decrease certain frequency content, as proven in the above mentioned study [29]. By reviewing the road roughness report conducted for the PG's OR road course [17], it was discovered that certain "severity degrading" of the surfaces was discovered due to extended (2-3 years) "el-Niño" weather patterns. Weather conditions such as high winds, or rains tend to smooth out some washes on the test courses. Under normal weather pattern conditions, the roads dry out quickly, and are expected to return to their "normal" conditions within 24-36 hours of use. However some degradation or changes in the roughness are surely expected to occur.

Lastly, the grouping of roads was further verified by comparing amplitude distribution functions for all channels of data and for all the road test sections studied. It was clearly shown that the probability density functions (PDF) for collected vehicle responses were overlaying each other if the roads were similar in nature. The PDF functions showed that the distribution of amplitudes is almost normal in nature, centered around zero mean. Some variations in comparing PDF functions were observed if raw (unfiltered) data was used, and if slight offsets were present in the data. The PDF comparison could be improved by filtering the data through a high-pass filter at 0.2 Hz, and by applying averaging functions to remove some irregularities in the PDF functions, resulting from the algorithm used to obtain them.

Due to number of files analyzed, all PSD and PDF plots could not be shown. Figures 57 and 58 plot respectively a PSD and PDF function for a single channel (Channel 25), and six different road sections (R1, R3, R8, R9, R10 and R7). Quick visual inspection of both functions allows one to see which roads are similar and which are distinct.

Figure 57 plots PSD functions for six different roads for one of the channels. The only two functions resembling one another are the red and yellow graphs representing R1 and R3 Roads. The remaining plots for R8 Road (green), R9 Road (navy), R10 (light blue) and R7 (black), show more distinctive features. The differences are easier to observe when plotted on y-log scale, as shown in Figure 58. A very clear distinction is observed between R10 and remaining road sections.

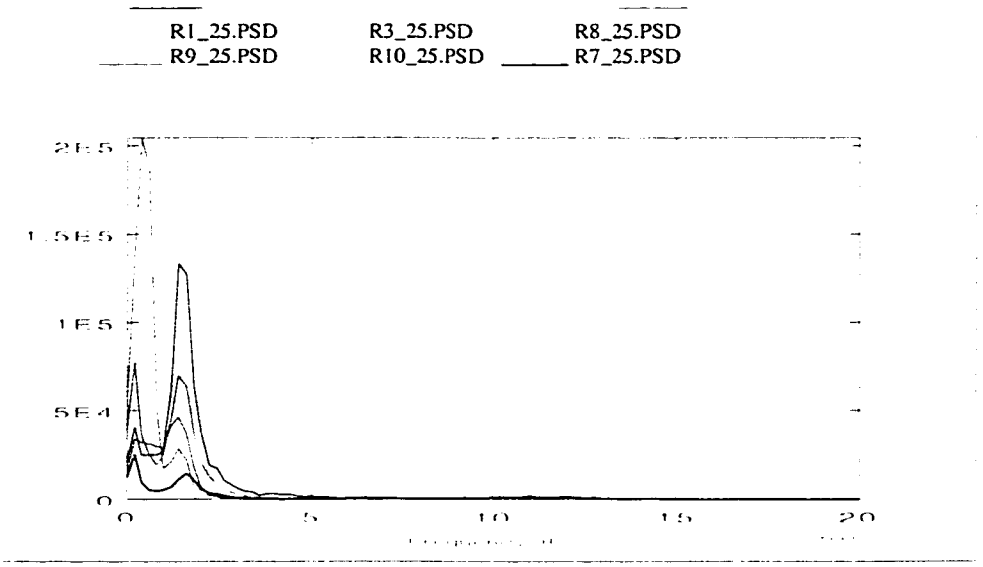

Figure 57. Plot of PSD functions for test #P1 at full rated load, for channel 25 data and for selected six roads: R1 (red), R3 (yellow), R8 (green), R9 (navy), R10 (light blue), and R7 (black). A simple visual check of PSD plots enables one to determine which roads are similar and which are distinct in nature.

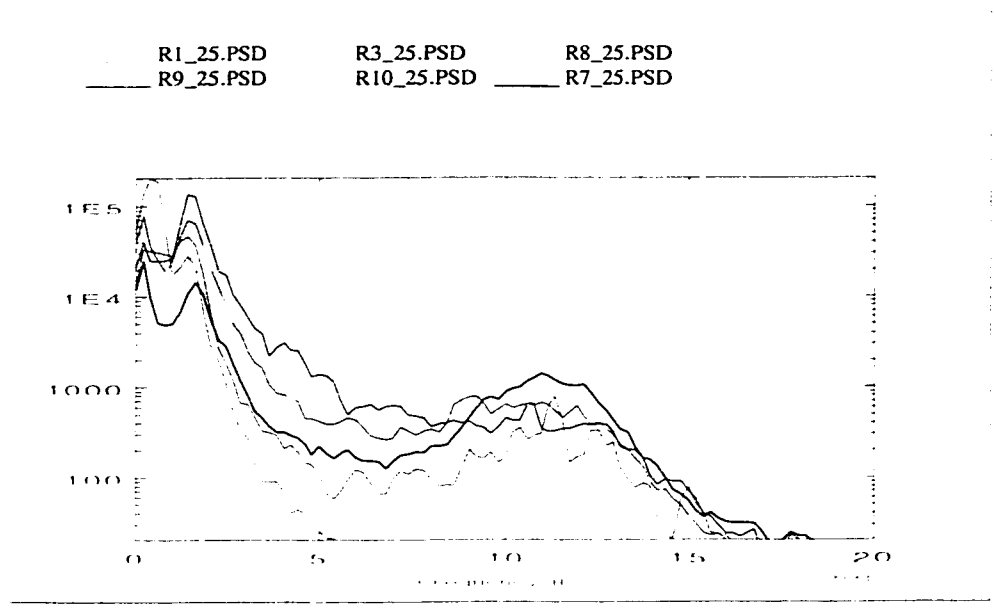

Figure 58. Plot of PSD functions for test #P1 at full rated load, for channel 25 data and for selected six roads: R1 (red), R3 (yellow), R8 (green), R9 (navy), R10 (light blue), and R7 (black) on a y-log scale.

Figure 59 plots PDF functions for six different roads and for one of the channels (Channel 25). The two PDF functions that follow each other the best are the red and yellow graphs representing R1 and R3 Roads. The remaining plots for R8 Road (green), R9 Road (navy), R10 (light blue) and R7 (black), show once again more distinctive features. The differences are easier to observe when plotted on y-log scale, as shown in Figure 60. A very clear distinction is observed between R10, R8 and R7 roads from remaining road sections.

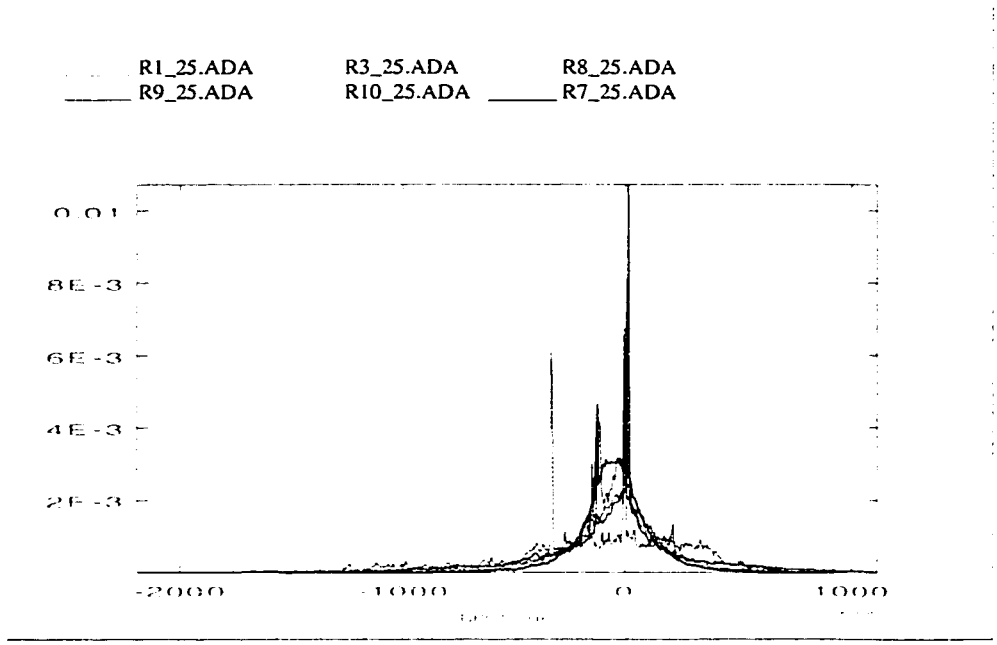

Figure 59. Plot of PDF functions for test #P1 at full rated load, for channel 25 data and for selected six roads: R1 (red), R3 (yellow), R8 (green), R9 (navy), R10 (light blue), and R7 (black). A simple visual check of PDF plots enables one to determine which roads are similar and which are distinct in nature.

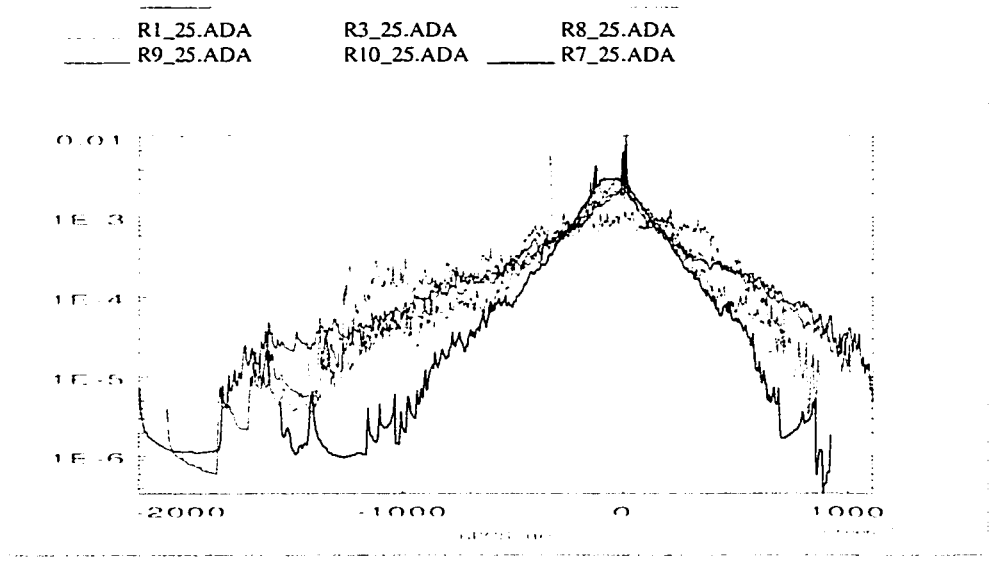

Figure 60. Plot of PDF functions for test #P1 at full rated load, for channel 25 data and for selected six roads: R1 (red), R3 (yellow), R8 (green), R9 (navy), R10 (light blue), and R7 (black) on a y-log scale.

This type of inspection was conducted for all roads, and all channels analyzed. Limitation of the software allowed files to be displayed only eight at a time on up to four screens (32 files in total). Since ten roads were investigated, some collected in two sections such as R6, R8 and R9, and all roads had to be compared relative to one another for all sixteen channels, this process proved to be very time consuming. In order to consider the roads to be similar, all channels had to show similarities in PSD and PDF functions. The distinctions of the roads were more apparent in some channels than others.

Based on analysis of P1 project data at full rated load, five groups of roads were formed, as stated at the beginning of this section. The roads revealing significant differences in characteristics were categorized as individual groups. These include R10, R8, and R9 roads. This discovery was supported by the descriptions of roads included in Chapters 3.2.2 and 3.3 of this study.

The same form of analysis was then applied to four other sets of data, in order to verify the results. These tests included the following:

- Project #P2 under 2-passenger load,
- Project #P2 under half payload,
- Project #P3 under 2 passenger load,
- Project #P3 under full rated load.

A brief discussion of the results from these tests will follow.

6.2 Project #P2

6.2.1 #P2 at Half-Payload

Verification of test results from P1 test at full rated load, was first conducted on test #P2 at half-payload. Since no significant offsets or drifts were exhibited in time histories, the analysis was conducted on raw (unfiltered) road data.

The only roads from Group 1 that correlated well for this test were R1, R3 and R4 Roads. Correlation of remaining roads in this group, consisting of R2 and R5 Roads, was not very satisfactory, especially for R5 Road.

Figure 61 presents a cycle correlation for Group 1 roads. The ratios of cycles in each of the 64 bins and for all channels of data, were close to one only in R1-R3 and R1-R4 road correlation. The correlation of cycles in R2 road to those of R1, showed uniform correlation however the ratios were on the order of 0.7. The linear regression between these two roads showed high RMS and absolute cycle errors, as well as low correlation coefficient factors.

The correlation of cycles in R5 road to R1 road was more erratic. Few channels showed very significant differences (Ch 14, 16, 28 and 29) between the two roads. Even after these channels were removed from linear regression analysis, the results were still very poor.

Despite this poor correlation between R2-R1 and R5-R1 Road combinations, all correlation coefficients relating Group 1 roads (R2, R3, R4, R5) to R1 Road are similar in both project #P1 at full rated load and in P2 at half-rated load (See legends of Figures 50 and 61).

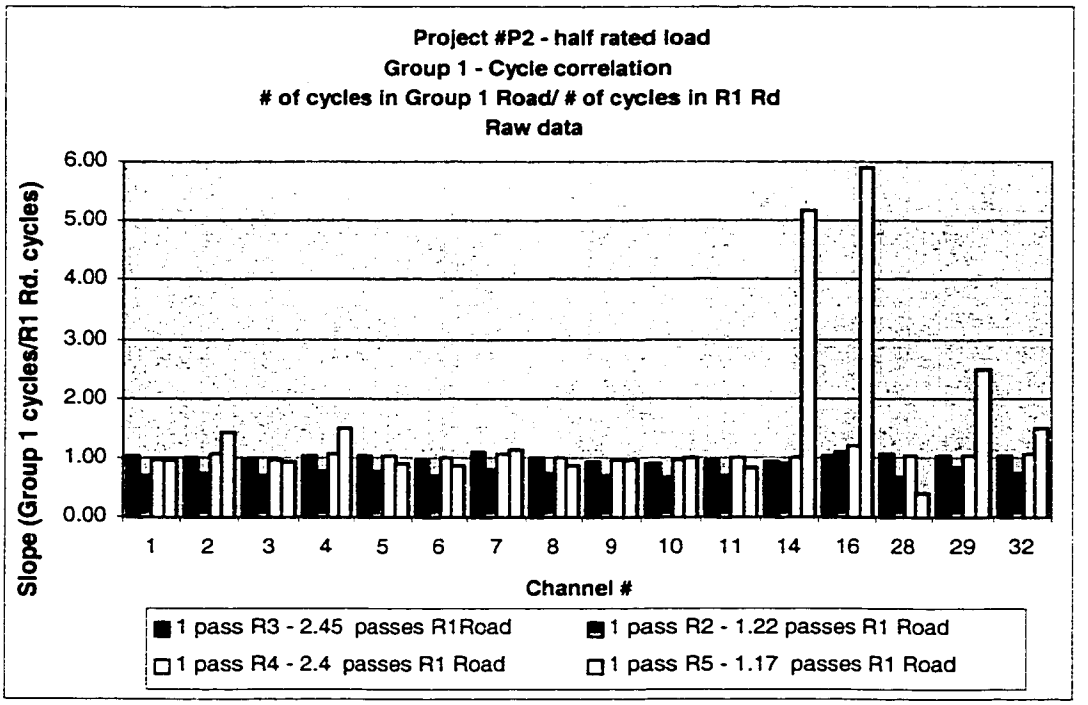

Figure 61. Verification of cycle correlation for Group 1 Roads: R1, R2, R3, R4 and R5 for P2 test at half rated load. The y-axis value represents a slope (rise/run) of a line obtained by linear regression, while trying to match number of cycles in each of 64 bins of data from R1 Road (run) to other Group 1 roads (rise). This test verifies only good correlation between R1, R3 and R4 roads.

Figure 62 presents a cycle correlation for Group 2 roads. The correlation of the two sections of R6 road to R7 road proved to be very inadequate. The linear regression results showed low correlation coefficients, and high errors. Figure 62, shows that the slopes relating number of cycles in R6 Road to R7 road (in all 64 bins) are very erratic across all the channels. Thus the performed cycle correlation could not justify the grouping of R7 and R6 Roads

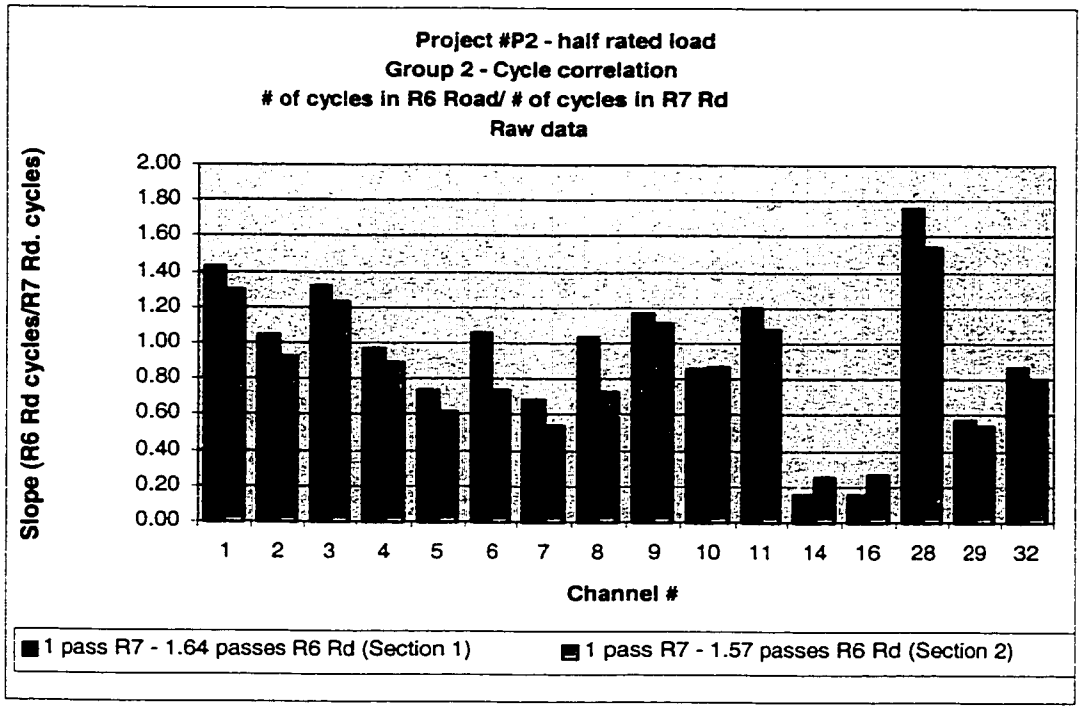

Figure 62. Verification of cycle correlation for Group 2 Roads: R7 and R6 (collected in 2 sections) for P2 test at half rated load. The y-axis value represents a slope (rise/run) of a line obtained by linear regression, while trying to match number of cycles in each of 64 bins of data from R6 Road (rise) to R7 Road (run). The results of the correlation were not satisfactory to verify the grouping of R7 and R6 roads.

Relative fatigue analysis of Group 1 and Group 2 showed similar results. These are presented in Figures 63 and 64 respectively. The ratios plotted in both figures were averaged out for the channels on which damage analysis was performed. In Group 1 only R3 and R4 roads showed a good correlation to R1 Road. Group 2 roads, R7 and R6, did not correlate well in damage analysis. These results were expected based on the results of cycle correlation.

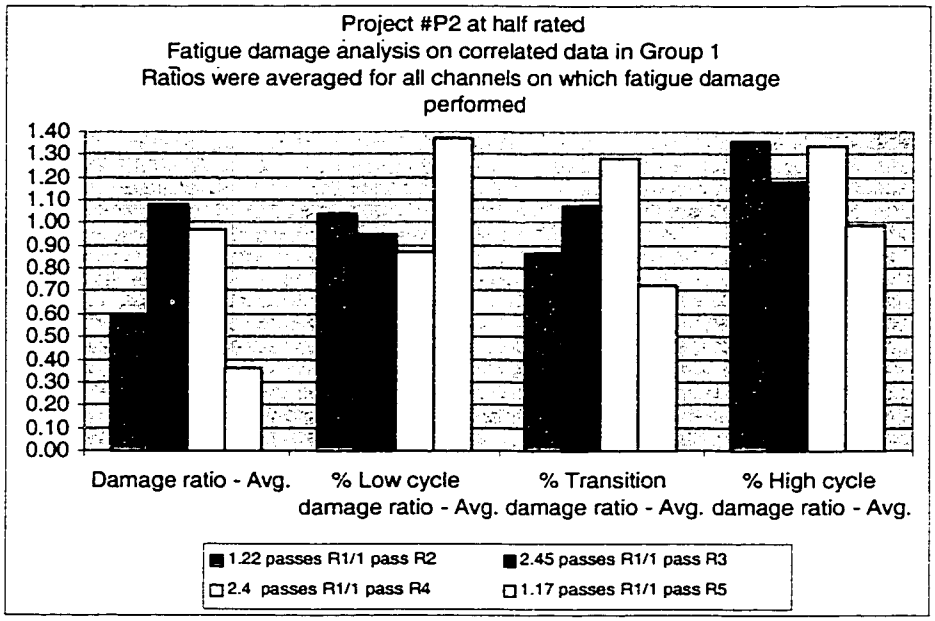

Figure 63. Fatigue damage correlation between R1 Road and the correlated roads of Group 1 (R2, R3, R4 and R5). Only R3 (red) and R4 (yellow) showed satisfactory correlation.

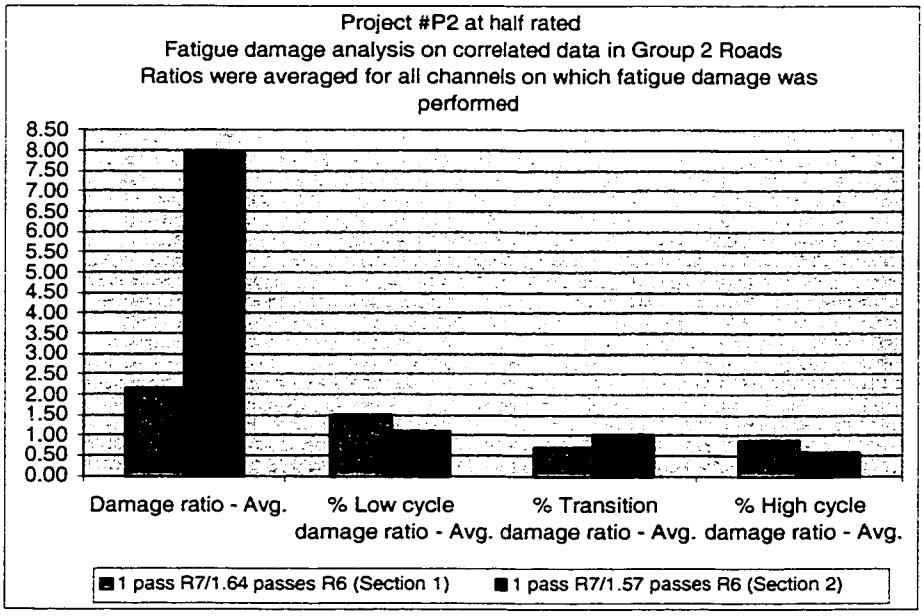

Figure 64. Fatigue damage correlation between R1 Road and the correlated R6 Road Sections. P2 test at half rated load showed poor correlation between R7 and R6 Roads.

It was decided to justify why the correlation of R5 and R2 Roads to other roads of Group 1 proved to be unsatisfactory. First an evaluation of the time histories was performed. The time histories for all channels did not show any abnormal behavior that could affect the correlation itself. Only channel 28 for both R2 and R5 road showed a failure of a transducer during data acquisition. However even when this channel was eliminated from correlating the number of cycles based on linear regression, the results were still very poor.

Next a closer look was paid to the PDF functions showing amplitude distributions of Group 1 roads. Plotting the PDF functions for all Group 1 roads for all channels considered, showed significant differences in amplitude distributions of vehicle responses collected from R5 and R2 Roads. One of those plots for channel 4 data is shown in Figure 65. Figure 66 shows the same plotted on logarithmic scale to attenuate the differences.

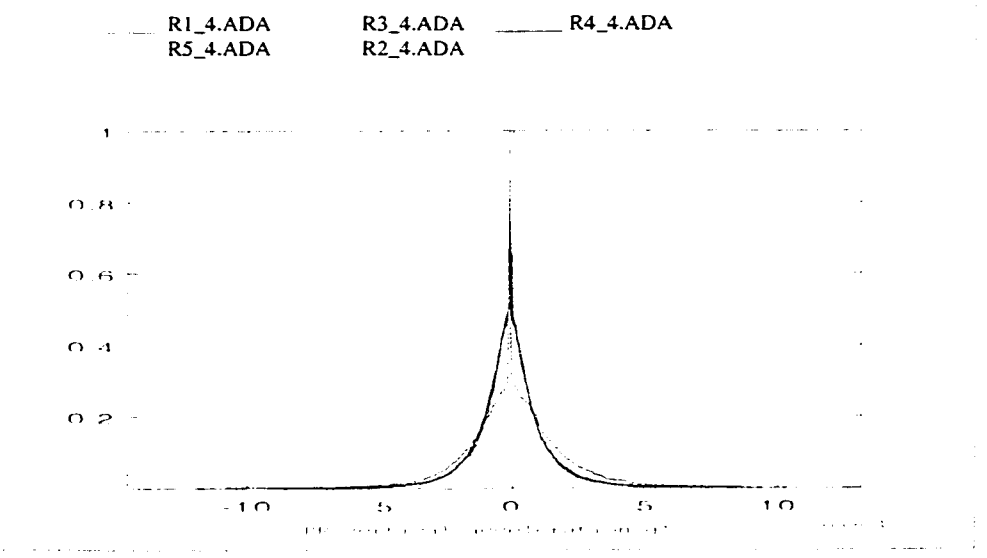

Figure 65. Plot of PDF functions of Group 1 roads for test #P2 at half rated load, for channel 4 data. Only PDFs of R1 (red), R3 (green) and R4 (navy) Roads showed resemblance, while R5 (light blue) and R2 (yellow) differed in amplitude distributions.

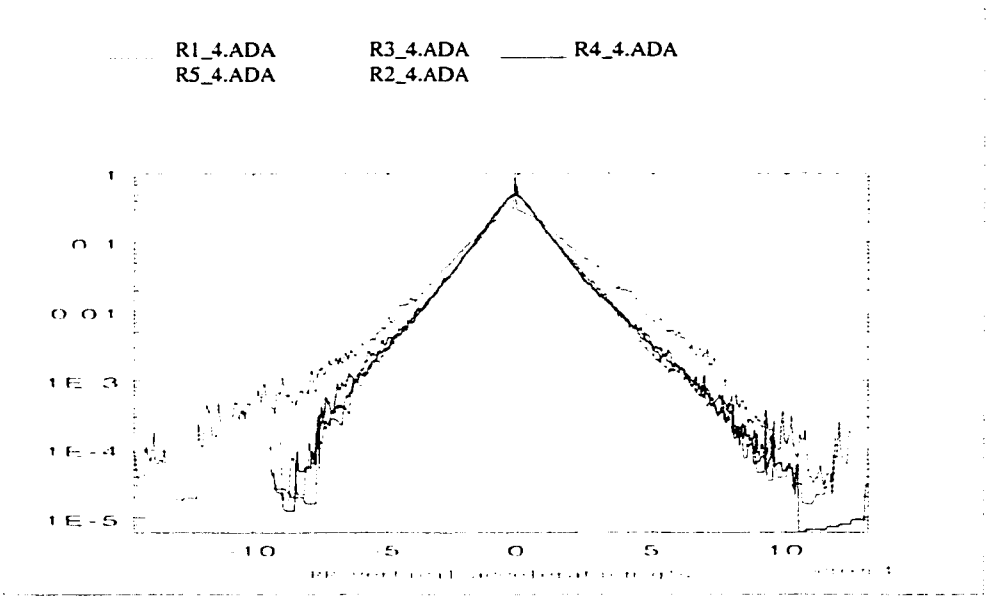

Figure 66. Plot of PDF functions of Group 1 roads for test #P2 at half rated load, for channel 4 data plotted on logarithmic scale. Only PDFs of R1 (red), R3 (green) and R4 (navy) road showed resemblance, while R5 (light blue) and R2 (yellow) differed in amplitude distributions.

The differences in amplitude distributions were very evident, especially in R5 Roads for all channels considered.

Next a closer look at the PSD functions for the Group1 roads was presented. Once again significant differences were observed in R5 and R2 Roads from remaining roads of Group 1, not only in PSD profile but also in frequency content. Figure 67 shows a PSD plot for Group 1 roads (channel 4), which illustrates these differences. Figure 68 is the same graph but plotted on y-log scale.

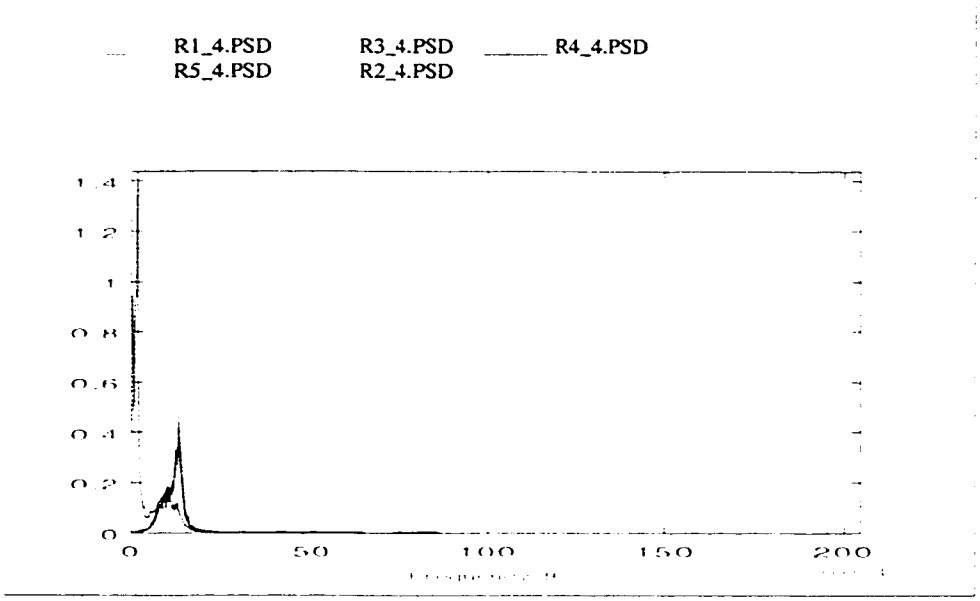

Figure 67. Plot of PSD functions for test #P2 at half rated load, for channel 4 data and for group 1 roads. Only PSDs of R1 (red), R3 (green) and R4 (navy) road showed resemblance, while R5 (light blue) and R2 (yellow) differed in amplitude distributions.

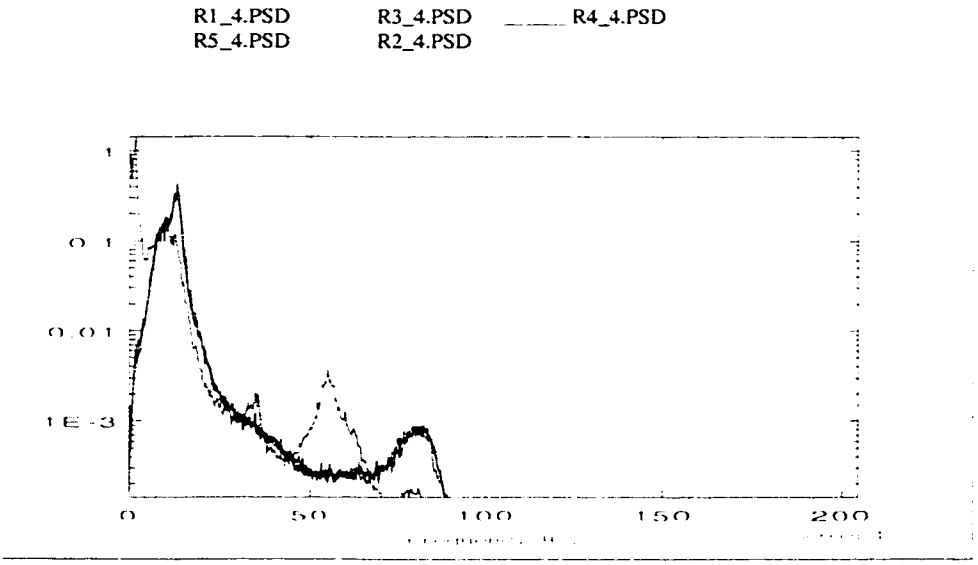

Figure 68. Plot of PSD functions for test #P2 at half rated load, for channel 4 data and for group 1 roads plotted on a logarithmic scale. Only PSDs of R1 (red), R3 (green) and R4 (navy) road showed resemblance, while R5 (light blue) and R2 (yellow) differed in amplitude distributions.

The question now is whether the poor correlation is attributable simply to the fact that the R2 and R5 Road conditions do not resemble those of the other Group 1 roads, or are the differences attributed to other factors.

During a conversation with Mr. Martin Vander Baaren, one of the engineers at ARDC working on P2 project, attention was brought to the fact that during data acquisition, problems were experienced with some transducers and the Megadac (data acquisition system). Analysis of time histories showed that in both R5 and R2 roads Channel 28 transducer failed, while in R7 Road the same situation happened for channel 32. Thus one explanation for the poor correlation among the R1, R5 and R2 roads (for Group1) and the R7 and R6 roads (for Group 2) in P2 test at half payload, could simply be attributed to problems during data acquisition.

Another possibility investigated was the fact that road conditions due to weather pattern, traffic use, or road maintenance could have changed drastically over the year period for the roads in question (R2, R5, R7, R6). These changes would then indeed affect the differences in amplitude distributions and frequency content. Since P1 test was collected in 1997 and P2 test was acquired in 1996, road roughness comparison for those years was necessary. To do that, road roughness report [17] conducted for OR course at the PG was used. In the report, a comparison of road roughness amplitude ratios was performed between June 1998, March 1997, August 1996, December 1995, and October 1994. The ratios were speed dependant (i.e. ft^2/Hz vs. Hz), and were unique to each course. Thus a normalization process was used, in which spectral density values for each of the courses were calculated and processed to a single value, roughness ratio [17]. This roughness ratio then provided an overall ratio of the energy input to the vehicle over 1 – 20 Hertz range (frequency range in interest).

In the report, roughness severity ratios are presented for October 1994, December 1995, August 1996, March 1997 and June 1998, with October 1994 used as a reference measurement. That is, all the October 1994 severity ratios are unity, and ratios from other years are compared relative to them.

The severity ratios for the individual roads included in the Off Road Course are presented in Table 14, for October 1994 (reference), August 1996 and March 1997.

Group	Road	Roughness Severity Oct-94 used as a reference		
		Oct-94	Aug-96	Mar-97
Group 1	R1	1	0.8	0.8
	R2	1	0.6	0.7
	R3	1	0.9	0.95
	R4	1	1.1	0.8
	R5	1	0.8	0.9
Group 2	R7	1	0.8	0.4
	R6	1	0.6	0.6

Table 14. Roughness Severity Ratio for Group 1 and Group 2 roads [17]. This table shows that with the exception of R7 Road, no significant differences were observed in road roughness during 1996 to 1997 period.

The overall severity has not altered much over 1996 to 1997 period. The variations that did exist were due to differences in the severity and the amount of washboard content present at time of profiling [17]. These type of changes are generally confined to the deeper sand sections of the courses that run with washes, such as R6 and R7. The general lack of the washboard seen during March 1997 profiling was most likely due to rainfall and run-off with the washes. This could explain why R6 Road and R7 road correlated well in 1997 but not in 1996. However the poor correlation results from P2 test for the R2 and R5 Roads still needs to be explained.

Four common channels were used in both P1 (full rated payload) and P2 (half rated payload) tests. They were the vertical acceleration channels. Thus PSD plots for these channels were plotted for Group 1 roads in both tests. Due to a limitation of the software only eight of the functions could be plotted on one graph. Figure 69 plots PSD functions of selected Group 1 roads: R1, R3, R2 and R5 for both tests and for the left front vertical acceleration channels. It is very easily observed that the PSD functions for all road sections are very similar in profile and frequency content, with the exception of R5 (light brown) and R2 (magenta) road collected for P2 test at half-payload.

Changes in frequency intensities between the two tests are expected as a result of using different vehicles, payloads, drivers, and changing weather conditions. Despite these variables however, the roads that correlated well (R1, R3, R4) show similarities in PSDs profiles for both tests. Vehicle responses from R2 and R5 Roads show some additional frequencies in a range of 0-7 Hz for the vertical acceleration channels. These frequencies could have appeared in a signal directly as a result of road inputs, or could be attributed to some vibrations internal to the vehicle or transducers, but not resulting from road input.

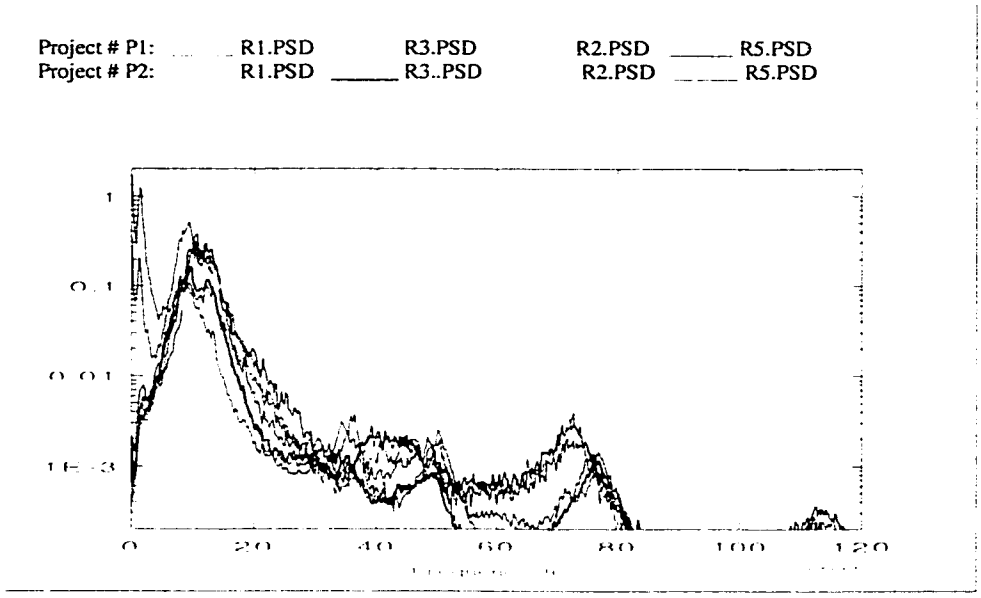

Figure 69. Plot of PSD functions for test #P1 at full rated load and test #P2 at half rated load for R1 R3, R2 and R5 Road, for left front vertical acceleration channel. Despite differences in vehicles, payloads, drivers, and weather, both tests show similar profiles and frequency content, except for vehicle V2 R5 (light brown) and R2 (magenta) PSD functions which show some additional frequency content between 0 to 7 Hz.

To see whether similar result will be present in Group 2 roads, PSDs for both project #P1 at full rated load and project #P2 at half rated load were plotted for all vertical acceleration channels. One of the graphs for right rear vertical acceleration is plotted in Figure 70. The PSD functions of the two sections of R6 Road (yellow and red) together with R7 road (green) from P1 test show similarities in profile and frequency content. The

two sections of R6 road (navy and light blue) from P2 test show similarities in profiles to project #P1 PSDs. The frequency intensities from the P2 tests are expected to be different than those from the P1 test, since a lower payload was used. Other factors such as tire pressure, or vehicle speed could have also contributed to these differences.

The P1 test shows no significant differences in PSDs between the two sections of R6 Road, whereas significant differences in frequency intensities between the two sections are observed in P2 test. In addition the vertical acceleration PSD plots for vehicle V2 R7 Road (black) show additional frequencies between 0 to 6 Hz, and a somewhat different profile in 50 to 70 Hz range.

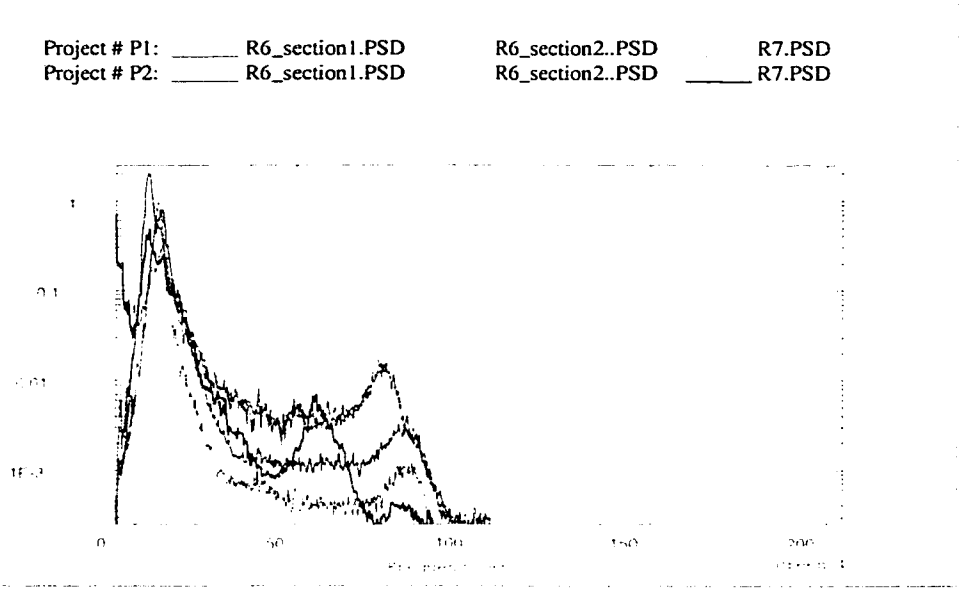

Figure 70. Plot of PSD functions for test #P1 at full rated load and test #P2 at half rated load for R6 and R7 roads for right rear vertical acceleration channel. Despite differences in vehicles, payloads, drivers, and weather, both tests show similar profiles and frequency content, except for vehicle V2 R7 (black) PSD functions which shows some additional frequency content between 0 to 7 Hz., and in the 50-70 Hz range.

If the additional frequencies in P2 test at half-payload were indeed present in the R2, R5, R6 and R7 Roads, as a result of road inputs, similar results should be produced for the P2 test at a 2-passenger payload. They will be discussed below.

6.2.2 #P2 at 2-Passenger Payload

Further verification of the results was conducted on test #P2 using a 2-passenger payload. Due to significant abnormalities, such as offsets or drifts, in time histories, the analysis was conducted on data that has been high-pass filtered at 0.2 Hz.

The correlation results obtained in analysis of P2 test at 2-passanger payload proved to be even less satisfactory for Group 1 roads, however an improvement was noticed in correlating Group 2 roads.

Figure 71 presents a cycle correlation for Group 1 roads. The only road sections that correlated well were R1 and R4 (yellow). The ratios relating number of cycles in each bin of rainflow matrix for the two roads were close to unity for all channels as shown in Figure 71. The remaining roads - R2, R3, and R5 - when correlated to R1 Road showed very inadequate and erratic relationships for different channels. The results of this correlation could be attributed to the poor quality of data itself.

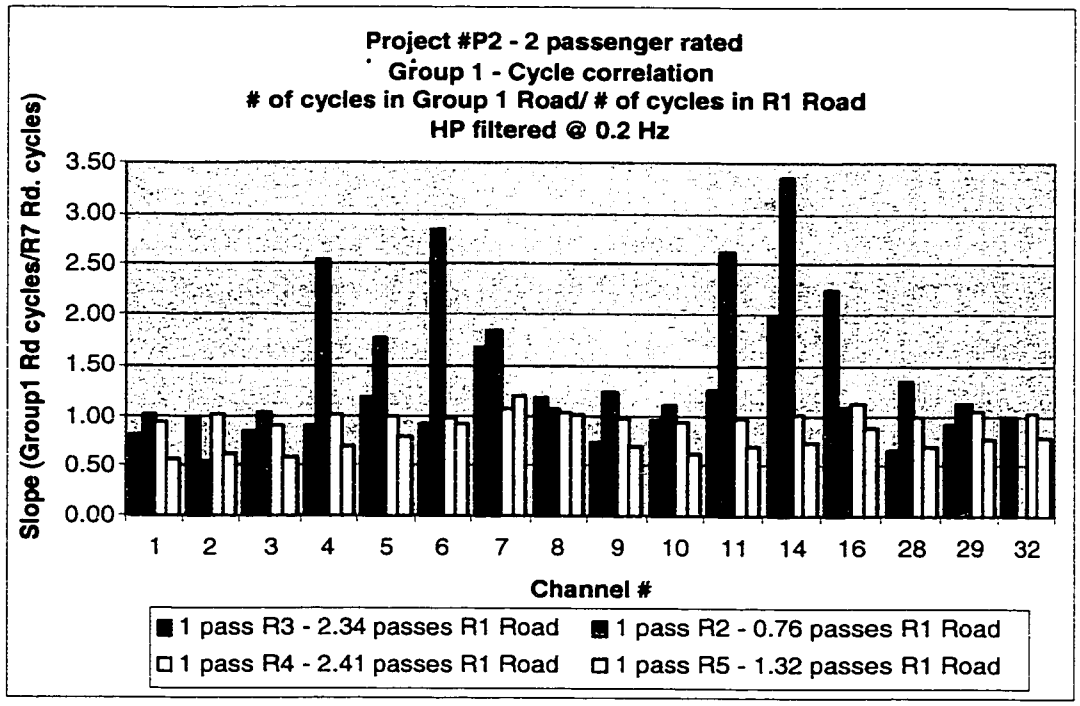

Figure 71. Verification of cycle correlation for Group 1 Roads: R1, R2, R3, R4 and R5 for P2 test at 2-passenger load. The y-axis value represents a slope (rise/run) of a line obtained by linear regression, while trying to match number of cycles in each of 64 bins of data from R1 Road (run) to other Group 1 roads (rise). Only the R1 and R4 roads showed good correlation in this test.

Figure 72 presents a cycle correlation for the Group 2 roads. An improvement was noticed in relating these two roads to each other through linear regression. The slopes relating number of cycles in R6 Road to R7 road at each bin of rainflow matrix and for all channels were close to one. Some irregular behavior was however observed in these slopes (not present if roads correlate well) as demonstrated in Figure 72.

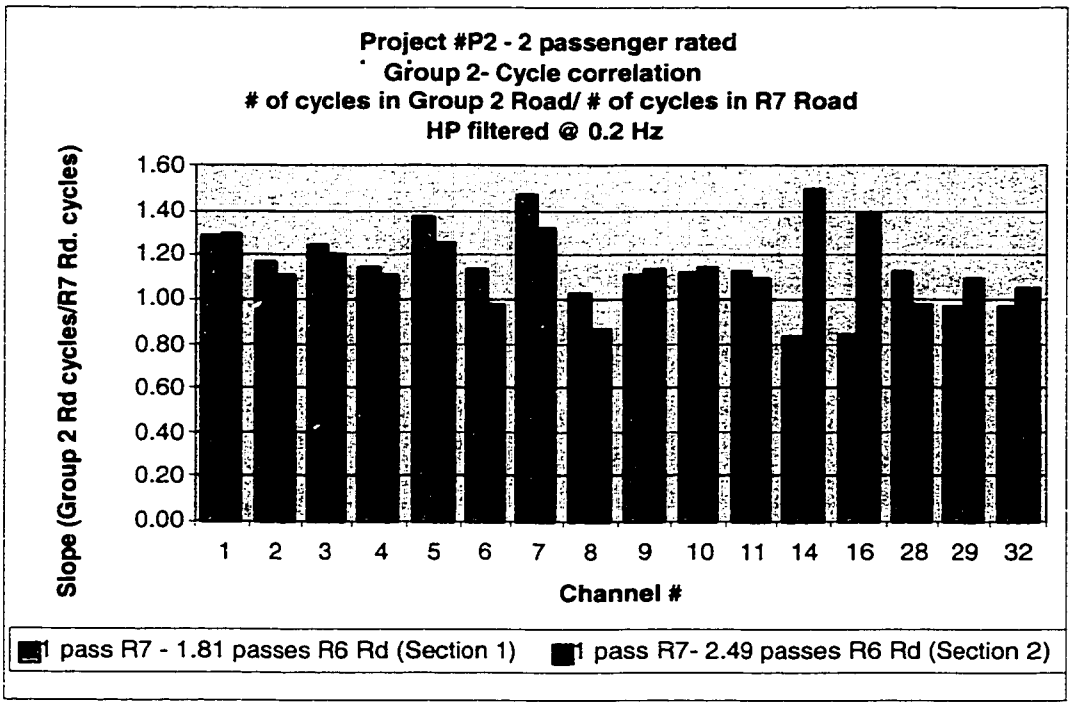

Figure 72. Verification of cycle correlation for Group 2 Roads: R7 and R6 (collected in 2 sections) for P2 test at two passenger load. The y-axis value represents a slope (rise/run) of a line obtained by linear regression, while trying to match number of cycles in each of 64 bins of data from R6 Road (rise) to R7 Road (run). An improvement in cycle correlation was observed (as compared to P2 test at half-payload), however the slopes still show some irregular behavior.

Fatigue analysis was performed on Group 1 and Group 2 string pot and coil spring data channels (channels 14, 16, 29 and 32) to further confirm the results of cycle correlation. The results are presented in Figures 73 and 74 for Group 1 and 2 respectively. The ratios plotted in both figures were averaged out for the channels on which damage analysis was performed. In Group 1 only R4 road showed a good correlation to R1 Road. Group 2 roads, R7 and R6 showed better correlation than at the half-payload data, with one section of R6 road showing better correlation to R7 Road than the other (see Figure 74). These results were once again expected based on the results of the linear regression for cycle correlation.

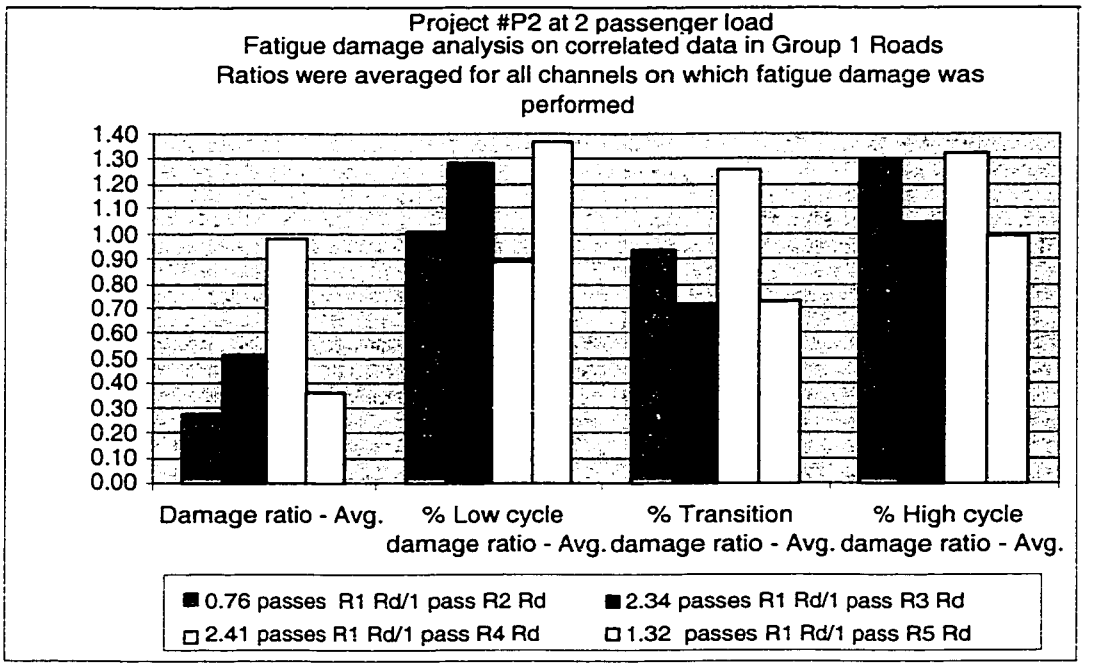

Figure 73. Fatigue damage correlation between R1 Road and the correlated roads of Group 1 (R2, R3, R4 and R5). Only R4 (yellow) road showed satisfactory correlation.

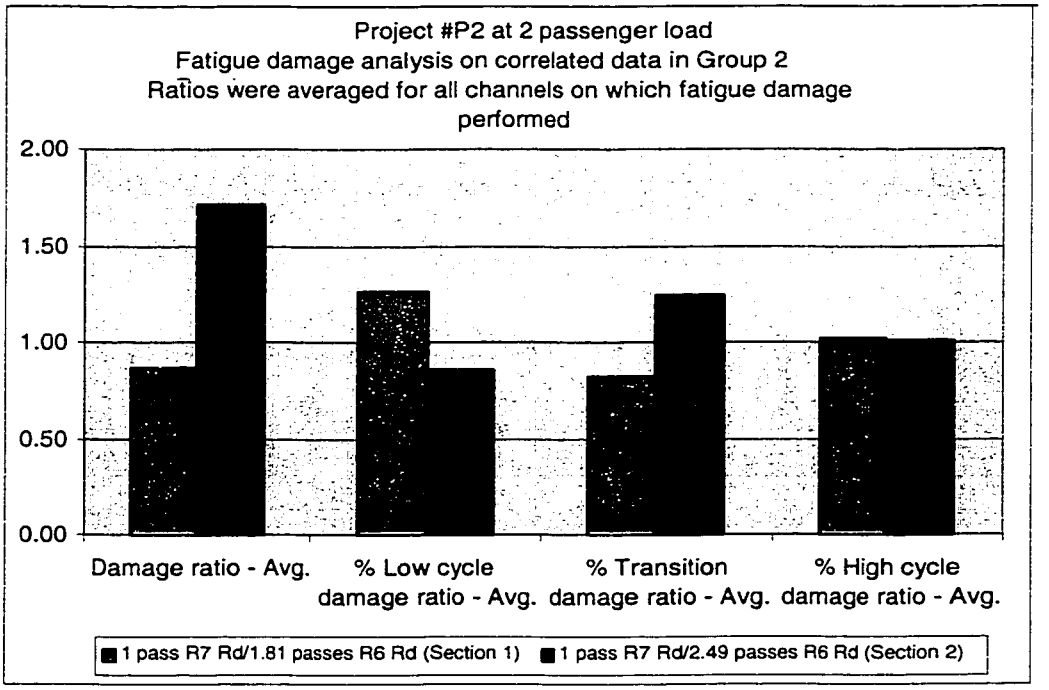

Figure 74. Fatigue damage correlation between R7 Road and the correlated R6 Road Sections. P2 test at 2-passenger load showed improved correlation between R7 and R6 Road as compared to the half-rated load, however significant differences were still observed.

The time histories of roads that did not correlate well (R2, R3, R5, R7 and R6) revealed no anomalies, since any offsets, or drifts were removed by passing data through a 0.2 Hz high pass filter.

Next a closer look was paid to the PDF functions showing amplitude distributions of Group 1 roads. Plotting the PDF functions for all Group 1 roads for all channels considered, showed significant differences in amplitude distributions of vehicle responses collected from R5, R3 and R2 Roads. One of those plots for channel 1 data is shown in Figure 75. Figure 76 shows the same plot but plotted on a logarithmic scale to attenuate the differences.

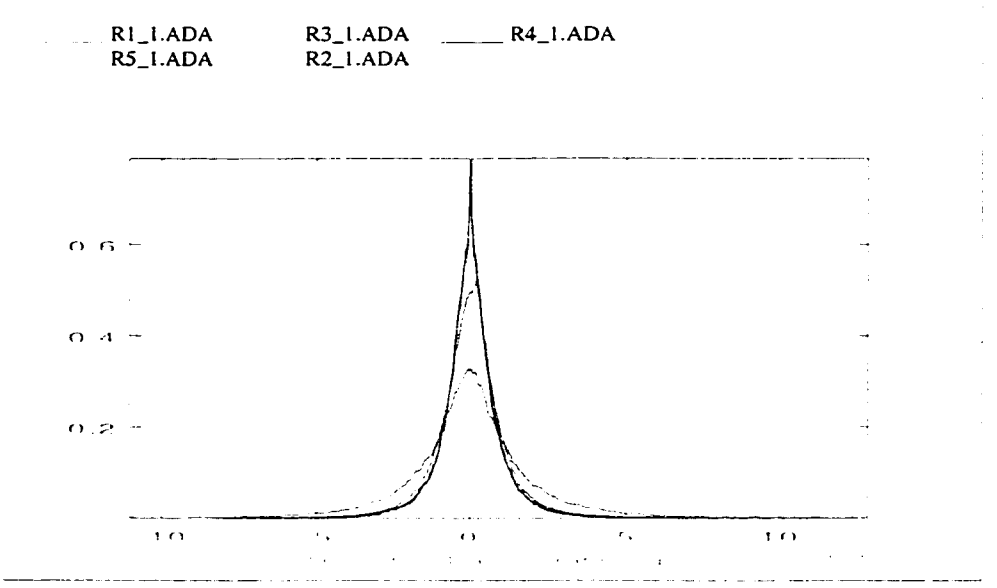

Figure 75. Plot of PDF functions for Group 1 roads of test #P2 at 2-passenger load, for channel 1 data. Only PDFs of R1 (red) and R4 (navy) Roads showed resemblance, while R5 (light blue), R3 (green) and R2 (yellow) differed in amplitude distributions.

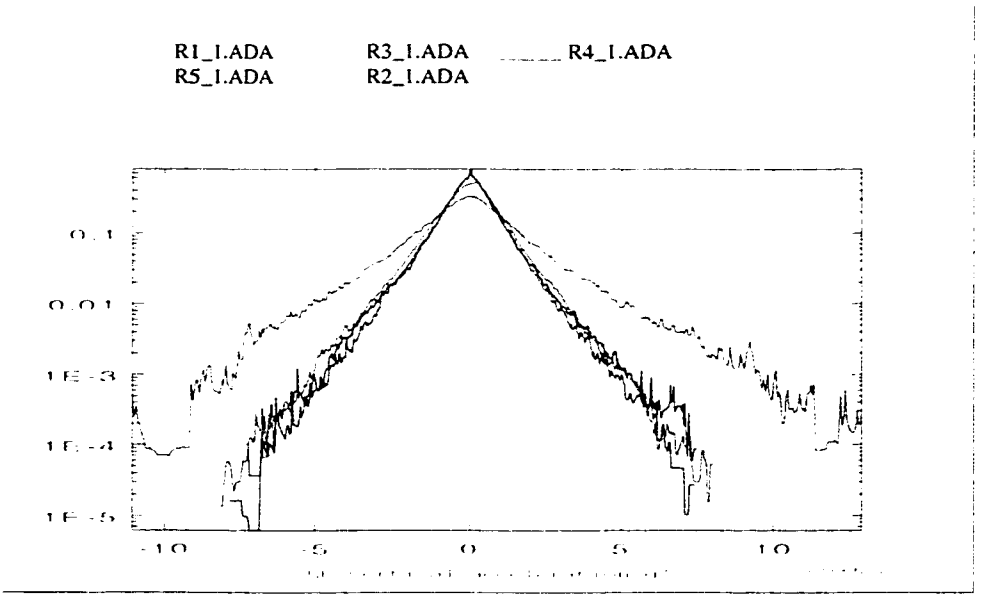

Figure 76. Plot of PDF functions for Group1 roads of test #P2 at 2-passenger load for channel 1 data plotted on logarithmic scale. Only PDFs of R1 (red) and R4 (navy) road showed resemblance, while R5 (light blue), R3 (green) and R2 (yellow) differed in amplitude distributions.

The differences in amplitude distributions were very evident, especially for R5 and R2 Roads for all channels considered.

Next, a closer look at the PSD for the Group 1 roads was taken. Once again significant differences were observed in R3, R5 and R2 Roads from the remaining roads of Group 1 (R1 and R4), not only in PSD profile but also frequency content. Figure 77 shows PSD plots for Group 1 roads (channel 1), which illustrates these differences. Figure 78 is the same graph but plotted on y-log scale.

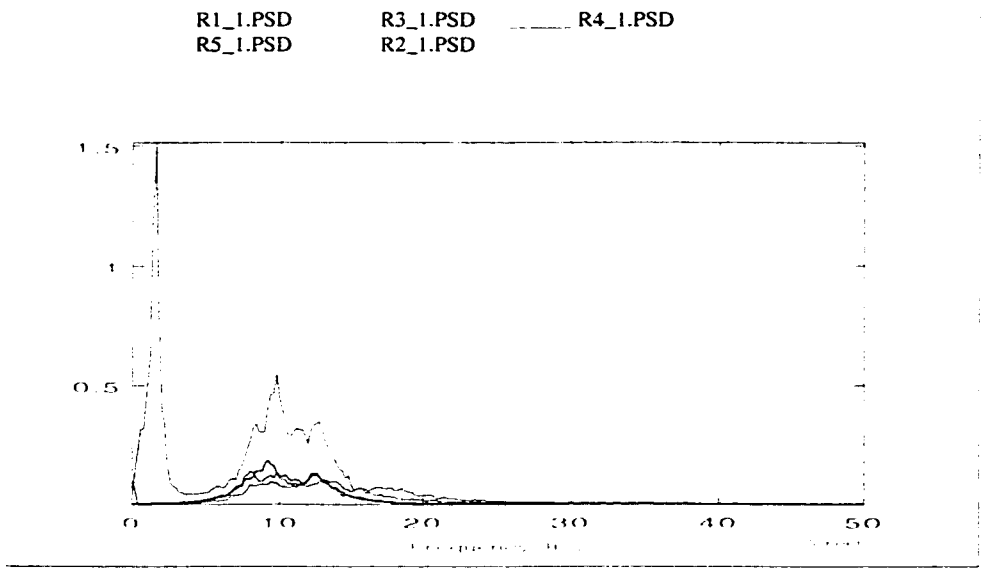

Figure 77. Plot of PSD functions for Group 1 roads of test #P2 at 2-passenger load, for channel 1 data. Only PSDs of R1 (red) and R4 (navy) road showed resemblance, while, R3 (green), R5 (light blue) and R2 (yellow) differed in both PSD profiles and frequency contents, especially R2 and R5

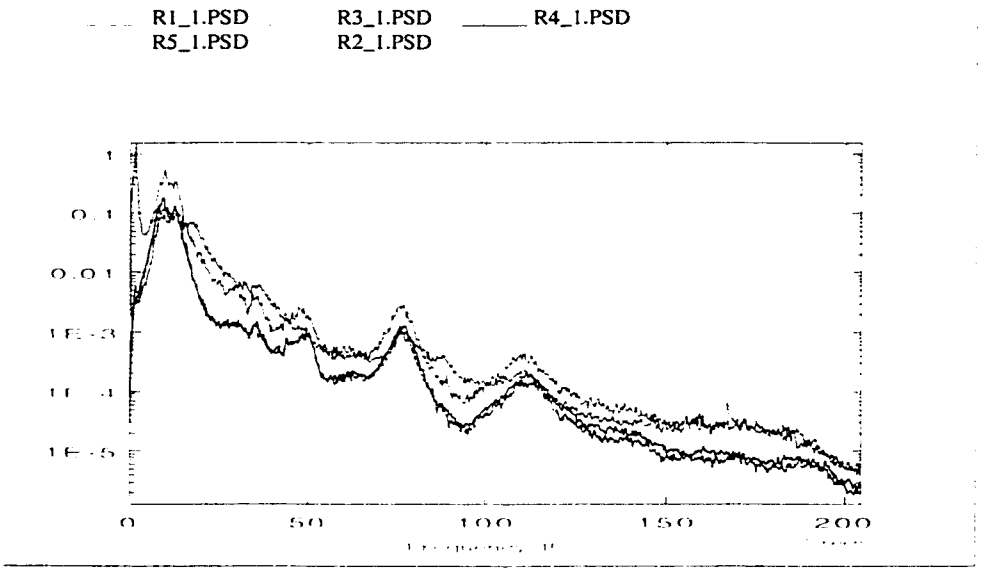

Figure 78. Plot of PSD functions for Group 1 roads of test #P2 at 2-passenger load, for channel 1 data plotted on a logarithmic scale. Only PSDs of R1 (red) and R4 (navy) road showed resemblance, while R3 (green), R5 (light blue) and R2 (yellow) differed in frequency contents, especially in a range of 0-7 Hz. These differences were mostly observed in R5 and R2 Roads.

The correlation for Group 1 roads proved to be even less satisfactory when using 2-passenger payload data than for half payload. Only R1 and R4 roads could be classified with some confidence as roads inducing similar behaviors in vehicles based on the data analysis of the P2 test at 2-passenger payload, whereas at half-payload all except R2 and R5 Roads correlated well. This shows that perhaps the quality of the data rather than road inputs caused the poor correlation of the roads of Group 1.

R6 Road and R7 Wash showed much better correlation when using 2-passanger payload data rather than half-payload, as shown in Figures 62 and 72, with one section (labeled 1) of R6 Road correlating better than the other.

The PDF plots, shown in Figures 79 and 80 (log-scale), of the R6 and R7 Roads for channel 1 data and for both half and 2-passenger load explain this phenomenon. The labeling system for these graphs is as follows: for 2-passanger loading, R6 Section 1 is colored red, R6 Section 2 is yellow and R7 Road is green, for half payload, R6 Section 1 is navy, R6 Section 2 is light blue and R7 is black.

The PDF functions of R6 Section 1 (red) and R7 (green) Road in 2-pasanger loading condition show a significant resemblance, while section 2 of R6 Road (yellow) shows a different amplitude distribution. For half-payload condition none of the roads show any likeness to one another. It is however apparent that both R6 Road sections show resemblance for the two loading conditions, while the R7 Road PDF functions stray from one another.

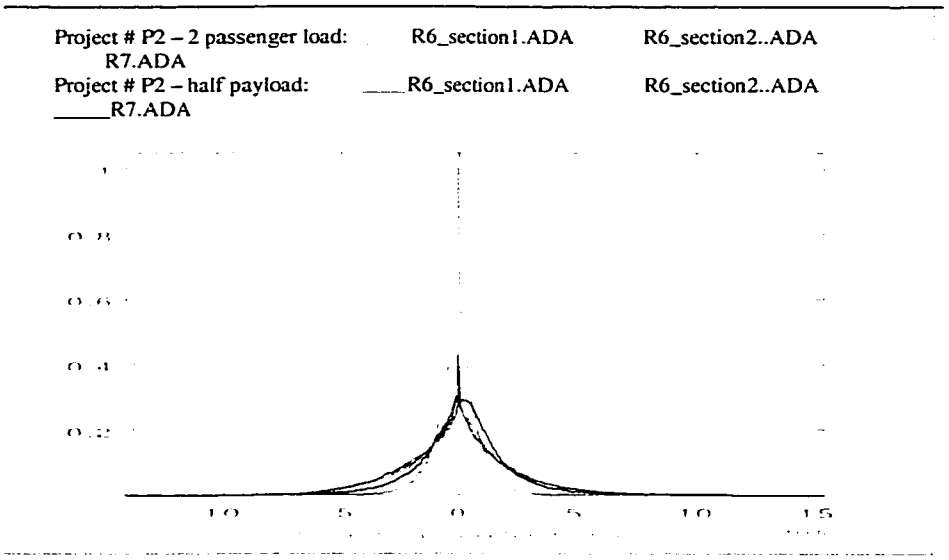

Figure 79. Plot of PDF functions of Group 2 roads in #P2 test, for channel 1 data. The 2-passenger data showed better correlation among group 2 roads than did half-payload data, with section 1 of R6 Road resembling R7 road better than section 2. The labeling system is as follows: for 2-passanger loading, R6 Section 1 is colored red, R6 Section 2 is yellow and R7 Road is green. For half payload, R6 Section 1 is navy, R6 Section 2 is light blue and R7 is black.

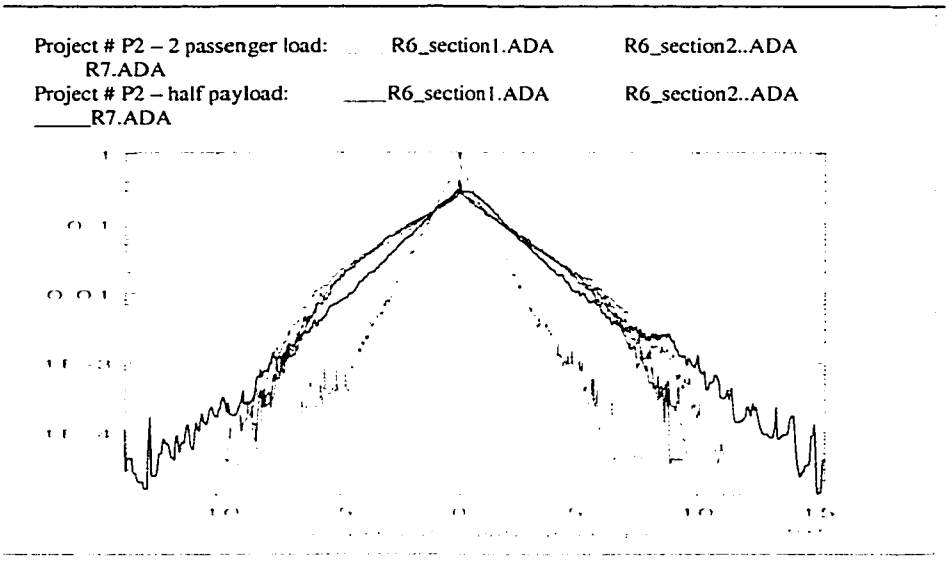

Figure 80. Plot of PDF functions for test #P2, for channel 1 data and for group 2 roads plotted on log scale. 2-passenger data showed better correlation among group 2 roads than did half-payload, with section 1 of R6 Road resembling R7 road better than section 2. The labeling system is as follows: for 2-passanger loading, R6 Section 1 is colored red, R6 Section 2 is yellow and R7 Road is green. For half payload, R6 Section 1 is navy, R6 Section 2 is light blue and R7 is black.

When PSD graphs were plotted for both the R7 and R6 Roads, for the two payloads and all channels, all except R7 at half payload (black) showed resemblance in profile and frequency content. One of the plots for channel 1 data is shown in Figure 81.

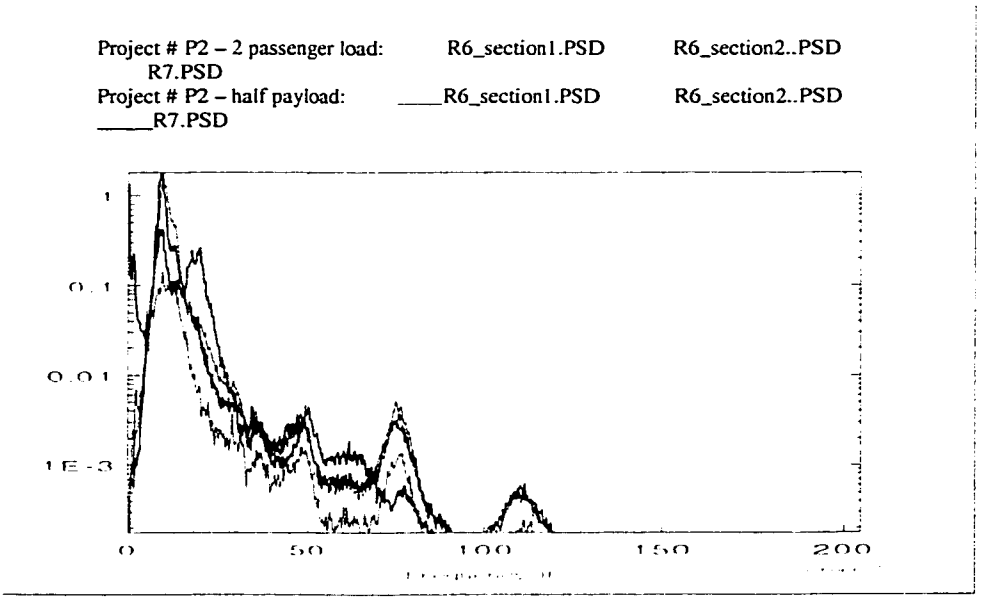

Figure 81. Plot of PSD functions of Group 2 roads in test #P2 for channel 1 data, plotted on log scale. The labeling system is as follows: for 2-passanger loading, R6 Section 1 is colored red, R6 Section 2 is yellow and R7 Road is green. For half payload, R6 Section 1 is navy, R6 Section 2 is light blue and R7 is black. Only R7 Road in half-payload condition (black) shows difference in profile than the other roads (especially between 0-6 Hz range), which could explain the poor correlation between the R7 and R6 roads, at that payload.

When the results of both P1 at full rated load and P2 at half and 2-passanger tests where compared to one another, it was shown that the roads that correlated well in P2 test showed significant similarities in PDF and PSD plots to those of project #P1 data. The roads that resulted in poor correlation in project #P2, either at half-payload or 2-passanger payload, showed considerable differences in amplitude distributions and frequency profiles. The question is whether the roads did not correlate well because of poor quality data, or due to changes in road conditions. It seems more likely however that it was the quality of the data that affected the results, especially in Group 1 roads. This can be explained by the fact that even if the road conditions changed significantly between years 1996 and 1997, similar results would still be expected from P2 test

regardless of which payload was used. Since however, some roads correlated well under one payload condition but not under the other, it is highly unlikely that the differences are attributable to road inputs.

The differences in Group 2 roads are most likely attributable to the changing road conditions of R7 Road, as shown in Table 14. However since the data analysis of P2 test produced inconclusive results, another two sets of data were analyzed.

6.3 Project #P3

Since the results obtained with P1 data were not totally verified by the project P2 data, possibly due to poor quality data, another substantiation was required. For that, data recently collected by Defiance/Manta for vehicle V3 was used, at both full and 2-passanger payloads. The full rated load data had to be filtered through a 0.2 high pass filter to remove significant offsets and drifts. Unfiltered (raw) data was used for 2-passenger load data. The results of correlation were indeed agreeable with project #P1, although some issues were raised with regard to grouping R7 and R6 roads. These will be discussed below.

Once again the R8, R9 and R10 Roads showed a substantial distinction from each other and other roads included in the OR test. Thus, inclusion of all three roads in the durability cycle is necessary to preserve the integrity of the test.

Correlation based on matching the number of cycles at particular range values of the rainflow matrix showed that two main groups of roads could be formed. The first group included R1, R2, R3, R4 and R5 roads, while the second group consisted of R7 and R6 Washes. The results of the cycle correlation are presented in Figures 82 and 83 for Group 1 at full payload and 2-passenger payload respectively. Figures 84 and 85 present the correlation outcomes for Group 2 at full payload and 2-pasanger payload respectively.

Both Group 1 and Group 2 cycle correlation results for both payloads, proved to be agreeable with the results of P1 test. Linear regression showed correlation coefficients close to one, "low" RMS and absolute errors (less than 300, and less than 100 respectively) as defined in Section 6.1. The only exception was in correlating R7 and R6 Road – Section 2, where although correlation coefficients were close to one, the RMS and absolute cyclic errors were higher than expected for good correlation.

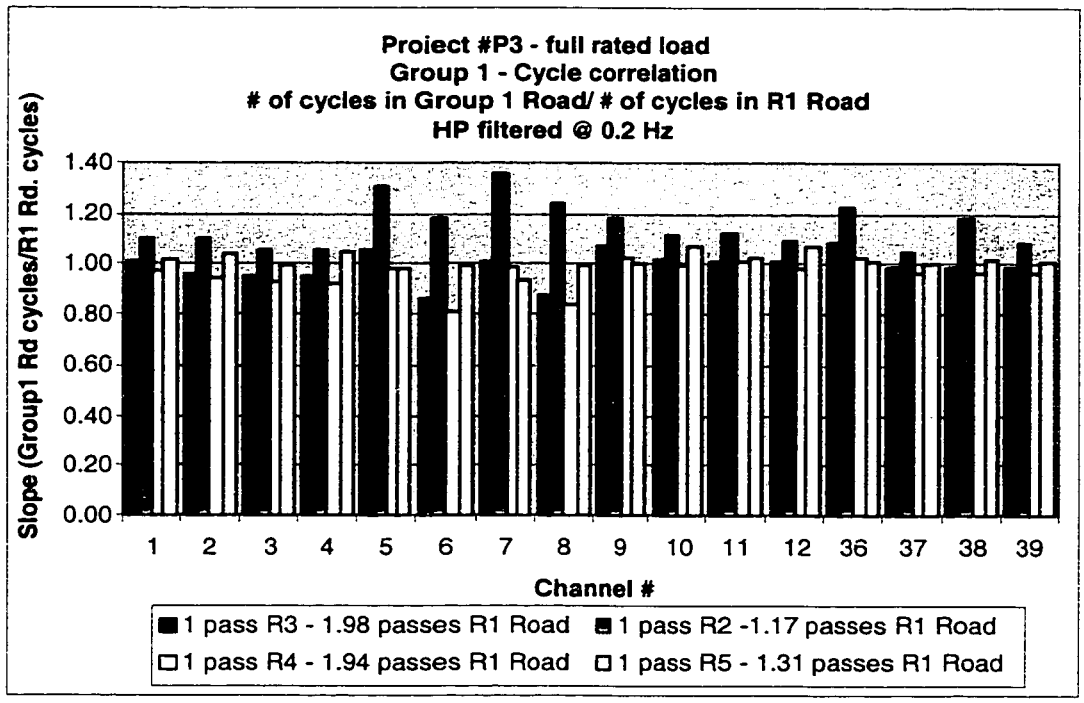

Figure 82. Cycle correlation between R1 Road and the remaining roads of Group 1 (R2, R3, R4 and R5) at full rated load. The y-axis value represents a slope (rise/run) of a line obtained through linear regression, while trying to match number of cycles in each of 64 bins of data from R1 Road (run) to other Group 1 roads (rise). This figure clearly illustrates that the Group 1 roads do indeed produce similar responses in a vehicle in all studied channels of collected data.

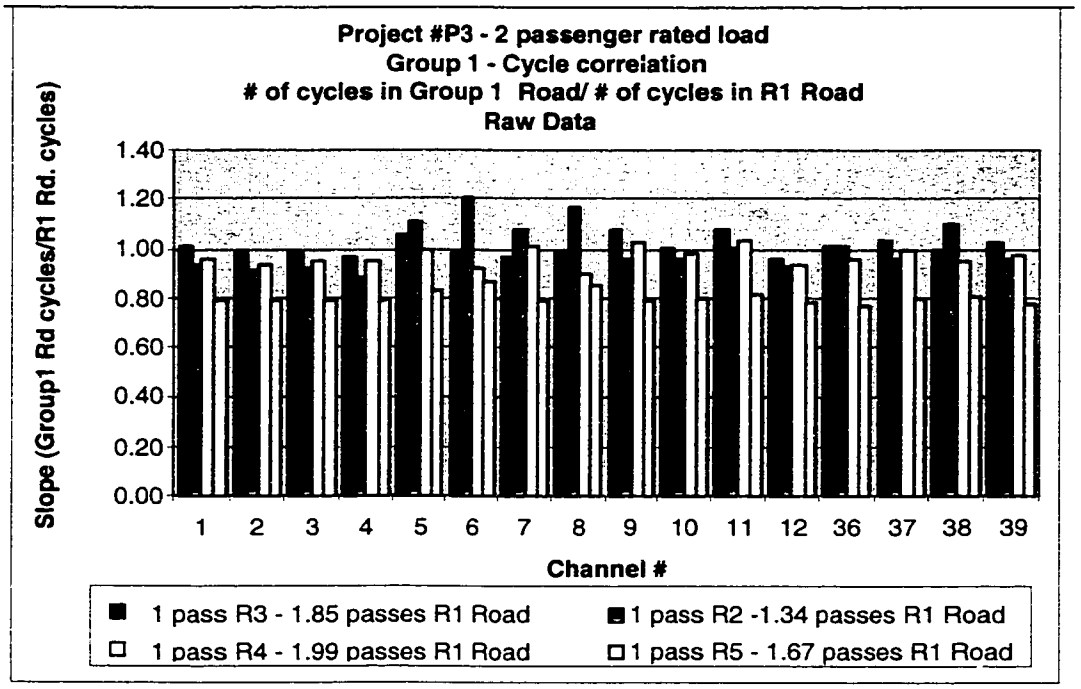

Figure 83. Fatigue damage correlation between R1 Road and the correlated roads of Group 1 (R2, R3, R4 and R5) at two-passenger load. The y-axis value represents a slope (rise/run) of a line obtained through linear regression, while trying to match number of cycles in each of 64 bins of data from R1 Road (run) to other Group 1 roads (rise). Once again, this figure clearly illustrates that the Group 1 roads do indeed produce similar responses in a vehicle in all studied channels of collected data.

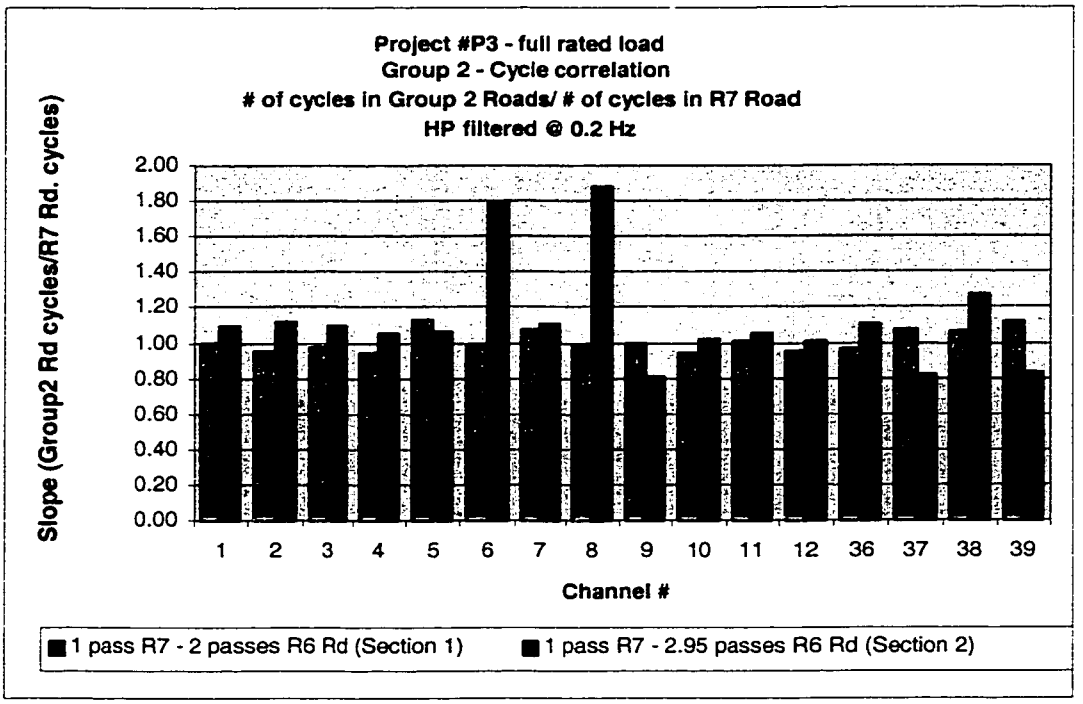

Figure 84. Fatigue damage correlation between R7 Road and the correlated roads of Group 2 (R6 Section 1 and Section 2) at full payload. The y-axis value represents a slope (rise/run) of a line obtained through linear regression, while trying to match number of cycles in each of 64 bins of data from R7 Road (run) to other Group 2 roads (rise). This figure clearly illustrates that the Group 2 roads do indeed produce similar responses in a vehicle in majority of studied channels, with the exception of channel 6 and 8 for R6 Road Section 2. This is because the absolute cyclic errors for these two channels were the highest.

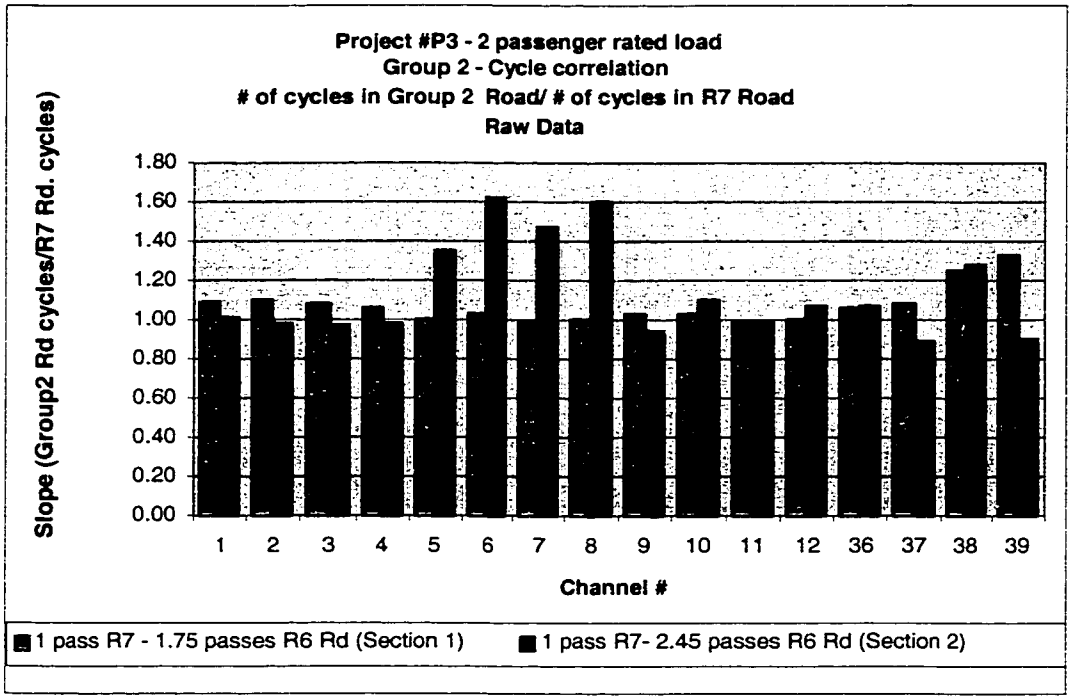

Figure 85. Fatigue damage correlation between R7 Road and the correlated roads of Group 2 (R6 Section 1 and Section 2) at 2-passenger payload. The y-axis value represents a slope (rise/run) of a line obtained through linear regression, while trying to match number of cycles in each of 64 bins of data from R7 Road (run) to other Group 2 roads (rise). This figure clearly illustrates that the Group 2 roads do indeed produce similar responses in a vehicle in majority of studied channels, with the exception of channel 5 to 8 for R6 Road Section 2.

Fatigue analysis was then performed to further verify the results. For Group 1, both full rated and 2-passenger load cases presented satisfactory damage correlations. The averaged damage ratios (for all channels condisered in damage analysis) and damage distribution ratios for Group 1 at full and 2-passenger payload are presented in Figures 86 and 87 respectively.

As shown in Figures 86 and 87, the roads of group 1 correlated well based on damage acquired and damage distribution.

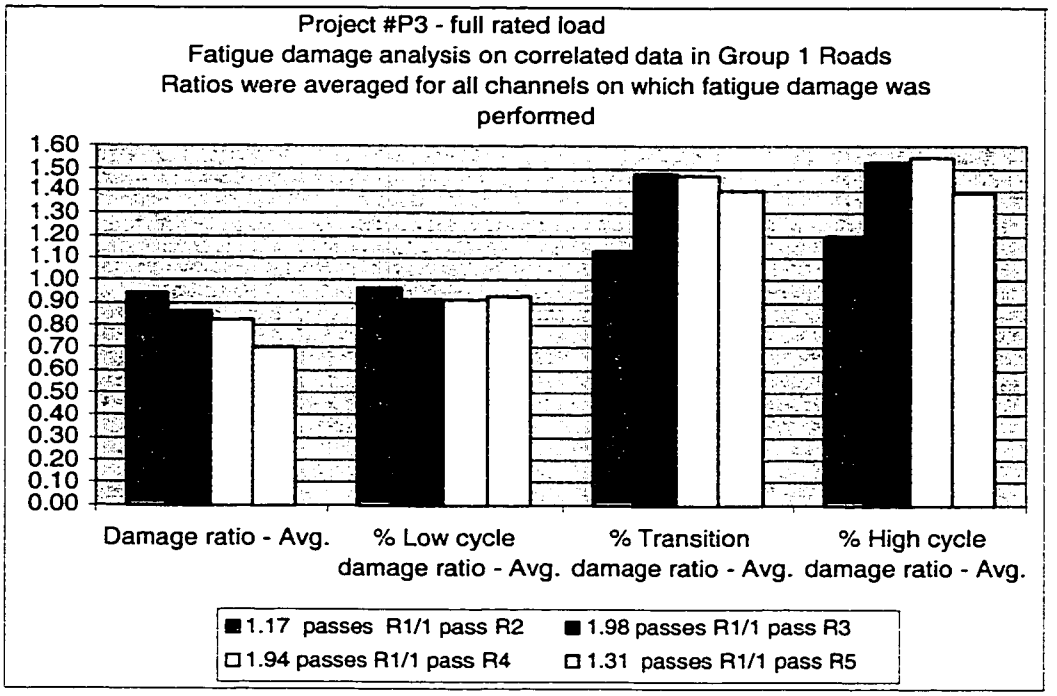

Figure 86. Fatigue damage correlation between R1 Road and the remaining roads of Group 1 (R2, R3, R4 and R5) at full rated load. This illustrates that all roads in Group 1 induce similar damage in the tested vehicle.

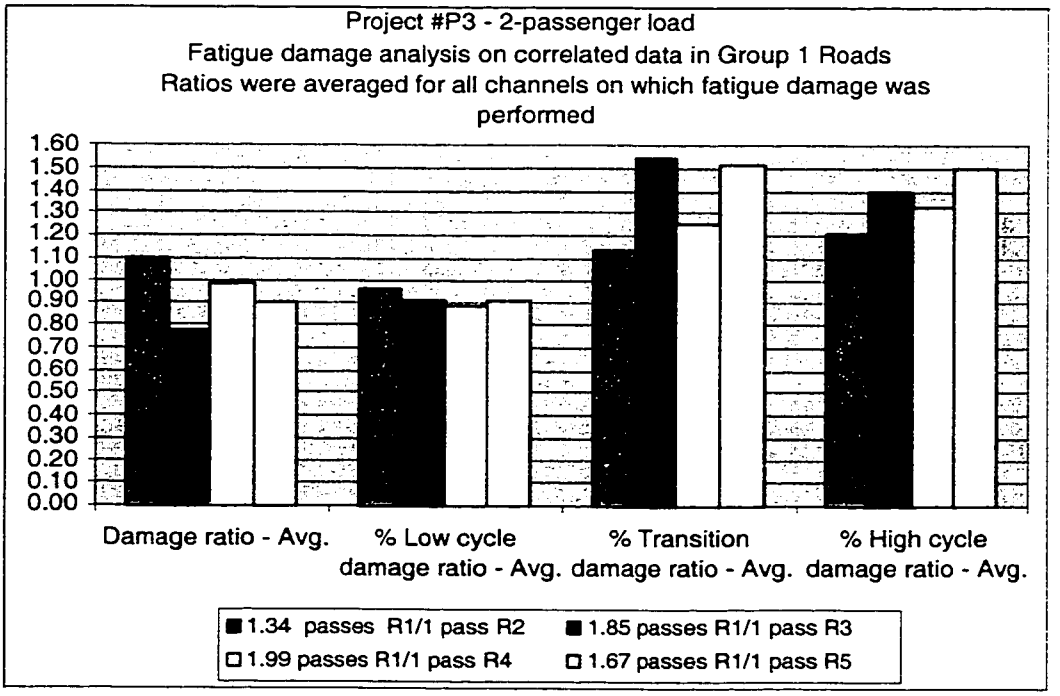

Figure 87. Fatigue damage correlation between R1 Road and the correlated roads of Group 1 (R2, R3, R4 and R5) at 2-passenger load. This illustrates that all roads in Group 1 induce similar damage in the tested vehicle.

When damage analysis was performed on Group 2 roads, the results were not that inadequate, especially when it came to damage distribution. The avergaged damage ratios (for all channels considered in damage analysis) and damage distribution ratios for Group 2 at full and 2-passenger payload are presented in Figures 88 and 89.

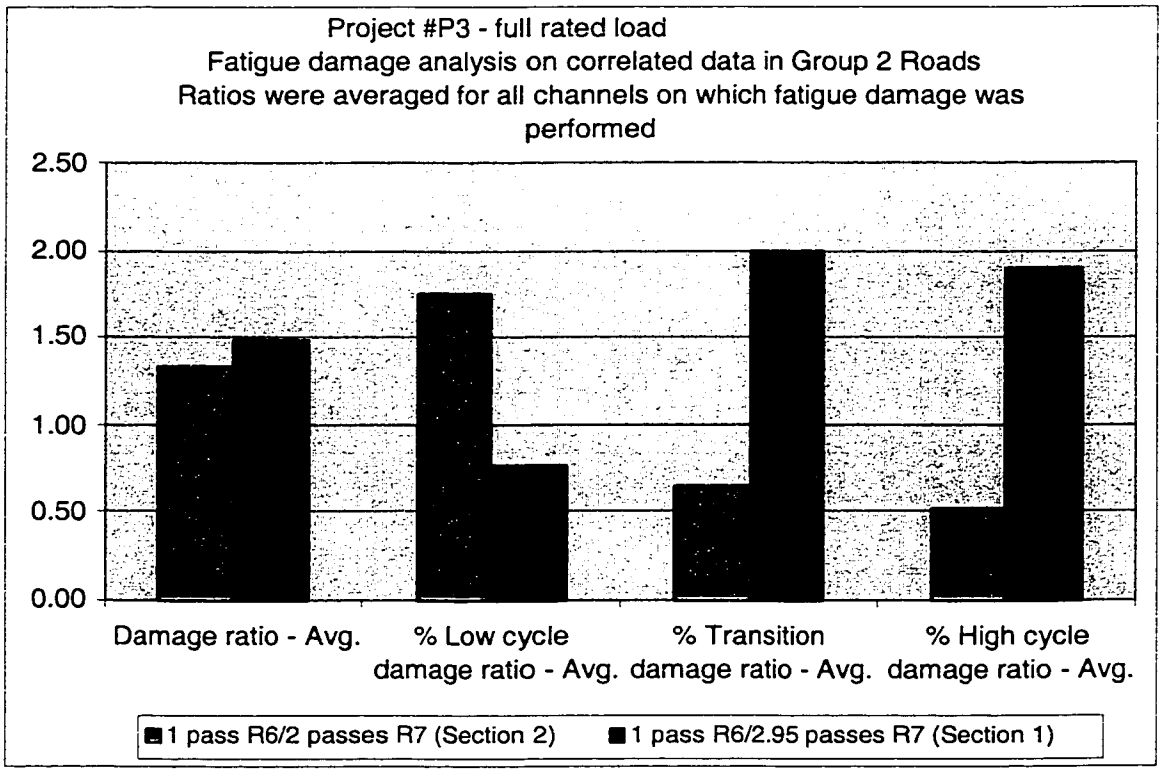

Figure 88. Fatigue damage correlation between R7 Road and the correlated roads of Group 2 (R6 Section 1 and 2) at full payload. The relative damage correlation proved to be unsatisfactory in relating R7 and R6 Roads, especially in damage distributions among high, low and transition life.

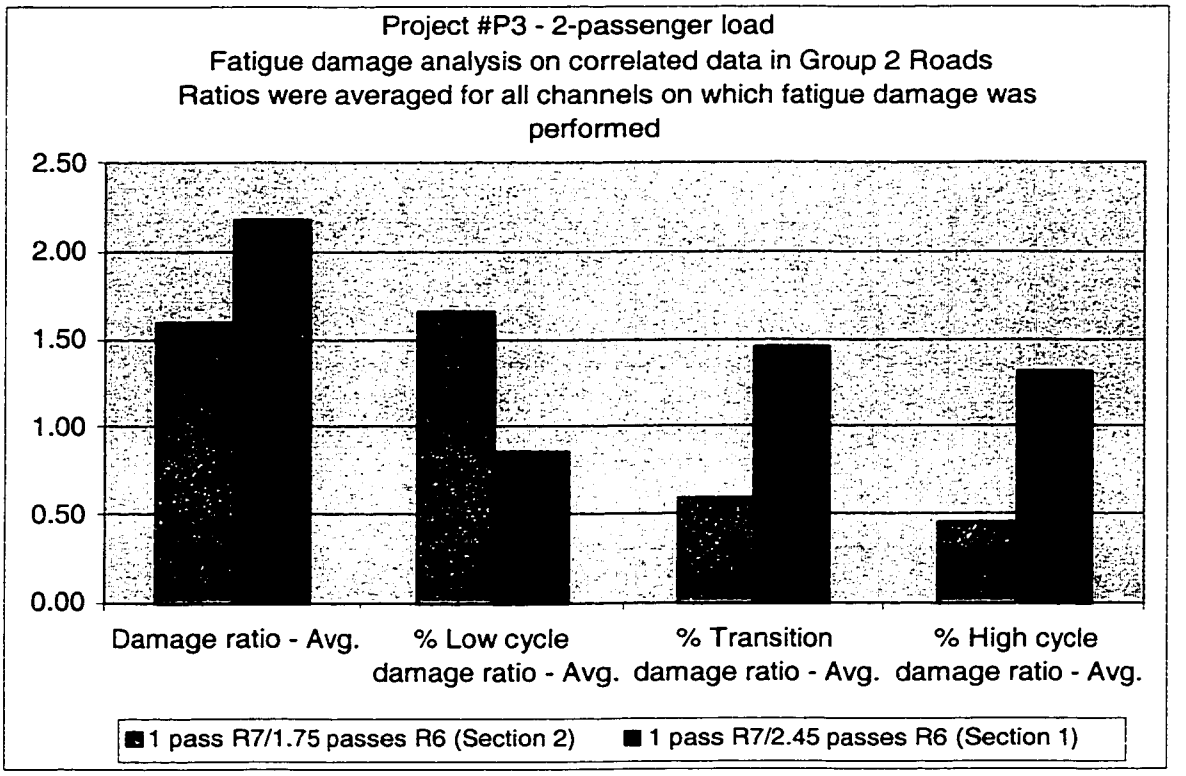

Figure 89. Fatigue damage correlation between R7 Road and the correlated roads of Group 2 (R6 Section 1 and 2) at 2-passenger payload. The relative damage correlation proved to be unsatisfactory in relating R7 and R6 Roads, especially in damage distributions among high, low and transition life.

To explain the reason behind the R7 and R6 roads not correlating very well, a close look at amplitude and frequency distribution will be taken.

First however, a further verification of Roads of Group 1 will be considered. The PDF plots for all channels of data showed a resemblance in amplitude distributions for all roads in Group 1, at both full and 2-passenger loading. This is demonstrated in Figures 90 and 91 respectively, for channel 38 data.

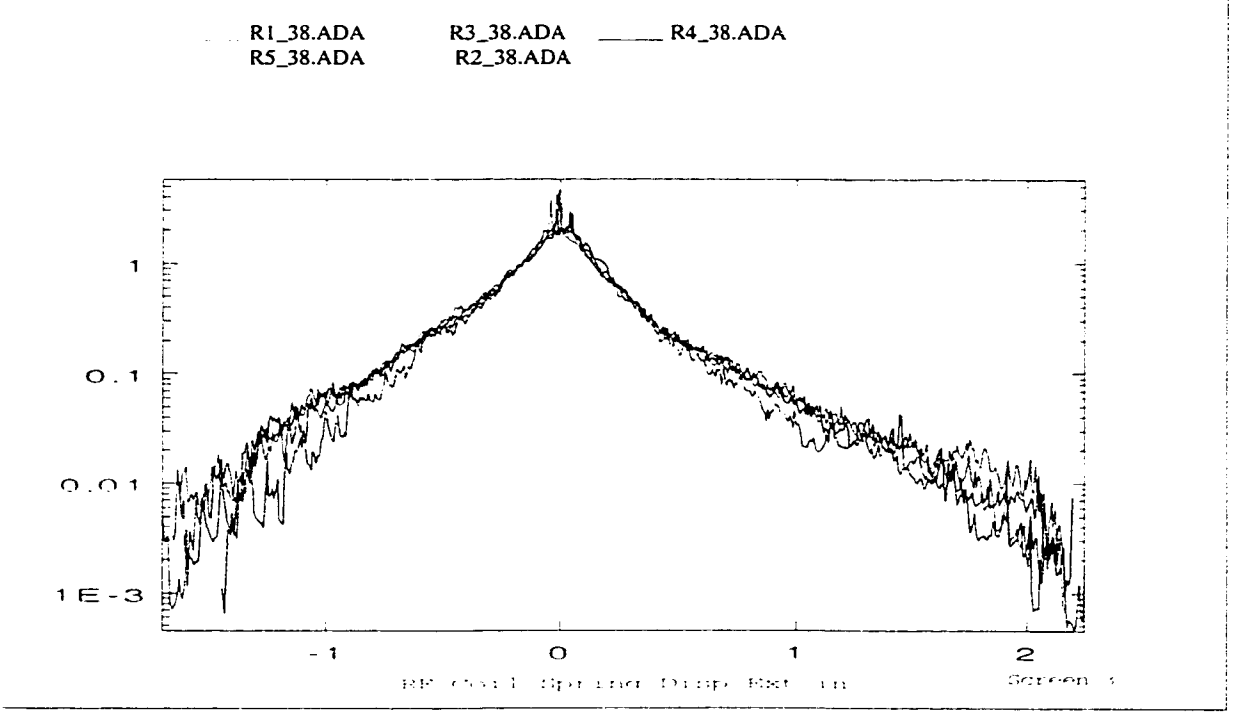

Figure 90. Plot of PDF functions for the P3 test at full rated load, for channel 38 data and for Group 1 roads plotted on log scale. All roads of Group 1 show similarities in amplitude distributions.

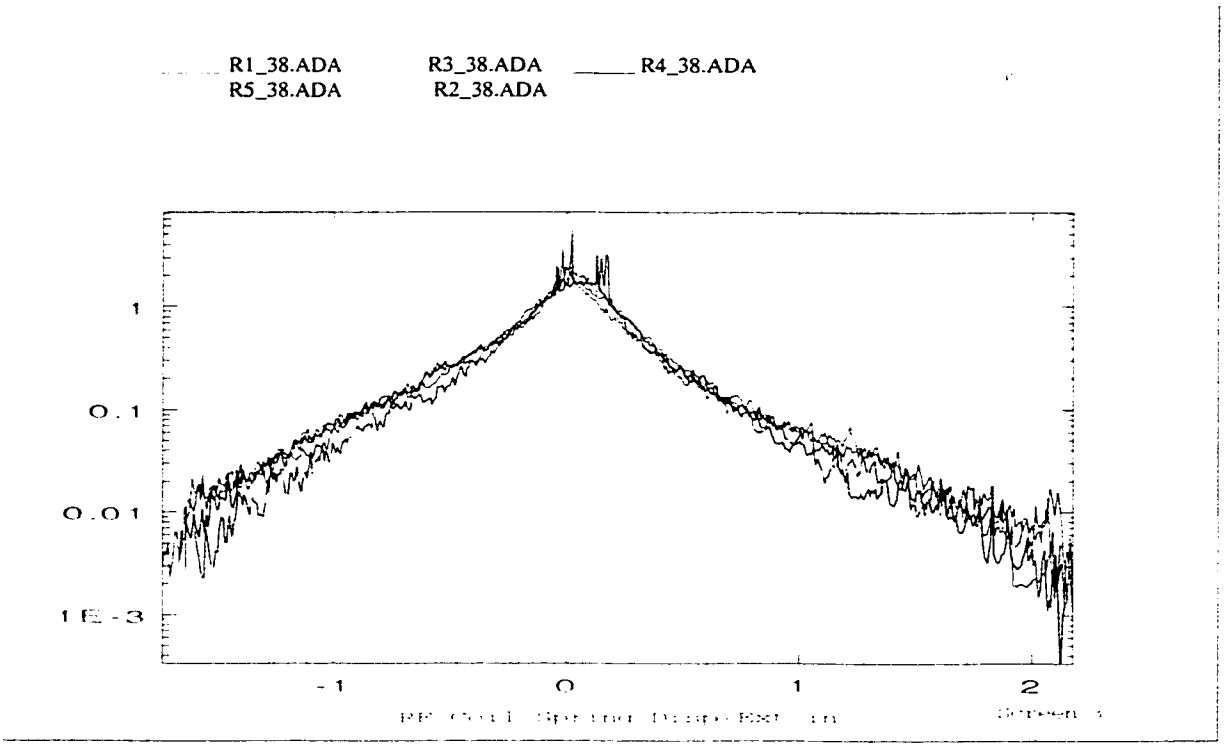

Figure 91. Plot of PDF functions for test P3 test at 2-passenger load, for channel 38 data and for group 1 roads plotted on log scale. All roads in Group 1 show similarities in amplitude distributions.

Similar resemblance was observed for Group 1 roads, and all channels considered, in frequency distribution. This is illustrated in Figures 92 and 93 which plot PSD functions for selected channel 38 for full and 2-passenger payload respectively.

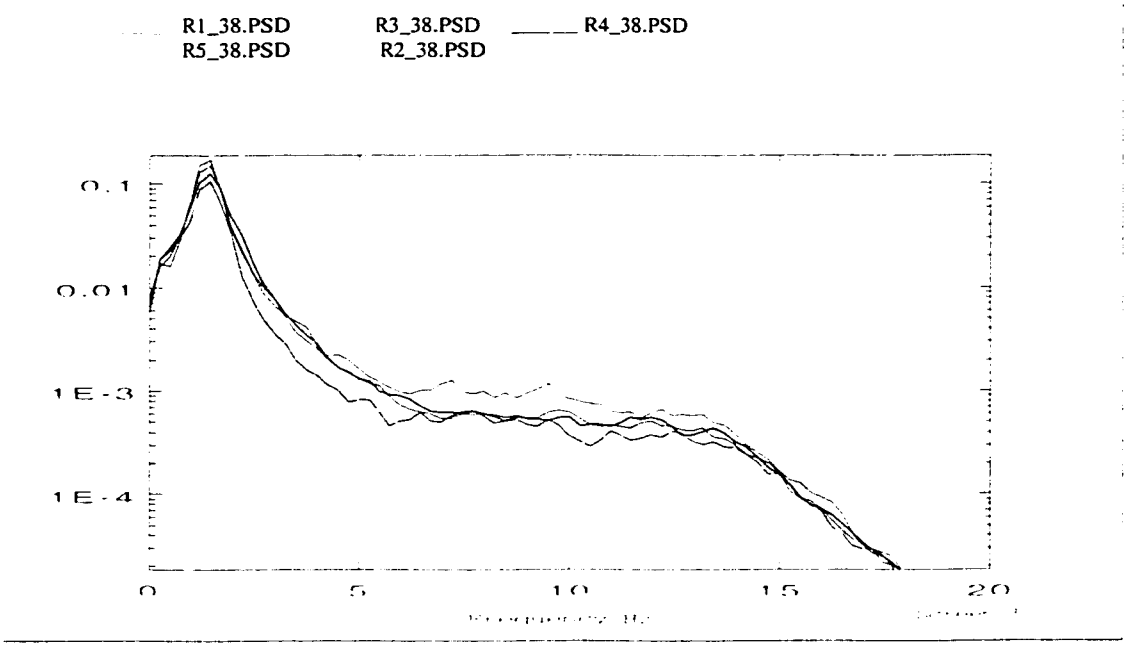

Figure 92. Plot of PSD functions for the Group 1 roads in the P3 test at full rated load, for channel 38 data plotted on log scale. All roads show similarities in frequency content and profile.

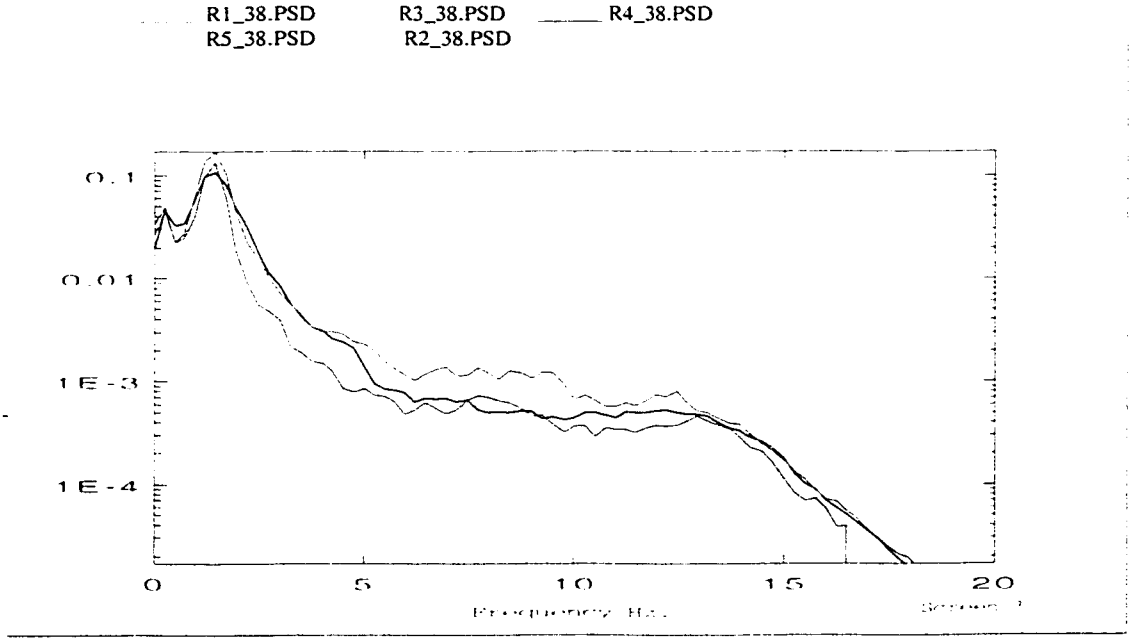

Figure 93. Plot of PSD functions for the Group 1 roads in the P3 test at 2-passenger load, for channel 38 data plotted on log scale . All roads show similarities in frequency content and profile.

The same analysis was conducted for the R7 and R6 Roads. Although cycle correlation proved to be reasonably adequate (see Figures 84 and 85), the damage analysis showed differences in damage distribution between these two roads.

The amplitude distributions of the responses, collected from R7 and R6 Roads, showed good correlation only for vertical acceleration channels, as shown in Figure 94 and 95 for full and 2-passenger payloads respectively. The body to spindle displacement channels based on which fatigue analysis was conducted, together with remaining channels, showed differences in their PDF plots. Coil Spring Channel PDF plots for R7 and R6 roads are shown in Figures 96 and 97 for full and 2-passenger payloads.

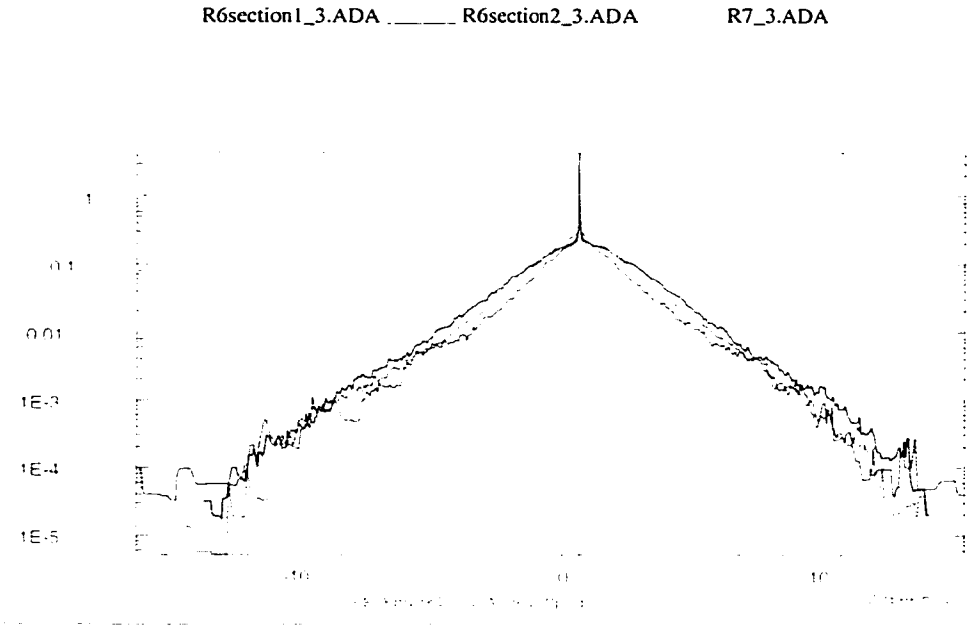

Figure 94. Plot of PDF functions for Group 2 roads in the P3 test at full rated load, for vertical acceleration channel (Ch 3) plotted on log scale. All roads show similarities in amplitude distributions.

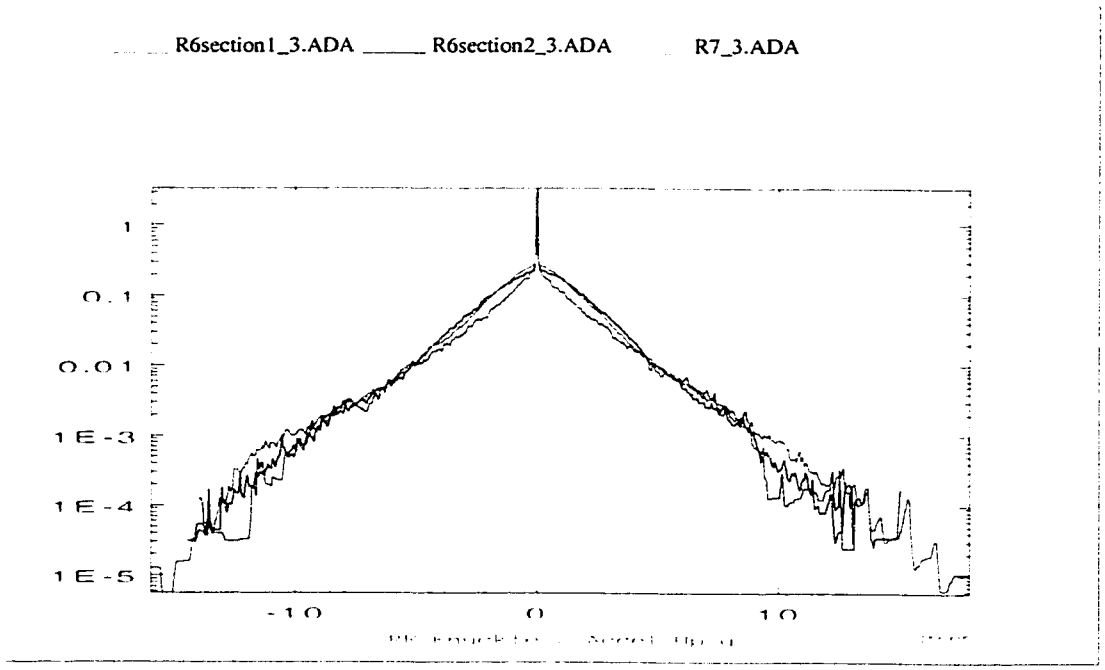

Figure 95. Plot of PDF functions for test project P3 data at 2-passenger load, for vertical acceleration channel (Ch 3) and for group 2 roads (R7 and R6) plotted on log scale. All roads show similarities in amplitude distributions.

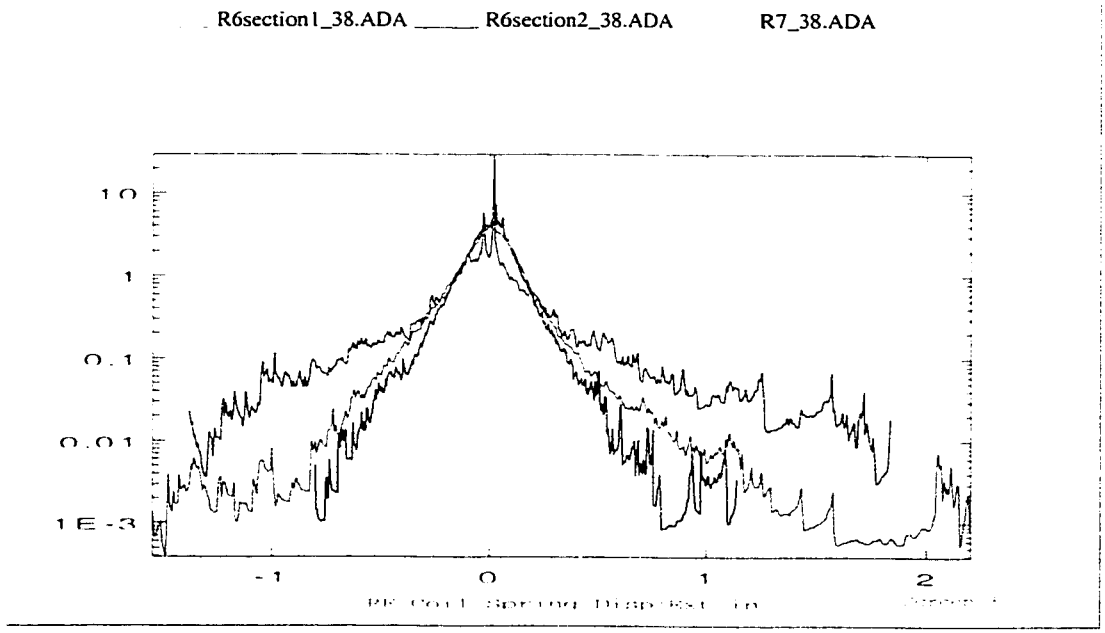

Figure 96. Plot of PDF functions for Group 2 roads in the P3 test at full payload, for coils spring displacement channel (Ch 38) and for group 2 roads plotted on log scale. Amplitude distribution varies tremendously in the roads of Group 2 for all channels except the vertical acceleration channels.

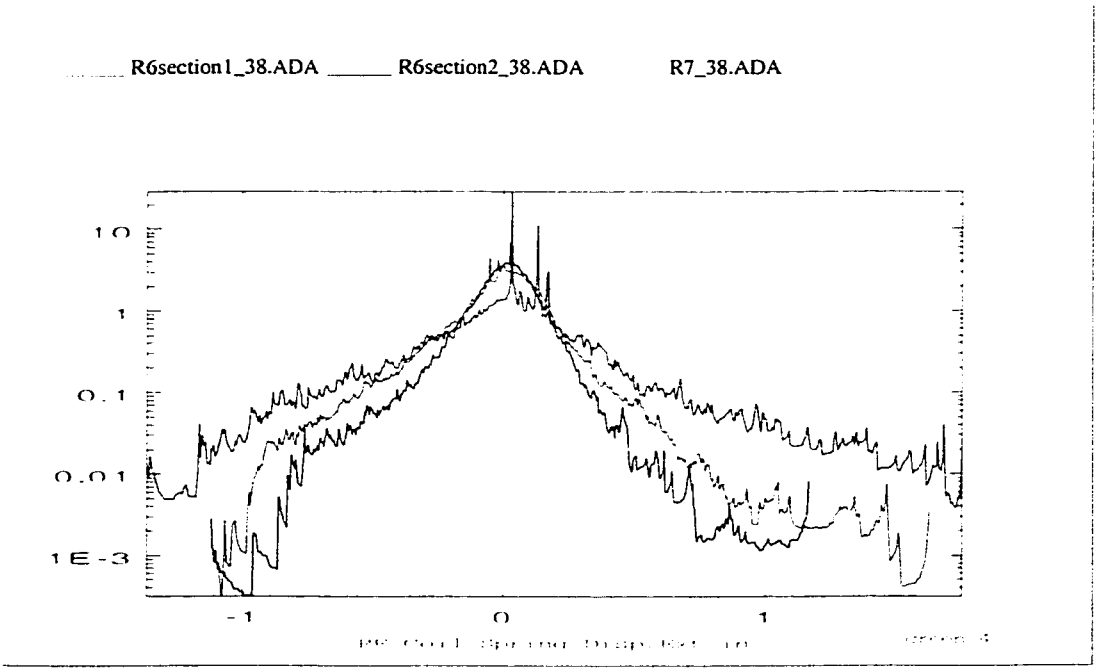

Figure 97. Plot of PDF functions for Group2 roads in the P3 test at 2-passenger payload, for coils spring displacement channel (Ch 38) plotted on log scale. Amplitude distribution varies tremendously in the roads of Group 2 for all channels except the vertical acceleration channels.

The PSD functions showed good correlation for all channels of R7 and R6 Roads, in both frequency content and profiles. The most noticeable differences were observed in the spindle to body displacement channels, where there were significant differences in energy content at some frequencies. PSD plots for a vertical acceleration channel are shown in Figures 98 and 99 for full and 2-passenger load respectively. PSD plots for a coil spring displacement channel are shown in Figures 100 and 101 for full and 2-passenger load respectively.

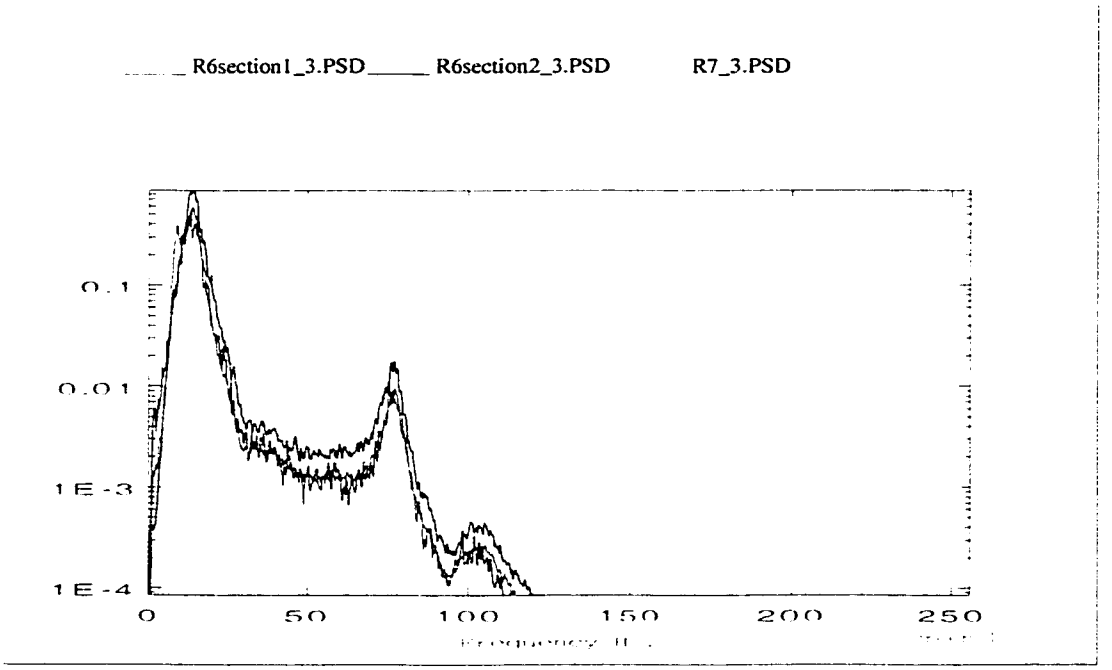

Figure 98. Plot of PSD functions for Group 2 roads in the P3 test at full payload, for vertical acceleration channel (Ch 3) plotted on log scale. Similarities in frequency content and PSD profiles were observed.

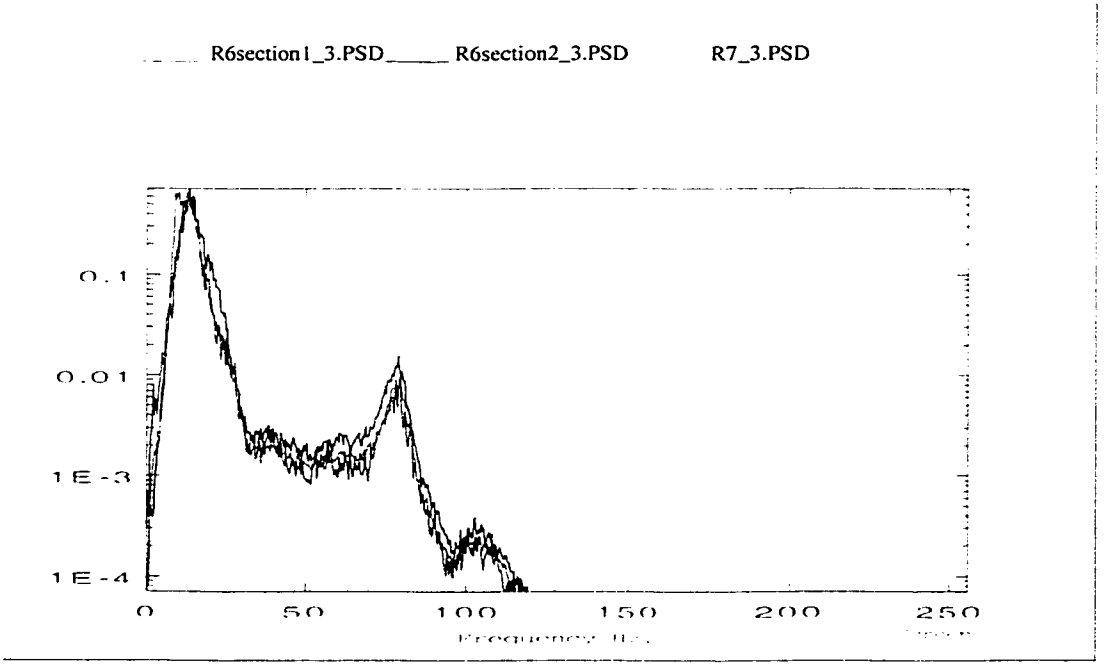

Figure 99. Plot of PSD functions for Group 2 roads in the P3 test, at 2-passenger payload, for vertical acceleration channel (Ch 3) plotted on log scale. Similarities in frequency content and PSD profiles were observed.

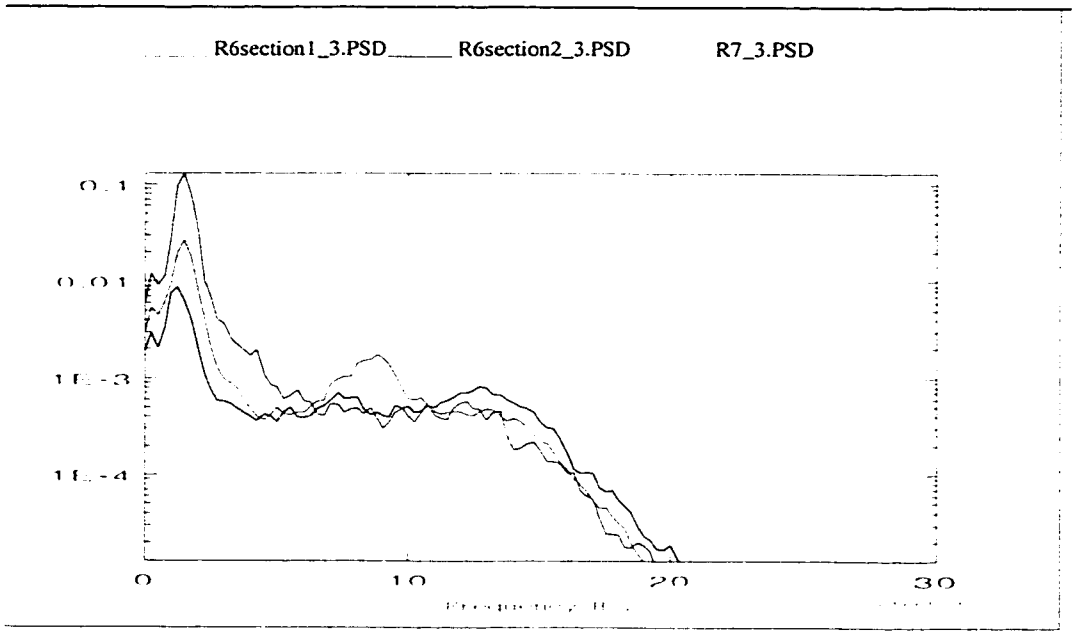

Figure 100. Plot of PSD functions for Group 2 roads in the P3 test at full payload, for coils spring displacement channel (Ch 38) plotted on log scale. Although frequency content was preserved, some differences were observed in intensities at some frequencies even when plotted on log scale.

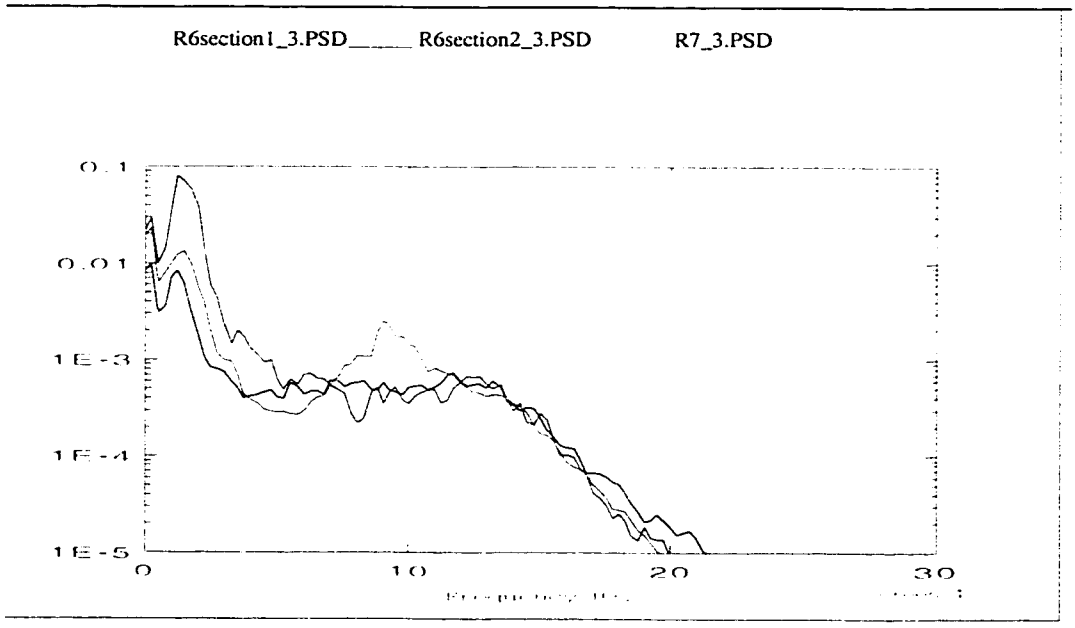

Figure 101. Plot of PSD functions for test P3 data at 2-passenger load, for coils spring displacement channel (Ch 38) and for group 2 roads (R7 and R6) plotted on log scale. Once again, we see that although frequency content was preserved some differences were observed in intensities at some frequencies even when plotted on log scale.

The differences in the vehicle responses collected from R6 and R7 Roads during the project #P3 data acquisition, put in question whether or not these two roads should be grouped together. The differences in the responses collected from these two roads could however be assigned to their dynamic/changing road conditions. The road profiling report [17], conducted over 5 year period, showed that the changes in severity and washboard content of OR courses are mainly confined to the deeper sand sections of courses that run with the washes such as the R6 and R7 Roads.

7 CONCLUSIONS/RECOMMENDATIONS

7.1 Summary

Acceleration of vehicle testing is a significant time and cost reduction technique utilized currently in the automotive industry. In the early days, automotive manufacturers relied exclusively on the experiences obtained from previous generation products, to improve their performance, reliability or fix any mishaps. With the increase of product complexity, competition, and customer expectations, a need for faster methods of testing were foreseen. Before putting vehicles in production, manufacturers began assessing their performance and durability on public roads. Then came the proving grounds, which proved to be more economic, safe, and reliable. Distant road surfaces, grades, and soil conditions could be included in the service cycle, in a close physical proximity to where the vehicle was being developed. With technology revolutions, laboratory simulations and analytical evaluations became the newest trend in the vehicle testing. As a result, vehicles or components could be tested faster, less costly, and in more controlled environments. Computer simulations allowed even prediction of critical locations without subjecting a vehicle/component through a physical test.

Thus, vehicle accelerated testing became one of the most crucial areas of vehicle testing. This essential component of product development has however some downfalls. For an ideal accelerated test to be accomplished, a correlation of failures with service vehicles should be established. Thus, a lot of questions are being raised on how to shorten the time while retaining the integrity of testing. A lot of time and money is being spent investigating "how good" the accelerated tests really are. With all these efforts however, it has been established that the benefits definitely outweigh the disadvantages. With constant research being employed in this area, accelerated vehicle testing continues to grow.

7.2 Conclusions

The method of data analysis, described in detail in Chapter 5, was developed to analyze. Within the laboratory simulation itself, further methods of accelerating vehicle testing are constantly being investigated. An example of this is the present project, which is being conducted for University of Windsor/DaimlerChrysler Canada ARDC in Windsor. The study was conducted to verify a method suggested by the Road Test Simulation (RTS) Department, which implied that some road courses included in the OR vehicle durability test produce similar vehicle responses. This observation was made through experiences of qualified engineers who have conducted many tests at the OR course. This in turn resulted in the grouping roads of similar characteristics, and including only one representative road in the durability schedule replicated in the laboratory. The questions posed by the RTS group with regard to applying this method of test acceleration were:

- Is this method feasible?
- If feasible, which roads should be grouped together and how should the representative road should be selected?
- If feasible, what benefits and disadvantages can be expected by utilizing this test acceleration method?
- Are there any cost and time saving benefits associated with this method?
- What recommendations can be put forth as a result of this study?

The results of this study show that accelerating the OR durability test by a road substitution method is, indeed, a feasible solution. A detailed analysis of vehicle responses collected at the OR test course showed that five groups of roads could be formed based on the similar behavior they induced in the vehicle. The groups formed are as follows:

Group 1: R1, R2, R3, R4 and R5
Group 2: R6 and R7
Group 3: R10
Group 4: R8

Group 5: R9

For a group to be formed, the vehicle responses collected from each road were required to show correlation in:

- cyclic content based on rainflow-counting methods,
- probability density function relating amplitude distribution,
- frequency content and profile,
- total damage and damage distribution.

The last three groups of roads, that is R10, R8 and R9 showed significant distinction from each other and the remaining roads included in the test. Thus, they had to be placed in groups of their own. This analytical observation was confirmed with the road profiling [17] report conducted at the PG off-road course.

The R10 Road is a discrete event constructed to provide torsional input. It is one of the two test courses that was man-fabricated (R9 Road is the second), whereas other roads exemplify natural desert-like conditions. The R9 Road individuality comes from R9 bed formations, which are not present in other road sections. These rough road inputs require very low speeds, and induce uniquely high vertical, longitudinal and lateral loads.

The R8 Road is a paved surface used to transverse to other surfaces. If in good condition, the road adds no value to the structural durability input. Even with some imperfections (surface wear over years), the road shows to produce low damage numbers (compared to other roads); thus many times it is not included in the durability schedule. However since the R8 road has been used by the RTS Department in Windsor in their testing, it was included in the study. In preparing the OR test schedule for laboratory simulation, it is recommended however to perform a comparative damage assessment with each test to determine whether or not the R8 Road could be omitted from the durability cycle. Factors such as road maintenance may significantly improve the condition of this road, making it inefficient to include it in the test.

Thus, to preserve the integrity of the test it is recommended that all three roads: R10, R9 and R8 be included in the test, although further investigation is recommended to study the benefits of including R8 Road in the test.

The first group of roads includes R1, R2, R3, R4, and R5 Roads. To a high degree of certainty, all roads showed similarities in the vehicle responses collected while driving through them. The closest resemblance was observed between R3 and R4 Roads.

The study showed that one representative road out of this group could be selected to represent the remaining roads. Producing multiple passes of the representative road allows the other roads to be replaced, while maintaining the same cyclic input, and damage distribution. The selection of the representative road should be based on three criteria. These are:

1. Stability of the road – Based on the test course roughness report [17] conducted at the PG off-road course, the dynamic nature of the roads, weather conditions, traffic type and density, affect the condition of the roads. A five year study, profiling the OR course, showed that R5 Trail has proved to be one of the most stable courses at the PG.

2. Duration of the time history – In order to reduce the time of the durability cycle, it would be most efficient to select a representative road that is the shortest in duration.

3. Fatigue Analysis – To accelerate the test, while achieving the most damage, it is recommended to select a representative road that is the most damaging one in the group.

It is recommended, in future work, to perform an optimization study to determine the best way of selecting the "representative" road, with all three factors serving as variables. All three criteria change however with time, vehicle type, speed, driver and his/her conduct. In addition, the present study showed that the severity of road inputs and intensity of frequencies varied from test to test, from channel to channel for each road. Thus it would be impossible to predict whether one individual road will always produce the optimal solution. A quick procedure/macro would need to be developed, that would allow the

engineer to decide which road should be used as a representative road for that particular test by satisfying all three criteria.

The second group included the R6 and R7 Roads. The only test that showed good correlation between the vehicle responses from these two roads came from project #P1 at full rated load, conducted in 1997. Poor correlation for the other data sets could be contributed to the quality of data itself or the change in road condition. Upon a close review of the test course roughness report [17], it is more likely that the variability of road conditions in Group 2 roads affected the results. The sand-based washes present in R7 and R6 Road are prone to transformations as a result of traffic but mostly due to weather conditions. The report notes that primary changes in washboard content were noticed in R6 Road, and the south end of R7 Wash over the last five years. The severity of the washboard changes significantly with the amount of rain, with washboard formation and amplitude being the greatest for unbound material in dry weather conditions.

The report however notes that the characteristics of R7 road "are much the same as what was noted in R6 Wash" [17]. Thus, it would be a judgment call of the testing engineer, preparing the durability schedule for simulation in the laboratory, to decide whether the changes in the two roads are significant enough to include both roads in the test or if road substitution is feasible. The same decision would have to be taken with respect to other groups of roads.

As with any type of test acceleration, the feasibility of using the method presented in this study can be judged based on its disadvantages and benefits. The benefits include:

- possible time-savings in data analysis, drive file development, and durability testing,
- cost savings resulting from the shortened duration of the test,
- ability/potential to substitute another road with reasonable confidence, if a data-set is corrupted or deemed unacceptable for some reason, thus likely saving on cost of another trip to the PG.

The possible disadvantages are:

- changing test integrity by not including all roads in the test,
- omission of input cycles and/or frequency inputs important in durability assessment, and
- change of failure modes.

These issues could be addressed with exploration of more sets of data collected at the PG OR course. This would not only further confirm or dispute the results, but it would also increase the reliability of the method presented in this work. In addition, maintaining the integrity of the test could be assured by constantly correlating the failures seen in the vehicles tested in the lab with those seen in service.

The time-savings acquired by accelerating the test through road substitution are confined to the laboratory simulation itself. It is recommended during data acquisition at the proving grounds, to collect the responses from all roads included in the test. This seems more efficient for two reasons, which are:

- The design of the course itself requires travel over each road in the group, even if the data were to be collected only from the "representative" road. Therefore, since one has to drive over the road, why not just collect the data?
- Secondly, in case of a transducer failure, or data acquisition system problems, it is "safer" to have back-up roads to use in place of the representative road.

The time-savings acquired in the lab environment can be divided into three sectors:

- Time spent on data analysis, and editing – the fewer roads are to be analyzed, the shorter the data preparation period. This step is however recommended to be performed on all road sections, to determine whether some roads in a particular group are of value, and need to be included in the test.
- Drive file development – the fewer roads included in the test, the fewer drive files need to be developed (iterated).

- Duration of the durability schedule- this is dependent on many factors such as the duration of the time histories of the "representative roads" and their damage content.

The interest of experienced engineers at the ARDC with the method of road substitution, is geared mainly towards time saving. The method although shown to be a feasible solution, however needs verification with each test, as shown in this study. The degree of confidence will however increase with more data being analyzed.

8 FUTURE WORK

It is recommended for future work that an efficient macro be designed which, based on method of analysis presented in this work, determines whether or not the roads induce similar vehicle responses in the vehicle. This would increase the level of confidence and decrease the time spent analyzing the data, prior to drive file development. Further implementation of a macro could allow an optimized selection of a "representative" road as discussed in the Chapter 7 of this thesis. The effects of editing the vehicle responses prior to grouping and optimization process should also be investigated.

The method of analyzing vehicle responses could be implemented even further in the future work. In this study, statistical analysis proved to be not a reliable method used for road classification. This is because the complex service load spectra (load amplitudes and their frequency of occurrence) are actually comprised of two categories of loading [14]:

- normal loads (stationary) – generated due to road roughness, and
- extreme loads (transient) - which occur due to unusual vehicle maneuvers, curb impacts, or deep chuckholes.

To obtain a meaningful statistical comparison between roads, the transients should be analyzed separately from the constant RMS sections. Computer software could be used to detect and extract transient events from the majority of the data, as presented in a study by Bruscella at the Victoria University of Technology [36]. In his study this technique was utilized on road profile data, for purpose of road classification used in the simulation of the road transportation process. Nine parameters were developed to characterize and evaluate road conditions. They were:

- for transient amplitude distributions:
  - mean,
  - standard deviation,
  - median,

- range,

- for constant amplitude distributions:

  - mean,
  - standard deviation,
  - median,
  - range,

- transient density.

In addition, road classification of OR course could include "true" road profile data collected at the PG. The method presented by Bruscella [36] could then be implemented to further verify the results of the present study. Although, collecting road profile data for road classification purpose seems ideal, it is a costly and time-consuming process. Extensive analysis of road profiles relies on their accurate measurements. The road profile can be described as a two-dimensional random surface, and description of such surface would require elaborate statistical parameters to be fully described [36]. Since a vehicle experiences inputs at each wheel, any road profiling simplification for vehicle simulation purpose, would have to account for the cross correlation between these inputs.

A difficulty in collecting road profiling data at the Proving Grounds could present itself due to the dynamic road conditions. According to conversations with Mr. Schlueter from APG [37], the only institution capable of collecting road profiles on off-road track conditions is the Nevada Automotive Test Center (NATC). The NATC has developed a Dynamic Force Measurement Vehicle (DFMV) capable of measuring the road roughness indexes of the type of roads present at the PG. According to Mr. Schlueter [37] however, it would be quite unrealistic to define a "true road profile" for the off-road tracks, which is necessary for road classifications method presented by Bruscella [36]. This is because the dynamic nature of the OR course causes a constant change of the surface while a vehicle travels through it. The displacement of the road surface would vary due to factors such us vehicle weight, speed, tire pressure, tire width and tread size. Therefore, until a profile-meter capable of collecting true profiles on off-road tracks is developed, the analysis based only on vehicle responses can be used to classify those types of roads.

If the true road profiling data would be available, it could also be used with the knowledge of vehicle suspension properties to predict the vibrational responses of vehicles [15]. This in turn can serve as another way of classifying the road characteristics present in the OR course. Since however only the vehicle response data was readily available during the present study, it seemed more cost-efficient to use it for road classification purposes. This would also determine whether or not it is possible to characterize road characteristics based on inputs they create in a vehicle.

The method of using vehicle dependent data as a way of determining the similarities and differences of road conditions could be even further verified with the use of "effective road profile control (ERPC)" [15]. This method was briefly described in Section 2.2.4 of this thesis. Developed by Ford Motor Company, ERPC incorporates vehicle/tire dynamics models with vehicle response data, to calculate "effective road profile". The estimated vehicle-independent road profile is then used as a control reference for other vehicle testing. With the access to the ERPC, effective road profiles could be created for each road, independent of a vehicle used. Vehicle responses collected from similar roads would then be expected to create similar road profiles.

Lastly, future work in this area could also consist of improvements in correlating the cyclic inputs of the vehicle responses based on linear regression. This could be done in three ways. Firstly, the non-damaging portions could be removed from the signals using fatigue damage analyses. The method of road analysis presented in this study could then be applied to the edited road sections to further accelerate the tests. Secondly, methods of data extrapolation [38] could be utilized in defining the Target and Sample test tracks in form of rainflow matrix. This would account for variability associated with data acquisition such as: driver type, or road severity. This concept was briefly described in Section 2.2.1. The third method of improving the correlation process based on linear regression of cyclic inputs could consist of including frequency characteristics of the responses. A given target PSD could be optimized in parallel with cycle related histograms. This concept was introduced by LMS of North America, and is included in their software package [38].

In conclusion, any method of test acceleration requires constant validation. The method of test acceleration introduced in this study can contribute a significant reduction in product design/development time. However, only through constant research in accelerated vehicle testing, standards can be established that would justify the development of more durable and reliable products at a cost of decreasing product development times.

REFERENCES

1. Philip Grote, "Fatigue Correlated Testing for Vehicle Components – Automated Tools to Test Smarter and Faster", SAE Paper 9434082.

2. K. B. Clark and T. Fujimoto, Product Development Performance, Harvard Business School Press, 1990.

3. Gail E. Leese and Robert L. Mullin, "The Role of Fatigue Analysis in the Vehicle Test Simulation Laboratory", SAE Paper 910166

4. Bernhard Gründer, Michael Speckert, Peter Pirro, "Optimal Configuration of Test Schedules", LMS Durability Technologies, and John Deere Zweibrücken, paper obtained directly from LMS North America, Troy, MI

5. W. A. McConnell, "How good is testing?, a correlation of customer, laboratory, and proving ground experience.", Ford Motor. Co, SAE paper #600060 presented at SEA Detroit Section meeting Dec. 7, 1959.

6. David F. Ensor, B.Sc. Ceng MIMechE, "Customer Correlation & Accelerated Proving", nCode International Ltd., 27 January, 1998

7. Scott R. Pajtas, "Team Test: Real World Instrumented Vehicle Quality/Reliability Testing", Automotive Systems Testing TOPTEC presentation, October 14-15, 1998

8. R. E. Canfield and M. A. Villaire, "The Development of Accelerated Component Durability Test Cycles Using Fatigue Sensitive Editing Techniques, SAE Paper 92. 0660

9. "No pain, no gain – ADR track at Chelsea Proving Grounds", DaimlerChrysler MAGAZINE for employees, Autumn 1999

10. Steven R. Haeg, "Steer Dynamics in Road Simulation", MTS Systems Corporation, Minneapolis, Minnesota, Paper 55424

11. J. De Cuyper, D. Coppens, C. Liefoofhe, J. Swevers, M. Verhaegen, "Advanced drive file development methods for improved service load simulation on multi axial durability test rigs", LMS North America, http://www.lmsna.com/apps/twr.htm

12. MTS publication, "Explaining the Six Steps of Remote Parameter Control", MTS Systems Corporation, USA

13. "RPC III Operation Training Manual", Version 4.2, by MTS System Corporation, 1996

14. Matyas Matolcsy, Narendra J. Sheth, "Determination of Extreme Structural Loads in Service", SAE paper #780107, SAE Congress and Exposition, Detroit, MI, Feb27-March 3, 1978

15. Larry Mianzo, David Fricke, Rakan Chabaan, "Road Profile Control Methods for Laboratory Vehicle Road Simulators", Ford Motor Company, Dearborn, MI

16. DaimlerChrysler Arizona Proving Grounds Web Site, http://wwwcais.cpg.chrysler.com/docs/ppoint/apgweb/

17. Thomas Wolcott, S. Colin Ashmore, "Arizona Proving Ground Off-Road Test Course Roughness Comparison" – June 1998 vs. March 1997 vs. August 1996 vs. December 1995 vs. October 1994 – Comparative Road Profile Analysis", NATC project no.: 20-17-786, Nevada Automotive Test Center, Carson City, Nevada

18. Correspondence with Steven E. Schlueter, Duty Cycle Specialist from DaimlerChrysler Arizona Proving Grounds., November 1999

19. D. Wong, R. Din-Lovinescu, G. Barnett, 'Road Simulation Drive File Development – AK3 Cycle for 1999 model vehicle V1, Volume 1 and 2", University of Windsor/DaimlerChrysler ARDC Product and Development Engineering, May 1997

20. Jennifer Heymans, Gerry Pettica, Martin Vander Baaren, "Durability Test Report – AK3 12 Channel Simulation for vehicle V2", University of Windsor/DaimlerChrysler ARDC Product and Development Engineering, July 1996

21. Correspondence with Martin Vander Baaren, Product Engineer at University of Windsor/DaimlerChrysler ARDC, October-November 1997

22. Jess J. Comer, "Fundamentals of metal fatigue analysis" SAE Seminar , July 12-14, 1999

23. Julie A. Bannantine, Jess J. Comer, James L. Handrock, "Fundamentals of Metal Fatigue Analysis", Prentice Hall, 1990

24. American Society for Testing and Materials, "Annual Book of ASTM Standards, Section 3: Metals Test Methods and Analytical Procedures", Vol. 03.01-Metals-Mehanical Testing; Elevated and Low-Temperature Tests, ASTM, Philadelphia 1986, pp. 836-848.

25. NCode nSoft V5.1 Online Documentation, Ncode North American Office, Southfield, Michigan, March 1998, pg. 6-3-17 to 6-3-18.

26. NCode nSoft V5.1 Online Documentation, Ncode North American Office, Southfield, Michigan, March 1998, pg. 6-2-4 to 6-2-5.

27. NCode nSoft V5.1 Online Documentation, Ncode North American Office, Southfield, Michigan, March 1998, pg. 6-2-8

28. NCode nSoft V5.1 Online Documentation, Ncode North American Office, Southfield, Michigan, March 1998, pg. 6-4-2 to 6-4-4

29. Ming Yu, Jihal Zhao, Huile Wu, "Effects of Test Conditions on Vehicle Structural Accelerated Testing", SAE paper #958480

30. NCode nSoft V5.1 Online Documentation, March 1998, pg. 5-2

31. NCode nSoft V5.1 Online Documentation, March 1998, pg. 5-31

32. M. R. Mitchell, R.M. Wetzel, "Cumulative Fatigue Damage Analysis of a Light Track Frame", SAE paper #750966, Automobile Engineering Meeting, Detroit, MI, Oct. 13-17, 1975.

33. H. Neuber, Trans. ASME, J. App. Mech., 8, 1961

34. "Fatigue Design Handbook – SAE 10", SAE 1988

35. Paul Weal, Christophe Liefooghe, LMS International; Klauss Dressler, TECMATH, "Improving the Durability Engineering Process", http://www.lmsna.com/apps/cashist/s&vdur.htm

36. Ben Bruscella, "The Analysis and Simulation of the spectral and statistical properties of road roughness for package performance testing", Victoria University of Technology, Victoria, Australia, March 1997

37. Conversation with Steven E. Schlueter, Duty Cycle Specialist from DaimlerChrysler Arizona Proving Grounds during trip to APG, December 7, 1999.

38. Bernhard Gründer, Michael Speckert, Mark Pompetzki, "Design of Durability Sequences Based on Rainflow Matrix Optimization", SAE paper # 980690, International Congress and Exposition, Feb. 23-26, 1998, Detroit, MI.

VITA AUCTORIS

Mirella T. Rennert was born on October 16, 1974 in Swiętochłowice, Poland. She graduated from Catholic Central Secondary School in Windsor, Ontario in 1994. From there she went to the University of Windsor, Ontario, Canada where she received the degree of Bachelor of Applied Science Honors in Mechanical Engineering, with co-operative education program option in 1998. She was awarded the 1998 Board of Governors Medal in engineering and the 1998 Association of Professional Engineers of Ontario Medal for her scholastic achievements. Mirella is currently a candidate for the Master's degree of Applied Science in Mechanical Engineering at the University of Windsor and is scheduled to graduate in Fall of 2000. She is also currently employed as an Impact Safety Vehicle Development Engineer by DaimlerChrysler Jeep and Truck Engineering in Detroit, Michigan, USA.

APPENDIX I

PROJECT #P1 – TRANSDUCER LOCATION

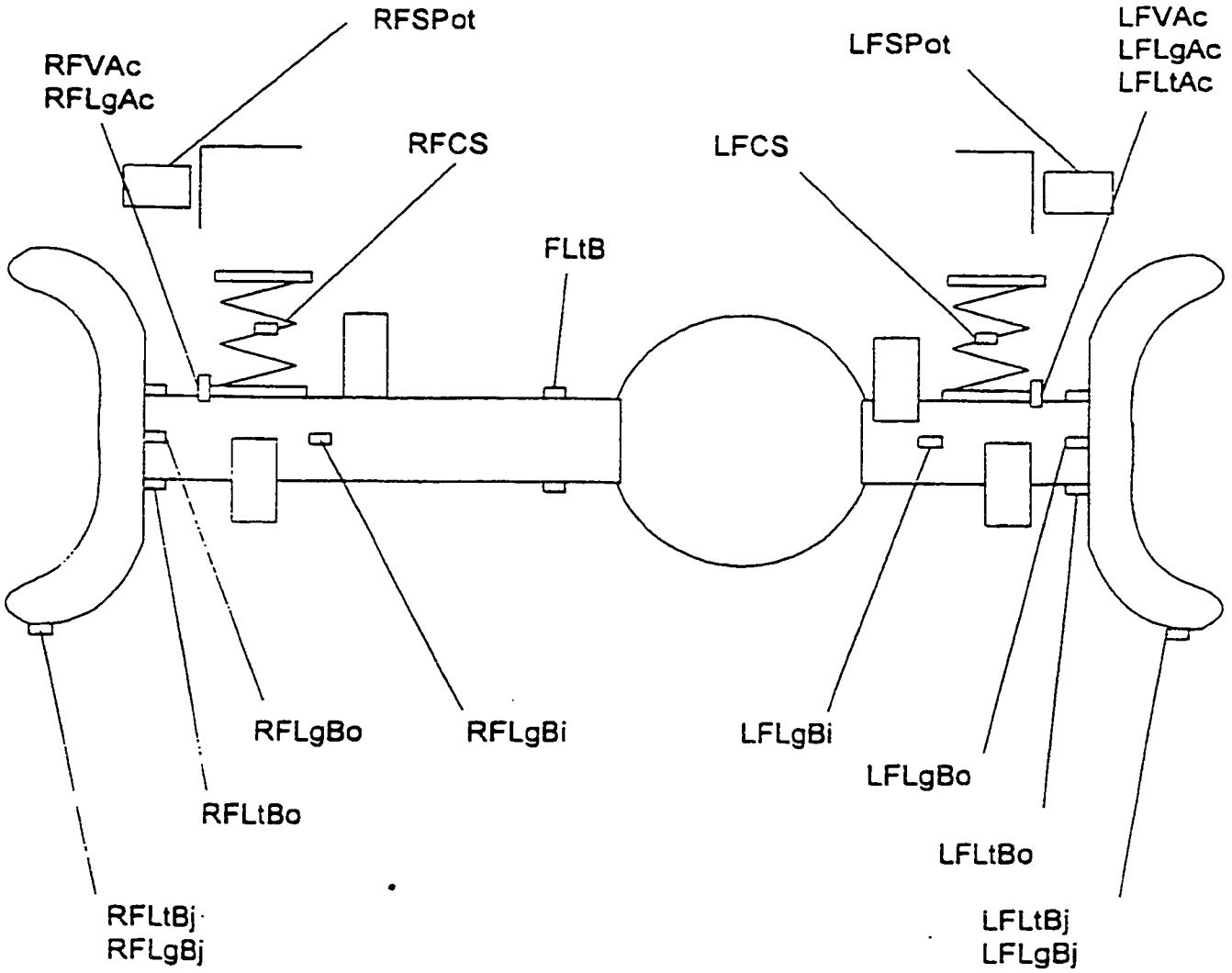

Front View

Instrumentation for Road Simulation - Front Axle

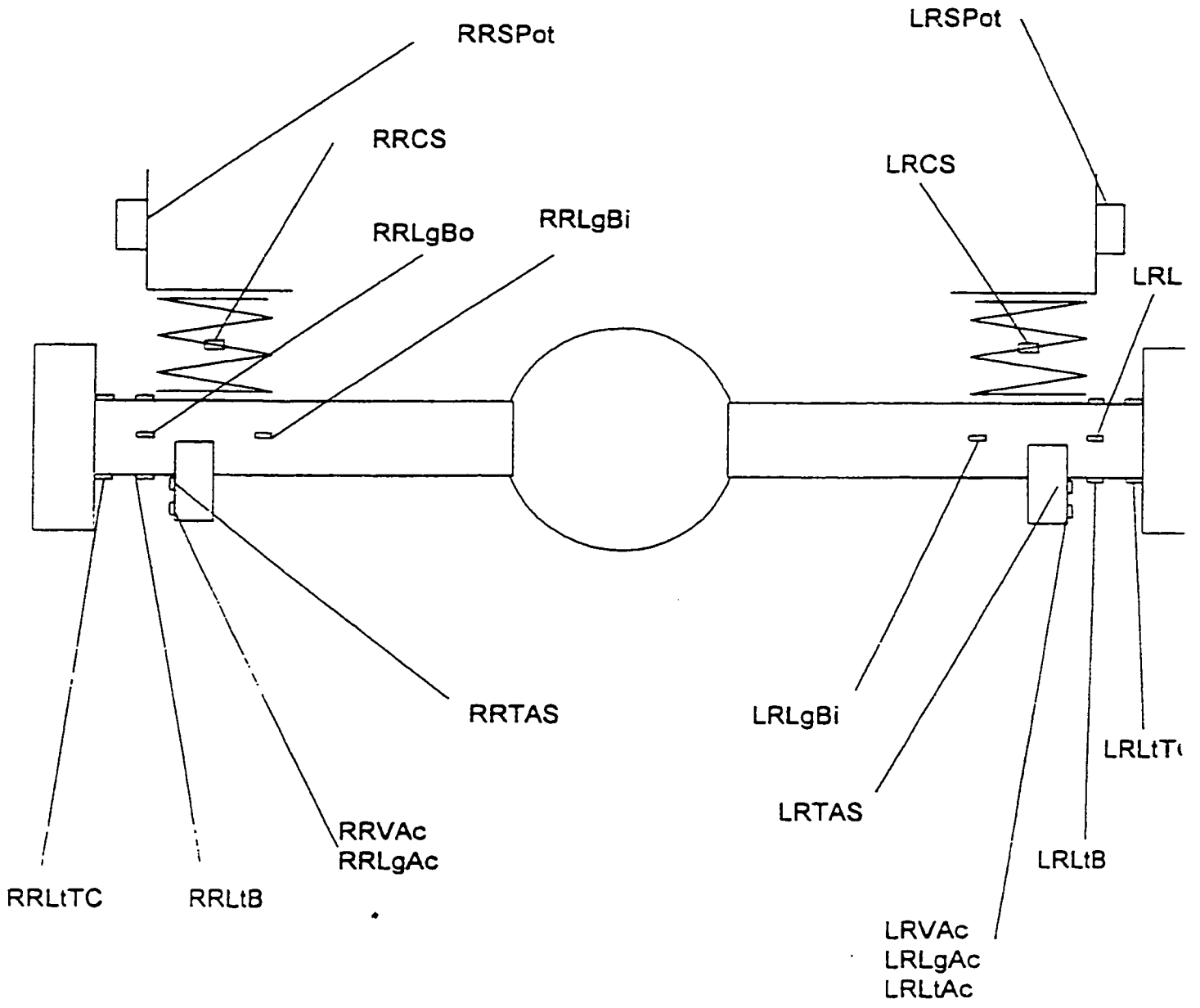

Front View

Instrumentation for Road Simulation - Rear Axle

APPENDIX II

TRN, CSD AND ASD CALCULATIONS

How to Calculate the FRF (1 of 2)

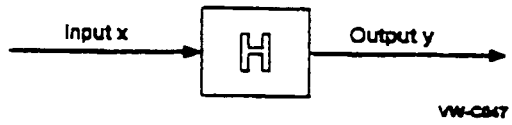

- **Magnitude**

For Each Frequency:

The input amplitude is x and the output amplitude is y.

$$H = \frac{y}{x} = \frac{y}{x} * \frac{x}{x} = \frac{y * x}{x^2}$$

x^2 is proportional to the power of the input signal.

$y * x$ is proportional to the combined power between the input and the output signal.

$$x^2 \sim G_{xx}$$

Autospectral density, G_{xx}, describes the power of a signal for each frequency.

$$y * x \sim G_{yx}$$

Cross-Spectral density, G_{yx}, describes the combined power of two signals for each frequency.

For All Frequencies:

$$\text{Magnitude of } H(f) = \frac{\text{Magnitude of } G_{yx}(f)}{\text{Magnitude of } G_{xx}(f)}$$

How to Calculate the FRF (2 of 2)

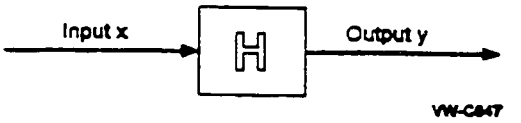

- **Phase**

  For Each Frequency

  $$\text{Phase of } H =$$

  $$[\text{Time delay between } x \text{ and } y] \times [\text{Frequency}] \times 360°$$

  $$\text{Phase of } G_{xx} = 0$$

  The phase of G_{xx} is always 0.

  $$\text{Phase of } G_{yx} =$$

  $$[\text{Time delay between } x \text{ and } y] \times [\text{Frequency}] \times 360°$$

  For All Frequencies

  $$\text{Phase of } H =$$

  $$[\text{Phase of } G_{yx}] - [\text{Phase of } G_{xx}] = [\text{Phase of } G_{yx}] - 0$$

- **Magnitude and Phase**

$$H(f) = \frac{G_{yx}(f)}{G_{xx}(f)} = \frac{[\text{Cross} - \text{Spectral Density}]}{[\text{Autospectral Density}]}$$

Autospectral Density

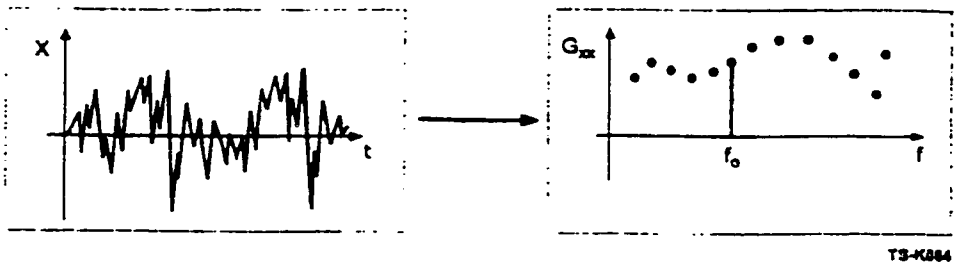

- ## Power as Function of Frequency

  The Autospectral Density (ASD) gives information about the frequency content of a signal. The ASD shows the power at each frequency line. The power is relative to the amplitude squared.

  Another name for Autospectral Density is Power Spectral Density (PSD).

  The ASD for a sinusoidal signal is just one point at that frequency line.

- ## No Phase Information

  The ASD shows the power and has no phase information.

- ## Original Method – Bandpass Filters

  The original way to calculate the ASD for a signal was to use many narrow bandpass filters. There was one filter per frequency line in the spectrum.

  The average for the squared signal from each filter was measured and plotted in the ASD.

  This method gives an ASD which is sensitive to the bandwidth of the filters used in the process. If the filters are very narrow, less signal passes through the filters and the ASD has a lower magnitude than if the filters were wider.

- ## Normalized to Bandwidth

  By normalizing the ASD to the bandwidth of the filters, it is possible to compare ASD's from different systems. This is done by dividing the measured value by the bandwidth of the filters.

  The units of the ASD are: (Eng. Units)^2/Freq.

Original Method of Creating an Autospectral Density (1 of 2)

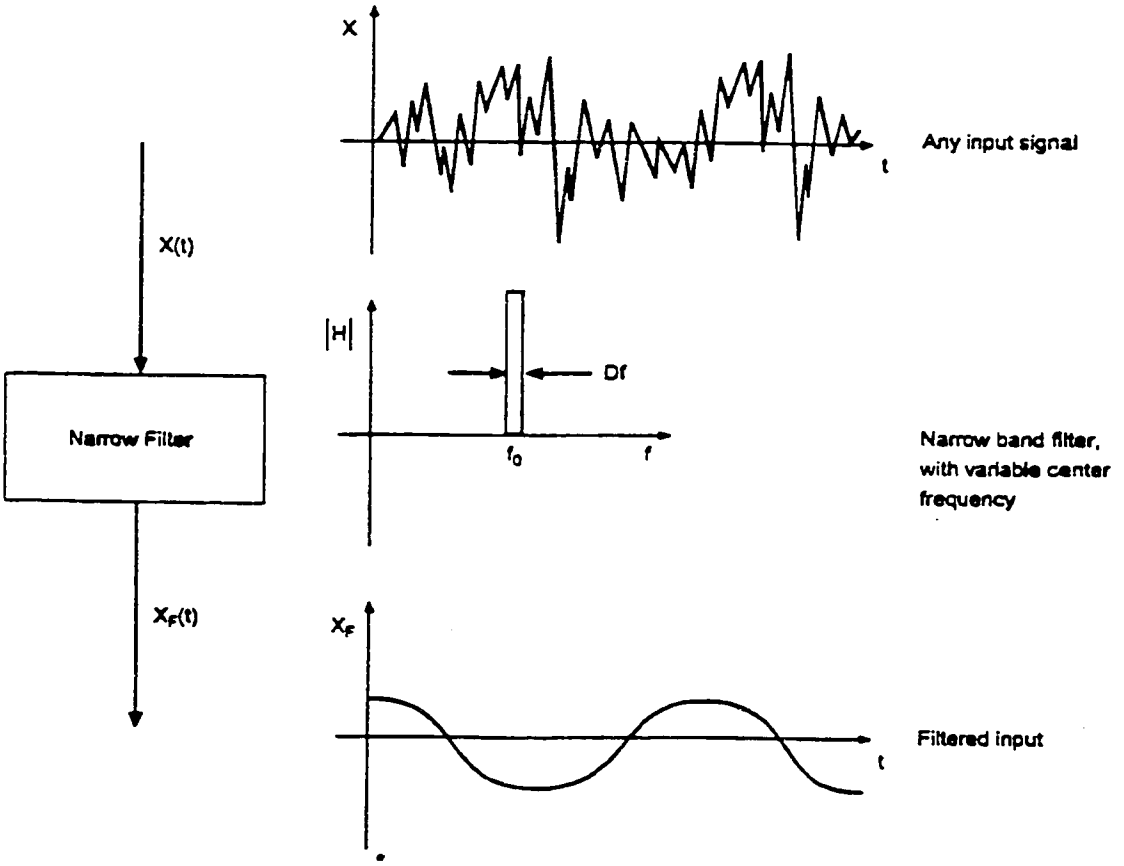

Continued on next page

TS-K088

Original Method of Creating an Autospectral Density (2 of 2)

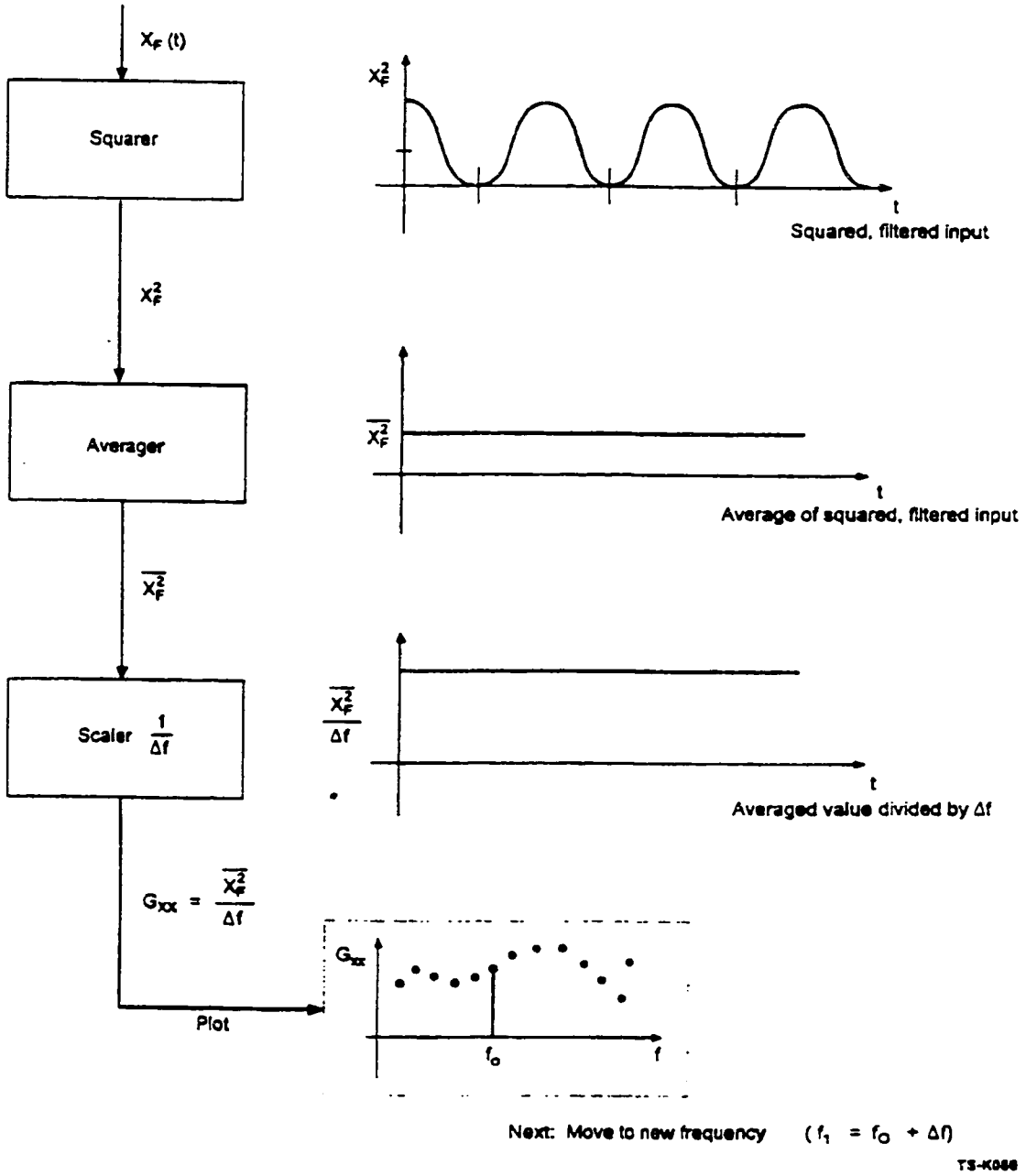

Calculating an ASD

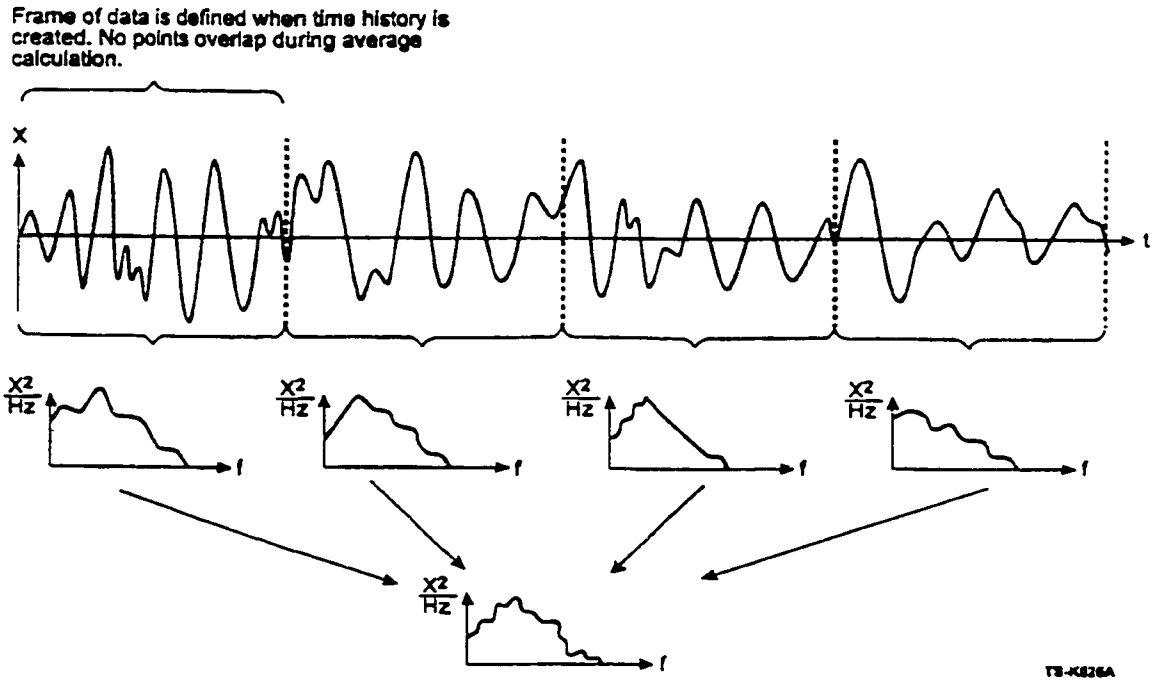

- **Frequency Domain**

  RPC uses digitized data to calculate the ASD. Transferring the data to the frequency domain produces the frequency spectra of the data. The units in the frequency domain are the same as those used in the time domain. To calculate the normalized ASD, RPC multiplies the frequency spectra by itself and then divides by the bandwidth. The bandwidth is the frequency increment in the ASD.

- **Fast Fourier Transform – FFT**

  The Fast Fourier Transform (FFT) algorithm transfers the data from the time domain to the frequency domain.

• Average ASD

The FFT algorithm uses a predefined number of points. In RPC, the number of points is equal to one frame of a time history. If the signal is longer than one frame, an ASD is calculated for each frame, and the average of all ASD's becomes the ASD for the entire signal.

The bandwidth is 1/(frame length).

Normally a frame has 1024 points, and its length is 5 seconds. Therefore, normal frames have a bandwidth of 0.2 Hz.

• Reducing External Random Noise

Averaging helps reduce the effects of external noise on the ASD.

A measured signal will have some amount of random noise in it. When doing averages, the effect of the random noise is reduced and the content of the signal shows up better.

Cross-Spectral Density

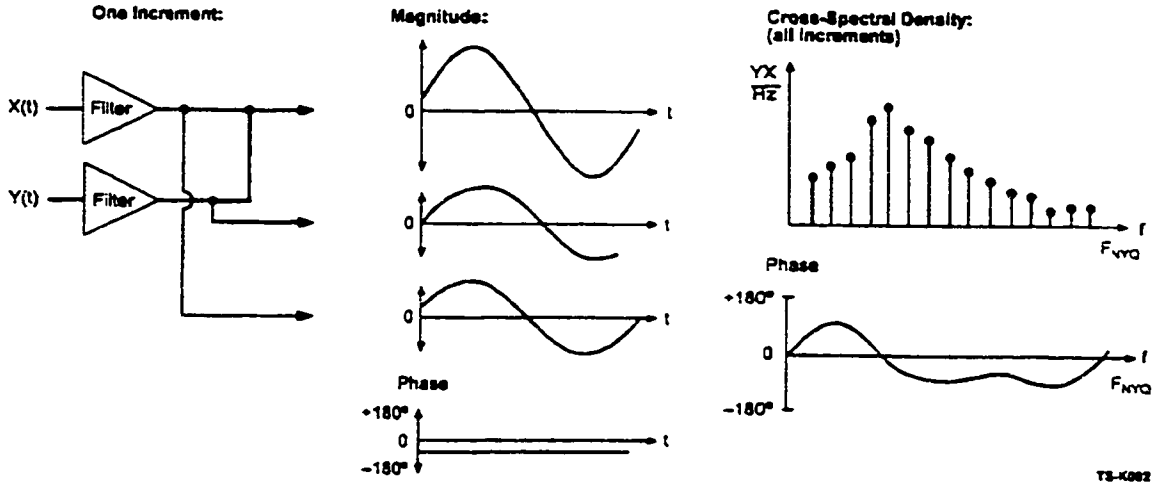

- ## Combined Power of Two Signals

  For each frequency line, the Cross-Spectral Density (CSD) shows the combined power of two signals. The magnitude is relative to the product of the amplitudes of both signals.

- ## Original Method – Bandpass Filters

  The original method used to measure the CSD is similar to the original method used to measure the ASD. The method uses one bandpass filter per frequency line. The product of filtered amplitudes are calculated and then averaged. This average is divided by the bandwidth to get the magnitude.

- ## Phase Between the Signals

  At each frequency line, the phase difference between the two signals becomes the phase in the CSD.

- ## ASD Special Case of CSD

  When you use the same signal as both inputs in creating a CSD, the result is an ASD.

Calculating a CSD

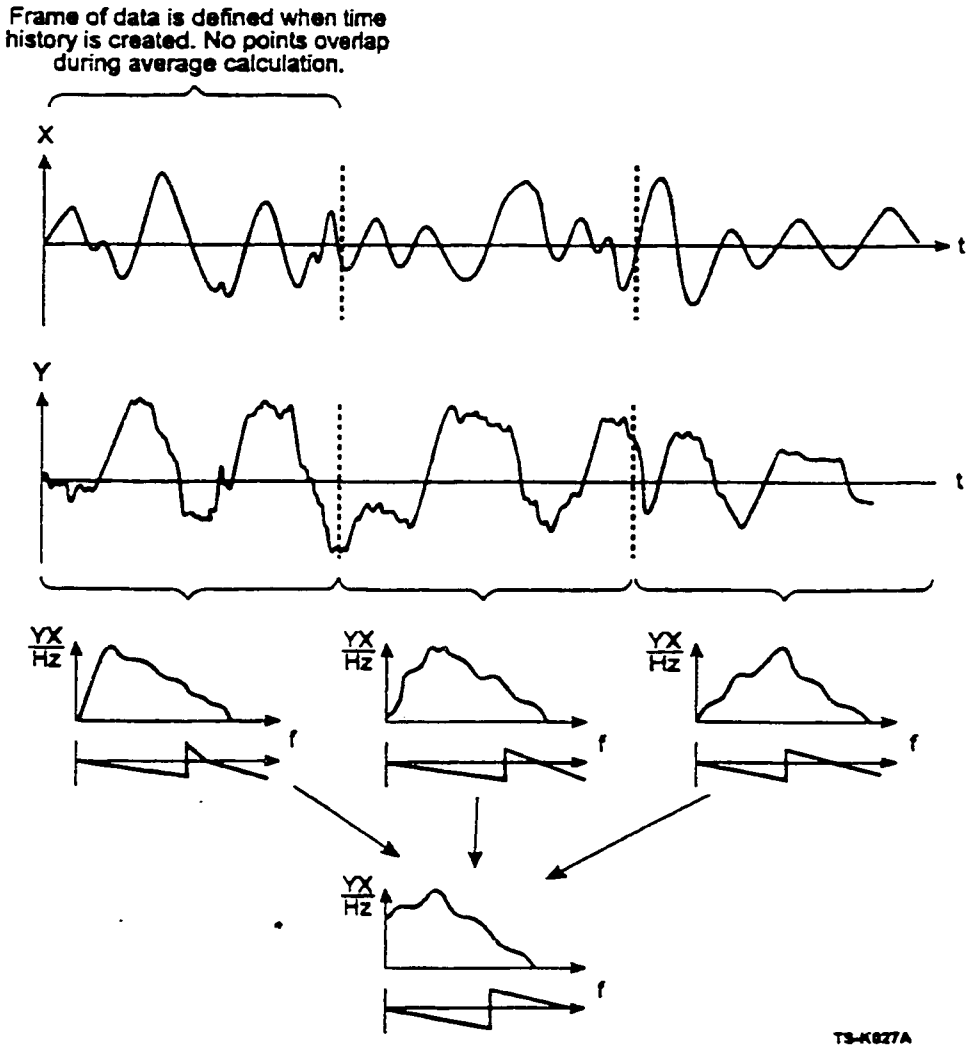

- **Frequency Domain**

  To calculate a CSD, RPC transfers input and output data to the frequency domain. To calculate the normalized CSD for each frame, RPC multiplies the input frequency spectra by the output frequency spectra and then divides by the bandwidth.

- ## Fast Fourier Transform – FFT

  The Fast Fourier Transform (FFT) algorithm transfers the data from the time domain to the frequency domain.

- ## Average CSD

  The FFT algorithm uses a predefined number of points. In RPC, the number of points is equal to one frame of a time history. If the signal is longer than one frame, a CSD is calculated for each frame, and the average of all CSD's becomes the CSD for the whole signal.

- ## Reduce Effect of External Noise

  Averaging helps reduce the effects of external noise on the CSD.

FRF Calculation

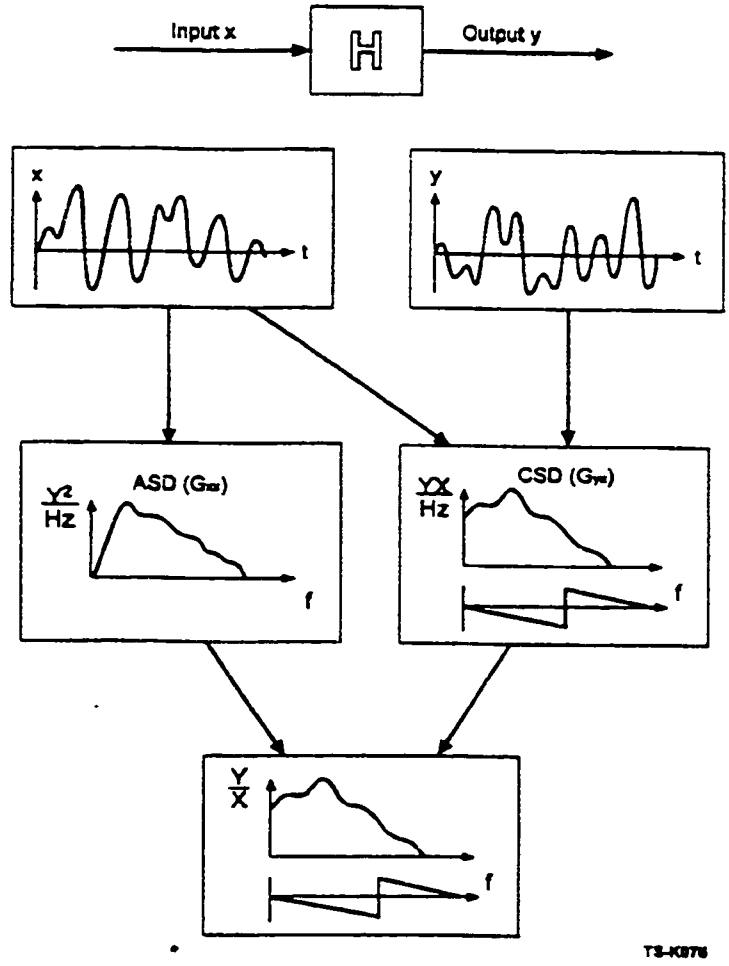

- **Random Noise Input**

  To calculate the Frequency Response Function (FRF) over a range of frequencies, it is necessary to use an input signal that has data throughout all frequencies in the range.

  The signal can be either a sine sweep or a random signal that contains all frequencies. Using a random signal is most common because it allows various amplitudes at each frequency (unlike a sine sweep).

- ## System Output – Response Signal

  At the same time you give input to the system, you can measure its output. Measuring the system output produces a response signal. The response signal gives information about how the system reacts to different inputs.

- ## ASD for Input

  ASD for the input is proportional to the square of the input amplitude. The spectrum has no phase information.

- ## CSD between Input and Output

  The CSD between input and output is proportional to: (output amplitude) * (input amplitude). The CSD also has phase information between input and output. This phase becomes the phase for the FRF.

- ## FRF

  The FRF is calculated from the ASD of the input and the CSD of the input and output.

  The gain comes from the magnitude ratio Y/X, and the phase comes from the cross spectrum.

  A single input, single output FRF is stored as a |X| matrix.

APPENDIX III

CORRELATION EQUATIONS

Fit Coeffs Grid (RMS cyclic error)

$$RMS = \frac{\sum_{1}^{n}(Target[i]-Solution[i])^2}{n}$$

Fit Coeffs Grid (R2 value)

$$R^2 = 1 - \frac{\sum_{1}^{n} (Target[i] - Solution[i])^2}{\sum_{1}^{n} (Target[i] - \text{Mean of solution bins})^2}$$

Fit Coeffs Grid (average absolute cyclic error)

$$Absolute = \frac{\sum_{1}^{n} Absolute(Target[i] - Solution[i])}{n}$$